Potential of proximal teledetection and modeling as a way to assess canopy structure and functioning

Gabriel Hmimina

UNIVERSITE PARIS-SUD

ÉCOLE DOCTORALE : SCIENCES DU VEGETAL

DISCIPLINE BIOLOGIE

THÈSE DE DOCTORAT SUR TRAVAUX

soutenue le 29/11/2013

par

Gabriel HMIMINA

Préparée au Laboratoire Ecologie, Systématique et Evolution

UMR 8079, Université Paris Sud, CNRS, AgroParisTech
Faculté des Sciences d'Orsay

Apports de la télédétection rapprochée et de la modélisation à l'étude de la structure et du fonctionnement des couverts végétaux.

Directeur de thèse : Kamel Soudani MdC (ESE – Faculté des Sciences d'ORSAY, Université Paris Sud)

Composition du jury :

Stéphane Jacquemoud (Pr, Université Paris 7- Denis Diderot)	**Rapporteur**
Nicolas Viovy (Dr, LSCE, CEA Saclay)	**Rapporteur**
Paul Leadley (Pr, Orsay, Université Paris Sud)	**Examinateur**
Valérie Le Dantec (MdC, CESBIO, Université Paul Sabatier, Toulouse)	**Examinateur**
Guerric le Maire (CR, Eco&Sols, CIRAD, Montpellier)	**Examinateur**
Nicolas Barbier (CR, AMAP, IRD, Montpellier)	**Examinateur**

« Un seul a toujours tort : mais avec deux commence la vérité.

Un seul ne peut se prouver : mais il suffit de deux pour qu'on ne puisse plus les réfuter. »

Friedrich Nietzsche, « Le gai savoir »

Deux n'auraient pas suffi : la liste complète serait longue. Je tiens avant tout à remercier les membres du jury, qui ont accepté d'examiner ce travail : Stéphane Jacquemoud, Nicolas Viovy, Paul Leadley, Valérie Le Dantec, Guerric le Maire et Nicolas Barbier.

Merci à l'Université Paris-Sud XI, ainsi qu'au GIP ECOFOR et à F-ORE-T «Observatoires de Recherche en Environnement (ORE) sur le Fonctionnement des Écosystèmes Forestiers» ECOFOR, INSU, Ministère de l'Enseignement Supérieur et de la Recherche pour avoir financé ce travail de thèse.

Merci à Kamel Soudani, mon directeur de thèse, sans qui rien de tout cela n'aurait été possible. Merci particulièrement pour ta pédagogie et ta patience, mise à rude épreuve. Merci également pour la grande liberté dont j'ai joui tout au long de cette thèse. Cette liberté d'explorer des voies plus ou moins fructueuses, voire de me tromper a fait de ces quelques années la meilleure formation qui soit.

Merci à Eric Dufrène pour son soutien tout au long de ce travail. Merci à Daniel Berveiller pour son soutien et son efficacité, et à Jean-Yves Pontailler pour ces années de travail sur le site de Barbeau et sur le capteur NDVI dont j'ai pu bénéficier. Merci à Gabriel Cornic, Peter Streb, Zoran Cerovic, Jean Marc Ducruet, Gwendal Latouche, Nicolas Delpierre, qui ont toujours été disponibles pour répondre à mes questions de néophyte. Merci à Laurent Vanbostal, dont l'aide a été précieuse. Merci à l' « équipe CASTANEA », merci à Claire Damesin et Christophe François sans qui la vie de l'équipe EV serait bien morne. Un grand merci d'ailleurs à toute l'équipe EV pour cette atmosphère inégalée dans laquelle j'ai eu la chance de travailler : merci à ceux qui sont passés ; Alissar Cheaib, Sébastien Bellow, Constance Laureau, Alice Michelot, Touhami Rzigui... Et bon courage à tous ceux qui suivront : Joannès Guillemot, Lydie Blottière, Alice Delaporte ; votre tour approche !

Merci à l'école doctorale "Sciences du Végétal" et particulièrement à Jacqui Shykoff. Merci à Nathalie Lecat, Aude Ballouard et Sandrine Dessaints pour leur efficacité.

Merci enfin à mes parents (doublement !) sans qui rien de tout cela n'aurait été possible, à mon frère, et à Karla Perez-Toralla, qui m'a supporté et porté tout au long de ces dernières années.

Merci à tous ceux que je n’ai pas cités mais que je n’oublie pas : c'est une page qui se tourne, et que je relirais volontiers.

Résumé

L'anticipation des effets des changements climatiques nécessite une bonne compréhension du fonctionnement carboné des écosystèmes continentaux. L'une des principales contraintes liées à l'étude de ces écosystèmes est la forte variabilité à la fois spatiale et temporelle de leurs flux de carbone et de leurs réponses aux contraintes abiotiques. L'usage de méthodes de télédétection optiques pourrait permettre de suivre de façon spatialisée le fonctionnement des couverts végétaux. Ce travail vise à évaluer le potentiel de méthodes de télédétection pour décrire la structure et le fonctionnement de couverts végétaux à des échelles spatiales et temporelles variées. Pour ce faire, les relations entre indices optiques et phénomènes biologiques ont été étudiées en suivant une démarche de transfert d'échelle, des échelles les plus fines aux plus larges. Il a été montré que le PRI (Photochemical Reflectance Index), utilisé en tant qu'indicateur du LUE (Light Use Efficiency), est par nature un signal composite qui reflète principalement la régulation du rendement de la photosynthèse sur des échelles de temps fines, et la structure et composition biochimique du couvert à l'échelle de la saison. L'analyse de courbes de réponse du PRI au PAR (Photosynthetically Active Radiation) a permis de déconvoluer ces deux sources de variabilité, via l'introduction du concept de PRI_0 ou PRI d'une feuille idéalement adaptée à l'obscurité. Ce PRI_0, capturant la variabilité du PRI indépendante du LUE, a pu être mesuré à l'échelle de la feuille, et estimé à l'échelle de jeunes couverts végétaux et de la parcelle. Cette variabilité a pu être expliquée à l'échelle de la feuille et de jeunes couverts végétaux par les variations du contenu en pigment des feuilles. A l'échelle de peuplements adultes et de l'année, elle résulte cependant d'effets combinés de la composition biochimique et de la structure des couverts qui n'ont pu être séparés. Ces effets sont susceptibles aux échelles larges de masquer en bonne partie, voire de biaiser la relation entre PRI et LUE. Il a en outre été montré que la représentativité du PRI est limitée aux strates supérieures des canopées et dépend de la structure du couvert et du climat lumineux, ce qui peut limiter son intérêt en tant qu'estimateur du LUE à l'échelle de l'écosystème. Ces résultats soulignent la nécessité de prendre en compte la structure et la composition biochimique des couverts végétaux dans le cadre d'une utilisation du PRI en tant que proxy du LUE de l'écosystème.

Summary

In order to assess the effect of global warming, a good understanding of carbon functioning of terrestrial ecosystems is needed. The study of terrestrial ecosystem carbon fluxes and responses to abiotic stress remain challenging due to their high spatial and temporal variability. The use of remote sensing may help us to describe those sources of variability. The aim of this work is to assess the potential of remote sensing as a way to describe canopy structure and functioning over a broad range of temporal and spatial scales. The relationships between optical indices and biological phenomenon were investigated over a range of increasing scales. The PRI (Photochemical Reflectance Index), used as a proxy of the LUE (Light Use Efficiency) was shown to be a composite signal, mainly impacted by the regulation of the LUE at short time scales, and by canopy structure and pigment content at seasonal scale. The analysis of PRI response to PAR (Photosynthetically Active Radiation) allowed us to deconvolve those two sources of variability thanks to the introduction of the PRI_0 defined as the PRI of ideally dark adapted leaves. The PRI_0 was shown to efficiently describe the LUE unrelated PRI variability, and could be measured at leaf scale, and estimated at the leaf, canopy and stand scales. This variability could be explained by changes in leaf pigment content over the growing season at leaf and canopy scales. At the stand scale and over the year, this LUE independent PRI variability resulted from combined effects of canopy structure and pigment content, which could not be separated. These effects may result in biased or masked PRI versus LUE relationships at larges scales. Moreover, it was shown that the in-situ PRI measurements mainly responded to the LUE of sunlit leaves, depending on canopy structure and sky conditions. This may considerably hamper the use of the PRI as a proxy of the whole ecosystem LUE. These results illustrate the need to take canopy structure and pigment content into account while using the PRI as a proxy of the ecosystem LUE.

Sommaire :

Introduction générale

La photosynthèse terrestre est un des éléments clefs du cycle du carbone et un des puits nets qui contribuent à atténuer les effets des dégagements anthropiques de CO_2 (Houghton, 2003). Elle est cependant particulièrement sensible aux contraintes abiotiques. Les principaux facteurs limitant la photosynthèse terrestre sont la température et le rayonnement incident, la disponibilité en nutriments minéraux, et la disponibilité en eau. Elle est donc impactée par l'augmentation des températures qui génère dans l'hémisphère nord un allongement de la saison de croissance (Menzel & Fabian, 1999 ; Penuelas et al. 2002, Lebourgeois et al. 2010). Par ailleurs, l'acidification des sols et les dépôts azotés impactent la disponibilité des nutriments minéraux (Schoenholtz et al. 2000, Peñuelas et al. 2012). Enfin, l'augmentation annoncée de la fréquence des évènements de sécheresse risque de limiter localement la photosynthèse (Sheffield & Wood 2008, Coumou & Rahmstorf, 2012) et d'impacter fortement des écosystèmes sensibles. Ces effets viennent accentuer ou compenser des contraintes géographiques locales, liées à la topographie, aux propriétés des sols, ou à un microclimat.

L'anticipation des conséquences des changements climatiques est d'autant plus complexe que la variabilité des flux de carbone des écosystèmes continentaux - spatiale et temporelle - est forte (Falge et al. 2002, Le Quere et al. 2009) et que la réponse de ces écosystèmes aux contraintes abiotiques sont non-linéaires. Il en découle une nécessité d'améliorer notre compréhension du fonctionnement de la photosynthèse terrestre, de ses limitations, de sa régulation, et de sa sensibilité aux contraintes abiotiques.

La photosynthèse terrestre est en effet particulièrement contrainte par la disponibilité en eau qui limite de manière importante et récurrente la quantité de lumière effectivement utilisable par les plantes, tandis que la quantité de lumière absorbée ne peut pas être régulée sur des échelles de temps courtes. Les réactions de la photosynthèse peuvent être divisées en deux groupes ; les réactions photosensibles qui ont lieux dans la membrane des thylakoïdes, et les réactions « d'obscurité ». Ces deux ensembles de réactions sont limités par des facteurs différents ; principalement par la quantité de lumière absorbée pour les réactions photosensibles, et par les échanges gazeux de CO_2 pour les réactions « d'obscurité ». Ces deux ensembles sont susceptibles de limiter la photosynthèse.

Une partie de la lumière incidente est absorbée par les pigments photosensibles de deux complexes protéiques nommés Photosystème I (PSI) et Photosystème II (PSII) situés dans la

membrane des thylakoïdes, au sein d'organites appelés « chloroplastes », et transmise sous forme d'exciton à leurs molécules de chlorophylle dont le potentiel d'oxydoréduction diminue en conséquence. Cette excitation de molécules de chlorophylle initie une chaine de transfert d'électrons (Figure 1) qui constitue un ensemble de réactions d'oxydo-réduction nommée « réactions photochimiques » de la photosynthèse.

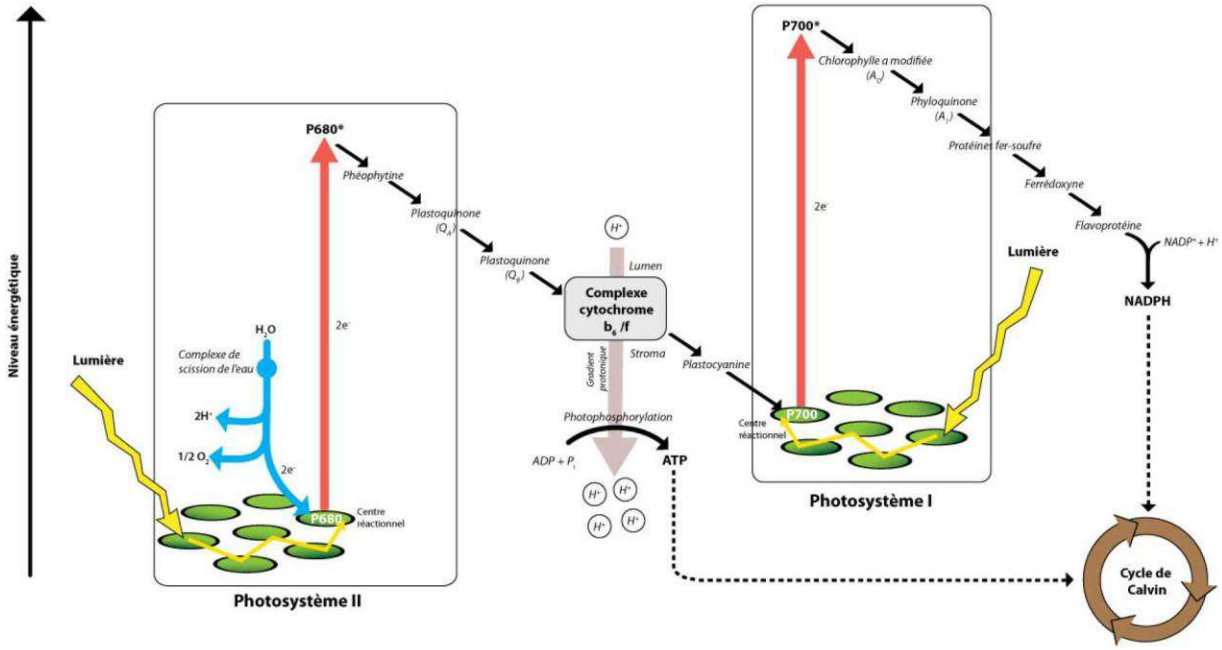

Figure 1 : schéma de la chaine de transfert d'électrons, d'après Raven et al. 2003.

Ce transfert d'électrons s'accompagne d'un stockage d'énergie sous forme chimique, via la réduction d'un coenzyme nommé NADP+ en NADPH et de la formation d'un gradient de protons de part et d'autre de la membrane des thylakoïdes qui fournit l'énergie nécessaire à la phosphorylation d'ADP en ATP par une pompe à protons. Cet ensemble d'échanges d'électrons permet aux cellules chlorophylliennes de convertir via une série de réactions à faible énergie la lumière absorbée en énergie sous forme chimique utilisable par les cellules.

Parallèlement à ces réactions photosensibles se déroulent les « réactions sombres » du cycle de Calvin, qui implique la réduction du CO_2 atmosphérique absorbé par les feuilles via les stomates. Cette réduction est réalisée via la déphosphorylation de l'ATP et l'oxydation du NADPH produits par les réactions photosensibles. Le flux entrant de CO_2 s'accompagne en outre d'un flux sortant d'eau qui dissipe la chaleur générée par ces réactions et par la lumière incidente sous forme de chaleur latente d'évaporation, permettant de maintenir la feuille en deçà des températures à partir desquelles les enzymes impliquées dans ces réactions perdent leur fonctionnalité.

Ce système peut être limité, non seulement par la quantité de rayonnement absorbé, mais également par la capacité du cycle de Calvin à oxyder le NADPH et à dé-phosphoryler l'ATP produits par les réactions photosensibles. Les plantes peuvent donc être soumises à un excédent d'énergie lumineuse absorbée, notamment lorsqu'une perte trop importante en eau est limitée par une fermeture stomatique, qui entraine une baisse de la disponibilité du CO_2. Le flux d'électrons généré par l'appareil photosynthétique est alors susceptible d'entrainer la formation de composés réactifs de l'oxygène qui endommagent l'appareil photosynthétique. Pour lutter contre le stress oxydatif provoqué par un excès de lumière, les plantes ont développé plusieurs mécanismes afin de dissiper l'énergie excédentaire.

- La réémission sous forme de chaleur connue sous le terme de NPQ (non photochemical quenching) par opposition au quenching photochimique par la voie de la photosynthèse.
- La réémission sous forme de fluorescence chlorophyllienne.

Les trois voies de gestion du rayonnement absorbé (photosynthèse, NPQ et fluorescence) sont en compétition (Baker, 2008) et le flux d'électrons est, en cas d'excès, activement dirigé vers l'une des deux voies de « quenching ». Le rendement de conversion de l'énergie lumineuse absorbée par les végétaux est donc particulièrement dynamique, et est tributaire de la quantité d'énergie incidente et de l'état hydrique des plantes.

Ce rendement de conversion peut être exprimé en fonction de différentes ressources, notamment en fonction de la quantité d'eau utilisée et transpirée par la plante (Water Use Efficiency ou WUE), ou en fonction de la quantité d'énergie lumineuse absorbée par la plante (Light Use Efficiency ou LUE ou aussi Radiation Use Efficiency ou RUE qui correspond au rendement d'utilisation de la lumière absorbée). De nombreux travaux ont porté sur la compréhension et l'estimation du LUE, des échelles fines (cellulaires) aux échelles larges (satellitaires). Le LUE, défini par Monteith & Moss, 1997 comme étant la production de biomasse carbonée (GPP, gross primary production) par unité de rayonnement absorbé (aPAR), a dans un premier temps été utilisé à des échelles temporelles larges pour décrire le rendement maximum de la photosynthèse de cultures en conditions optimales (Muchow et al. 1990). Le LUE était alors estimé comme étant la pente d'une relation linéaire entre la productivité de matière sèche par surface de culture et le rayonnement incident ou intercepté cumulé sur la même période, ou d'une relation linéaire entre productivité de matière sèche cumulée et rayonnement cumulé à intervalle de temps régulier (Kemanian et al. 2004). Outre les faiblesses méthodologiques liées à l'usage de variables cumulées (Spitters et al. 1990,

Mallet et al. 1997), la pertinence d'une relation linéaire entre productivité primaire et rayonnement incident a été plusieurs fois remise en question (Demetriades-Shah et al. 1992) et l'accent a été mis sur la variabilité du LUE à différentes échelles (Arkebauer et al. 1994). La qualité des relations linéaires entre productivité primaire et rayonnement intercepté se dégrade en effet pour les échelles temporelles les plus larges (inter-annuelles) du fait de l'accumulation de sources de variabilité indépendantes du PAR, et aux échelles de temps les plus fines du fait de l'apparition de comportements non-linéaires (Figure 2).

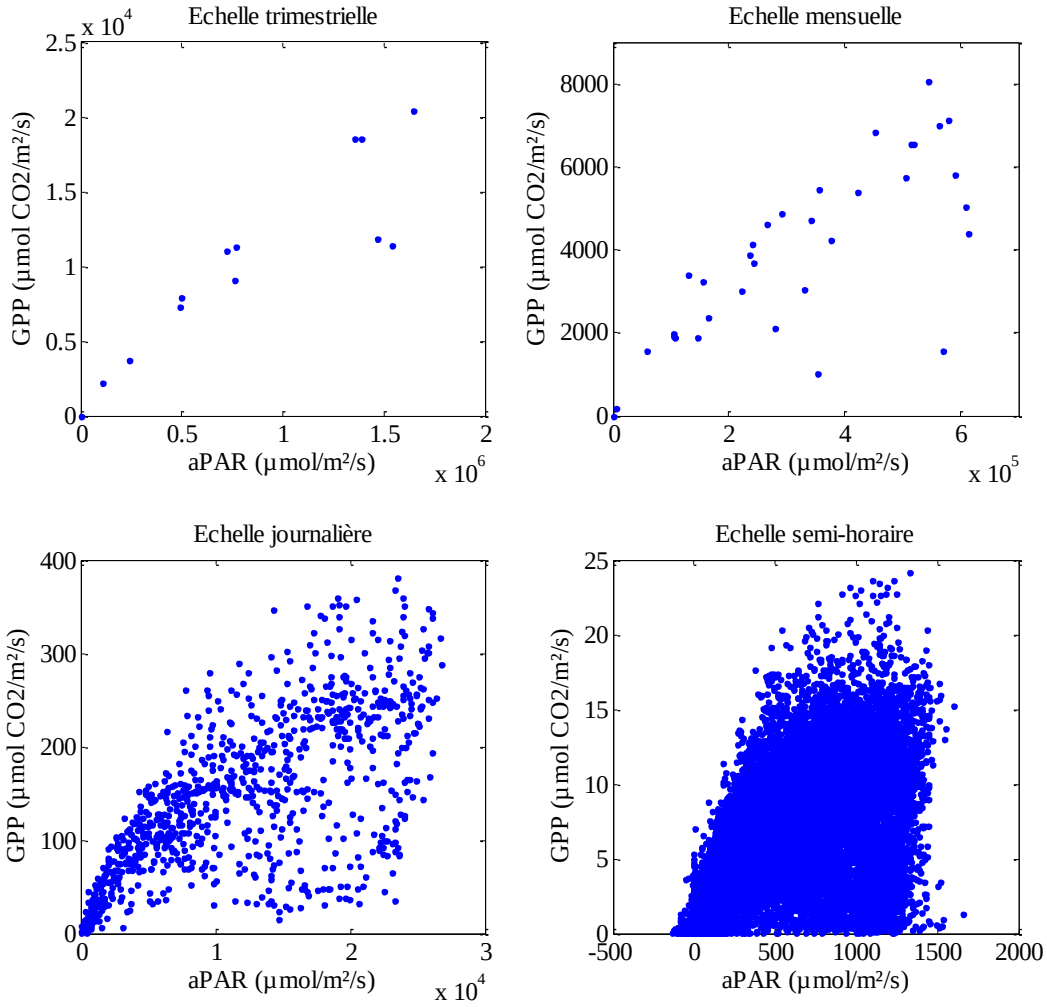

Figure 2 : Relations entre productivité primaire (GPP) et rayonnement absorbé (aPAR) sur le site de Puéchabon et sur 2 années. Les deux variables d'intérêt ont été cumulées sur l'ensemble de la série temporelle, puis cumulées à des échelles de temps variables : trimestrielle, mensuelle, journalière et semi-horaire.

Le LUE montre en effet une très forte variabilité temporelle, et constitue un proxy pertinent permettant de décrire finement l'effet de contraintes environnementale sur la photosynthèse aux échelles de temps fines. Il est la principale variable expliquant la baisse de la GPP en réponse aux évènements climatiques (Garbulsky et al. 2011) et reflète donc à la fois la régulation et la limitation de la photosynthèse. La compréhension de sa variabilité spatiale et temporelle aux échelles fines permettrait donc d'améliorer significativement l'estimation de la productivité des écosystèmes terrestres.

Un premier pas dans ce sens a été réalisé avec la mise en place du réseau de mesure de flux d'eau et de CO_2 (FLUXNET, Baldocchi et al. 2001). Ce réseau de 500 sites permet de mesurer localement avec une résolution temporelle fine (semi-horaire) ces flux de carbone. Chaque site est équipé d'un système de mesure de flux de CO_2 par eddy-covariance et y associe des mesures de flux d'eau, d'énergie, et climatiques. Les mesures de flux de carbone et d'eau ainsi obtenues ont une représentativité limitée à une zone d'un km² et ne peuvent pas être extrapolées à l'échelle de biomes du fait d'un sous-échantillonnage au sein d'écosystèmes clefs (Jung et al. 2009) et de l'importance de l'hétérogénéité spatiale à des échelles bien inférieures à la maille du réseau FLUXNET. De même, les relations empiriques entre mesures locales de flux et variables climatiques ne peuvent pas être systématiquement appliquées à des mesures globales, ou à des prédictions climatiques. Elles n'ont donc pas la portée prédictive nécessaire pour nous renseigner sur l'impact présent ou futur des changements climatiques.

Ce dispositif permet néanmoins de décrire le fonctionnement d'écosystèmes variés via l'étude des relations entre ces flux et des variables climatiques. La description et la mise en équations des mécanismes physiques et biologiques en jeu permettent de concevoir et de calibrer des modèles mécanistes qui nous renseignent sur le fonctionnement d'écosystèmes à des échelles fines (Hanson et al. 2004), tout en ayant une portée prédictive. Ces modèles mécanistes sont cependant basés sur des hypothèses et des approximations dont le choix relève d'un compromis entre réalisme et complexité du modèle. La complexité du modèle est contrainte non seulement par nos moyens de calculs mais également par l'accès aux variables nécessaires à sa calibration. Ce compromis limite dans les faits le potentiel prédictif d'un modèle aux situations ou scénarios pour lesquels ses hypothèses de base et approximations sont valides. En conséquence, les approches de modélisation mécanistes sont multiples, et répondent à des objectifs variés.

On peut ainsi distinguer :

- Des modèles destinés à la modélisation fine de couverts végétaux à l'échelle de la parcelle, tels que CASTANEA (Dufrene et al. 2005), qui sont capables de décrire avec précision le fonctionnement écophysiologique d'une canopée, au prix d'une initialisation et d'une calibration nécessitant une description précise de sa structure et de son état. De tels modèles permettent de reproduire fidèlement et à une résolution temporelle fine les effets non-linéaires de contraintes abiotiques sur le fonctionnement des végétaux. Cependant, leur généralisation à des échelles spatiales supérieures n'est possible qu'au prix d'hypothèses fortes qui dégradent sensiblement cette fidélité ou cette résolution temporelle.
- Des modèles destinés à la modélisation à une échelle régionale ou globale, tels que les modèles ORCHIDEE (Krinner et al. 2005), et BIOME-BCG (White et al. 2000), qui modélisent un comportement moyen par type fonctionnel de végétation. En outre, les écosystèmes sont représentés comme étant des systèmes à l'équilibre avec leur environnement, et subissant des perturbations, ce qui a pour effet de simplifier considérablement l'initialisation de ces modèles. En conséquence, ces approches reproduisent efficacement un comportement moyen à des échelles spatiales et temporelles larges, mais ne permettent pas de décrire finement le fonctionnement écophysiologique des peuplements.

Si cette multiplicité d'approches recouvre effectivement une large gamme de résolutions spatiales et temporelles, le compromis entre complexité et facilité d'initialisation du modèle ne permet pas en l'état une bonne prise en compte de la variabilité spatiale de la structure et de l'état des couverts végétaux. Une première réponse à ce problème a été le recours à des données obtenues par télédétection en vue de décrire de façon spatialisée la structure des couverts végétaux. La mesure de la réflectance (ratio du rayonnement réfléchi au rayonnement incident en fonction de la longueur d'onde) des couverts végétaux apporte en effet des informations sur leur structure (Verstraete et al. 1996), et leur composition biochimique (Sims & Gamon 2002) tel qu'illustré dans la figure 3.

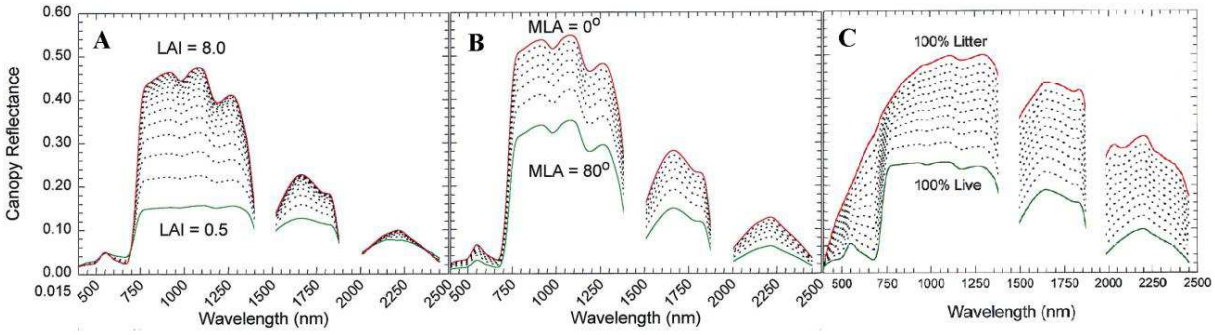

Figure 3 : Impact des propriétés structurales et biochimiques des couverts végétaux sur leur spectre en réflectance (d'après Asner, 1998). 3.A : effet de la variabilité du LAI (indice foliaire) sur la réflectance d'un couvert végétal, pour un angle foliaire de 45°. 3.B : effet de la variabilité de l'angle foliaire sur la réflectance d'un couvert végétal, pour un LAI de 5. 3.C : effet de la fraction de litière (feuilles sèches) sur la réflectance d'un couvert herbacé, pour un LAI (leaf area index – indice foliaire) de 2 m² de surface foliaire/m² du sol et un angle foliaire moyen de 60°.

Cette figure illustre les variations de réflectance de couverts végétaux associées à des variations de densité du couvert (LAI, « Leaf Area Index » ou surface de feuilles par surface au sol en mètre carré par mètre carré), de structure du couvert (MLA ou angle foliaire moyen), ou d'état du couvert. Il est donc possible à partir de mesures de réflectance de décrire et de suivre la structure et l'état phénologique des couverts végétaux. Ce type de mesure optique revêt un intérêt d'autant plus important qu'il est réalisable dans une très large gamme de résolutions temporelles (de la micro-seconde à l'année) et spatiale (de l'échelle de la feuille à l'échelle du peuplement).

A ce jour, les mesures de réflectances sont principalement utilisées sous la forme d'indices spectraux, conçus de façon à refléter la variabilité de la réflectance dans une bande de longueur d'onde donnée tout en minimisant les effets de la variabilité de facteurs exogènes tels que la contribution du sol, la géométrie de visée et les conditions atmosphériques. Ces indices sont construits de façon à rapporter la réflectance dans une bande fortement impactée par le phénomène d'intérêt (Figure 3) à la réflectance dans une bande de référence, peu impactée par ce phénomène. Différents schémas de constructions ont été développés de façon à minimiser les erreurs additives (via une différence entre une bande de référence et la bande d'intérêt), et les erreurs multiplicatives telles que les effets angulaires de visée ou d'éclairement via le calcul de ratio. Différents indices spectraux sont listés en Table 1.

Phénomène d'intérêt	Ratios simples	Différences normalisées	Autres
LAI, fAPAR	$SR = \frac{\rho_{NIR}}{\rho_{red}}$	$NDVI = \frac{(\rho_{NIR} - \rho_{red})}{(\rho_{NIR} + \rho_{red})}$	$EVI = \frac{2.5 \times (\rho_{NIR} - \rho_{red})}{(\rho_{NIR} + 6 \times \rho_{red} - 7.5 \times \rho_{blue} + 1)}$
Contenu en Chlorophylle	$SR_{680} = \frac{\rho_{800}}{\rho_{680}}$ $SR_{705} = \frac{\rho_{750}}{\rho_{705}}$	$ND_{680} = \frac{(\rho_{800} - \rho_{680})}{(\rho_{800} + \rho_{680})}$ $ND_{705} = \frac{(\rho_{750} - \rho_{705})}{(\rho_{750} + \rho_{705})}$ $mSR_{705} = \frac{(\rho_{750} - \rho_{445})}{(\rho_{705} + \rho_{445})}$	$mND_{705} = \frac{(\rho_{750} - \rho_{705})}{(\rho_{750} + \rho_{705} - 2 \times \rho_{445})}$
Caroténoïdes/Chlorophylle		$PRI = \frac{(\rho_{531} - \rho_{570})}{(\rho_{531} + \rho_{570})}$	$SIPI = \frac{(\rho_{800} - \rho_{445})}{(\rho_{800} + \rho_{680})}$ $ND_{705} = \frac{(\rho_{680} - \rho_{500})}{(\rho_{750})}$

Table 1 : Indices spectraux en tant qu'indicateurs de la structure ou de la composition biochimique des couverts végétaux (d'après Huete et al. 1994 et Sims & Gamon 2002). SR – Simple Ratio ; NDVI – Normalised Difference Vegetation Index ; EVI Enhanced Vegetation Index ; ND Normalised Difference ; mSR, mND modified Simple Ratio and modified Normalised ; PRI – Photochemical Reflectance Index ; SIPI Structural Independent Pigment Index.

Les indices de végétations les plus utilisés (NDVI et EVI) le sont pour décrire la structure des couverts végétaux en relation avec l'indice foliaire (LAI) ou avec la fraction du rayonnement utile à la photosynthèse absorbé ou intercepté (PAR – Photosynthetically Active Radiation) (Soudani et al. 2006).

Le lancement de plate-formes satellitaires équipées de capteurs passifs tels qu'AVHRR (Advanced Very High Resolution Radiometer, Reed et al. 1994), puis MODIS (Moderate Resolution Imaging Spectroradiometer, Zhang et al. 2003) a permis de quantifier à l'échelle globale et avec une résolution spatiale kilométrique et temporelle infra-journalière la quantité de lumière réfléchie par les couverts végétaux dans des bandes de longueur d'onde préalablement définies pour estimer certaines variables biophysiques clés (PAR absorbé, LAI, albédo, taux de couverture, etc.). Une illustration du positionnement de certaines bandes MODIS sur le spectre de réflectance d'un couvert végétal est donnée dans la Figure 4.

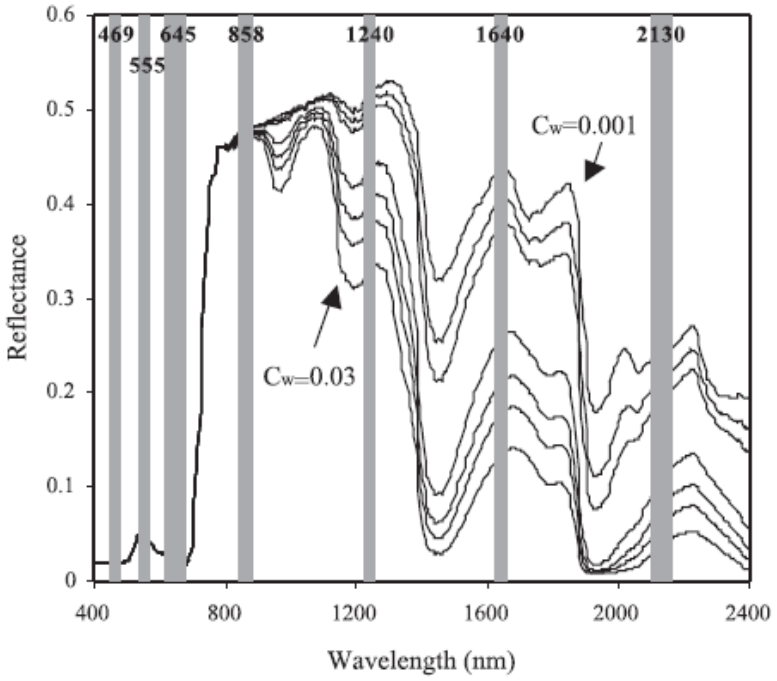

Figure 4 : Localisation des principales bandes spectrales MODIS superposées sur des spectres de réflectance simulés de couverts végétaux pour des contenus en eau différents à l'aide du modèle PROSPECT-SAILH (d'après Zarco-Tejada et al. 2003).

La structure des couverts végétaux peut ainsi être décrite avec une résolution spatiale approchant 250 m avec MODIS et une résolution temporelle journalière, et être utilisée pour paramétrer, forcer ou valider des modèles mécanistes. Cette approche a en effet permis de mieux représenter la variabilité spatiale et temporelle des flux de carbone (Demarty et al. 2007, Maselli et al. 2009). Si ces approches de télédétection permettent de façon relativement directe de spatialiser la structure et la phénologie des couverts végétaux, la variabilité spatiale de leurs réponses aux facteurs abiotiques reste un problème récurrent et est une source majeure d'erreurs d'estimation des flux de carbone à l'échelle globale (Jung et al. 2007, Turner et al. 2006, Anav et al. 2010).

En effet, les travaux de télédétection de la végétation se sont principalement intéressés à l'estimation de certaines variables qui caractérisent ses propriétés structurales et biochimiques mais peu de travaux se sont intéressés à la caractérisation de son fonctionnement écophysiologique carboné et hydrique. Toutes les approches par télédétection qui s'intéressent au fonctionnement des couverts végétaux utilisent le concept de LUE en tant que proxy permettant de tenir compte de la réponse photosynthétique aux contraintes abiotiques. Dans le but d'estimer la GPP à l'échelle du globe par télédétection, l'usage d'indices spectraux initialement définis pour estimer la densité des couverts végétaux, tels que

le NDVI ou l'EVI (Table 1) s'est avéré peu efficace en l'absence de stress hydrique sévère (Myneni et al. 1995). Ces indices spectraux rendent compte de variations de biomasse chlorophyllienne et sont corrélés à la fraction du PAR absorbée. S'ils permettent effectivement de détecter les stress hydriques et azotés intenses, ils ne permettent pas de suivre des changements fins de rendement photosynthétique. Le rendement de la photosynthèse est en effet particulièrement variable ; il est finement régulé et baisse de façon très rapide en présence d'un excès de lumière.

L'exposition de la feuille à un excès de lumière génère la formation d'un fort gradient de protons de part et d'autre de la membrane des thylakoïdes. Ceci stimule la désépoxydation d'un pigment xanthophylle, la violaxanthine, en anthéraxanthine, puis en zéaxanthine (Yamamoto 1979, Pfundel and Bilger, 1994, Demmig-Adams & Adams, 1996) comme illustré dans la figure 5.

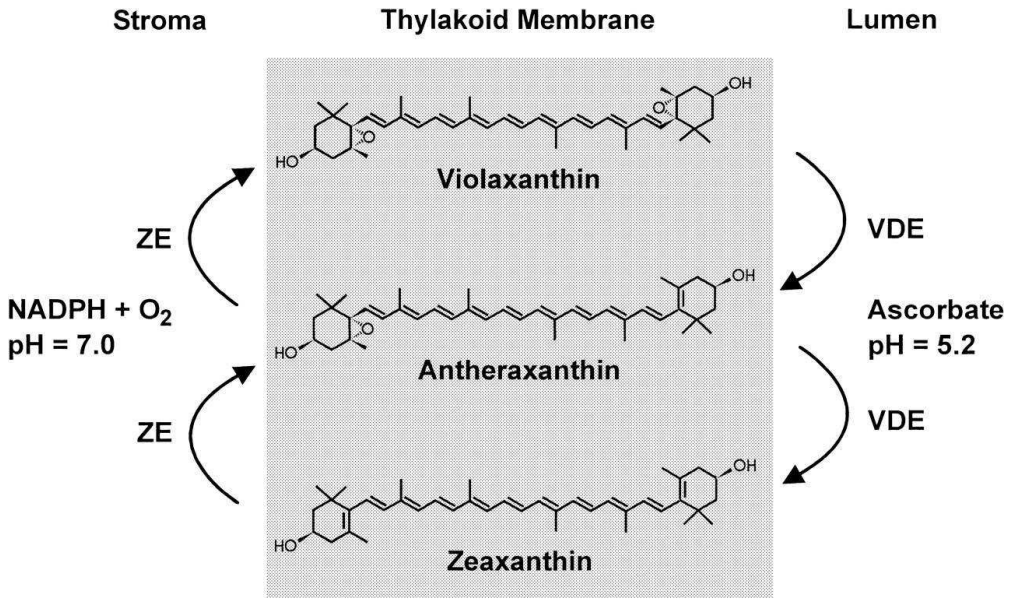

Figure 5 : schéma du fonctionnement du cycle xanthophylle, d'après Hieber et al. 2004.

Outre ses propriétés photoprotectrices, la zéaxanthine agit sur la sensibilité de l'antenne collectrice du photosystème II au pH, et le taux de dé-époxidation du pool de pigments xanthophylles est enfin positivement corrélé au NPQ (Johnson et al. 2008). Deux principaux mécanismes expliquant ce lien entre l'état du cycle xanthophylle et le quenching sont actuellement proposés ;

- une action directe de la zéaxanthine via sa capacité à intercepter les excitons de molécules de chlorophylle excitées et à les dissiper sous forme de chaleur.

- Une action indirecte via une différence de conformation entre violaxanthine et zéaxanthine ayant un effet sur la conformation de la membrane des thylakoïdes, réduisant ainsi les interactions entre les éléments du PSII.

Ce cycle xanthophylle (Figures 5 et 6) a été pointé comme étant « l'interrupteur » des mécanismes de photoprotection de l'appareil photosynthétique (Ruban et al. 2012) et est nécessaire à la régulation de la dissipation d'un excédent d'énergie (Bonente et al. 2008). Il répond aux variations d'aPAR à l'échelle de quelques minutes et est lentement réversible à l'obscurité. La proportion de l'énergie absorbée par l'appareil photosynthétique et ensuite dissipée via la fluorescence et le NPQ est de 2 à 12% et de 14 à 88% respectivement lors d'une transition ombre/lumière (Rosema et al. 1991).

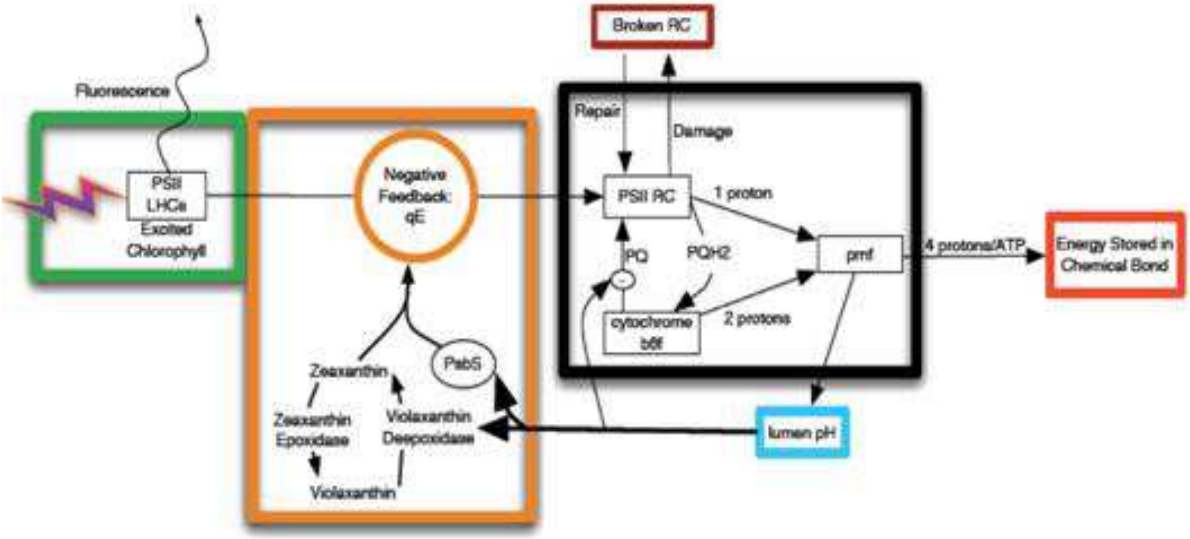

Figure 6 : schéma de la boucle de régulation de l'appareil photosynthétique mettant en jeu le cycle xanthophylle. Le flux d'électron au sein de l'appareil photosynthétique (de l'antenne collectrice LHC du PSII aux cytochromes) génère la formation d'un gradient de pH. Ce gradient de pH stimule le cycle xanthophylle, qui y sensibilise le PSII, entrainant un contrôle négatif sur le flux d'électrons. Ce flux d'électrons est en conséquence redirigé vers la fluorescence et la dissipation thermique.

En outre, l'action de ce cycle xanthophylle s'accompagne d'un changement d'absorbance de la feuille à une longueur d'onde de 505 nm, et d'un changement de réflectance foliaire à environ 531 nm (Figure 7) mis en évidence par John Gamon (Gamon et al. 1990). Cette relation revêt un intérêt particulier du fait du rôle central que ce cycle xanthophylle joue au sein du système de régulation du rendement de la photosynthèse.

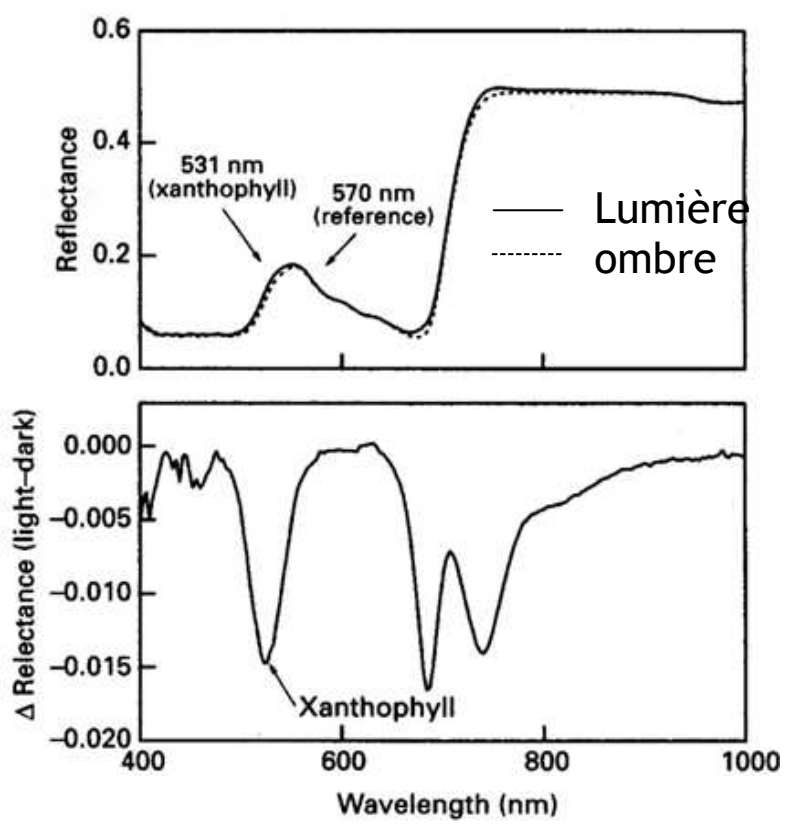

Figure 7 : Réflectance et variabilité de la réflectance d'une feuille soumise à une variation brutale de la lumière incidente, d'après Gamon et al. 1990.

Cette observation a donc permis le développement d'un indice optique, le photochemical reflectance index (PRI) (Table 1), corrélé chez de nombreuses espèces avec le rendement du PSII mesuré par analyse de la fluorescence, et le LUE (Gamon et al. 1992, Gamon et al. 1997, Gamon et al. 1999, Stylinsky et al. 2002).

Des efforts conséquents ont été déployés pour évaluer cette approche de l'échelle de la feuille (Gamon et al. 1990, 1992, 1997, Penuelas et al. 1995, Stylinski et al. 2002) à celle de l'écosystème (Nichol et al. 2000, Asner et al. 2004, Drolet et al. 2005, Goerner et al. 2009). Les principaux résultats obtenus et analysés dans Garbulsky et al. (2011) mettent en évidence l'impossibilité d'utiliser directement les mesures de PRI en tant que proxy du LUE. Il a été montré que le signal PRI est sensible à la structure des couverts végétaux, dont la variabilité spatiale et temporelle est susceptible d'affecter sa réponse au PAR et aux stress (Barton et al. 2001, Hall et al. 2008, Hilker et al. 2009, 2009b). En outre, le PRI est fortement impacté par la composition en pigments des feuilles (Moran et al. 2000, Gamon et al. 2001, Sims et al. 2002, Filella et al. 2004, Nakaji et al. 2006). Cette dépendance à la composition biochimique des feuilles est évoquée en tant que l'origine du lien potentiel entre PRI et LUE à l'échelle saisonnière (Garbulsky et al. 2011), mais n'impacte pas nécessairement de la même façon ces

deux variables, et peut être espèce-dépendante. Le PRI est donc un signal composite particulièrement difficile à interpréter. Malgré son usage croissant à des échelles variées, les relations observées entre PRI et LUE ainsi que leur variabilité restent en grande partie inexpliquées. Une bonne compréhension de la variabilité du PRI est néanmoins nécessaire pour juger de la pertinence des mesures à haute résolution spatiale et faible résolution temporelle dont l'usage connait actuellement un essor important (Zarco-Tejada et al. 2009, 2011, Suarez 2009).

L'objectif principal de ce travail est d'évaluer et de comprendre les relations entre le PRI et le fonctionnement écophysiologique, carboné et hydrique, des couverts végétaux. Plus précisément, les objectifs sont :

- Décrire et expliquer la variabilité temporelle du PRI en la reliant aux contraintes climatiques, aux propriétés structurales, et au fonctionnement écophysiologique des couverts végétaux.
- Evaluer l'intérêt du PRI en tant qu'indicateur du fonctionnement carboné et hydrique à différentes échelles, de la feuille aux peuplements adultes, en conditions naturelles en passant par la mise en place de mesures en conditions semi-contrôlées.
- Evaluer le potentiel de la télédétection satellitaire pour l'estimation du LUE aux échelles larges.

Afin d'aborder ces questions, trois approches ont été utilisées :

- Des approches expérimentales, basées sur le suivi des propriétés écophysiologiques et spectrales de jeunes peuplements de chêne (*Quercus robur* L.), de hêtre (*Fagus sylvatica* L.) et de pin (*Pinus sylvestris* L.) soumis à deux régimes hydriques différents via une exclusion de pluie.
- Des approches de télédétection rapprochée reposant sur l'analyse de mesures de PRI *in situ* sur des peuplements matures de chêne sessile (Fontainebleau) et de chêne vert (Puéchabon) et de télédétection satellitaire reposant sur des séries temporelles NDVI et PRI utilisant les bandes MODIS sur les mêmes peuplements.
- Des approches de modélisation, via l'usage d'un modèle écophysiologique mécaniste à l'échelle de la parcelle, CASTANEA, en tant qu'outil pour décrire finement le fonctionnement écophysiologique des deux peuplements étudiés précédemment et en tant qu'outil aidant à la compréhension de la variabilité temporelle du signal PRI *in situ* observée. Les sorties du modèle CASTANEA préalablement calibré et validé ont

été mises en relation avec les mesures *in situ* du PRI de façon à investiguer son potentiel en tant que proxy du LUE à l'échelle de ces deux peuplements adultes.

Le manuscrit est organisé en 6 chapitres, chaque chapitre constituant un article soumis ou sous forme finale.

Le premier chapitre est basé sur une approche expérimentale à l'échelle de la feuille visant à décrire la variabilité saisonnière et à court-terme du PRI, et à la relier à des paramètres biochimiques et écophysiologiques. Il a abouti à une déconvolution des sources de variabilité du PRI à l'échelle de la feuille, et a fait l'objet d'un article publié dans Plant, Cell and Environment (Hmimina et al. 2013b).

Le second chapitre, basé sur une approche expérimentale et de modélisation empirique, dérive des résultats précédents une méthode de déconvolution du signal PRI à l'échelle de jeunes canopées, isole les sources de variabilité du PRI, et examine leur impact sur l'intérêt du PRI en tant que proxy du LUE. Il a fait l'objet d'un article soumis au journal Plant, Cell and Environment (Hmimina et al. soumis).

Le troisième chapitre, basé sur une approche de télédétection in situ, examine la variabilité du PRI mesuré sur deux peuplements forestiers adultes en conditions naturelles et identifie les principaux facteurs influençant les relations entre PRI et LUE. Il a fait l'objet d'un article soumis au journal Remote Sensing of Environment (Soudani et al. soumis).

Le quatrième chapitre, basé sur une approche de télédétection rapprochée couplée à une approche de modélisation mécaniste examine le lien entre PRI et fonctionnement écophysiologique des deux peuplements adultes citées précédemment. La relation entre PRI et LUE y est examinée à la lumière de variables écophysiologiques prédites par le modèle CASTANEA, afin de déterminer les limites de l'usage du PRI en tant que proxy du LUE à l'échelle de peuplement.

En raison du rôle important joué par la dynamique temporelle de la surface foliaire sur le signal PRI rendant son interprétation particulièrement très difficile lorsqu'il est mesuré par télédétection satellitaire, le cinquième chapitre évalue le potentiel de l'instrument satellitaire MODIS pour suivre la dynamique saisonnière de la structure des couverts végétaux dans différents biomes. Les mesures satellitaires MODIS sont comparées à des mesures *in situ* de manière à estimer leur précision, et la résolution temporelle maximale pouvant être obtenue. Ce travail a fait l'objet d'un article publié dans Remote Sensing of Environment (Hmimina et al. 2013a).

Chapitre 1. Relationship between PRI and leaf ecophysiological and biochemical parameters under two different water statuses: toward a rapid and efficient correction method using real-time measurements

Hmimina G.[a]; Dufrêne E.[b]; Soudani K.[a]

[a] Univ. Paris-Sud, Laboratoire Ecologie Systématique et Evolution, UMR8079, F-91405 CNRS, Orsay, France

[b] CNRS, Laboratoire Ecologie Systématique et Evolution, UMR8079, F-91405, Orsay, France

Abstract

The use of the photochemical reflectance index (PRI) as a promising proxy of LUE has been extensively studied, and some issues have been identified, notably the sensitivity of PRI to leaf pigment composition and the variability in PRI response to LUE due to stress. In this study, we introduce a method that enables us to track the short-term PRI response to LUE changes due to photosynthetically active radiation (PAR) changes. The analysis of these short-term relationships between PRI and LUE throughout the growing season in two species (Quercus robur L. and Fagus sylvatica L.) under two different soil water statuses showed a clear change in PRI response to LUE, which is related to leaf pigment content. The use of an estimated or approximated PRI_0, defined as the PRI of perfectly dark-adapted leaves, allowed us to separate the PRI variability due to leaf pigment-content changes and the physiologically related PRI variability over both daily (PAR-related) and seasonal (soil water content-related) scales. The corrected PRI obtained by subtracting PRI_0 from the PRI measurements showed a good correlation with the LUE over both of the species, soil water statuses and over the entire growing season.

1. Introduction

The terrestrial biosphere is one of the main components of the carbon cycle and is very sensitive to abiotic stresses. Climate change is expected to increase the frequency and intensity of drought events and will have a considerable impact on carbon and water budgets (Sheffield & Wood 2008). Understanding carbon and water fluxes, which exhibit wide spatial and temporal variability (Falge et al. 2002; Le Quere et al. 2009), is of considerable importance and is a subject of increasing interest. The direct measurement of carbon and water fluxes between the biosphere and the atmosphere is currently possible only locally using the eddy-covariance method. Over 500 tower sites from approximately thirty regional networks across five continents and covering the majority of terrestrial biomes, with different spatial densities and organized within the global network FLUXNET are used to track the temporal dynamics of carbon and water fluxes at an intra-daily scale **(**Baldocchi et al. 2001**).** Nevertheless, the acquired data is still insufficient to accurately describe the functioning of the biosphere and the global carbon exchange due to the great diversity of ecosystems and the wide range of variability of ecosystem structure, physiological functioning and environmental abiotic and biotic factors.

Remote sensing is considered to be an alternative method of estimating carbon fluxes and stocks on large scales while allowing for the consideration of the great diversity and spatial heterogeneity of terrestrial vegetation. Since 2000, the approach built around the MODIS project has provided maps of gross primary production (GPP) and annual net primary production (NPP) across the globe with an eight-day time step (for GPP) and a spatial resolution of 1 km². In this approach, MODIS daily imagery is used to derive the land cover, the fraction of absorbed photosynthetically active radiation (PAR),the leaf area index (LAI) and, based on the concept of light-use efficiency (LUE) developed by Monteith (Monteith and Moss, 1977), estimates of the GPP at the global scale. Data are available from February 2000 to the present. LUE is highly variable and sensitive to abiotic stress factors, and LUE is notably one of the main factors of the variation of GPP in response to climatic events (Garbulsky et al. 2011).Currently, this variability is accounted for by considering a daily biome-specific maximum LUE value, which is then downscaled according to the modeled daily minimum temperature and vapor pressure deficit (VPD), as described by Running et al. (2000). MODIS GPP and NPP values are validated across different biomes by comparison with eddy covariance measurements (Heinsch et al. 2006; Coops et al. 2007), and the

estimation of LUE is known to be a major source of uncertainty (Gebremichael and Barros, 2006; Turner et al. 2006).

At the leaf scale, the most widely used technique to measure LUE is analyzing chlorophyll fluorescence based on modulated fluorescence using the saturation pulse method (Maxwell et al. 2000).Fluorescence, photosynthesis (photochemistry) and heat dissipation are the three pathways of transformation of absorbed solar energy conducted by leaves. In natural conditions under actinic light, measurements of variable fluorescence (usually named F_s or F_v) and the maximum fluorescence under a saturating light pulse of a light-adapted leaf (F_m') enable an accurate estimate of the proportion of photons used in the PSII centers in chloroplast thylakoids according to the Genty parameter or the quantum yield of PSII photochemistry (Genty et al. 1989).Because the quantum yield of PSII is directly related to the quantum yield of CO_2 fixation in the absence of photorespiration (Baker, 2008), this parameter provides an accurate estimation of the LUE. Satellite-based measurements of solar-induced chlorophyll fluorescence are technically and methodologically challenging mainly because the fluorescence intensity of chlorophyll is very weak, i.e., approximately 1 to 2% of the absorbed radiation (Maxwell and Johnson, 2000), and is strongly affected by atmospheric absorption. Recent works (Rascher et al. 2009; Guanter et al. 2012) showed that the retrieval of sun-induced chlorophyll variable fluorescence (F_s) might be feasible but remains challenging. Moreover, satellite-based F_s measurements provide information about canopy photosynthetic activity, which depends on both LUE and other parameters, such as the leaf area index, chlorophyll concentration and light conditions, among other factors. Hence, F_s needs to be standardized using a reference, such as F_m'.

Spectral vegetation indices based on reflected radiation, such as the enhanced vegetation index (EVI) and the normalized difference vegetation index (NDVI), are ineffective in the absence of severe water stress (Myneni et al. 1995). These indices report changes in chlorophyll biomass but are not able to track changes of photosynthetic efficiency over short timescales. Other spectral indices, particularly the photochemical reflectance index (PRI), which uses reflectance measured at 531 nm, have proven to be effective to track the LUE of different species and under different conditions at both the leaf and canopy scales. Indeed, a change in leaf reflectance at 531 nm related to the state of epoxidation of the violaxanthin-antheraxanthin-zeaxanthin cycle has been shown (Gamon et al. 1990). The epoxidation state of the xanthophyll-cycle pigments is caused by excess light energy and allows the dissipation of this excess energy as heat (Yamamoto, 1979; Schreiber and Bilger, 1993; Pfündel and Bilger, 1994). This mechanism responds to changes in absorbed PAR over

short time scales of a few minutes and is slowly reversible in darkness (Jahns, 1995; Hartel et al. 1996; Nikens et al. 2010). At the leaf scale, the PRI has proven to be an accurate estimate of the quantum yield of PSII, as measured by fluorescence analysis, and LUE (Gamon et al. 1990; Gamon et al. 1992; Penuelas et al. 1995; Gamon et al. 1997; Stylinski et al. 2002). The first works of Gamon et al. opened the way for the assessment of the photosynthetic LUE from space.

Over the past ten years, considerable effort has been made to evaluate the potential use of PRI as a proxy of LUE based on *in situ* and satellite-based measurements (Nichol et al. 2000; Asner et al. 2004; Drolet et al. 2005; Goerner et al. 2009; Penuelas et al. 2011). At the canopy scale, the results are contrasting. The PRI versus LUE relationship was shown to be site-dependent (Garbulsky et al. 2011) and exhibited variability over the seasonal scale (Soudani et al. submitted). To explain this variability in the PRI response to LUE, many studies have focused on the PRI sensitivity to the proportions of sunlit and shaded leaves in the canopy, which depend on the 3D canopy structure and sun-view geometry (Barton et al. 2001; Hall et al. 2008; Hilker et al. 2008; Hilker et al. 2009; Hilker et al. 2010). Recently, the PRI sensitivity to leaf pigment content (Moran et al. 2000; Gamon et al. 2001; Sims et al. 2002; Filella et al. 2004; Nakaji et al. 2006), which was first shown to play a role in PRI response to LUE changes at seasonal scales (Garbulsky et al. 2011), was shown to introduce variability in PRI response to LUE at the leaf scale (Rahimzadeh-Bajgiran et al. 2012).Moreover, it was recently shown based on PRI kinetics following a dark to light transition (Gamon and Berry. 2012) that PRI variability could be separated in two components: a facultative component linked to leaf physiological response to light, and a constitutive component which was unrelated to the xanthophyll cycle.

Thus, PRI is a composite signal depending on the physical, chemical and physiological properties of leaves and canopies, and its variability is particularly difficult to interpret. A good understanding of this variability is necessary to judge the relevance of using PRI measurements as a proxy for LUE at the canopy scale, especially under different sun-view configurations and/or coarse temporal resolutions, which are extensively used based on satellite data (Drolet et al. 2005; Drolet et al. 2008; Goerner et al. 2009; Moreno et al. 2012) or aircraft remote sensing (Zarco-Tejada et al. 2005; Zarco-Tejada et al. 2012; Suárez et al. 2008; Suárez et al. 2010). The use of the PRI as a proxy for LUE is not directly feasible and requires further study. The most challenging issue at hand is the deconvolution of the different sources of variability in PRI versus LUE relationships mentioned above. The development of methods to disentangle the seasonal variability due to changes in leaf pigment content from

the variability due to climatic and edaphic constraints, which are related to the LUE, is particularly necessary.

In this study, we examine the temporal variability of the relations between PRI, fluorescence and the carbon assimilation at the leaf scale and throughout the season in two temperate deciduous tree species under two soil-moisture treatments. More precisely, this study was designed with the following aims: i) To assess PRI responses to PAR variations depending on the species and soil water status; ii) To assess the relationships between PRI and LUE; and iii) To attempt to disentangle the effects of seasonal variations of leaf biochemical properties on PRI vs. LUE relationships.

2. Materials and Methods

2.1. Plant materials and growth conditions

Two hundred saplings of oak (*Quercus robur* L.) and beech (*Fagus sylvatica* L.) that were three years old were divided into two groups of one hundred individuals each. For each species, the saplings were previously selected to have comparable sizes (approximately 45 to 60 cm for the oaks and 40 to 55 cm for the beeches). The saplings were planted in February 2011 in four planter boxes (50 individuals each), with two planter boxes for each species corresponding to the two soil water statuses. The planter boxes were 2 x 2 x 0.5 m each and were installed outside.

In the four planter boxes, the soil was identical and was composed of a mixture of 2/3 compost and 1/3 sand. The bottom of the planter box was permeable, and two drains were installed in each of the two planter boxes that were submitted to the drought treatment to facilitate drainage. With the aim of causing drought, the two planter boxes were also covered with clear plastic tarps only during rain events. The goal of this experiment was not to completely exclude rain, which may lead to a severe drought and therefore premature senescence and shedding of leaves, but to produce two contrasted conditions of soil moisture between the control and the treated plot. Therefore, the soil moisture in both the stands was controlled by watering.

2.2. Measurements at the canopy and leaf scales, and statistical analysis

2.2.1. Canopy scale and soil moisture measurements

The four planter boxes were topped by an arch-shaped greenhouse structure with a top height of 4.5 m and made with galvanized steel pipes (Fig.1). Optical fibers were placed on two cross bars of the greenhouse structure at approximately 2 m from the top tree canopy directly above the center of each planter box. The fibers (numerical aperture 0.37, core diameter 200 µm, field of view 43.4°; Thorlabs Inc., Newton, NJ, USA) pointed downward to collect the reflected radiation from the tree canopy in each planter box. The area covered by the field of view of each fiber was approximately 1.90 m in diameter. Two other optical fibers were used: one directed toward the sky and equipped with a cosine corrector was mounted on top of the structure and used to measure the incident photosynthetically active radiation (PAR), and the second fiber was installed at 7 cm from a Spectralon reference panel (Spectralon 99% reflectance, 25 cm x 25 cm; Labsphere Inc., North Sutton, NH, USA) and looking downward, collecting the reflected upwelling irradiance. The Spectralon reference panel was located next to the planter boxes and positioned at approximately 1.5 m height at the same level as the top of the tree canopy. All of the optical fibers were connected to input ports of an optical multiplexer (MPM2000, OceanOptics, Dunedin, FL, USA). The multiplexer had 16 input ports and one output port. The free input ports were blocked and used for dark-noise measurements (instrumental noise). The output port was connected to a spectrometer (USB2000 + 350-1100 nm, 0.33nm full width at half maximum [FWHM]; OceanOptics). Each port was scanned sequentially by the multiplexer, allowing a temporal resolution of approximately 7 minutes between two successive acquisitions on the same planter box. After the installation and at their final locations, each fiber was calibrated for radiance measurements (w/nm/m²) by measuring the spectrum at the output port of the multiplexer coming from a calibration lamp (HL-2000 CAL, OceanOptics, USA) connected at the end of the fiber.

Figure 1: Picture of the setup.

In this study, the spectral data acquired above the vegetation were used to derive spectral indices as indicators of the temporal variation of canopy greenness (leaf area index) during the experiment. The reflected radiances from vegetation and from the Spectralon reference panel were used to calculate the reflectance. The NDVI (normalized difference vegetation index), as an indicator of the canopy structure, was calculated based on the reflectance measured within a 25-nm wavelength band centered on 655 nm for the red and 800 nm for the near infrared using the following expression:

$$NDVI = \frac{\rho_{800} - \rho_{655}}{\rho_{800} + \rho_{655}}$$

The soil water content was monitored over the whole profile in the four planter boxes. An access tube was installed near the center of each box, allowing the monitoring of the soil water content every five or six days over a 5-cm resolution profile using a PR2 soil moisture-profile probe (Delta-T Devices, UK). The PR2 measurements were calibrated for volumetric humidity over ten 250 cm^3 soil samples for each box (with a total of 60 samples).

2.2.2. Leaf-scale measurements

At the leaf scale, measurements of fluorescence, photosynthesis and optical properties were begun when a sufficient contrast in terms of soil moisture was observed between the

treated and control plots and during a long period of NDVI stability to minimize the effects of strong eventual temporal changes in the canopy structure and leaf pigment content. More precisely, the measurement campaigns took place from early July (Doy 206) until late August (Doy 240).

For the planter boxes occupied by the oak saplings, data were acquired during four measurement campaigns (Doy 212, 215, 233 and 247). For the planter boxes occupied by the beech saplings, only two measurement campaigns were performed (Doy 213 and 234). The treatment and control plots were always sampled on the same day. From each plot, ten leaves (five leaves from the top and five leaves from the bottom of the tree crowns) on five different trees were randomly selected. The same leaves were numbered and monitored throughout the experiment.

The measurements were conducted on leaves still attached to the tree and previously wrapped in aluminum foil to keep them in the dark for fluorescence measurements. The leaves were dark-adapted for 12 h. The measurements were performed on the same leaves, at first using a PAM-2000 fluorometer and then using the LICOR 6400 for fluorescence and photosynthesis measurements on the other half of the leaf. The measurements of leaf optical properties were performed simultaneously with the PAM-2000 fluorescence measurements. The protocols are described in detail below:

For fluorescence measurements using the PAM-2000 and leaf optical properties, each leaf, still wrapped in aluminum foil, was clipped with a leaf-clip holder 2030-B (Walz, Effeltrich, Germany). An optical fiber (50 µm, FOV 25°, OceanOptics) fixed on the leaf-clip holder and equipped with a collimating lens (to reduce the field of view of the optic fiber) and connected to a USB2000 spectrometer (350-1100 nm, 0.66 nm full width **at** half maximu**m** [FWHM]; OceanOptics) was used to measure the leaf optical properties on the same portion of the leaf exposed to saturating light pulses generated by the PAM-2000.

The optical measurements started by measuring the radiance on a gray Spectralon panel (4% reflectance, Labsphere Inc., North Sutton, NH, USA) clipped to the leaf and then the radiance reflected by the leaf immediately after removing the gray Spectralon and the aluminum foil. The aluminum foil was removed only from the first half of the leaf. The other half was kept dark-adapted for LICOR measurements.

Immediately after the measurement of the leaf's reflected radiance (approximately one or two seconds after), the fluorescence parameters F_0 (dark-adapted initial minimum fluorescence)

and F_m (maximum fluorescence measured during the first saturation pulse on dark-adapted leaves) were measured. After these two measurements, the F_s (stationary chlorophyll fluorescence level) and F_m' **(**maximum chlorophyll fluorescence in a light-adapted leaf) were measured continuously for 24 minutes at different increasing and decreasing light intensities emitted by an LED-array actinic lamp (0-472 µmol/m²/s) to obtain light-response curves of the leaf under LED and natural light conditions. The quantum yield of PSII and its maximum value were determined as follows:

$$\varphi PSII = \frac{F'_m - F_s}{F'_m}$$

$$\varphi PSII_{max} = \frac{F_m - F_0}{F_m}$$

Simultaneously with the PAM-2000 measurements and throughout the sequence of increasing and decreasing light intensities, automatic measurements of the leaf optical spectrum were taken continuously at a very high temporal frequency (the maximum difference observed between two successive acquisitions of spectra was 0.5 seconds, and the mean difference was 0.13 seconds). At the end of the PAM-2000 measurements, another spectrum was measured on the Spectralon reference panel.

The spectra obtained from the leaves were then used to calculate PRI using the following formula:

$$PRI = \frac{\rho_{531} - \rho_{570}}{\rho_{531} + \rho_{570}}$$

where ρ_{531} and ρ_{570} represent the leaf reflectance integrated over a 10 nm wavelength band centered on 531 nm and 570 nm, respectively.

The first spectrum measured immediately after removing the aluminum foil and before switching on the PAM LEDs was also used to calculate the modified red-edge normalized difference index ($mNDI_{705}$) as an indicator of leaf chlorophyll content based on the reflectance measured within a 25-nm wavelength band according to the following formula given by Sims and Gamon (2002):

$$mNDI_{705} = \frac{\rho_{750} - \rho_{705}}{\rho_{750} + \rho_{705} - 2 \times \rho_{445}}$$

where ρ_{445}, ρ_{705} and ρ_{750}represent the reflectance integrated over a 25-nm waveband centered on 445 nm, 705 nm and 750 nm, respectively.

Note that only the PRI values computed from measurements taken two seconds after each PAM-2000 pulse were used to obtain a response curve of the PRI to increasing and decreasing PAR levels. This choice was made to avoid the contribution of the PAM pulses to the reflected radiation by the leaf. In addition, the spectrum of actinic light provided by the PAM-2000 LED sources and measured in this study peaked at 655 nm and ranged between 600 and 700 nm (FWHM 642-671 nm) and thus did not overlap the PRI wavelengths (531 and 570 nm).

After the PAM-2000 measurements, six out of ten leaves from each measurement campaign were kept for fluorescence and CO_2-assimilation measurements with a LICOR 6400with the 6400-40 leaf chamber fluorometer. CO_2-assimilation measurements were used to estimate the LUE and leaf stomatal conductance. LICOR fluorescence and CO_2-assimilation measurements were acquired simultaneously during a sequence of 30 minutes of an increasing and decreasing sequence of PAR (0-2000 µmol/m²/s) after removing the aluminum foil covering the remaining portion of the leaf.

2.2.3. Leaf biochemical measurements

During the entire experiment and throughout the growing season, a total of 45 oak and 25 beech non-dark-adapted leaves were sampled in each planter box. Before the sampling, their reflectance spectra were measured. Immediately after the sampling, the leaves were frozen in liquid nitrogen, lyophilized, weighed and ground. Fifteen micrograms of the resulting powder from each leaf was dissolved in 10 ml 90% acetone at 60°C during one hour. Then, the absorbance spectrum of the solution was measured using an Agilent 8453 UV-VIS spectrophotometer to determine the total chlorophyll concentration of the leaf. Reflectance and leaf chlorophyll concentration measurements were used to establish a calibration relationship between the $mNDI_{705}$ and leaf total chlorophyll content.

2.2.4. Data analysis

The spectra were processed using Matlab 7.0 (Mathworks, Natick, MA, USA). The reflectance spectra obtained using radiances measured from the leaves and the Spectralon reference panel were smoothed using a robust loess local regression. The spectra were then used to derive the spectral indices (NDVI, $mNDI_{705}$ and PRI) described above.

The spectral, fluorescence and CO_2-assimilation data were then analyzed to describe the temporal and treatment-related variability and to assess relationships between the PRI, PAR, fluorescence and LUE at the leaf scale. The temporal and treatment-related variability was described based on summary statistics and a Kruskall-Wallis non-parametric analysis of variance. Relationships between the PRI, PAR, fluorescence and LUE were described using regression analysis, and their robustness was assessed using the resulting R^2 values.

3. Results

3.1. General characterization of the soil water status, temporal patterns of canopy structure and leaf chlorophyll content in the experimental plots

The soil moisture and canopy-structure dynamics during the measurement campaigns are shown in Fig.2 A and 2 B.

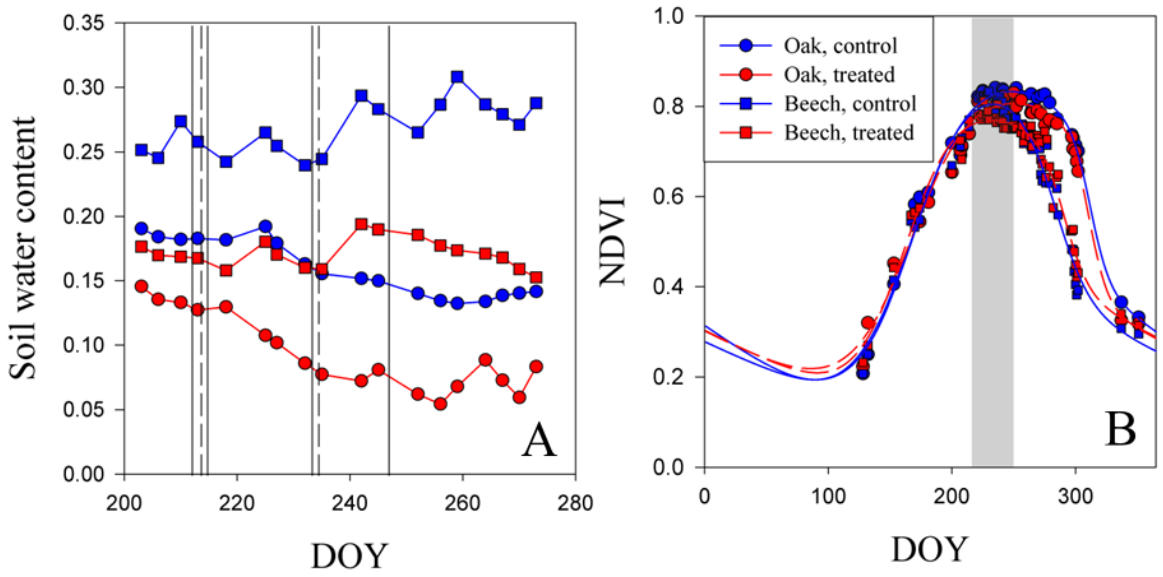

Figure 2: A - Soil moisture measured at a depth of 30 cm using a PR2 soil moisture-profile probe. The soil moisture was calibrated against gravimetric measurements. B - Canopy structure dynamics based on the NDVI time-series. Symbols: blue and red symbols for the control and treated plots, respectively, with circles for oak and squares for beech. The vertical continuous and dotted lines in Fig. 1 A delimit the oak and beech measurement campaigns, respectively. The gray area in Fig 1 B delimits the period of time of the measurement campaigns.

As stated in the Materials and Methods, the four plots were regularly watered to produce a difference in the soil water content between the control and treated groups. Intense hydric stress was avoided to prevent strong changes in the structural and biochemical canopy characteristics. Nevertheless, the soil moisture time courses (Fig. 2 A) showed different hydric statuses between the plots. For the oak, the soil moisture varied between 13% and 19% for the control plot and between 6% and 15% for the treated plot. Throughout the duration of the experiment, the average difference in soil moisture in the control and treated oak plots was approximately 7%. For beech, the soil moisture varied between 24% and 31% for the control plot and between 15% and 19% for the treated plot. During the entire experiment, the average absolute difference in soil moisture between the control and treated beech plots was approximately 10%. These absolute differences did not lead to perceptible changes of the canopies structural properties. As shown in Fig. 2 B, the NDVI time courses did not show any significant variation in canopy structure between the control and treated plots. Finally, between the two species, the lower soil moisture reached in the treated oak plot can be explained by a higher canopy leaf area index, as suggested by the level and length of the stable NDVI region during the measurement campaigns.

At the leaf scale, temporal patterns of chlorophyll content were investigated based on $mNDI_{705}$ measurements calibrated against direct measurements, as described above (§2.5.3) and are shown in Figure 3. A robust linear calibration relationship (R^2=0.95, RMSE=0.4) was obtained, with a slope of 17.5 mg/g and an intercept of -9.8 mg/g (Fig. 3 A).No significant differences in leaf chlorophyll content were observed between the treatments during the measurement campaigns (Fig. 3 B and C).

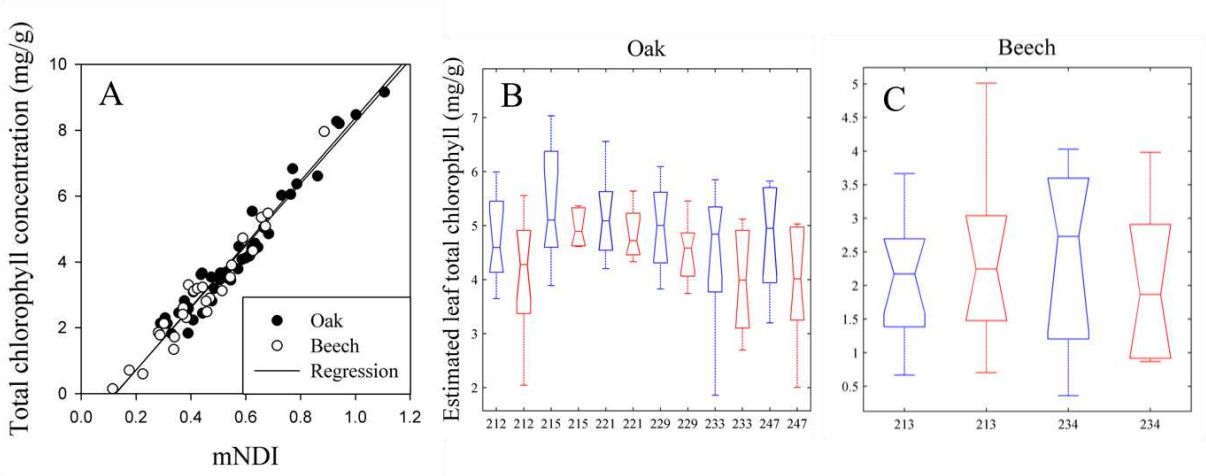

Figure 3: A - Calibration relationship between the leaf total chlorophyll content (mg/g) and mNDI705. B and C - Estimated leaf total chlorophyll dynamics over the survey for oak (B) and beech (C). The top of each bar is the median chlorophyll content of the group with 10 leaves, and the whiskers indicate the estimated error (95% confidence interval) around the mean. The control groups are presented in blue, and the treated groups are presented in red.

3.2.Dynamics of ecophysiological responses and PRI

As noted above, ecophysiological responses of the four plots were investigated during the NDVI plateau period. Photosynthetic functioning at the leaf scale was assessed through measurements of CO_2 and water exchange (Fig. 4) and through parameters of chlorophyll fluorescence measurements under different levels of imposed PAR (Fig. 5).

Summary statistics of the leaf stomatal conductance and light-use efficiency are illustrated in Fig. 4. As described in the Materials and Methods, the leaf stomatal conductance was determined based on the LICOR measurements made in the same conditions and over the same PAR range for every leaf. For oak, Fig. 4 A does not show any significant difference between the control and treated plots at the beginning of the experiment. However, significant differences can be observed on the Doy 233 and 247 (P<0.001 and P<0.0015, respectively). Significant differences between the beech control and treated plots were also observed at the end of the experiment, as shown in Fig. 4 B (P<0.003).

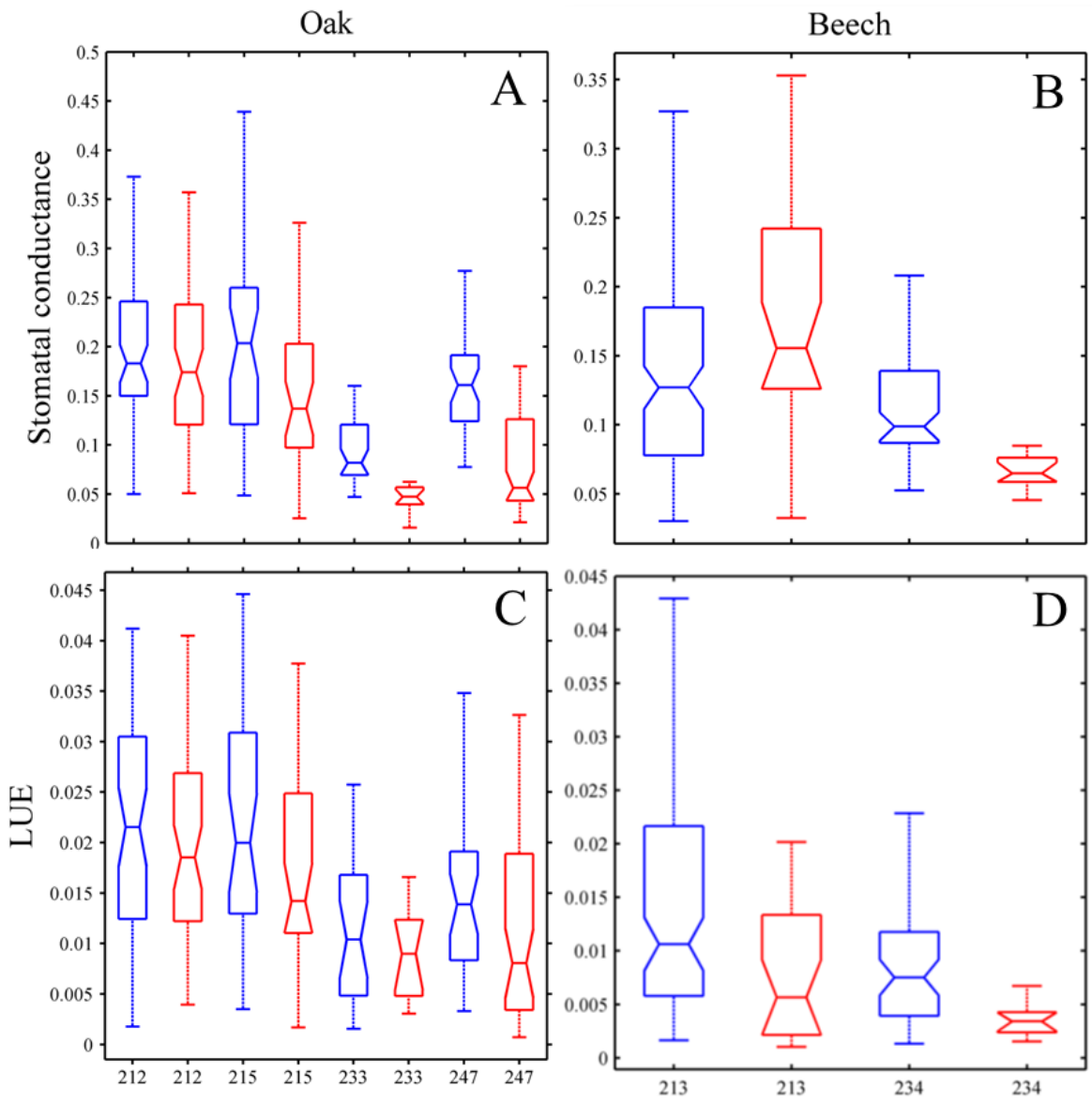

Figure 4: A and B - Leaf stomatal conductance (gs – mol/m2/s) measured on oak (A) and beech (B) leaves in the control and treated plots. The vertical bars are the means of 6 leaves and were used to calculate the summary statistics. C and D - Light-use efficiency (LUE) measured on oak (C) and beech (D) leaves in the control and treated plots. The vertical bars are the means from 6 leaves and were used to calculate the summary statistics.

Fig. 4 (C and D) shows the temporal variability of the LUE. No significant differences between the control and treated plots were observed for oak (Fig. 4 C). Nevertheless, during the entire period of measurements, the average LUE was always lower in the treated plot. In the beech plots (Fig. 4 D), LUE was significantly lower during the end of the experiment (P<0.027).

Summary statistics of the maximum fluorescence yield from PAM measurements are illustrated in Fig. 5. The results confirm the conclusions derived based on the LUE measurements. The maximum fluorescence yield was measured on dark-adapted leaves and consequently was not PAR-dependent. A decrease in maximum fluorescence yield is observed, as well as significant difference between the control and treated plots for oak at the end of the experiment, and for beech (Fig. 5.A and B).

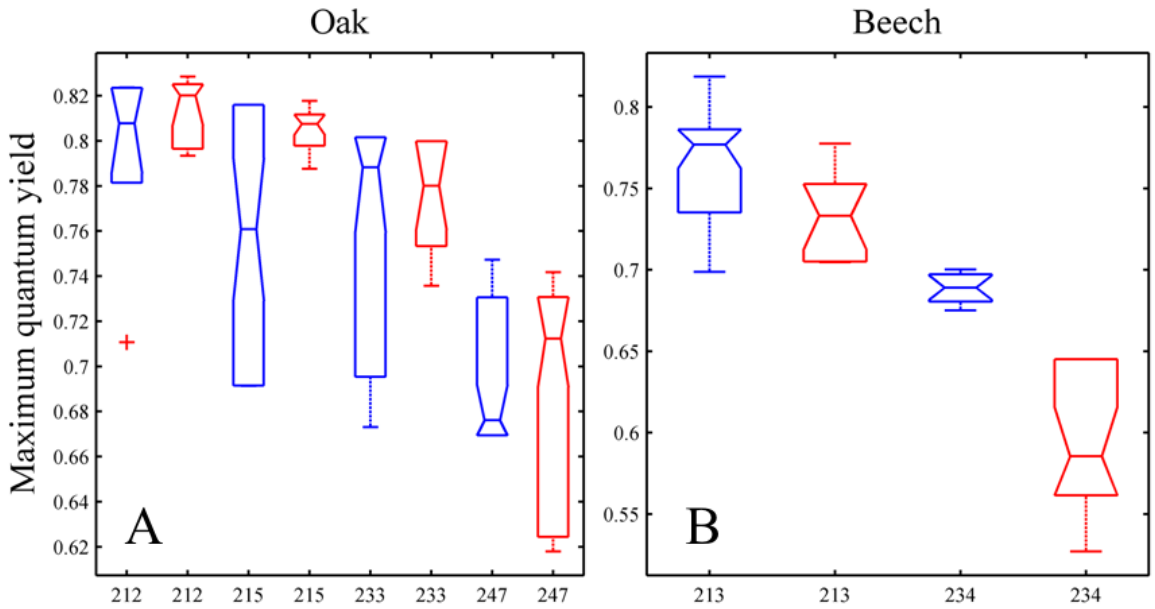

Figure 5: Leaf maximum yield measured on oak and beech leaves in the control and treated plots. The vertical bars are the means of 6 leaves and were used to calculate the summary statistics.

3.3. Relations between the PRI and leaf ecophysiological and biochemical parameters

3.3.1. Relations between the PRI and ecophysiological responses

Simultaneous reflectance spectra and fluorescence measurements are illustrated in Fig.6 A and 6 B and Fig. 7.Typical reflectance spectra measured at the leaf scale under different levels of incident radiation coming from PAM LEDs and from ambient light conditions are illustrated in Fig. 6 A. PAM LED radiation was applied in increasing and decreasing sequences. The general shape of the reflectance spectrum was similar to that typically measured above leaves. In the visible spectrum, reflectance peaked in green and as

low in the blue and red regions. Then, reflectance increased sharply at the red-edge with an inflection point around 720 nm and reached its maximum in the near infrared. The peaks observed around 655 nm were due to the increased actinic red light that came from the PAM LEDs. As noted above (§ 2.2), the emission spectrum of the PAM LEDs did not overlap with the wavelengths used in PRI. Measurements of this spectrum (data not shown) showed that the emission spectrum was limited between approximately 611 nm and 687 nm. In addition, the peak located at approximately 760 nm was largely due to the sun-induced chlorophyll fluorescence in the Fraunhofer line of the oxygen absorption.

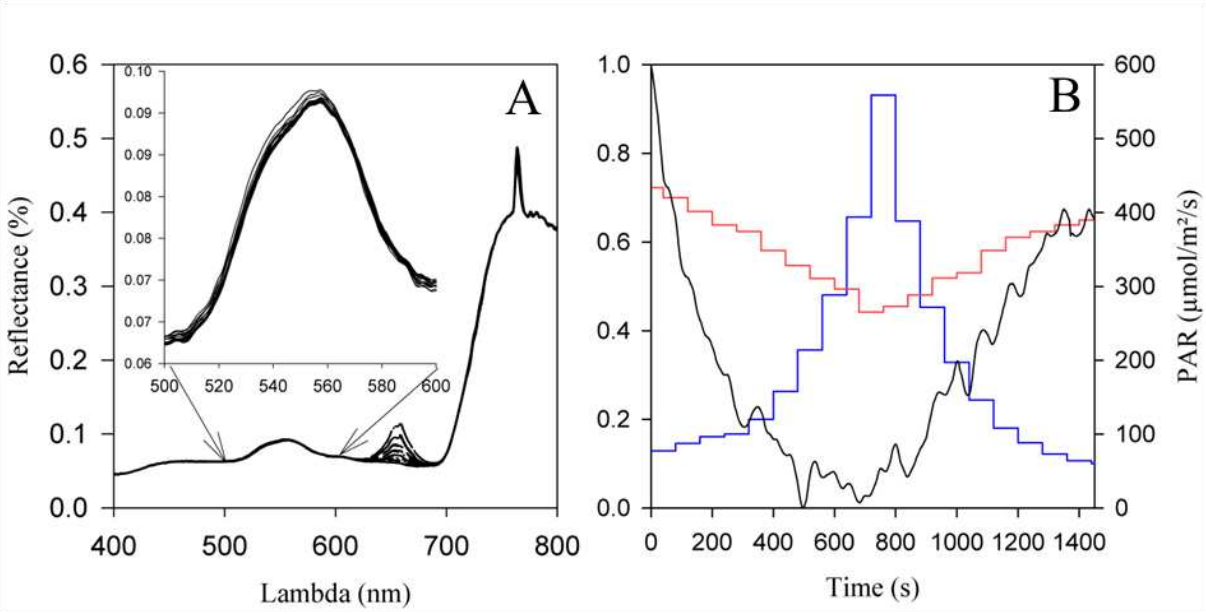

Figure 6: A - Temporal series of typical reflectance spectra measured over the same leaf under increasing then decreasing PAR. The inset shows the reflectance variability around 550 nm. B - Typical PRI and fluorescence yield dynamic in response to an imposed PAR sequence, derived from the same series. The imposed PAR (µmol/m²/s) is represented in blue, the fluorescence yield is represented in red, and the standardized PRI is represented in black. The highest PRI value (shown as 1 here) was -0.0286. The lowest PRI value (shown as 0 here) was -0.0409.

Fig. 6 A (insert) shows a significant temporal variability of the reflectance in the region surrounding the peak at 555 nm due to increasing and decreasing variations of PAR. This variability was asymmetrical and more important in the left side than in the right side.

The corresponding sequence of imposed PAR and the resulting typical PRI and fluorescence kinetics are illustrated in Fig. 6 B. The PRI and fluorescence yield were both negatively correlated with the PAR, and their variation was not completely reversible. The PAR-

dependent variability of the reflectance calculated for every wavelength as the relative difference between the reflectance at time *t* and reflectance at the beginning of the increasing sequence of PAR (time zero) is illustrated in Fig. 7.

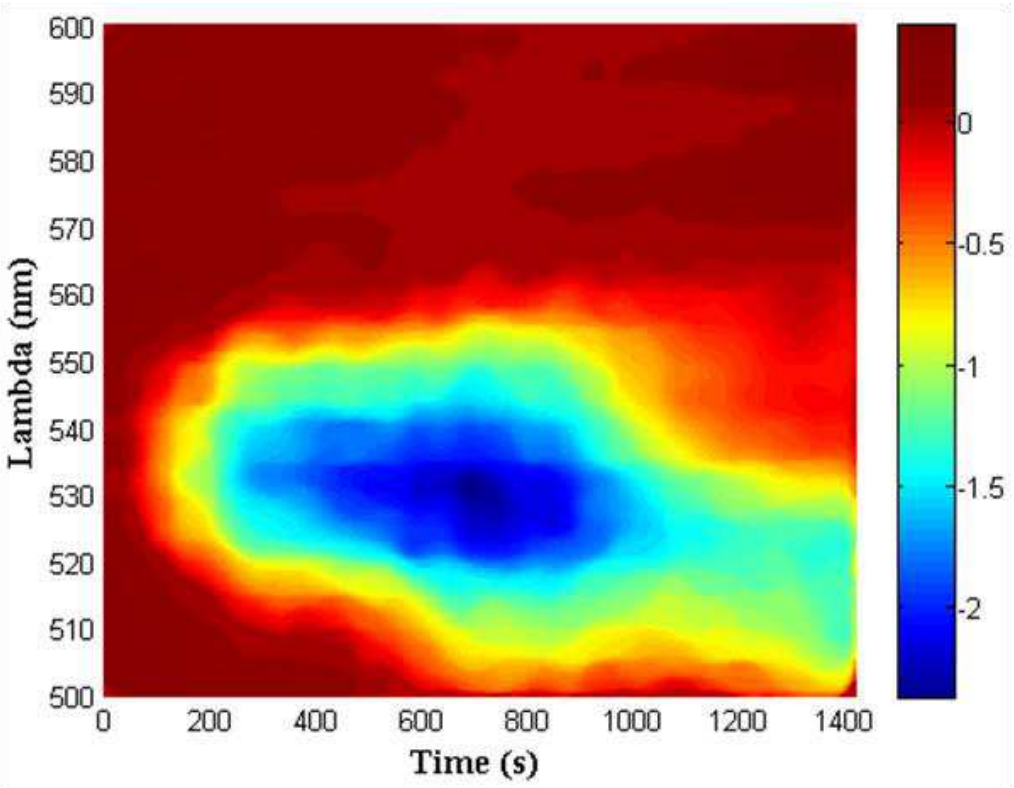

Figure 7: Relative reflectance difference (%) calculated using the first spectrum as a reference over time (s).

First, over the entire kinetic path from the beginning of the increasing sequence of PAR to the end of the decreasing sequence, the reflectance level remained lower than the level of reflectance measured at time zero. This result indicates a hysteresis phenomenon, meaning that the curve of the decrease of reflectance produced by the increase of PAR does not overlap the curve of the increase of reflectance produced by the decrease of PAR. This figure also shows an important variability depending on the wavelength. The maximum variation was found in two spectral bands centered on 525 nm and on 540 nm. The variation observed in the 525-nm band was not completely reversed with decreasing PAR (the R_{525} nm at the end of the decreasing sequence remained lower than the R_{525} nm at time zero). On the contrary, the variation observed around the 540 nm spectral band appeared with low PAR values as soon as the leaf was exposed and was quickly reversed under increasing red light.Based on measurements of PRI and fluorescence from all the leaves under increasing and decreasing sequences of PAR according to the protocol described in § 2.2, the relationships between PAR, fluorescence yield, LUE and PRI are shown in Fig. 8.

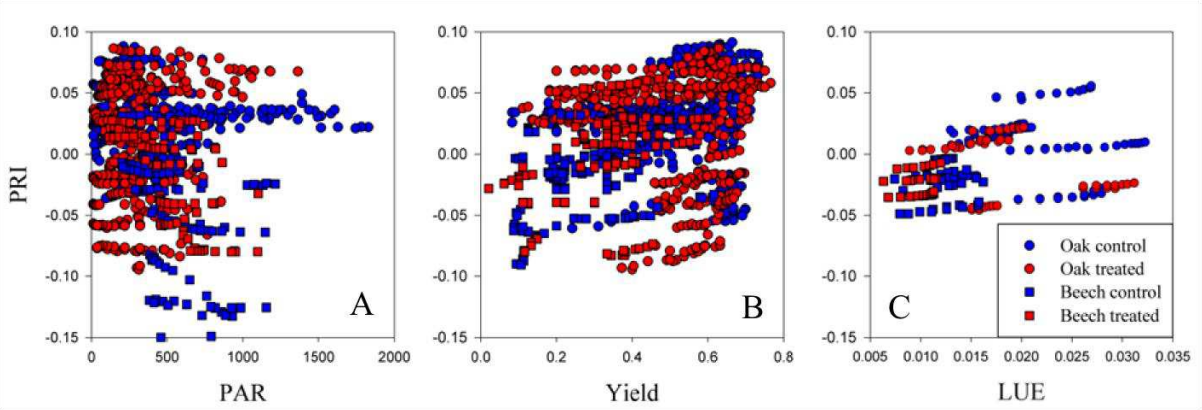

Figure 8: A - PRI versus PAR (µmol/m2/s). Symbols: blue and red symbols for the control and treated plots, respectively, with circles for oak and squares for beech. B - PRI versus fluorescence yield. Symbols: blue and red symbols for the control and treated plots, respectively, with circles for oak and squares for beech. C- PRI versus LUE. Symbols: blue and red symbols for the control and treated plots, respectively, with circles for oak and squares for beech. All of the relationships are shown (oak control, n=44; oak treated, n=41; beech control, n=20; beech treated, n=14).

As shown in Fig. 8, the relationships between PRI and PAR, fluorescence and LUE at the leaf scale were very scattered because of the strong variability of the intercepts.

3.3.2. Investigating causes of the variability of the relations between PRI and fluorescence yield

As noted above, the PRI, as well as the intercept of the linear regressions of PRI vs. PAR (Fig. 8), hereafter called regression-based PRI_0 (the hypothetical PRI at PAR near 0), exhibited a strong variability between the leaves. Fig. 9 shows summary statistics of the PRI and PRI_0 for the oak and beech during the different measurement campaigns.

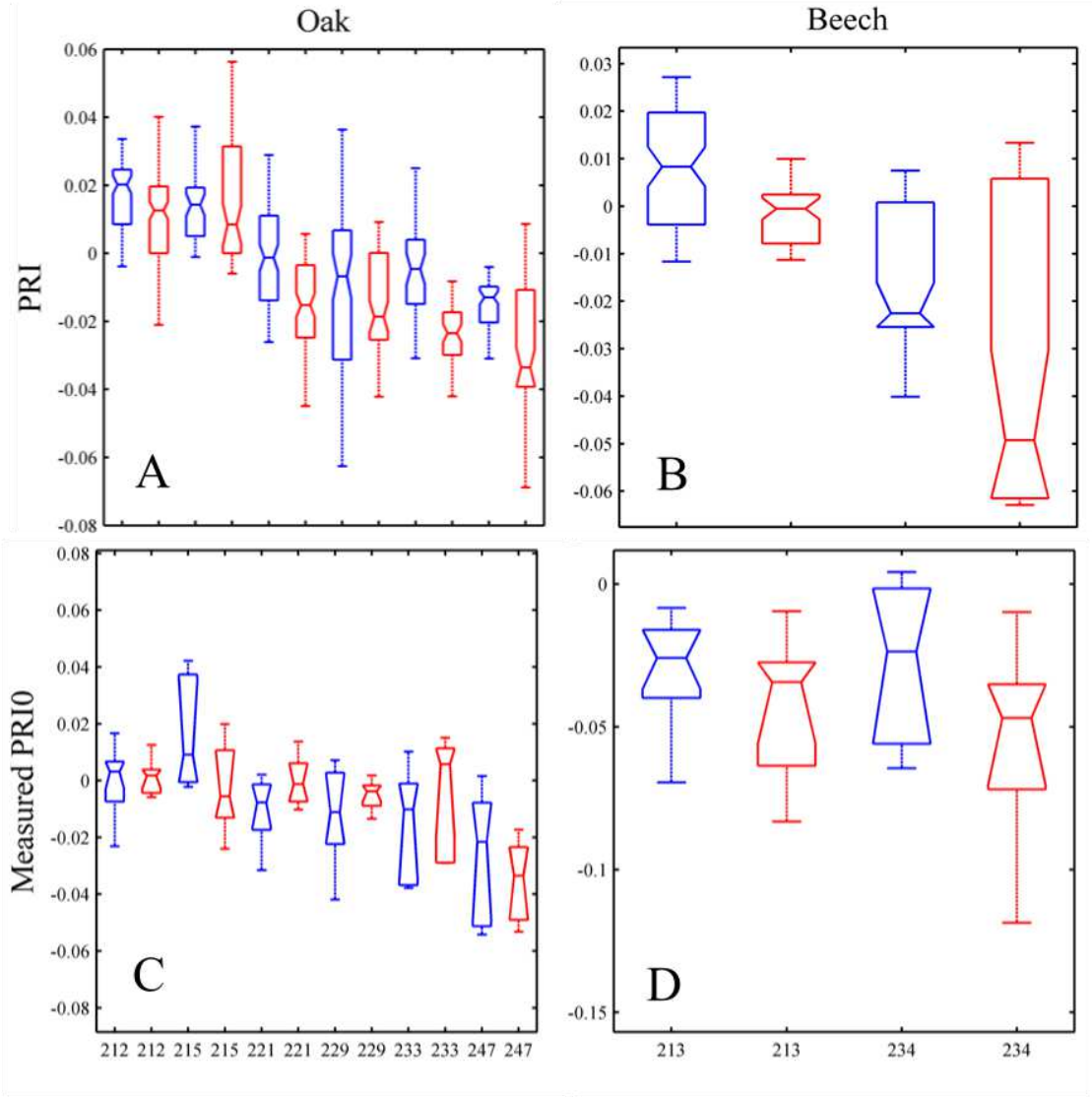

Figure 9: A and B - Leaf PRI measured on oak (A) and beech (B) leaves in the control and treated plots. The top of each bar is the mean PRI of the leaf group, and the whiskers indicate the estimated error (95% confidence interval) around the mean. The control groups are presented in blue, and the treated groups are presented in red. C and D - Leaf PRI0 measured on oak (C) and beech (D) leaves in the control and treated plots. The top of each bar is the mean PRI0 of the leaf group, and the whiskers indicate the estimated error (95% confidence interval) around the mean. The control group is presented in blue, and the treated group is presented in red. (oak: n=10 for each bar; beech: n=10 for each bar).

Note that regression-based PRI_0 values were estimated from PRI vs. PAR relationships established from measurements acquired on dark-adapted leaves. The comparison of the regression-based PRI_0 estimates to the PRI values measured on the same leaves immediately after the removal of the aluminum foil that covered each leaf is shown in Fig. 10 A. Significant correlations between the offsets and the dark-adapted PRI values were obtained

(R^2=0.84, P<0.001, RMSE=0.006). Moreover, the measured and estimated dark-adapted PRI_0 were positively correlated (R^2=0.83, P<0.001, RMSE=0.33) with the leaf chlorophyll content as estimated using the calibrated $mNDI_{705}$ (Fig. 10 B).

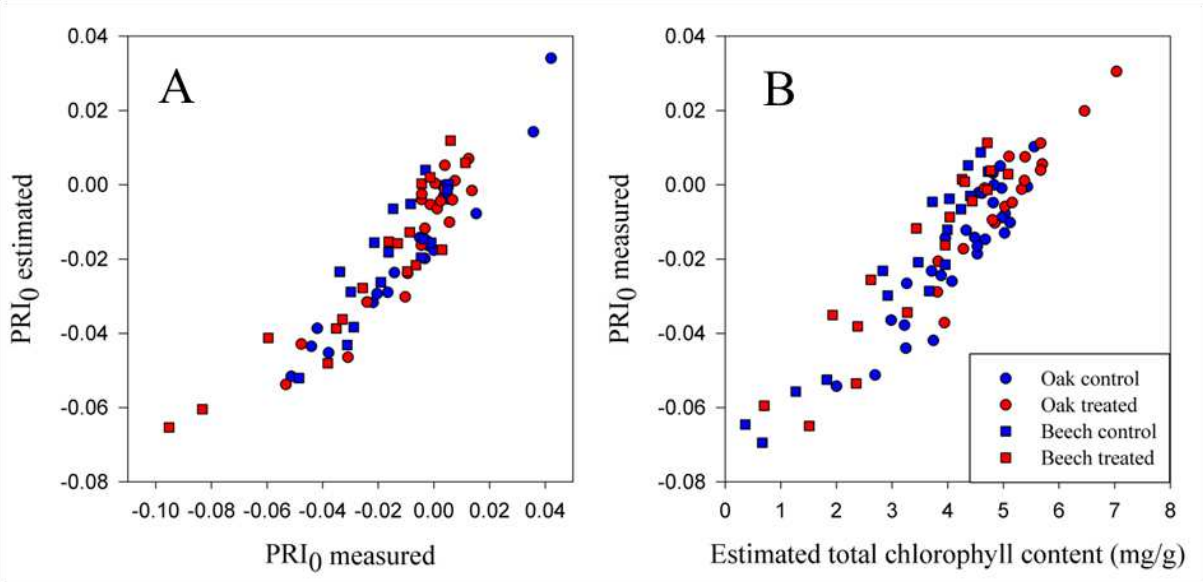

Figure 10: A - PRI_0 estimated as the intercept of PRI PAR regressions versus PRI_0 measured immediately after dark adaptation. Symbols: blue and red symbols for the control and treated plots, respectively, with circles for oak and squares for beech. B - Measured PRI_0 versus the estimated total leaf chlorophyll content of leaves (mg/g). Symbols: blue and red symbols for the control and treated plots, respectively.

A simple procedure for disentangling the dependencies of PRI on the variability of leaf chlorophyll content between leaves and during the season may consist of subtracting the corresponding PRI_0 values from the PRI measurements achieved during the different campaigns. The relationships between the corrected PRI and fluorescence yield from PAM and between the corrected PRI and LUE from Licor data are shown in Fig.11 A and 11 B. Whereas the correlation between the PRI and fluorescence yield and LUE was poor (R^2=0.09, P<0.001, RMSE=0.039 and R^2=0.09, P<0.001, RMSE=0.038 respectively), the obtained corrected PRI versus LUE over 260 measurements made on 16 oak leaves and 8 beech leaves (4 leaves per sampling date) was strong (R^2=0.72, P<0.001, RMSE=0.0042 and R^2=0.93, P<0.001, RMSE=0.0016 respectively) and linear, accounting for both inter-leaf and seasonal variability.

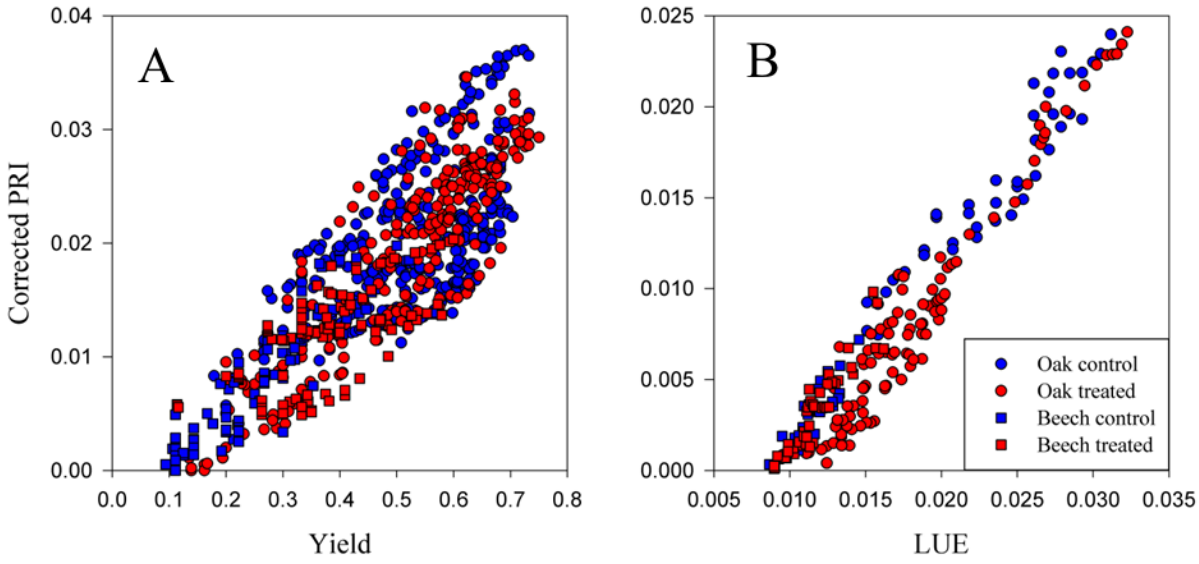

Figure 11: A - Corrected PRI (PRI minus PRI0 for each measurement series) versus fluorescence yield. Symbols: blue and red symbols for the control and treated plots, respectively, with circles for oak and squares for beech. B - Corrected PRI versus LUE. Symbols: blue and red symbols for the control and treated plots, respectively, with circles for oak and squares for beech.

4. Discussion

Previous studies (Gamon et al. 1990; Gamon et al. 1992) showed a clear response of PRI to the xanthophyll cycle epoxidation state and the LUE. However, other studies obtained much more contrasting results over the season at the leaf (Rahimzadeh-Bajgiran et al. 2012) and canopy scales (Grace et al. 2007; Garbulsky et al. 2011). Indeed, at the seasonal scale, a relationship between PRI and LUE may not always be observed (Gamon et al. 2001; Filella et al. 2004; Nakaji et al. 2006; Rahimzadeh-Bajgiran et al. 2012). Hereafter, we summarize the reasons that may explain the apparent loss of relationship between PRI and LUE, i.e.:

- Insufficient light-use efficiency variability (for example, due to abiotic and biotic stress conditions).
- Dependency of the PRI on other factors (e.g., leaf biochemical composition, leaf area index, 3D canopy structure and sun-view geometry) regardless of LUE.
- Loss of PRI response to LUE changes (e.g., xanthophyll cycle inhibition or saturation and zeaxanthin-independent quenching).

At the leaf scale, most of the previous works focused on the steady-state response of PRI under fixed PAR, after stabilization (Gamon et al. 1990; Gamon et al. 1992; Gamon et al. 1997; Penuelas et al. 1997; Rahimzadeh-Bajgiran et al. 2012), rather than the dynamic response of PRI to PAR variability. Under natural conditions, the steady-state response of PRI may not be reached because of high PAR variability over very short time scales. Therefore, steady-state PRI measurements may not be similar to PRI responses under natural conditions, as suggested by Rasher et al. (2006).On the other hand, some studies focused on the PRI kinetic under fixed PAR and after dark-light transition (Penuelas et al. 1995, Gamon and Surfus 1999, Gamon and Berry 2012).In Gamon and Berry (2012), it was shown that two components of PRI variability could be distinguished: a constitutive component depending on leaf pigment content, and a facultative component, varying at short time scale due to the xanthophylls cycle. The constitutive component could be isolated using the first PRI measurement over dark-adapted leaves.

In the present study, PRI kinetics after dark-light transition were coupled with PRI light curve measurements under semi-controlled PAR variability. This enabled us to track the quantitative response of PRI to PAR variation under constant leaf pigment composition. Our results showed the same responses of reflectance at 525 nm and 540 nm as those reported by Gamon et al. (1997). The band centered on 525 nm which respond to the whole range of PAR may be linked to the xanthophylls cycle, while the band centered on 540 nm may be due to the reflectance variation due to light scattering changes due to dark-light transition, as observed in Gamon et al. (1997) around 545 nm. These reflectance changes were clearly associated with the PRI changes related to the imposed sequences of PAR and to the resulting quantum yield changes (Fig.6 and 7).The protocol adopted in this study allowed us to avoid considering the possible causes of the deterioration of the relationship PRI vs. LUE that are described above. The measurements were made at very high temporal resolution under an imposed variability of PAR over leaves for which the biochemical composition remained unchanged during the measurements.

Our results were obtained based on measurements achieved over the entire growing season from two species (*Quercus robur* and *Fagus sylvatica*) and under different soil water contents. The soil water content differential triggered a significant decrease in leaf conductance in the treated groups of both species (Fig.4 A and 4 B) as well as a decrease in LUE (Fig. 4 C and4 D) and a decrease in maximum quantum yield (Fig. 5.A and 5.B). In contrast, the leaf biochemical and canopy structural properties of the plots were not significantly different, as illustrated by the canopy NDVI dynamics and leaf chlorophyll

content (Fig. 2 and Fig. 3).The PRI seasonal variability (Fig. 9 A and B) exhibit both a difference between treatment, in accordance with the soil water content measurements, and a seasonal trend comparable to the one observed in leaf chlorophyll content (Fig. 2 and 3). At the leaf scale and over the entire season, the correlations between PRI and quantum yield and between PRI and LUE were significantly higher than those reported in the review of Garbulsky et al. (2011) (the mean R^2 was 0.78 and 0.73 between PRI vs. quantum yield and PRI vs. LUE, respectively, in this study, and values of 0.5 and 0.25, respectively, were reported by Garbulsky et al. 2011). These values are comparable to those obtained on an intra-daily scale (Gamon et al. 1992; Penuelas et al. 1997; Guo and Trotter, 2004). Moreover, these relations, shown in Fig. 8, were stable over the entire season for both species and both treatments. On the other hand, these relation exhibit a strong variability in intercepts between leaves and over the season.

In light of the results discussed above, we can conclude that we did not observe any loss of the robustness of the PRI response to PAR and to LUE over the growing season, but this PRI response changed depending on other factors unrelated to leaf physiological responses to PAR variability. This change is clearly shown in Fig. 8. This figure also shows that the PRI variability between leaves was much higher than the variability induced by PAR. To explain this variability, we defined PRI_0as the PRI of a completely dark-adapted leaves (analogous to the ground [F_0] fluorescence of a dark-adapted leaf). We used two different methods to determine the PRI_0. The first method consisted of estimating PRI_0 as the intercept of a PAR versus PRI regression, and the second method consisted of directly approximating PRI_0 as the PRI measured immediately (less than 100 ms on average) after the removal of the aluminum foil used for the leaf dark adaptation, as done previously in Gamon and Surfus (1999) and in Gamon and Berry (2012). We noticed that the estimated and measured PRI_0 were highly correlated (Fig. 10 A), meaning that the PRI_0 measured directly after leaf dark adaptation can be used to track the PRI variability that is unrelated to leaf physiological responses.

The results show that PRI_0 was highly linearly correlated with the leaf chlorophyll content (Fig. 10 B), in accordance with Gamon and Berry (2012). Therefore, there was a strong influence of leaf pigment content on PRI, as shown by Filella et al. (2004) and Garbulsky et al. (2011). After subtracting the PRI_0 from PRI measurements, the relations between the corrected PRI ($PRI - PRI_0$) and LUE significantly improved over the entire growing season for both species and both treatments, as shown in Fig. 11 A and 11 B, respectively. The uncorrected PRI vs. LUE relationship is shown in Fig. 8 C.

Based on these results and as reported in Gamon and Berry (2012), the PRI variability can be separated into two components:

- A constitutive component that is mainly due to the leaf biochemical composition, which exhibited a seasonal pattern and a strong inter-leaf variability. This component was captured using the PRI_0.

- A physiological component due to LUE variability, mainly explained by the PAR and soil water status. This component was recovered as the corrected PRI.

The use of high-temporal-resolution measurements on dark-adapted leaves under controlled PAR conditions, which allowed us to disentangle the PRI variability correlated to LUE from the effects of pigmentation changes, was clearly not suitable to correct the PRI acquired over vegetation canopies at large spatial and temporal scales. This constitutive PRI variability related to leaf pigment composition may therefore make it difficult to use the PRI as a proxy of the ecosystem LUE. Nevertheless, we think that the PRI_0 at the canopy scale could be obtained following a variety of approaches, including:

- Using PRI measurements acquired under low light after sunrise to minimize the contribution of the xanthophyll cycle to the measured signal. However, precautions should be taken because, as shown by Gamon et al. (1992) and confirmed in this study (Fig. 7), the PRI shows an exponential decline as soon as leaves are exposed to light.

- Using high-temporal-resolution PRI measurements to obtain a PRI versus PAR regression and to estimate PRI_0 as the intercept of this regression. In this study, the PRI_0 estimated using this approach was strongly correlated with the measured PRI_0 (Fig. 10 A). However, the intercept estimation depends on the quality of the PRI versus PAR relationship, which may not be conserved at larger scales because of high spatial heterogeneity or when photosynthesis is limited by other factors than the PAR (Soudani et al. submitted).

- As suggested by Rahimzadeh-Bajgiran et al. (2012), combining PRI with optical indices sensitive to leaf pigmentation, such as the $mNDI_{705}$, which was shown to be well correlated with the PRI_0 in this study. Nevertheless, special caution should be taken when using optical indices to correct the PRI because it is unclear whether there is a single relationship over different species, scales, acquisition conditions and plant physiological statuses.

5. Conclusion

In this study, measurements at a high temporal resolution of PRI on dark-adapted leaves in controlled PAR conditions showed strong relationships between the PRI, quantum yield and LUE at the leaf scale, but these relationships were strongly impacted by the leaf pigment content. These impacts may account for most of the PRI variability measured over coarse temporal and spatial scales. This effect may significantly hamper the use of PRI as a proxy of canopy light-use efficiency. Moreover, we showed that this PRI variability could be corrected using PRI measurements in low light or immediately after leaf dark adaptation or the estimation of dark-adapted PRI based on light curve analysis. The new correction procedure allowed for the disentanglement of the effects of seasonal variations in leaf pigment content on the relation between the PRI and LUE. Nevertheless, this correction method needs to be assessed at the leaf scale over a wide range of species under much more constraining conditions. At the canopy scale, the application of such a procedure using satellite data might be possible but must be tested.

Chapitre 2. Deconvolution of pigment-related and physiological related PRI variability at canopy scale, over a whole growing season.

Hmimina G.[a]; Dufrêne E.[b]; Soudani K.[a]

[a] Univ. Paris-Sud, Laboratoire Ecologie Systématique et Evolution, UMR8079, F-91405 CNRS, Orsay, France

[b] CNRS, Laboratoire Ecologie Systématique et Evolution, UMR8079, F-91405, Orsay, France

Abstract

The photochemical reflectance index (PRI) sensitivity to leaf pigmentation and its impact on the potential of the PRI as a proxy of the light use efficiency (LUE) was recently shown to be a major issue at leaf scale. Most of the leaf to leaf and seasonal variability could be explained by such confounding effect, which could be alleviated based on PRI measurements under low light or PRI light curve analysis. The present work relies on PRI light curve analysis at canopy scale, in natural conditions in order to derive a precise deconvolution of pigment and physiological related PRI variability. Both sources of variability are then explained in the light of measured or estimated physiologically relevant variables such as the soil water content, used as an indicator of water availability, and the $mNDI_{705}$, used as an indicator of canopy pigment content. Most of the PRI variability could be explained. The effect of PRI sensitivity to canopy pigment content on its potential use as a proxy of the LUE over broad temporal and spatial scales are discussed in details.

1. Introduction

Direct measurements of canopy carbon fluxes is achieved locally over five hundred flux tower sites organized in the FLUXNET network using the eddy-covariance method **(**Baldocchi et al. 2001). Yet, the extrapolation of such measurement over whole biomes raises issues, since flux tower sites density may not be sufficient to describe carbon fluxes spatial heterogeneity, particularly in tropical ecosystems which exhibit the highest growth primary production (GPP) (Jung et al. 2009). An alternative was provided by the MODIS project, which aim to derive maps of GPP (Gross primary production) and annual NPP (Net primary production) across the globe with an 8-day time step (for GPP) and a spatial resolution of1 km² from MODIS measurement. The LUE estimation used in the MODIS model rely on biome-specific maximum light use efficiency values which are modulated based on daily minimum temperature and vapor pressure deficit (VPD) as described in Running et al. (2000). The resulting modeled GPP were compared to flux tower based measurements and it was shown that inaccurate estimation of LUE is a major source of uncertainty (Gebremichael and Barros, 2006; Turner et al., 2006). The retrieval of canopy LUE is therefore a key issue in order to accurately estimate global carbon budget.

During the last twenty years, considerable efforts were focused on the use of the photochemical reflectance index (PRI) in order to access LUE over broad spatial scales. The PRI, based on canopy reflectance in two bands centered on 531and 570 nm (Gamon et al. 1992) was developed as a way to track the violaxanthin-based xanthophyll cycle (Gamon et al. 1990, 1992, 1997), which plays a central part in the regulation of the LUE (Demmig-Adams and Adams 1996). Being based on reflectances, it can be estimated using satellite data, such as MODIS images, which were extensively used in order to compute PRI at daily temporal resolution, and 1 km spatial resolution (Drolet et al., 2005; Drolet et al., 2008; Goerner et al., 2009; Moreno et al., 2012).

Good relationships between PRI and LUE over short time scales were shown across several species at leaf scale (Penuelas et al. 1995, Gamon et al. 1992 and 1997, Guo and Trotter 2004, Nakaji et al. 2006, Meroni et al. 2008) and at canopy scale (Filella et al. 1996, Trotter et al. 2002, Wu et al. 2009). Leaf scale relationships between PRI and LUE were shown to deteriorate at seasonal scale (Garlbulky et al. 2011, Rahimzadeh-Bajgiran et al. 2012, Hmimina et al. 2013b). The PRI was shown to be strongly related to leaf total chlorophyll content (Moran et al. 2000) and to the carotenoid to chlorophyll ratio (Sims and Gamon 2002; Stylinski et al. 2002; Filella et al. 2009). As shown in previous works

(Rahimzadeh-Bajgiran et al. 2012, Gamon and Berry 2012, Hmimina et al. Submitted), while the LUE account for most of the facultative diurnal PRI variability, the constitutive pigment-related PRI variability at the seasonal scale introduce a change in PRI versus LUE relationships.

The effects of this constitutive PRI variability on PRI versus LUE relationships at canopy scale are still unclear; while a clear decrease in PRI versus LUE correlation was shown at leaf scale due to leaf pigment content changes, no such thing was observed at canopy level and at seasonal scale in the review of Garbulsky et al. (2011). The observed PRI versus LUE relationships at such scales may in fact be due to correlations between LUE and LAI or leaf pigment content, and may therefore be year, site and scale dependant as suggested in Hmimina et al. 2013b.

In summary, the PRI was shown to be a composite signal at leaf and canopy scale, responding to both leaf pigment content, and leaf physiological response to environmental conditions. Those effects could be disentangled at leaf scale, showing a strong impact of leaf pigment content on the PRI versus LUE relationship as shown in Hmimina et al. 2013b. At canopy scale, these effects are poorly documented. Strong effects of canopy pigment content on PRI versus LUE relationships are expected, but are yet to be described.

The aim of this study is to assess the variability in PRI in natural conditions over different species, a wide range of total chlorophyll content, and soil water status. More precisely, we focus on distinguishing between the variability due to plant ecophysiological functioning and due to canopy structural and biochemical properties.

2. Materials and methods

2.1. Plant materials and experimental setup

As described in Hmimina et al. 2013b, one hundred of three years old saplings of oak (*Quercus robur* L.), beech (*Fagus sylvatica* L.) and pine (*Pinus sylvestris L.*) were divided into two groups of one fifty individuals each. The two groups of each species were composed in order to have comparable sizes (about 45 to 60 cm for oaks, 40 to 55 cm for beech, and 30 to 40 cm for pines). Each group was assigned to a 2 x 2 x 0.5 m planter box installed outdoor. For each species, one of the planter box is equipped with one drain placed at its bottom, and the other one with two drains, aiming to introduce a difference in soil water content. The saplings were planted in February 2011 in a 2/3 compost and 1/3 sand mixture. Thorough the whole experiment, the 6 planter boxes were covered by a plastic tarp during strong rain

events, and were differentially irrigated in a way to introduce a difference in soil water content while avoiding severe stress.

2.2.Measurements

2.2.1. Canopy scale measurements

The six planter boxes are disposed under a 3 to 5 m adjustable height galvanized steel pipe greenhouse structure. Two cross bars of the greenhouse structure directly above the center of each planter box were used for attaching optical fibers. Six fibers (Numerical aperture 0.37, core diameter 200 µm, field of view 43.4°, Thorlabs, Inc., USA) are pointing downwards to collect reflected radiation from each planter box. The whole setup height was adjusted so that the distance between the optical fibers and the planter boxes soil is 2.5 m, allowing each fiber's field of view to cover approximately 1.90 m in diameter at ground level. Each fiber's field of view and alignment was checked at the start of the experiment, and the effective field of view diameter at canopy-level for the oak, beech and pine were respectively 1.42 m, 1.53 m and 1.6 m. One optical fiber is directed towards the sky and equipped with a cosine corrector (Ocean optics, IL, USA) is mounted on top of the structure and is used for measurements of incident photosynthetically active radiation (PAR). Another fiber is pointing downward at 7 cm from a Spectralon reference panel (spectralon 99%, 25 cm * 25 cm, Labsphere, Inc., USA), collecting the reflected upwelling irradiance. The Spectralon reference panel is located just next the planter boxes and positioned at about 1.5 m height at the same level than the top of tree-canopy. All optical fibers are connected to a 16 input ports optical multiplexer (MPM2000, OceanOptics, IL, USA). The 8 unused input ports were masked and used to measure dark noise (instrumental noise) associated with each used input port. The output port is connected to a spectrometer (USB2000 + 350-1100 nm, ~ 0.3nm at FWHM - full width at half maximum, OceanOptics, IL, USA). The whole optical setup was calibrated for radiance measurements (w/nm/m²) using a calibration lamp (HL-2000 CAL, OceanOptics, IL, USA) connected at the end of each fiber. The multiplexer and the spectrometer are interfaced using a Visual Basic script under OOIBase32 software (OceanOptics, IL, USA). The interfaced spectrometer and multiplexer were programmed to scan each input port sequentially. When the multiplexer settle on an incoming fiber port, the signal versus noise ratio is checked, and when needed, the spectrometer integration time is adjusted.

PAR is computed from radiance data acquired over the spectralon panel and the cosine corrector by integrating the radiance spectra over the 400-700 nm interval. Reflectance of each planter box is computed as the ratio between reflected radiance from each planter box and the radiance reflected by spectralon. The reflectance spectra were then used to compute three spectral indices:

- The canopy NDVI (Normalised Difference Vegetation index) as an indicator of canopy structure dynamics using the following formula :

$$NDVI = \frac{(R_{800} - R_{650})}{(R_{800} + R_{650})} \qquad \text{(Eq.1)}$$

where R_{800} and R_{650} stands for the leaf reflectance integrated over a 40 nm and 20 nm wavelength bands centered on 800 nm and 650 nm, respectively.

- The canopy $mNDI_{705}$ (modified Red-edge Normalized Difference index) as an indicator of canopy chlorophyll content which is calculated to the following formula given in Sims and Gamon (2002):

$$mNDI_{705} = \frac{(R_{750} - R_{705})}{(R_{750} + R_{705} - 2 * R_{445})} \qquad \text{(Eq.2)}$$

where R_{445}, R_{705} and R_{750} stands for the reflectance spectrum integrated over a 25 nm waveband centered on 445 nm, 705 nm and 750 nm, respectively.

- The canopy PRI calculated using the following formula:

$$PRI = \frac{(R_{531} - R_{570})}{(R_{531} + R_{570})} \qquad \text{(Eq.3)}$$

where R_{531} and R_{570} stands for the leaf reflectance integrated over a 10 nm wavelength band centered on 531 nm and 570 nm, respectively.

Soil water content was monitored in the six planter boxes over the whole soil profile in an access tube installed near the center of each box. Measurements were done weekly every 5 cm using a PR2 soil moisture profile probe (Delta-T Devices, UK). The PR2 measurements were calibrated for volumetric humidity over ten 250 cm^3 soil samples for each box (total of 60 samples).

2.2.2. Leaf scale measurements

From leaf maturation to leaf senescence from Doy 197 To 250, in order to estimate leaf LUE, 9 measurement campaigns of photosynthesis were done for oak and 6 for beech

respectively, using a LICOR 6400 (LICOR, Lincoln, Nebraska USA) with the 6400-40. All measurements were done in open flow, under a PAR adjusted to the incident PAR using the LICOR quantum sensor. In each planter box, twenty sun leaves were chosen and measured repeatedly from 9 am to 8 pm. Each leaf is measured 5 times per day in average.

It is important to notice that no LUE measurements were done in Scots pine plots for practical reasons (instrumental limits). Nevertheless, in order to compare the three species, temporal variability of PRI responses to PAR and canopy structure and biochemistry was analyzed.

2.2.3. Data analysis.

At canopy scale and on daily basis, canopy PRI vs. PAR (canopy PRI light curves) were analyzed using a non-linear regressions described below:

$$PRI(t) = a_j + b_j * erf\left(\frac{PAR(t)}{c_j}\right) \qquad \text{(Eq.4)}$$

$$erf(PAR(t)/c_j) = \frac{2}{\sqrt{\pi}} \int_0^{PAR(t)/c_j} e^{-z^2} dz$$

with a, b, and c three parameters determined on a daily basis using mean square minimization, and erf the Error Function described above. The rate of xanthophylls deepoxidation as well as the change in absorbance around 505 nm which are associated with changes in PRI was shown to vary in a gaussian way with changes in light intensity (Takizawa et al. 2007). Therefore, the use of the Erf function which is a gaussian integral between 0 and x may be able to account for the continuous regulation process of the xanthopyll cycle between a PAR value of 0 and x.

This model allows the direct retrieval of the PRI_0, which is the parameters a, of the full ranges of PRI variation which is the parameters b, and of the saturating PAR values, which is the parameters c.

PRI time series at seasonal scale were analyzed using the following non-linear model:

$$PRI\ (t) = d * mNDI_{705}(t) + e + f * Erf\left(\frac{PAR(t)}{(g*RH(t)+h)}\right) \qquad \text{(Eq.5)}$$

with RH the soil moisture content. d, e, f, g and h are the fitted parameters of the model at seasonal scale. The model goodness of fit was assessed using its R^2 and the observations versus predictions. Significance level was fixed at 5%.

At leaf scale, LUE versus PAR relationships were established on a daily basis using the LICOR measurements in order to describe canopy ecophysiological functioning. A non-rectangular hyperbola model (Thornley 1998), modified in order to express the A_{max} (maximum photosynthesis) and θ (maximum photosynthesis efficiency) parameters as function of canopy $mNDI_{705}$ and soil moisture content, was fitted on those relationships.

Photosynthetic assimilation is expressed as follows:

$$A = \frac{PAR * A_{max} * \theta}{\theta * PAR + A_{max}} + R_d \qquad \text{(Eq.6)}$$

With A_{max} and θ expressed as follow:

$$\theta = k * mNDI_{705} + l$$

$$A_{max} = m * mNDI_{705} + n * RH_{soil} + p$$

k, l, m, n and p are fitted parameters. The LUE is then calculated as.

$$LUE = \frac{A}{PAR}$$

For days between measurement campaigns, the LUE is estimated using the above-described model and measured PAR, soil moisture content and $mNDI_{705}$.

3. Results

3.1. Seasonal variability of soil water content, canopy structure, biochemistry and functioning

The seasonal dynamic of the NDVI, the $mNDI_{705}$ and the soil water content are shown in Figure 1.

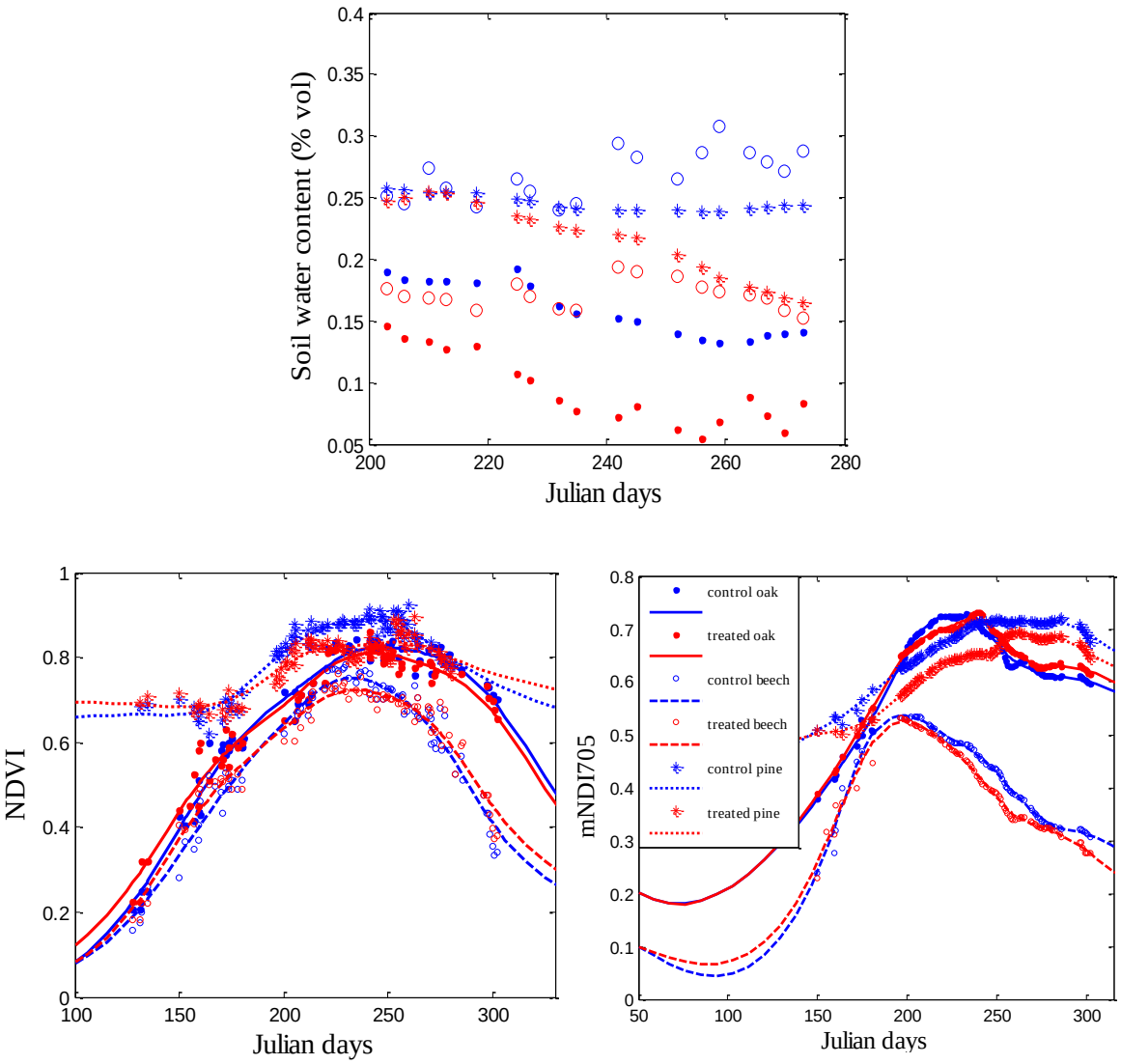

Figure 1: 1.a- seasonal dynamic of soil water content at 30 cm depth, 1.b- canopy NDVI, 1.c- $mNDI_{705}$. blue for control plots, and red for treated plots; points for oak, empty circles for beech, and stars for Scots pine..

Temporal dynamics of soil water content showed in Figure 1.a exhibit an increasing difference between control and treated plot through the whole period experiment for the three species. The difference appears particularly after the start of the rain exclusion (Doy 219).

Temporal dynamics of canopy NDVI showed in Figure 1.b show an increasing trend until Doy 220 to reach a plateau and then a decreasing trend starting from Doy 265 in deciduous oak and beech plots. In Scots pine plots, The NDVI exhibit a continuous increase until Doy 245, then a slight decrease in pine. The NDVI is relatively stable between DoY 190 and DoY 280.

The $mNDI_{705}$ showed in Figure 1.c exhibits different patterns than NDVI. Moreover, these patterns and their magnitude differ between species. In oak plots, $mNDI_{705}$ shows a slight increase from the beginning of the study to Doy 220, coinciding with the beginning of NDVI increase. Then, $mNDI_{705}$ decreases slowly while the NDVI remain stable. On the other hand, in beech plots, $mNDI_{705}$ is lower and exhibits a linear decrease through the whole experiment period. No significant differences can be seen between control and treated plot for oak and beech species. In Scots pine, there is a linear increase in mNDI705 through the experiment period, and a significant difference can be seen between control and treated plots, following the same pattern as the NDVI.

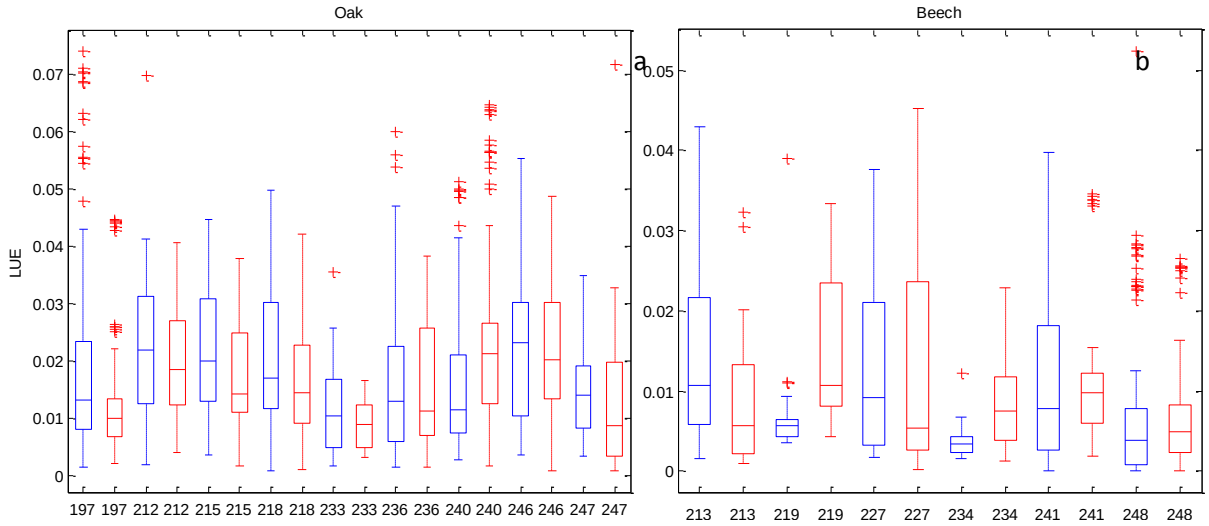

Figure 2: seasonal dynamic of mean leaf LUE (µmol CO_2/µmol photon) in oak (2.a) and beech (2.b) (blue boxes in control and red boxes in treated plots). The center of each box is the median and bounds correspond to the median 95% confidence interval.

Leaf LUE shown in Figure 2 exhibit non-significant differences between control and treated plots for the both species ($P > 0.05$) except for measurements achieved in Doy 219 and Doy 234 in beech, ($P < 0.01$ and $P < 0.04$, respectively). Moreover, temporal patterns of LUE over the whole experiment period are similar for the two species. We notice that these patterns were different than those of soil water content, NDVI and $mNDI_{705}$ as shown Figure 1.

Canopy PRI variations over the whole experiment period are shown in Figure 3. PRI exhibits a high daily dispersion. While the PRI increase until DOY 220 in oak and 240 in pine, the beech PRI show a linear decrease through the whole experiment. Those patterns are highly similar to those observed in $mNDI_{705}$, as shown in Figure 1.

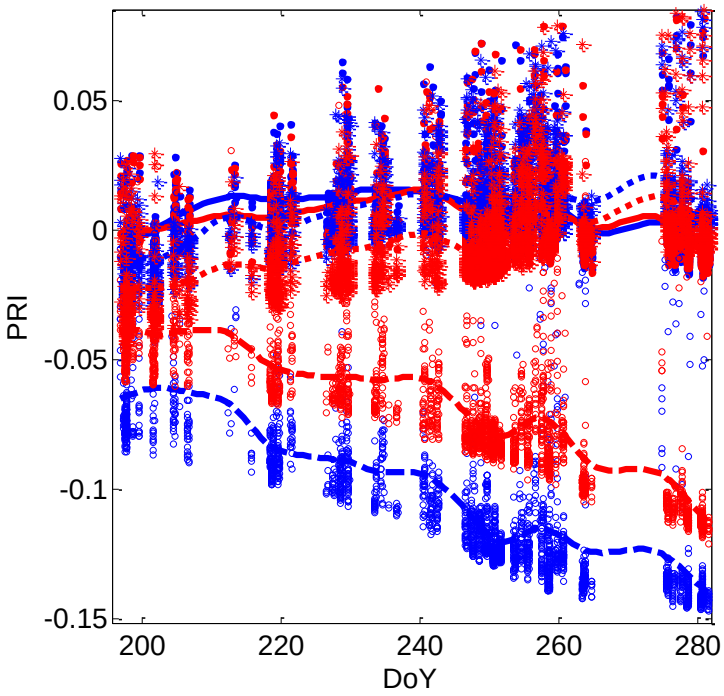

Figure 3: PRI over the whole experiment period for the three species (blue symbols stands for control plots, and red symbols for treated plots; points for oak, circles for beech and stars for Scots pine). (Number of reflectance spectra used in PRI calculation is of about 5000 samples par species and treatment).

3.2. Canopy physiological and optical responses to PAR variations

The canopy ecophysiological responses to environmental factors were described for each measurement campaign using daily light-curves. Figure 4.a shows these curves over the whole experiment period. For days between measurements campaigns, LUE versus PAR relationships are interpolated following the procedure described in Materials and Methods section (Eq.6).

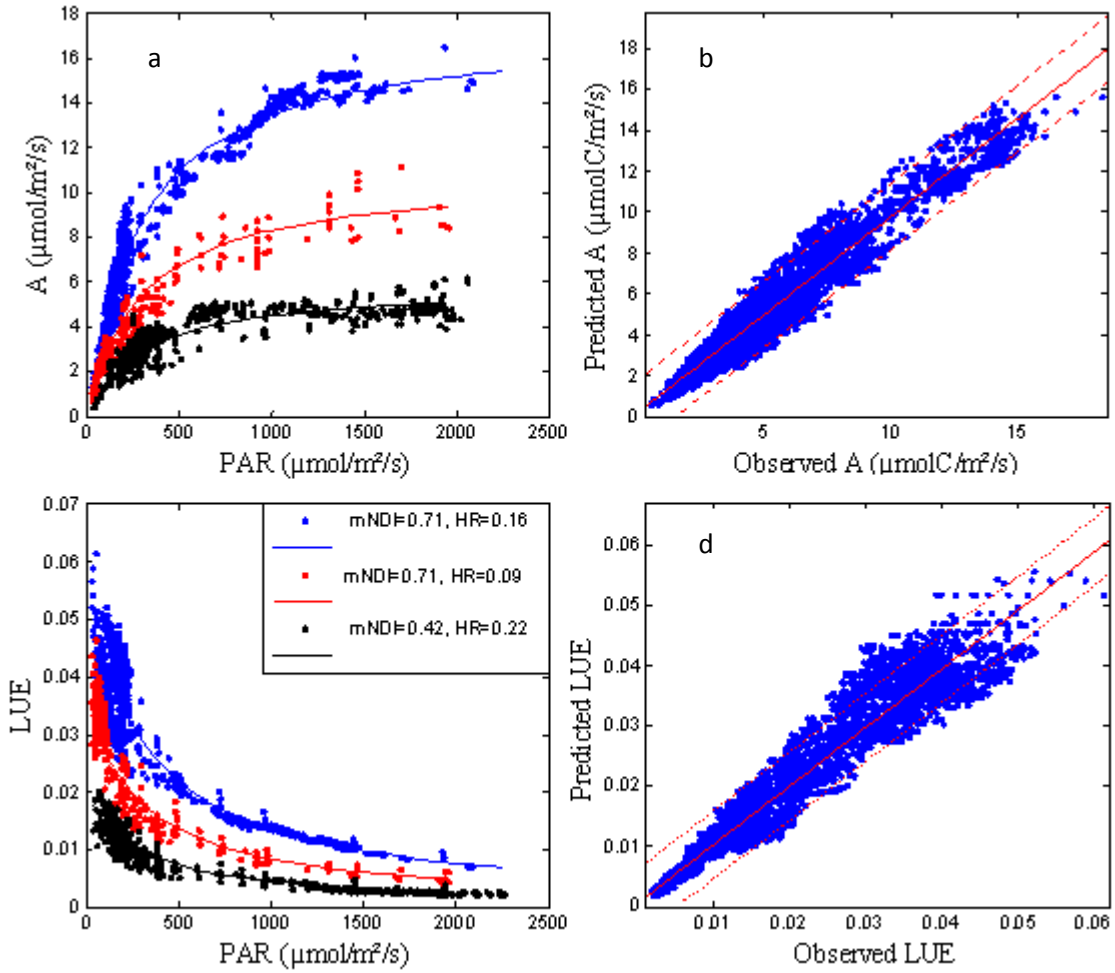

Figure 4: 4.a – Examples of A versus PAR relationships (measurements (dots), and model (line)) and 4.b- Observed versus predicted .4.c- Examples of LUE versus PAR relationships (measurements (dots), and model (line)). 4.d- Observed versus predicted LUE. Three different series over beech planter boxes are represented, covering a wide range of $mNDI_{705}$ and soil moisture content. (R^2 range from 0.67 to.0.98 for LUE versus PAR).

Daily PRI versus PAR light curves were fitted as described in the Material and methods section (Eq. 4). These relationships are illustrated in Figure 5. Residuals distribution were checked, and outliers outside two standard deviations (15% of the whole dataset, N=4457) were excluded from all the following analysis.

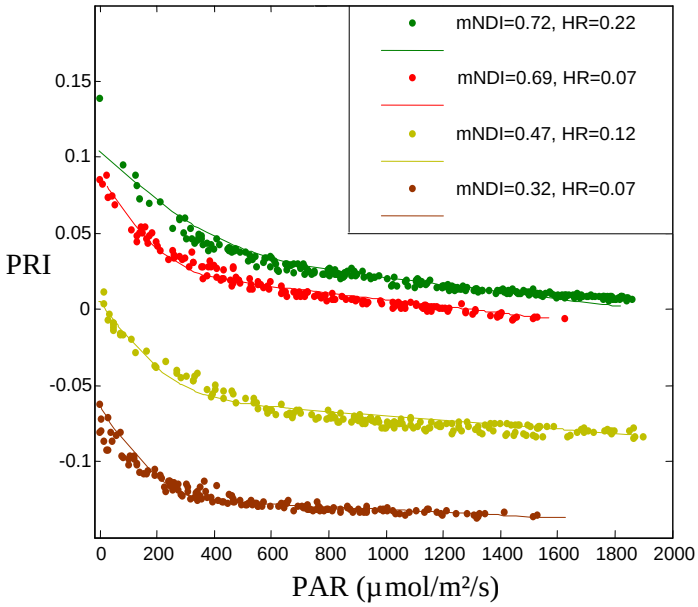

Figure 5: Examples of daily fitted PRI light curves under varying soil moisture content and leaf $mNDI_{705}$.

3.3. Analysis of PRI vs PAR relationships

Estimated parameters (PRI_0, PRI range and saturating PAR) of Eq.4 which expresses PRI variability at daily scale shown above (Fig. 5) were analyzed using simple linear regression with NDVI, $mNDI_{705}$ and soil moisture content. Results of regressions are shown in Table 1.

	PRI_0	PRI range	Saturating PAR
NDVI	R^2=0.1, p>0.08	R^2=0.02, p>0.37	R^2=0.01, p>0.42
$mNDI_{705}$	R^2=0.92, p<0.001	R^2=0.04, p>0.17	R^2=0.03, p>0.33
Soil moisture content	R^2=0.02, p>0.22	R^2=0.02, p>0.34	R^2=0.88, p<0.001

Table 1: Simple linear regression goodness of fit (R^2 and P-value) with NDVI, $mNDI_{705}$ and soil moisture content as explanatory variables (lines) and the PRI_0, PRI range and saturating PAR (columns). Data are pooled over all species and all treatments.

While the NDVI did not seem to be linearly correlated to any of the estimated parameters, the $mNDI_{705}$ is a good estimator of the PRI_0, and the soil moisture content is correlated to the saturating PAR. On the other hand, the PRI range was not correlated with any of the explicative variables, and exhibits low variability over the whole experiment (mean

value = 0.072, standard deviation = 0.0056). Relations between these variables are shown in Figure 6.

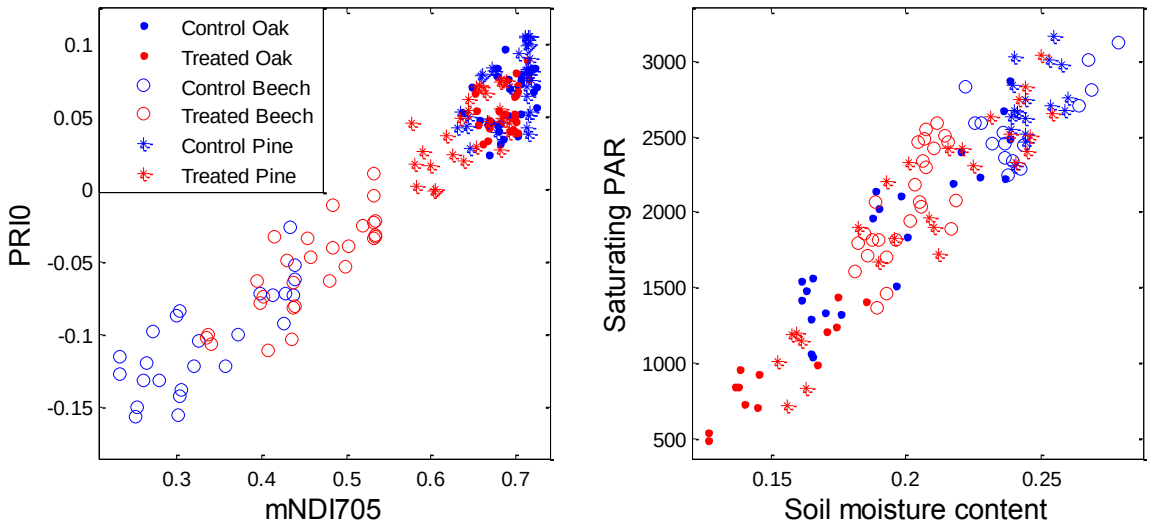

Figure 6: relationships between PRI_0 and $mNDI_{705}$ (left), and between the saturating PAR and soil moisture content (blue symbols for control plots, and red symbols for treated plots; points for oak, empty circles for beech, and stars for pine plots).

Since measurements show that the PRI_0 and the saturating PAR were linearly correlated with the $mNDI_{705}$ and the soil moisture content (Figure 6), respectively, the PRI model (Eq. 4) described in the Materials and methods section used at daily basis was modified in order to build a generic model at seasonal scale following Eq. 5 by replacing the two parameters PRI_0 and saturating PAR by their expressions as linear functions of $mNDI_{705}$ and soil moisture content, respectively. The range (parameter c in Eq.5) was kept as a parameter in the generic model. This generic model allows expressing PRI as a continuous function of PAR, soil moisture content and $mNDI_{705}$. The expression of the generic model is given in Eq. 5.

The parameters of this generic model were estimated using the whole dataset over the whole experiment period and over all species and treatments. The measured versus predicted PRI are shown in Figure 7.

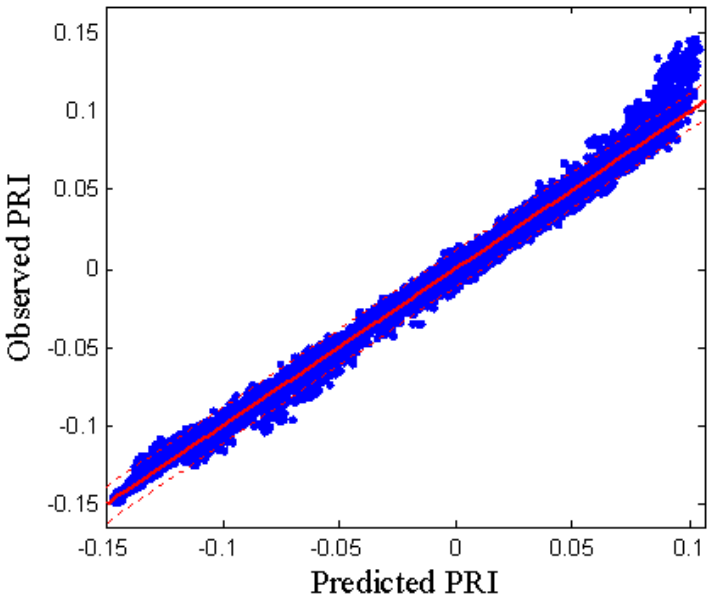

Figure 7: Measured versus predicted PRI over the whole experiment period using the generic model (Eq.5) applied on the whole dataset (without distinction between neither species nor treatments).

The model R^2 over the whole experiment (N=19412) was 0.98, and the model RMSE was 0.0058, accounting for 6.9% of the estimated daily PRI range.

The regression statistics are summarized in Table 2.

	Oak	Beech	Pine	Whole dataset
R^2	0.84	0.94	0.85	0.98
RMSE	0.0095	0.0098	0.0097	0.0058
RMSE/daily range	12.5%	16.4%	12.9%	6.9%

Table 2: PRI model goodness of fit over each species and over the whole dataset. RMSE/daily range corresponds to the ratio between RMSE and the parameter f in Eq.5.

We note that there are no significant differences in parameters between species.

3.4. Deconvolution of PRI variability

In order to disentangle the effects of pigment content, PRI_0 expressed as a linear function of $mNDI_{705}$ in the generic model fitted above was subtracted to PRI to obtain a

corrected PRI called PRI_c hereafter over the whole season. Temporal patterns of PRI, PRI_c and LUE for the full range of PAR are shown in Figure 8.

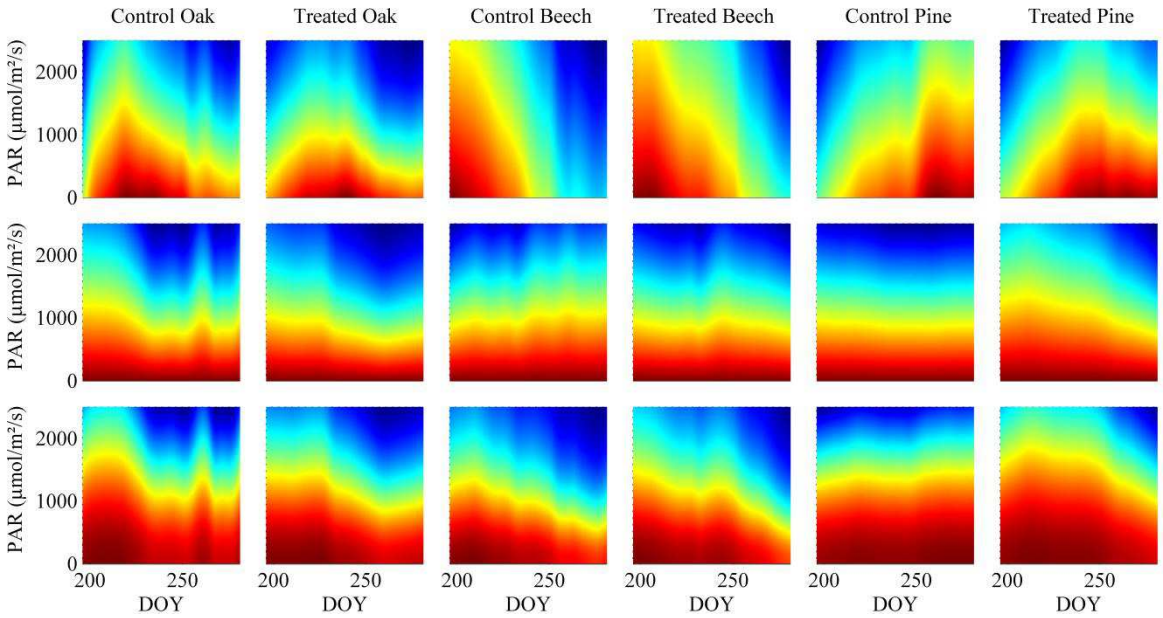

Figure 8: Surface plots of PRI from the generic model Eq.5 (upper line), corrected PRI (PRIc) after subtracting PRI0 (middle) and LUE (bottom line) for each experimental plot, over the full range of PAR and the whole experiment duration. To facilitate the reading of these figures, the three variables were standardized. Hot colors correspond to the maxima of each planter box and cool colors to the minima.

Figure 8 shows different patterns between species and treatments. After correction, patterns of PRIc and LUE become similar. This indicates that much of the PRI pattern is explained by leaf pigment content and that a residual part depends on the canopy physiological functioning. This is particularly the case in beech and pine.

Relationships between PRI, PRI_c and LUE are shown in Figure 9. Note that in this figure, only PRI measurements are used.

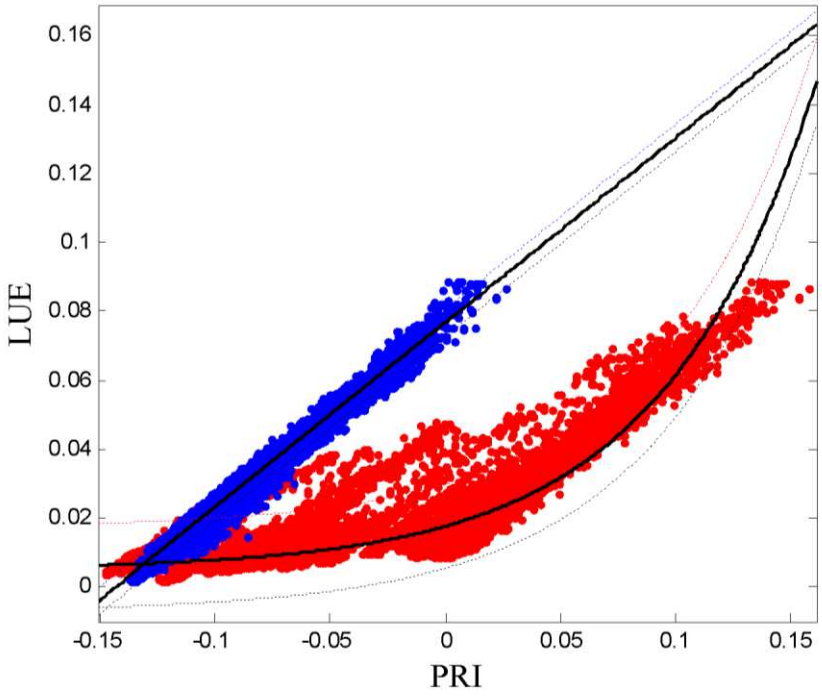

Figure 9: PRI and PRI_c versus LUE. Red symbols stand for uncorrected PRI, blue symbols stand for corrected PRI after subtraction of PRI_0. PRI and PRI_c based on measurements (N = 19412)

As also shown in Fig. 9, the PRI exhibits two distinct point clouds, the upper one being data acquired on oak and pine planter boxes and the lower one being data acquired on beech. PRI and LUE are exponentially related (R^2=0.77, P < 0.001, RMSE=0.0062) but residuals are non-uniformly distributed (P < 0.001). On the other hand, PRI_c and LUE are highly correlated (R^2=0.97, P < 0.001, RMSE=0.002), and residuals are normally distributed (P > 0.22). Note that this relationship between PRI_c and LUE does not depend on species or treatment.

4. Discussion

The six experimental plots corresponding to sapling of three different species (oak, beech and pine) were submitted to two different water statuses. As shown in Figure 1.a, differences in soil water statuses between species can be seen through the whole experiment. Differences can also be seen between control and treated plots starting from DOY 219. A wide range of soil water contents (from 5% to 35%) were therefore investigated. Punctual soil watering by irrigation introduced peaks in soil water content which can be seen, particularly in control plots.

The experiment spanned from the end of the sharp NDVI increase due to green-up to the start of the sharp drop in NDVI due to leaf senescence in deciduous species. In Pine plots,

NDVI shows a continuous increase until DOY 245 due to green-up and then a slight decrease which is probably due to lower branch needle shedding observed at the middle of summer. Small differences in NDVI between control and treated plots in deciduous species can be seen in Figure 1.b. A pronounced difference between pine control and treated plots can be seen around DOY 240, which may be due to the effects of drought.

As shown in Figure 1.c, the $mNDI_{705}$ which is used as a proxy of leaf chlorophyll content (Sims et al. 2002) exhibit different patterns between species, and low differences between control and treated plots. While beech plots exhibit a linear decrease in $mNDI_{705}$, oak plots exhibit an increase until DOY 220 to reach a plateau and then a linear decrease from Doy 240. This observation is in agreement with Damesin et al. 2003 which shows that in beech, leaf chlorophyll per area concentration sharply increases at the start of budburst and then decreases. In pine, the $mNDI_{705}$ exhibits a steady linear increase which can be explained by the formation of new cohorts of needles. Differences in trends between $mNDI_{705}$ and NDVI suggest that these two indices bring different information during the experiment.

As shown in Figure 2, measured leaf LUE exhibit a slight seasonal pattern which cannot be explained solely by soil water content, LAI or $mNDI_{705}$. This pattern is similar for both deciduous species (oak and beech) and is mostly explained by PAR variability due to bad weather around DOY 230. Daily LUE variability is of the same order of magnitude than the seasonal variability.

The measured LUE showed a decrease with increasing PAR following an asymptotic pattern at high PAR values. The saturating PAR value varies with the DOY according to both leaf chlorophyll content and soil water content as reported in Ogaya et al. 2003 and Xu et al. 2003. As observed on the LUE measurements (Figure 2), the resulting overall seasonal variability is of the same order than the daily variability. Both seasonal variability, linked to leaf chlorophyll content and soil moisture content, and daily variability due to PAR could be reproduced accurately as shown in Figure 4.

The measured PRI shown in Figure 3 exhibits strong daily variability and strong seasonal patterns that differ between species. While oak and pine measurements do not significantly differ in both PRI level and PRI seasonal dynamic, beech PRI is significantly lower through the whole experiment. While those seasonal trends as well as differences between species cannot be compared to those seen in LUE (Figure 2), they are similar to those observed in $mNDI_{705}$ (Figure 1.c). These results are comparable to those showed at leaf scale in Hmimina et al. 2013b, and suggest a strong sensitivity of PRI to leaf pigment content, as

shown in Moran et al. 2010, Rahimzadeh-Bajgiran et al. 2012 and Gamon and Berry 2012. In order to determine the impact of this sensitivity, leaf pigment and LUE related PRI variability must be disentangled.

PRI measurements were then fitted on a daily basis for each plot. The model described in the Materials and method section provides three biologically relevant parameters: the PRI_0, as defined in Hmimina et al. 2013b, the maximum daily PRI range, and the saturating PAR value. The linear correlations between those parameters and the NDVI, the $mNDI_{705}$, and the soil moisture content are summarized in Table 1. The PRI range exhibited very low variability, which can be explained by the absence of noticeable change in total xanthophylls pool size (Gamon & Surfus, 1999). The saturating PAR value was highly correlated to soil water content. The $mNDI_{705}$ versus PRI_0 and soil moisture content versus saturating PAR values are shown in Figure 6. As reported at leaf scale in Gamon and Berry (2012) and in Hmimina et al. 2013b, two distinct component of PRI variability can therefore be distinguished:

- A physiological component explained at daily scale by the PAR, and at seasonal scale by soil moisture content variability.
- A structural component explained at seasonal scale by the $mNDI_{705}$.

Since these relationships at canopy scale between PRI_0 and $mNDI_{705,}$ and between saturating PAR and soil moisture content are strong and linear across species and treatments, a generic PRI model integrating these variables was designed and fitted to each species, and to the whole dataset (Table 2). The parameters of this generic model relating $mNDI_{705}$ and soil moisture content to PRI_0 and saturating PAR respectively are not significantly different from those obtained using specific models in Figure 7. The generic model can therefore be used to deconvolve the PRI variability due to physiological response to PAR from variability due to leaf pigment content over the whole experiment.

Temporal variability in PAR vs PRI, PAR vs PRIc and PAR vs LUE relationships shown in Figure 8 exhibits strong discrepancies between PRI and LUE, which could be greatly alleviated by subtracting the estimated PRI_0. We may conclude that PRI would not be an accurate LUE proxy without taking into account canopy biochemical properties. Indeed, canopy chlorophyll content variability may leads to non-functional relationship when chlorophyll content incidentally matches LUE seasonal pattern.

This strong sensitivity of PRI versus LUE relationship and leaf pigment content may explain the observed variability in PRI versus LUE relationship strength between sites, and across different temporal resolution scales as shown in Grace et al. (2007) and Garbulsky et al. (2011). Spatial and temporal changes of leaf pigment content may mask the physiological related PRI variability and this effect may be amplified at low temporal resolution (high leaf pigment content variability between observations) and high PAR (low LUE variability).

In fact, while the relationship between the PRIc and the LUE shown in Figure 10 is strong and unique across all plots, the relationship between PRI and LUE is poorer and non-linear. This PRI vs LUE relation is mainly due to the strong PRI_0 variability in beech, as well as differences in PRI_0 level between species.

Moreover, the PRI versus LUE relationship exhibit a non-linear pattern, similar to those previously reported (Garbulsky et al. 2011), while PRIc versus LUE relationship is clearly linear. The reported non-linearity of PRI versus LUE relationship reported in Garbulsky et al. 2011 for deciduous species (Nichol et al. 2000, Nakaji et al. 2008) and combined sites may therefore be due to the shift in PRI versus LUE relationship due to leaf pigment content changes.

5. Conclusion

In concordance with previous study at leaf scale, the PRI was shown to be a composite signal, varying with both LUE (facultative variability) and leaf pigment content (constitutive variability). The PRI exhibits different seasonal patterns than the measured LUE. While the LUE seems to be mostly driven by the PAR at the seasonal scale, the PRI dynamic differ significantly between species, and exhibit features similar to the dynamic of leaves pigment content.

The high temporal resolution and high dynamic range of the setup described in this work allowed to describe PRI changes under a broad range of PAR. The PRI_0 was therefore precisely estimated and could be related to the $mNDI_{705}$, used as an indicator of leaf pigment content changes. Moreover, the range of daily PRI variation, of PRI facultative change, was shown to be constant in each species and treatment, and the saturation PAR was shown to be correlated to the soil water content. This description of PRI variability enabled us to design a

continuous seasonal scale model which was shown to be able to reproduce accurately seasonal PRI variability.

The continuous PRI model was used to interpolate the PRI measurements in order to describe the PAR-related, and pigment related temporal patterns, and to disentangle the constitutive and facultative PRI variability. The obtained PRI_c, calculated as the measured PRI minus estimated PRI_0, was shown to be highly correlated to the interpolated LUE. Moreover, while the relationship between PRI_c and LUE is clearly linear, the relationship between the mostly pigment-related PRI and the LUE is exponential, as reported in previous studies. The observed PRI versus LUE relationships may therefore be strongly affected by temporal and spatial of LAI and leaf pigment content. Their use over broader scales may lead to inaccurate estimation of LUE.

The described continuous model may be usable over broader scales, but require the use of reliable proxy of the canopy pigment content, and water availability. The described daily-scale PRI light-curve analysis may also be used in order to provide a coarser estimation of the PRI_0, but may require a high temporal resolution, and reliable PRI measurements in low light. Moreover, while these methods were shown to be able to deconvolve the LUE and the pigment-related PRI variability, the effect of different and varying canopy structures were not assessed in this work. The PRI potential as a LUE proxy, before and after deconvolution, need to be assessed over broader temporal and spatial scales, over forest exhibiting different structural properties, and under varying climatic constraints.

Chapitre 3. Tower-based photochemical reflectance index measurements to assess light-use efficiency in deciduous and evergreen broadleaf forests

Kamel Soudani[a*], Gabriel Hmimina[a], Eric Dufrêne[b], Daniel Berveiller[b], Nicolas Delpierre[a], Jean-Marc Ourcival[c], Serge Rambal[c], Richard Joffre[c].

[a] University of Paris-Sud, UMR CNRS, AgroParisTech, Université Paris Sud. Laboratoire Ecologie Systématique et Evolution, Faculté des Sciences d'Orsay, France.

[b] CNRS, UMR CNRS, AgroParisTech, Université Paris Sud. Laboratoire Ecologie Systématique et Evolution, Faculté des Sciences d'Orsay, France.

[c] CNRS, Centre d'Ecologie Fonctionnelle et Evolutive, Montpellier, France

Abstract

In this study, we evaluate the relationships between the photochemical reflectance index (PRI) and light-use efficiency (LUE) based on continuous *in situ* measurements acquired on a half-hourly basis for PRI, NDVI (Normalized Difference Vegetation Index) and net CO_2 exchange data in two deciduous and evergreen mature forests. Eight years of simultaneous measurements of PRI, NDVI and carbon and water fluxes and the main micrometeorological variables are analyzed in this study. More specifically, the objectives of this study include investigating the daily, seasonal, and interannual variations of PRI and LUE; linking PRI variations to the main influencing meteorological and eco-physiological variables; and evaluating the performance of PRI as a remote-sensing proxy of LUE under different environmental conditions. Two mature forests, Fontainebleau and Puéchabon, (FR-Fon and FR-Pue; www.fluxnet.ornl.gov) that differ mainly in their vegetation types and climates are evaluated in this study. The first one, located southeast of Paris, corresponds to a temperate forest representative of the main deciduous broadleaf forest type in Europe. The second forest,

located in southern France, is characteristic of the evergreen Mediterranean oak forest. On a seasonal scale, the temporal patterns of PRI and NDVI were similar, demonstrating that the temporal changes of PRI are primarily controlled by temporal changes in phenology, which affect both the structure and biochemical properties of canopies. At shorter time scales and in the stable total canopy leaf area during summer, the short-term variations of PRI were greater than those in the NDVI, suggesting that these two indices are relatively independent and provide different information. On a seasonal scale, statistical analyses revealed positive relationships between PRI and absorbed photosynthetically active radiation (aPAR) and negative relationships between PRI and LUE. Over shorter periods of a few days, the signs of these relationships remained unchanged; however, their correlations were strongly improved. The highest correlations were most often observed over periods characterized by clear or slightly overcast skies. However, all the periods of clear skies did not involve improvements in the relations of PRI vs. aPAR or PRI vs. LUE. Temporal variations of the intercept (called PRI_0 in this study) of PRI vs. aPAR regressions suggest the presence of a temporal trend that may reflect seasonal changes of the biochemical characteristics of the canopy. Regardless of the cause of this trend, it is important to note that once PRI_0 was subtracted from the measured PRI, the relationships between the corrected PRI and LUE for each year were significantly improved, and a stable multi-year model was obtained. Nevertheless, further studies are required to explain the temporal changes of PRI_0 during the season and to develop a more accurate disentangling approach that would make PRI-based remote-sensing of ecosystem light-use efficiency less sensitive to spatial and temporal changes in the structural and biochemical properties of the canopy.

1. Introduction

Forests are subjected to climate events with different intensities. Severe droughts can cause significant effects such as leaf discoloration, leaf browning, and early leaf loss (Carnicer et al. 2011; Bréda, 2006). The effects may lead to a decrease of forest productivity and a higher vulnerability to fire and to the proliferation of devastating opportunistic pathogens in the following years (La Porta et al. 2008). Under moderate water, temperature (heat), or light stress, the effects are not as significant; however, the physiological state of the trees, the water use, and carbon exchanges may be significantly affected. Under such environmental conditions, the available energy exceeds the capacity of the utilization of light in photosynthesis and the excess of energy is dissipated as fluorescence and heat according to many mechanisms, which are grouped under the generic term of non-photochemical quenching (NPQ) (as opposed to the photochemical processes involved in photosynthesis). As highlighted by Ort (2001), most plants encounter an excess of available energy and NPQ constitutes a short-term response by which plants dissipate excess energy as heat (Szabo et al. 2005; Li et al. 2009). The most important mechanism involved in NPQ processes is associated with changes in the composition of carotenoid pools known as the "xanthophyll cycle". Under excess light energy, violaxanthin (V) is converted into antheraxanthin (A) and then into zeaxanthin (Z) by losing a first and a second oxygen atom, respectively (Demmig-Adams & Adams, 1996). For this reason, the ratio between epoxidized forms of (Z + A) and the total pool of xanthophyll pigments (Z + A + V) is often used as an empirical approximation of the general state of the de-epoxidation of the xanthophyll cycle and the intensity of NPQ (Holt et al. 2005; Yamamoto, 2006). When light conditions become non-saturating, the concentration of zeaxanthin decreases according to the reverse process by epoxidation of zeaxanthin to antheraxanthin and violaxanthin. These reactions are fast (Jahns & Holzwarth, 2012) - a few minutes - and are used by the plant to respond to changes in light conditions above and within the canopy. Changes in the concentration of xanthophylls are accompanied by changes in light absorption in a narrow band between approximately 535 nm and 505 nm (Morales et al. 1990; Pfündel and Bilger, 1994) and in reflectance at approximately 531 nm (Gamon et al. 1992, 1997). Gamon et al. (1992, 1997) developed the photochemical reflectance index (PRI) from the narrow-band reflectance at 531 nm and a reference band at 570 nm – assumed to be insensitive to variations in the concentrations of xanthophylls – and suggested using this index as a remotely sensed proxy to track changes in the xanthophyll cycle pigment content at the leaf scale and to predict the light-use efficiency (LUE) for many herbaceous and woody

species (Gamon and Surfus, 1999; Sims et Gamon, 2002). These works laid the basis for the direct estimation of the ecosystem LUE from space.

Remote sensing is a powerful tool that provides important information concerning the structure and functioning of forest ecosystems due to its unique potential in terms of spatial and temporal resolutions. The potential use of this tool was mainly evaluated to monitor the temporal change of the forest canopy structure when this change is accompanied by significant variation in the amount of green leaf biomass or in the chlorophyll content. However, there are still limited studies that focus on the evaluation of remote sensing to monitor the ecophysiological responses at the canopy scale. It may be noted that LUE-based models of gross primary production (GPP) (Hilker et al. 2008) such as the MODIS GPP model (Turner et al. 2006), Glo-PEM (Prince and Goward, 1995), and CASA (Potter et al. 1993) applied at regional and global scales using remote-sensing data do not explicitly account for the large variations in LUE at short time scales. In the MODIS-based GPP approach, a constant biome-specific maximum LUE is used, and short-term temporal variations of this parameter are implicitly considered using modulation factors that depend only on the VPD (vapor pressure deficit) and air temperature. This type of modulation may be insufficient to account for the effects of the soil water deficit on GPP because meteorological and edaphic factors are decoupled at short time scales (Turner et al. 2005; Pan et al. 2006; Hwang et al. 2008). The explicit consideration of these effects in the model may be necessary, as suggested by Gebermichael & Barros (2006) and Mu et al. (2007).

The pioneering works of Gamon and colleagues (Gamon et al., 1992, 1997; Penuelas et al. 1995; Fillela et al. 1996) demonstrated that it is possible to track short-term changes in LUE at the leaf and canopy scales by clearly demonstrating the sensitivity of PRI to the photosynthetic activity due to variations in environmental conditions. At the canopy scale, especially above complex structures such as forests, recent studies have reported contrasting results, highlighting the combined effects of exogenous factors, especially solar and viewing angles, and the structural and biochemical attributes of the canopy. Using MODIS bands, Drolet et al. (2005, 2008) observed good relationships between PRI and LUE in the back-scattering direction (relative azimuth angle - difference between the sensor and sun azimuth angles < 60°) and under a relative zenith angle (difference between the sensor and sun zenith angles) less than 10° and explained these results based on the lower proportion of shaded leaves compared with the forward-scattering direction. Hall et al. (2008) and Hilker et al. (2009) showed the strong dependency of PRI on within-canopy light conditions and established two distinct relationships between PRI and LUE for sunlit and shaded foliage

surfaces, respectively. These authors explained these differences based on the changes in the xanthophyll cycle that lead to the decrease in LUE for the sunlit foliage surface exposed to strong light above a saturating point. Hall et al. (2008) noted that the PRI-LUE relationship is better for a sunlit foliage surface, confirming the findings of Gamon et al. (1997). The effects of illumination and viewing angle on the relationship between MODIS-based PRI and LUE were also highlighted by Goerner et al. (2009). The strongest relationships were obtained for viewing angles close to the nadir and in the range of 30-40° from the zenith. In addition to these factors, Goerner et al. (2009) noted the direct and indirect effects of atmospheric conditions that severely degrade the quality of the PRI signal and introduce bias in the relationships between PRI and LUE by restricting the LUE variability to a narrow range because only cloud-free MODIS images can be used.

The studies cited above highlight the difficulty in assessing the relationships between PRI and LUE at canopy scale. This is due to a multitude of factors that may influence the reflectance in PRI bands directly through the effects of biochemical and structural canopy characteristics, sun-view geometry and atmospheric conditions and indirectly through the xanthophyll cycle and thus canopy photosynthesis (light conditions, soil water content, VPD, temperature, etc.). In addition, it is still more complicated to achieve this task using satellite data because the spatial, temporal, and spectral data of the sensors available onboard spatial platforms are not optimal.

In this study, we evaluate the relationships between PRI and LUE from continuous *in situ* measurements of PRI and net CO_2 exchange data acquired on a half-hourly basis in two deciduous and evergreen mature forests in France. Eight years of simultaneous measurements of PRI and carbon fluxes are analyzed in this study. To the best of our knowledge, this data set is the longest time-series data set of *in situ* PRI measurements. Specifically, the objectives of this study involve the following: (1) investigating the daily, seasonal, and interannual variations of PRI and LUE; (2) linking the PRI variations to major influencing meteorological and eco-physiological variables; and (3) evaluating the performance of PRI as a remote-sensing proxy of the ecosystem LUE under different environmental conditions.

2. Materials and Methods

2.1. Study site

This study was undertaken in two mature forests (FLUXNET site codes: FR-Fon and FR-Pue; www.fluxnet.ornl.gov) differing in their vegetation types and climates. The first one, located near Fontainebleau (48°28'35"N/2°46'48"E) – southeast of Paris, corresponds to a temperate forest representative of the main deciduous broad leaf forest type in Europe. The forest stand is managed as mature deciduous forest occupied by two main overstory species of pedunculate and sessile oaks (*Quercus robur* L. and *Quercus petraea* (Matt.) Liebl) and a dense understory of coppiced hornbeam (*Carpinus betulus* L.). The age of the overstory is 150 years, and the average height is approximately 25 m. The leaf area index is approximately 5.5 m^2/m^2 on average. The elevation is approximately 90 m (a.s.l.), and the climate is a temperate climate characterized by an average annual temperature of approximately 11°C and an average annual rainfall of approximately 680 mm.

The second forest, Fr-Pue, the Puéchabon experimental forest, is situated in the south of France (43°44'29"N/3°35'45"E), 60 km northwest of Montpellier. Puéchabon forest is an evergreen broadleaf forest dominated by a dense overstory of holm oak (*Quercus Ilex* L.), the most typical tree of the Mediterranean climate. The age of the stand is 70 years, and the average height is approximately 6 m. The leaf area index is approximately 2.9 m^2/m^2. The elevation is approximately 270 m (a.s.l.), and the climate is Mediterranean with an average annual temperature of 13.4°C and an average annual rainfall of 907 mm. The climate is characterized by mild and wet winters and hot and dry summers, during which long periods of drought are frequent.

2.2. Flux and meteorological data

The measurements available were those usually made using the eddy covariance technique to estimate the net carbon exchange and latent and sensible heat fluxes between the forest ecosystem and the atmosphere. At the study site, these measurements include the net carbon exchange (*NEE*), the evapotranspiration (*ETR*), and the main bioclimatic variables (wind speed, incident, reflected and transmitted radiation, *VPD*, precipitation, air temperature, etc.). All these variables were recorded in the two forests at a half-hour time step.

The gross primary production (*GPP)* - the total amount of photosynthetic production of organic matter in the ecosystem - was calculated according to the CARBOEUROPE database standards (see Delpierre et al. 2012 for more details).

$$GPP\ (gross\ primary\ productivity) = NEE_{CO_2}(net\ ecosystem\ exchange) + ER\ (ecosystem\ respiration)$$

From the expression given in Kumar and Monteith (1981), the GPP can be expressed as

$$GPP = f_{PAR} \times PAR \times LUE_{maximum} \times \rho,$$

where PAR is the incoming photosynthetically active radiation used in the photosynthesis process, f_{PAR} is the fraction of PAR absorbed by the green canopy, $LUE_{maximum}$ is the maximum light-use efficiency, and $\rho \leq 1$ is the reduction factor used to consider the effect of other environmental factors, mainly soil water content, temperature and VPD that control the photosynthesis process.

The parameter $f_{PAR} \times PAR$, called $aPAR$ hereafter, is the absorbed PAR determined using

$$aPAR = iPAR - rPAR - tPAR,$$

where $i\ and\ r$ denote the incoming and reflected radiation measured above the canopy, respectively, and t represents the transmitted radiation measured below the canopy. In the expression above, all the $aPAR$ is assumed to be absorbed by leaves, and the portion absorbed by woody parts is assumed to be negligible.

Finally, in this study, the apparent ecosystem light-use efficiency LUE is calculated as

$$LUE = \frac{GPP}{aPAR}$$

It is important to note that the *GPP* is not measured directly but is estimated by subtracting the modeled ecosystem respiration (*ER*) during the day from *NEE*; consequently, *LUE* is subject to two main sources of error – errors inherent in *NEE* measurements from using the eddy covariance technique and uncertainties in the model predictions of *ER* during the day.

2.3. *In situ* measurements of PRI and NDVI

In each of the two forest sites, measurements of PRI and NDVI were acquired using sensors fixed side-by-side on a mast located approximately 7 m and 5 m from the upper layer

of tree crowns in Fontainebleau forest and Puéchabon forest, respectively. For the PRI measurements, we used the model SKR 1800 manufactured by Skye Instruments, Ltd. (Llandrindod Wells, UK). The NDVI sensors were laboratory-made following the description given in Pontailler et al. (2003) and Soudani et al. (2012). Both the PRI and NDVI sensors facing downward were inclined at an angle of approximately 20° from vertical and oriented to the south to avoid hotspot effects in canopy reflectance when the viewing direction was collinear with the solar direction. The measurements reported in this study were acquired from 2006 to 2011 in Fontainebleau forest and from 2010 to 2011 in Puéchabon forest.

Two PRI sensors were used; one sensor measured the incident solar radiation, while the second sensor simultaneously measured the radiation reflected upward. The PRI sensors measured radiance (or irradiance) in two narrow bands of 10-nm bandwidths centered on 530 nm and 570 nm. The PRI sensor facing downward had a field of view (FOV) of 25°, whereas the sensor facing upward had a cosine-correcting diffuser covering a 180° FOV. The area viewed at the top layer of the canopy was approximately 8 m² in Fontainebleau forest and 4 m² in Puéchabon forest.

In the two forests, a single NDVI sensor measured the radiances above the canopy in the red and near infrared bands, 640-660 nm and 780-920 nm, respectively. The field of view was initially 100° but was collimated to consider viewing constraints encountered at each site. The area viewed was approximately 100 m² in Fontainebleau forest and 60 m² in Puéchabon forest.

PRI was computed from reflectances (*R*) according to the expression given in the first work of Gamon et al. (1992):

$$PRI = \frac{R_{[565-575]} - R_{[525-535]}}{R_{[565-575]} + R_{[525-535]}}$$

The NDVI was computed from radiances (*Rd*) as:

$$NDVI = \frac{Rd_{[780-920]} - Rd_{[640-660]}}{Rd_{[780-920]} + Rd_{[640-660]}}$$

The values between brackets indicate the bandwidths in nanometers. At the two forest sites, the radiances used in the PRI and NDVI calculations are half-hourly average values from radiance measurements scanned every minute and recorded every half hour.

2.4. Statistical data analysis

The statistical data analysis was performed at different time scales within a season using moving temporal windows and between years. In the first analysis, the

strength and the direction of the relationships between PRI and the main bioclimatic variables at different time scales were measured using the coefficient of determination (R^2). In a second step, and because of the interdependence and the strong and complex interactions between the bioclimatic variables and PRI, the contribution of each variable to the temporal variability of PRI was evaluated using a nonparametric method based on the Random forest machine learning algorithm (Breiman, 2001) using the Random forest package (the library randomForest - Version 4.6.1). Briefly, for regression analysis, RF is an extension of the tree-based regression method that allows the prediction of a numeric dependent variable from one or more numerical or categorical predictors without any assumptions such as the normality of distributions of the predictors or the form of regression between the dependent variable and the predictors. Starting from the original data (with the root node corresponding to the entire PRI data set in this study), the tree was constructed using binary recursive partitioning of independent variables into subintervals, allowing for smaller deviations between the observed and predicted values of the dependent variable (PRI). Instead of a single tree, RF predicts the dependent variable from a large number of trees (a few hundred) built from subsamples selected in the original data by random sampling with replacement (bootstrap samples of the same size as the original data set). Each subsample was used independently to build a tree. During the building of the tree, all the predictors were not used simultaneously; instead, a second randomization was performed by selecting a random subset of the predictors for each partition. The predictions were averaged over all the trees of RF.

RF also allows the predictive variables to be hierarchized in terms of importance in prediction accuracy. In this study, the importance of each predictive variable was measured as the average decrease in node impurity (Gini index) over all trees in RF due to the introduction of the predictor in the analysis (Breiman, 2001). In addition to this overall measure, the relationships between PRI and the predictive variables were assessed through partial dependence plots, which measure the marginal effect of each predictor on the predicted variable (PRI). An excellent presentation of regression analysis using Random forest with R is given in Berk (2008).

It is important to underline that the purpose of statistical analyses undertaken and results shown in the next sections is not to predict PRI from meteorological and eco-physiological factors but to assess the strength of the relationships between PRI and LUE and to investigate the effect of each factor on the variability of PRI and on PRI vs. LUE relationships.

3. Results

3.1. Temporal patterns of the NDVI, aPAR, GPP, LUE, and PRI in the two forests

Figure 1 illustrates the seasonal and interannual variations of the NDVI, aPAR, GPP, LUE, and PRI in 2010 in the two forest stands.

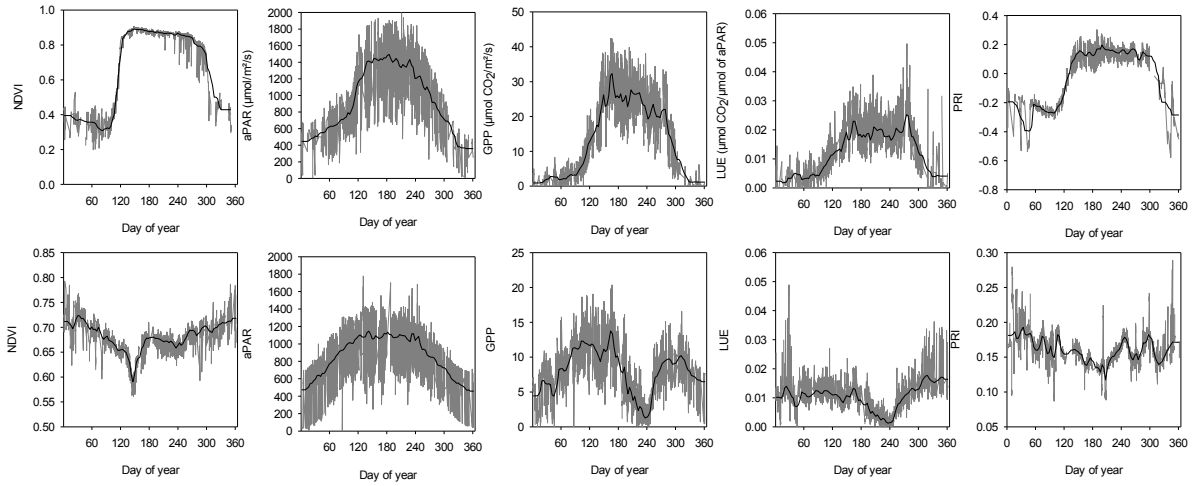

Figure 1: Seasonal variations in 2010 of NDVI, aPAR, GPP, LUE, and PRI measured every half-hour above a deciduous oak forest canopy (Fontainebleau flux-tower site – upper figures) and above an evergreen holm oak forest canopy (Puéchabon flux-tower site - bottom). The data presented were acquired between 8 h - 18 h TU. Continuous line: smoothed data using a moving average window of approximately ten days.

In Fontainebleau forest from 2006 to 2011, the NDVI, aPAR, GPP, LUE, and PRI exhibit similar patterns to that presented in Figure 1. The temporal pattern of the NDVI indicates the typical seasonal variations of green canopy foliage in deciduous forests. This seasonal dynamic is characterized by two main phases: the leafy season during mid-spring and summer and the dormancy season during late autumn and winter. These two main seasons are separated by two short phases, delimited by two major phenological events: a first phase of budburst, leaf development, and maturation in spring and a second phase of onset of yellowing, senescence, and leaf fall in autumn. On average, over the six available years of NDVI measurements, the NDVI starts to increase on day (day of year) 92 (± 1 day of standard error). The maximum value of the NDVI is reached in the late spring on day 126 (± 4). During the summer, the NDVI is at its maximum level and then starts decreasing on day 276 (±5) in early autumn at the beginning of leaf yellowing and leaf fall. During this period, the

NDVI decreases rapidly until day 330 (±8). On average, over all the years, the length of the main period of the growing season corresponding to the period of the NDVI plateau is approximately 150 days (± 2 days).

Seasonal patterns in the aPAR and GPP are similar to those usually observed in temperate deciduous forests and result from the seasonal climatic cycle and phenology. During the nonleafy season, the aPAR records correspond to the radiation absorbed by woody parts. During this period, there is no photosynthesis, and the GPP corresponds mainly to the contribution of herbaceous understory species and also to uncertainties in the modeled GPP estimates. During the leafy season, the GPP is driven by radiation and soil water content because the temperature is usually not a limiting factor during this period.

It is important to note that in temperate deciduous forests, at the end of the leaf expansion phase when NDVI reaches its maximum value, the leaves are not fully mature and their biochemical properties, in particular, the leaf chlorophyll content and leaf mass area, have not yet reached their maximum level (Demarez et al. 1999; Gond et al. 1999). In addition, the maximum photosynthetic capacity is not yet reached because this capacity depends strongly on the leaf biochemical properties. This phenomenon may partially explain the time shift between the occurrences of the maximum GPP and maximum NDVI.

In Puéchabon forest, the temporal dynamics of the NDVI during the two years of the study are similar. The NDVI temporal variations are significantly dampened compared with those observed in deciduous forests. However, the NDVI decreased significantly, reaching its lowest value in late April to early May. This temporal pattern of the NDVI is consistent with the temporal dynamic of litterfall measured in this forest (Limousin et al. 2012; Soudani et al. 2012). The decrease in the NDVI corresponds to the period during which the peak of litterfall is reached and also coincides with the slow emergence of a new cohort of leaves. The value of aPAR in Puéchabon forest is, on average, slightly lower than that in Fontainebleau forest during the growing season because of the lower LAI.

Regarding the GPP and LUE, Puéchabon forest experienced severe drought in summer 2010. Indeed, the total annual rainfall was 948 mm and 1157 mm in 2010 and 2011, respectively. However, the contrast between the two years is much more pronounced in the average summer rainfall. During the three summer months of June to August, the total rainfall was 57 mm in 2010 and 154 mm in 2011. The average rainfall during these three months from 1984-2011 is 109 mm. Consequently, in comparison with 2011 (data not presented), the GPP in 2010 decreased by approximately 20% during the three months of summer.

In the two forests, the seasonal patterns of PRI and NDVI are similar, emphasizing the control of canopy foliage dynamics on canopy PRI variations. However, in Puéchabon forest, it may be noted that during the GPP decline due to drought during midsummer in 2010, the NDVI remained nearly constant, whereas PRI increased significantly and covered the entire range observed over the entire year.

For the reasons described above and to accurately assess the relationships between PRI and LUE independently of the effects of temporal changes of canopy structural and biochemical characteristics, only the period from days 180 to 255 during the NDVI plateau, which corresponds to the period during which the LAI remains constant near maximum values, is included in the analysis of the PRI data. This period was also selected to avoid the inclusion of data acquired when the leaves were not yet fully mature or senescent because the PRI signal is strongly driven by the effects of temporal variations of leaf pigment pools.

3.2. Assessment of the relationships between PRI and climate meteorological, carbon, and water flux variables at different time scales

Three categories of variables related to climatic conditions and water and carbon fluxes were selected for this analysis: i) aPAR and the ratio of direct-to-total solar radiation (direct/total PAR) above the canopy were used as indicators of the amount of radiation available for photosynthesis and sky conditions; ii) the air vapor pressure deficit (VPD) and the ratio of real evapotranspiration-to-potential evapotranspiration (Etr/Etp) were used as indicators of the evaporative demand of the atmosphere and water stress; and finally, iii) the GPP and LUE were used as indicators of the amount and apparent quantum yield of photosynthesis.

The relationships between PRI and the variables described above were established on a half-hourly time step basis and during a period of NDVI stability from day 180 to day 255. In addition, to avoid diurnal variations of PRI, only measurements acquired between 10 h and 14 h were selected for analysis.

The strengths of these relationships are summarized in Table 1.

PRI vs.	aPAR	Direct/total PAR	VPD	Etr/Etp	GPP	LUE
FR Fon						
(n [581-760)	[0.60 – 0.74]	[0.51 – 0.76]	[0.55 – 0.67]	[-0.00 – -0.30]	[0.14-0.50]	[-0.38 – -0.65]
FR Pue						
2010 (n=603)	0.04 ns	0.15	-0.04 ns	-0.33	-0.53	-0.48
2011 (n=712)	0.61	0.65	0.51	-0.12	0.02 ns	-0.53

Table 1: Pearson's correlation coefficient [r] between PRI and aPAR, direct/total PAR, VPD, Etr/Etp, GPP, and LUE. The value of r was calculated per year during the period of nearly constant NDVI from day 180 to 255, and the measurements were acquired every half-hour between 10 h and 14 h TU. In Fontainebleau forest, because of the small variation between years, the data were pooled over the six years. In Puéchabon forest, to consider the differences between the two years due to drought, the data were analyzed separately for each year. n is the number of observations used in the regression each year. In Fontainebleau, the range (min-max) of n and r is given. ns: not significant (P >0.05).

In Fontainebleau forest, the best coefficients of correlation (in descending order) were observed between the following pairs: PRI vs. aPAR, PRI vs. Direct/total PAR, PRI vs. VPD, PRI vs. LUE, and PRI vs. GPP. The relationships between PRI and Etr/Etp were weaker at both sites. In Puéchabon forest, we observe the same hierarchy of variables correlated to PRI as in Fontainebleau forest, but only for 2011. During 2010, in which drought occurred, the results contrast with those of 2011. The correlations were not significant between PRI and aPAR and were significant between PRI and Etr/Etp, PRI and LUE, and PRI and GPP.

Figures 2 and 3 illustrate the form of the relationships between PRI and aPAR and between PRI and LUE in the two forests. For each forest site, the relationships are presented for two years, corresponding to the highest and the lowest values of the coefficient of correlation.

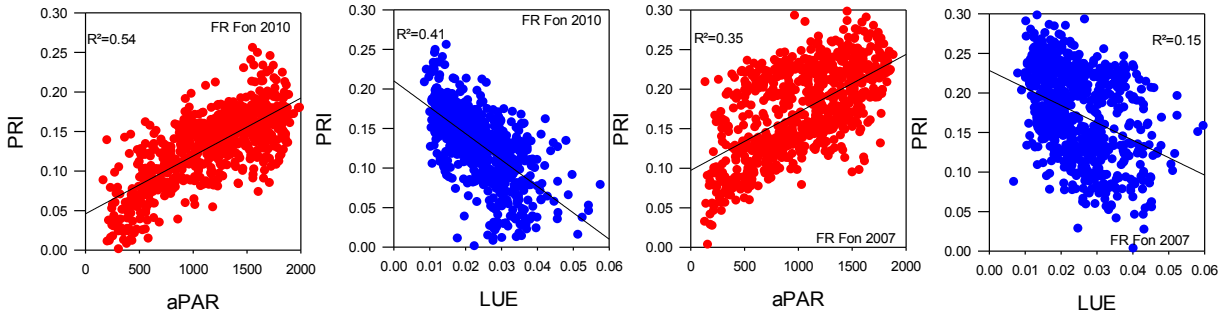

Figure 2: Relationships between PRI, aPAR, and LUE for 2010 (best correlations) and 2007 (lowest correlations) in Fontainebleau forest. The measurements were acquired every half-hour between 10 h and 14 h TU during a period of nearly constant NDVI from day 180 to 255.

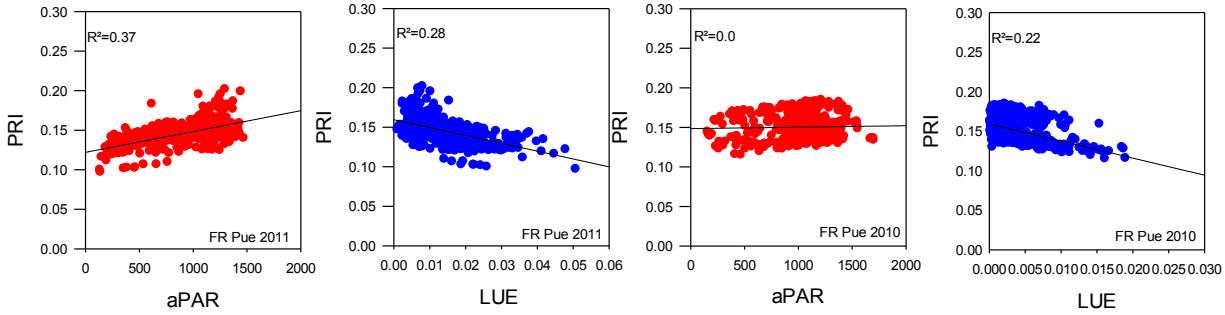

Figure 3: Relationships between PRI, aPAR, and LUE for 2011 (best correlations) and 2010 (lowest correlations) in Puéchabon forest. The measurements were acquired every half-hour between 10 h and 14 h TU during a period of nearly constant NDVI from day 180 to 255.

Despite the relatively high correlations between PRI vs. aPAR and PRI vs. LUE, these relationships are scattered. At first glance, this scattering may be due to the long period examined in the analysis (day 180-255), as PRI is known to vary at very short time scales. During the period of day 180-255, the structure and ecophysiological functioning of the canopy may have been subjected to changes associated with climatic events and with subtle temporal variations of the biochemical properties of the leaves, although the NDVI remained constant. To account for these considerations, regressions between PRI and aPAR and between PRI and LUE were performed at short-time scales using moving windows within the leafy season – from the beginning of the growing season (including the onset of the NDVI increase in spring – day 126) to the early autumn in Fontainebleau (day 276) and over the entire year (day 1-365) in Puéchabon forest. For both of the studied forests, statistical

analyses were conducted for two years (the years mentioned in Figures 2 and 3), for which the relationships between PRI, aPAR, and LUE on a seasonal scale (day 180 to 255) have the highest and lowest coefficients of correlation. The results are summarized in Figures 4 and 5, which illustrate the variations of the coefficient of determination (R^2) within a 20-day moving window throughout the season and at different hours of the day at two-hour time intervals. The selection of the size of the moving window is somewhat arbitrary; however, we assume that over 20 days, changes in the leaf biochemical properties are lower than what can be expected over the entire season. We also note that smaller sizes (one and two weeks) were also tested, and the general patterns of R^2 were similar to those observed in Figures 4 and 5.

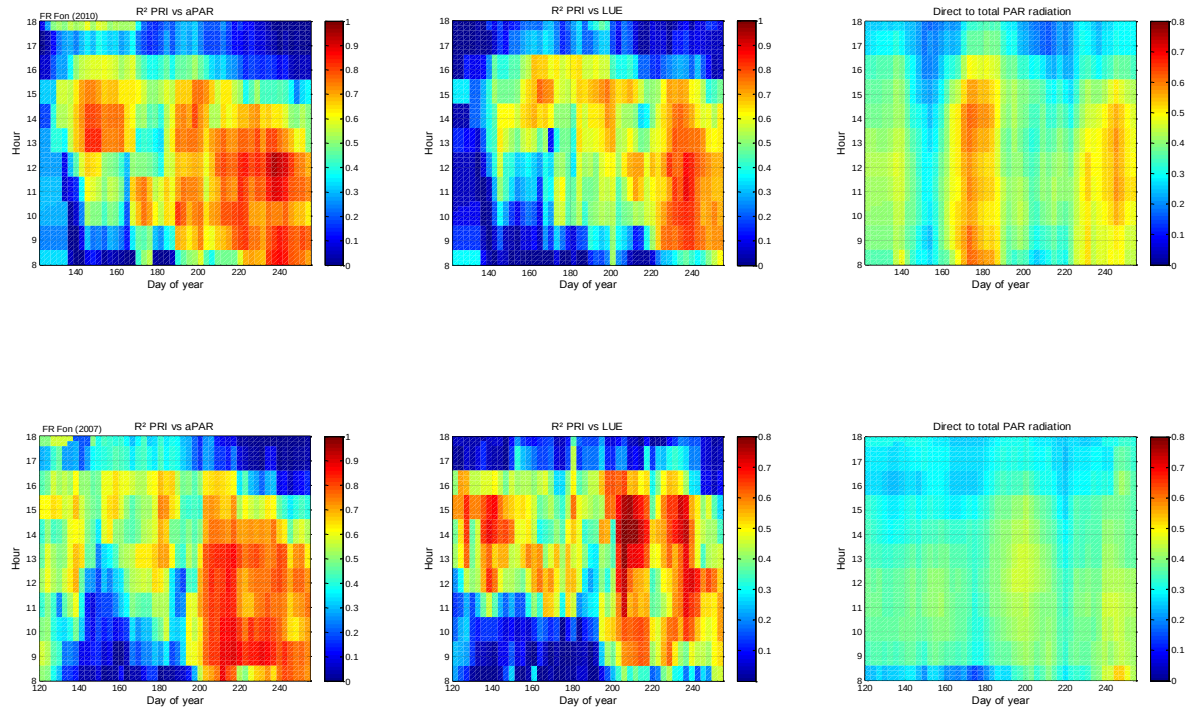

Figure 4: Images of the temporal variations of the coefficient of determination of the relationships between PRI vs. aPAR and PRI vs. LUE obtained from the measurements acquired in Fontainebleau forest in 2010 (upper three plots: best correlation) and 2007 (lowest correlation). The R^2 values were determined from data acquired separately in two-hour intervals during the day and within a moving window of 20 days over the entire period of the NDVI plateau (day 126-275). The plots on the right correspond to the ratio of direct-to-total PAR radiation.

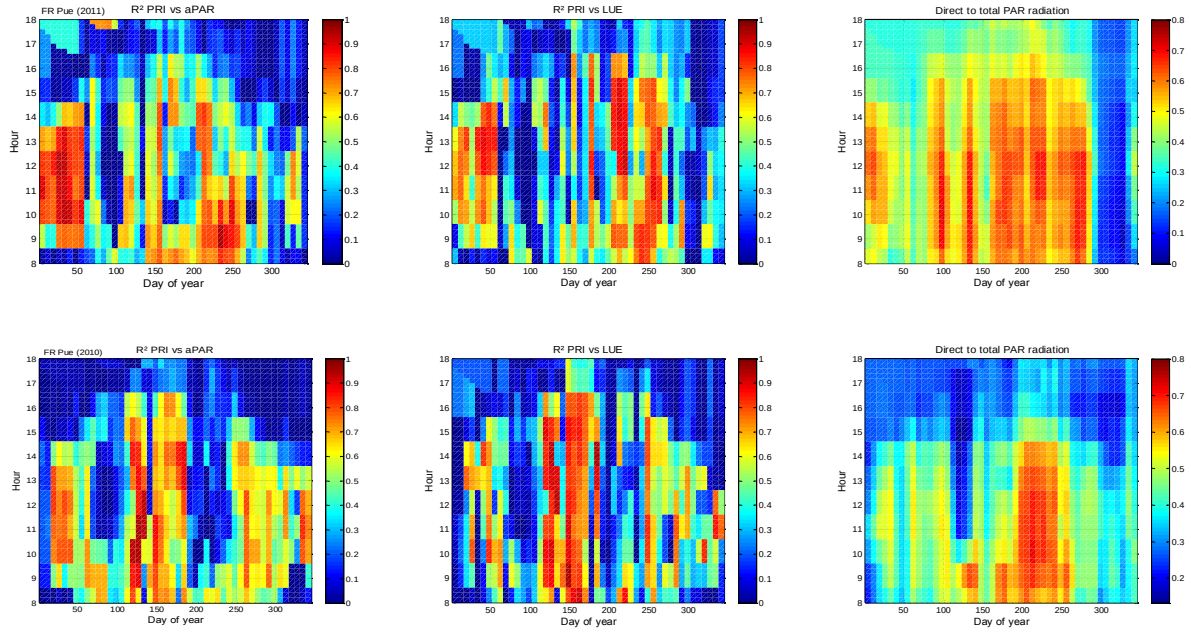

Figure 5: Images of the temporal variations of the coefficient of determination of the relationships between PRI vs. aPAR and PRI vs. LUE obtained from the measurements acquired in Puéchabon forest in 2011 (upper plots, best correlations) and 2010 (severe drought, low correlations). The R² values were determined from data acquired separately in two-hour intervals during the day and within a moving window of 20 days and over the entire year. The plots on the right correspond to the ratio of direct-to-total PAR radiation.

In Fontainebleau forest (Fig. 4) and from data acquired in 2010 (highest R^2), significant R^2 values (P <0.05) over the moving window of 20 days at two-hour intervals range between 0.05 and 0.94 for sample sizes varying between 21 and 80 observations, respectively. In 2007 (lowest R^2), significant R^2 values range between 0.04 and 0.89 for sample sizes varying between 29 and 80 observations, respectively.

In Puéchabon forest (Fig. 5) and from the data acquired in 2011 (highest R^2), significant relationships between PRI and aPAR and between PRI and LUE can be observed in winter under clear sky conditions (from day 1 to day 60). Significant relationships were also observed in summer periods, particularly from day 213 to day 265. In 2010, the highest correlations (reaching a peak of 0.9) between PRI and aPAR and between PRI and LUE were observed during two long periods from day 124 to 175 and from day 240 to 300. Between these two periods, from day 175 to 240, which coincides with the period of drought, the relationships between PRI vs. aPAR and PRI vs. LUE were insignificant.

Figure 6 presents the best regressions observed between PRI and aPAR and between PRI and LUE in 2010 in Fontainebleau forest and in 2011 in Puéchabon forest. In Fontainebleau forest, a maximum R^2 at an hourly time step (0.94) is reached from day 236 to 255. The R^2 value of the PRI vs. LUE relationship over the same period is 0.87. Over this period and when all the data acquired between 10 h and 14 h are pooled, R^2 is approximately 0.76 for PRI vs. aPAR and 0.70 for PRI vs. LUE. In Puéchabon forest, the maximum R^2 (0.93) between PRI and aPAR is reached between days 230 and 249. The maximum R^2 of PRI vs. LUE is approximately 0.92 and is reached between days 213 and 232. In Puéchabon forest from day 230 to 249 and when all the data acquired between 10 h and 14 h are pooled, R^2 is approximately 0.59 for PRI vs. aPAR and PRI vs. LUE.

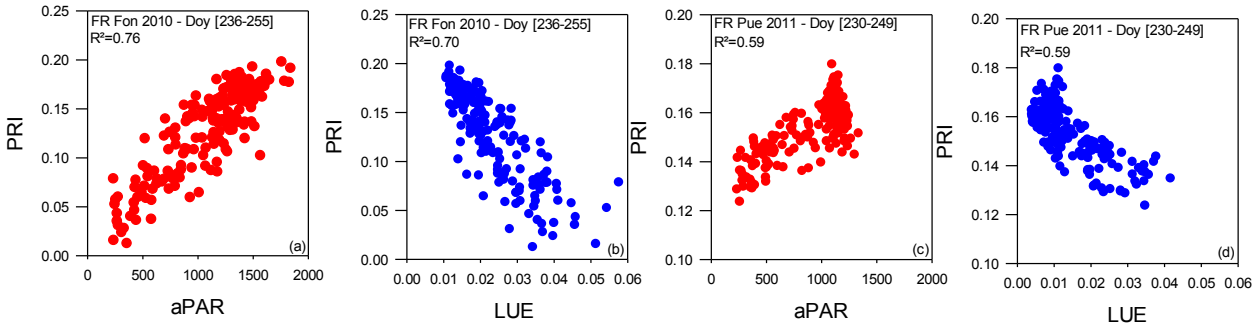

Figure 6: Illustrations of best correlations between PRI and aPAR and between PRI and LUE in Fontainebleau forest and in Puéchabon forest. The data used were acquired between 10 h and 14 h during the period of maximum R^2 given between brackets.

In conclusion, R^2 between PRI and LUE is less than that between PRI and aPAR, and high correlations between PRI and aPAR do not necessarily imply high correlations between PRI and LUE. Note that the best relationships between PRI and LUE often coincide with periods of clear skies dominated by a high direct-to-total PAR radiation ratio (Fig. 4 & 5).

3.3. Investigating the main drivers of PRI variations and PRI vs. LUE relationships

As underlined in Materials and Methods section, because of both the strong nonlinear interactions and dependencies between different variables, it is difficult to rank the variables in terms of explanatory power of the variability of PRI based on coefficients of correlation (Table 1) that measure the overall linear covariation over the entire range of explanatory variables. Nonlinear technique regression based on Random Forest Regression (RF) analysis is performed using the same dataset used for the statistical correlation analysis summarized in

Table 1 (days 180-255, 10 h-14 h) to assess the contribution of the main variables to the variability of PRI. The results are presented in Figures 7, 8, and 9.

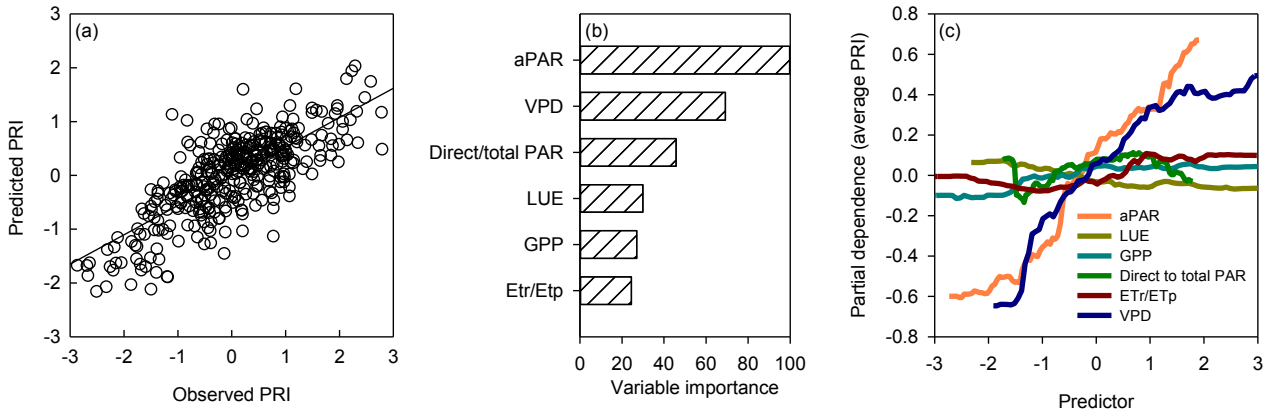

Figure 7 – 7.a: Observed vs. Predicted PRI from RF regression in Fontainebleau forest established based on a validation sample composed of 10% of the entire sample that was randomly selected (R^2 = 0.54, RMS = 0.45). The data were pooled over the six years – day 180-255 between 10-14 h. 7.b: Rank of importance based on RF regression of the predictor variables in determining PRI. 7.c: Partial dependence describing the marginal effect of each variable on PRI. The x-axis is the considered variable, and the y-axis is the average value of PRI obtained by fixing the values of X, whereas the other predictors are not fixed (All the variables – PRI and predictors – are centered and reduced).

In Fontainebleau forest and using data pooled over the six years of measurements (Fig. 7), the RF regression of PRI on variables presented in Fig. 7b explains approximately 54% of the total variance of PRI (Fig. 7a). aPAR appears to be the most important variable, followed by VPD and the direct/total radiation ratio. LUE, GPP, and Etr/Etp play insignificant roles (Fig. 7b). Fig. 7c reveals a monotonic positive relationship between PRI and aPAR over the entire range of aPAR. The relationship between PRI and VPD is also positive; however, a saturation feature is observed at high VPD values. The other variables have insignificant effects on the PRI variation.

In Puéchabon forest, the RF regression was performed separately for the 2010 and 2011 data to consider the contrast between the two years due to the effects of drought. The RF results are presented in Figures 8 and 9.

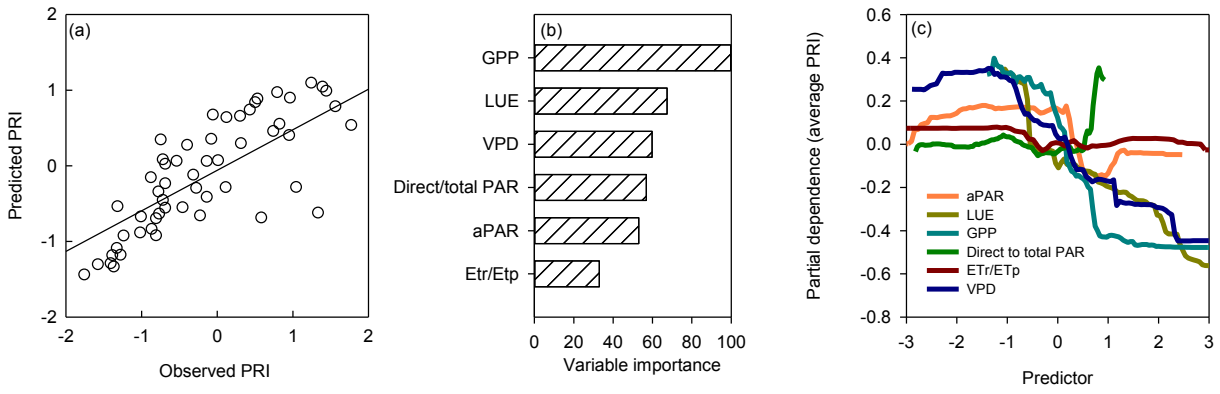

Figure 8 – 8.a: Observed vs. Predicted PRI from RF regression in Puéchabon forest (2010) established based on a validation sample composed of 10% of the entire sample that was randomly selected data (overall R^2 = 0.61, RMS = 0.39). 8.b: Rank of importance based on RF regression of the predictor variables in determining PRI. 8.c: Partial dependence describing the marginal effect of each variable on PRI. The x-axis is the considered variable, and the y-axis is the average value of PRI obtained by fixing the values of X, whereas the other predictors are not fixed (All the variables – PRI and predictors – are centered and reduced).

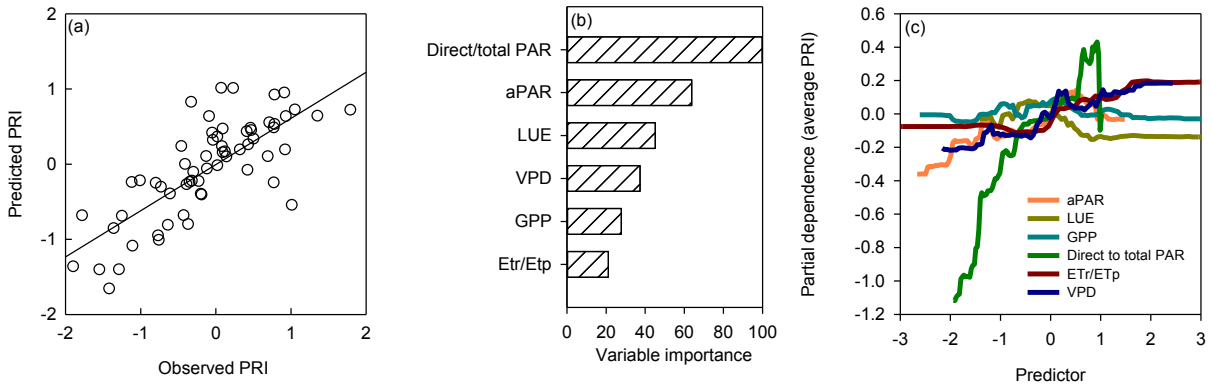

Figure 9 – 9.a: Observed vs. Predicted PRI from RF regression in Puéchabon forest (2011) established based on a validation sample composed of 10% of the entire sample that was randomly selected (R^2 = 0.56, RMS = 0.44). 9.b: The rank of importance based on RF regression of the predictor variables in determining PRI. 9.c: Partial dependence describing the marginal effect of each variable on PRI when all the other variables are fixed. The x-axis is the considered variable, and the y-axis is the average value of PRI obtained by fixing the values of X, whereas the other predictors are not fixed (All the variables – PRI and predictors – are centered and reduced).

The results demonstrate that the hierarchy of the predictive variables computed from variable importance criteria and the form of relationships between these variables and PRI are very different between the two years. In 2010, the year of severe drought, GPP, LUE, and VPD appear to be the most important variables over the entire range of PRI variation. The relationships between PRI and these three variables are negative. In 2011, the results presented in Figure 9 are quite similar to those obtained in Fontainebleau forest, highlighting a significant effect of the direct/total aPAR on PRI variation. The main variables affecting PRI are aPAR, direct/total PAR, and VPD. These three variables are linearly related to PRI (Fig. 9c). In contrast, the effects of GPP, LUE, and Etr/Etp on PRI are insignificant.

3.4. An approach for disentangling the effects of factors that affect the PRI vs. aPAR and PRI vs. LUE relationships on a seasonal scale

As demonstrated in Figures 4 and 5, statistically significant "moving window" relationships between PRI and aPAR or PRI and LUE appear or disappear over periods during the leafy season in Fontainebleau forest or during the year in Puéchabon forest. Moreover, even when these relationships are statistically significant, the parameters of regressions vary from one period to another. The temporal variability of the intercept of the linear regression of PRI vs. aPAR is particularly interesting to analyze. Indeed, this parameter corresponds to PRI at very low radiation levels. Because the xanthophyll cycle activity is expected to be slow at low radiation levels, a large portion of the temporal variability of the intercept throughout the season may be interpreted as being due to the effects of temporal variations of other factors, particularly the canopy structure and leaf biochemical properties.

Figure 10 illustrates the temporal variability of intercepts of regressions of PRI vs. aPAR within a moving window of one week in the two studied forests for all the years investigated. We note that the selection of a one-week moving window size is a compromise that we consider adequate for an accurate interpretation of temporal variations in the intercept. If using larger temporal windows, eventual variations in leaf biochemical properties may bias the interpretation of results, whereas narrower temporal windows may artificially increase the temporal variations of the estimates of regression coefficients because of the small sample sizes used.

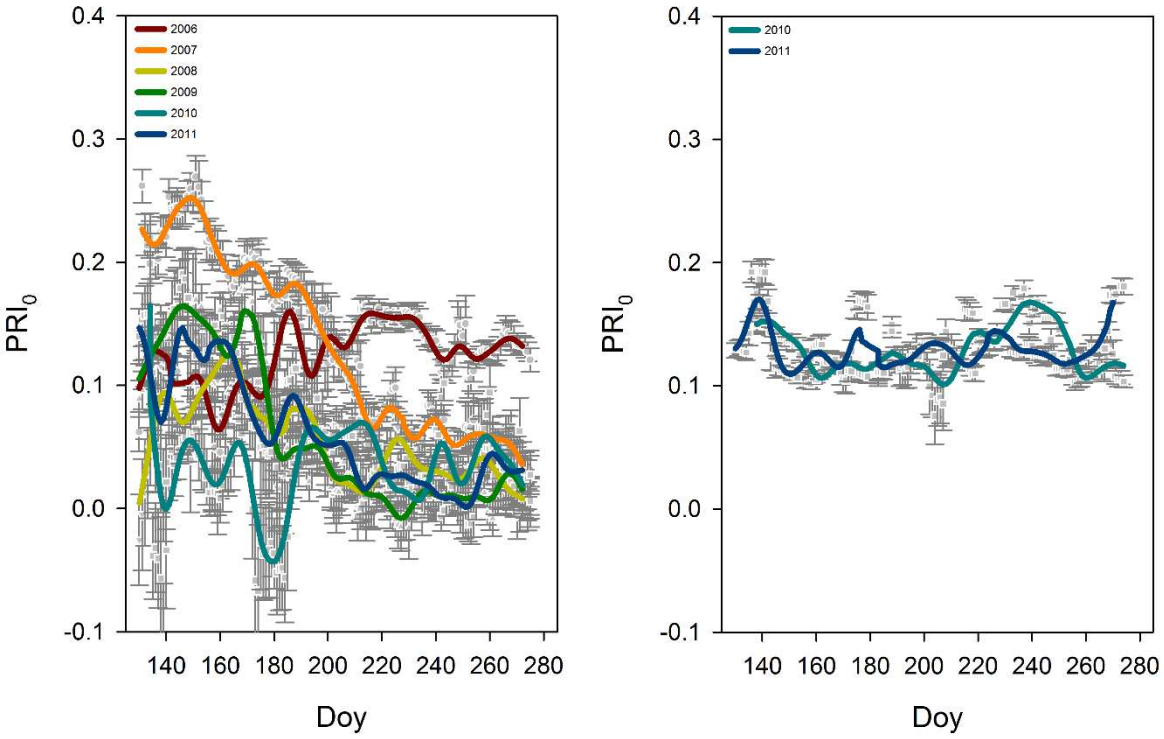

Figure 10– Variation of the intercept of the regression of PRI on aPAR in Fontainebleau forest (10.a) and in Puéchabon forest (10.b) within a 6-day moving window. The intercepts and errors determined from regressions are presented in gray. The continuous lines are the intercepts interpolated for each day using weighted smoothing splines. The weights are proportional to R^2.

In Fontainebleau forest, Figure 10a presents the temporal variations of the intercepts of the "moving window" PRI vs. aPAR regressions. At short time scales on the order of a few days, the intercepts vary rapidly and sharply. At the seasonal scale, with the exception of 2006 and 2010, we observe a general tendency for the intercepts to decrease during the season, especially during the period of the NDVI plateau. We also note that interannual intercepts are different at the beginning of the season in the spring and become very close at the end of the season in early autumn. The intercepts become very close except for in 2006.

In Puéchabon forest, Figure 10b demonstrates that the level of intercepts of PRI vs. aPAR is relatively stable throughout the year and that the range of intercept variations is narrower than in Fontainebleau forest.

As suggested above, a large portion of the temporal variability of the intercept of PRI vs. aPAR (called PRI_0 hereafter) can be interpreted as being due to the effects of temporal variations in the canopy structure and leaf biochemical properties. To disentangle the contribution of these effects from the PRI signal, PRI_0 is subtracted from the PRI observations, and the regressions between the corrected PRI (PRI_c) and aPAR and between PRI_c and LUE are reevaluated. Figure 11 presents these relationships before and after applying this correction method.

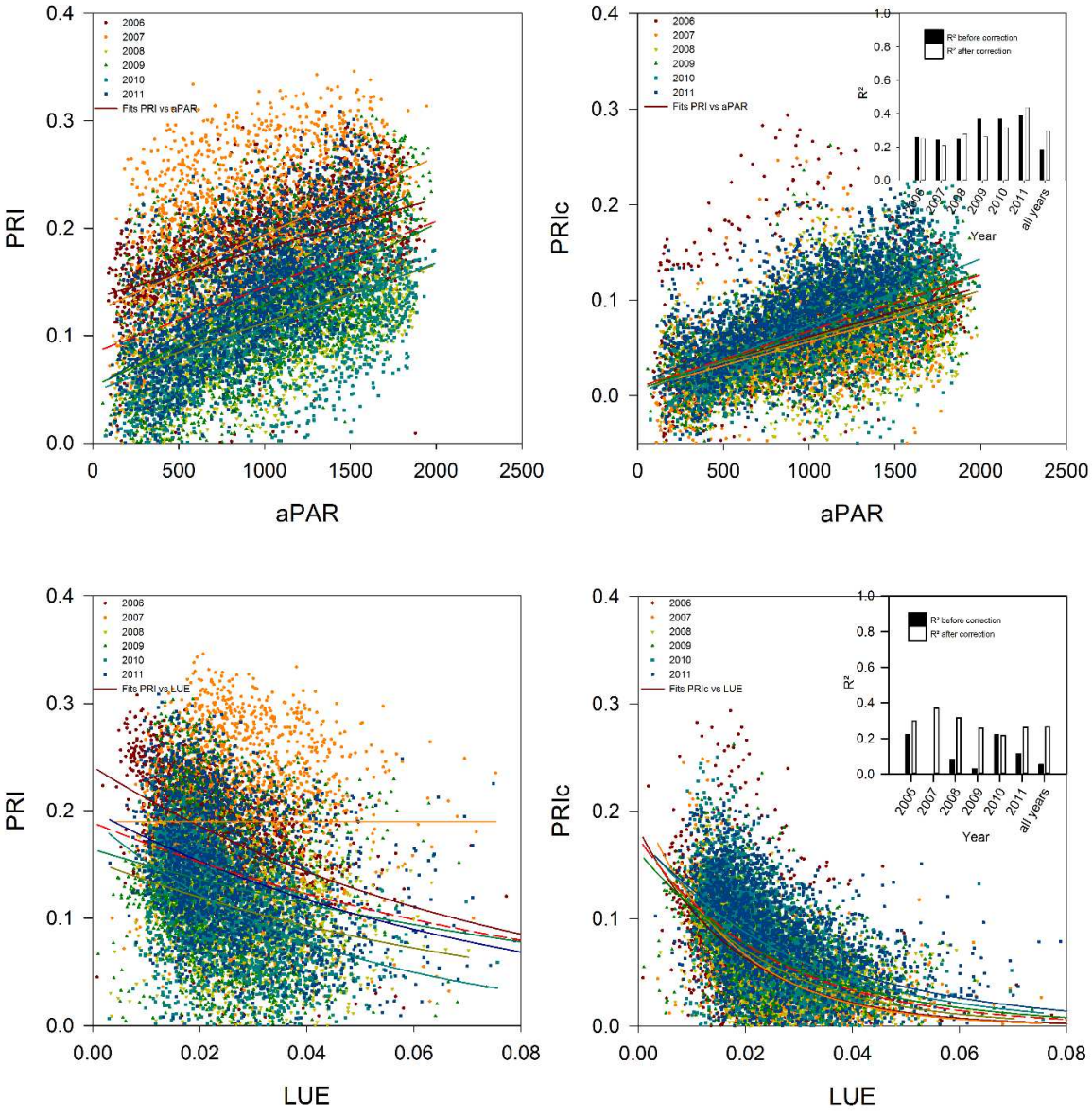

Figure 11– Relationships between PRI and aPAR (upper) and between PRI and LUE (bottom) in Fontainebleau forest. On the left and on the right, the relationships before and after PRI correction (PRIc) by subtracting PRI_0 from PRI observations are presented, respectively. The continuous curves represent the regression lines for each year. The short dashed curve in red represents the general model using data pooled over all the years.

We first note that to assess the relevance of this disentangling method, we extended the period of analysis to include periods during which foliar biochemical properties are supposed to be significantly contrasted. At the Fontainebleau site, the analysis period is from day 130 to day 280, including periods of immature, mature, and early senescent leaves. At the Puéchabon site, we considered the entire year.

For Fontainebleau forest, the disentangling procedure does not provide a significant improvement in the annual PRI vs. aPAR relationships. However, as demonstrated in Figure 11a, the dispersion around the general model with pooled data over the six years is reduced, and R^2 increases significantly (from 0.18 to 0.30 after the corrections). Concerning PRI vs. LUE, a notable increase of R^2 was measured for all years. The most important improvement was measured for 2007, for which R^2 increases from 0 to 0.37. The general model has also been significantly improved. R^2 increases from 0.05 to 0.26. As expected, in Puéchabon forest (data not presented), the correction procedure does not improve the relationships between PRI vs. aPAR or PRI vs. LUE because of the small variations of PRI_0 during the year (Fig. 10b).

4. Discussion

At the seasonal scale (Fig. 1), the temporal patterns of PRI and NDVI are similar, indicating that the temporal changes of PRI are primarily controlled by the seasonal phenology that modifies both the leaf area and biochemical properties of the canopies. Figure 1 also demonstrates that during periods of stable total canopy leaf area during summer, the short-term variations in PRI are greater than those in NDVI, suggesting that these two indices are relatively independent.

At the seasonal scale, from day 180 to day 255 (Fig. 2 and 3), our results indicate positive and significant relationships between PRI and aPAR in Fontainebleau forest over the six years of the study and in Puéchabon forest in 2011. These results are consistent with previous studies at both the leaf (Gamon et al. 1997; Peñuelas et al. 1998) and canopy (Evan et al. 2004, Peguero-Pina et al. 2008) scales. These studies emphasized the strong dependence of PRI on the incident radiation across a wide range of species and hydric conditions. Although the physiological mechanisms involved are complex and not fully understood (Holt et al. 2005; Demmig-Adams & Adams Demmig, 2006), the increase of PRI when absorbed PAR increases is explained by the decrease in reflectance at 531 nm due to an increase in light

absorption associated with the conversion of violaxanthin into antheraxanthin and zeaxanthin pigments (Gamon et al. 1997).

In contrast, the PRI vs. LUE relationships are negative (Fig. 2 & 3). At the leaf scale, Gamon et al. (1997) and Peñuelas et al. (1997, 1998) have demonstrated negative relationships between PRI and LUE and between PRI and the photochemical efficiency of PSII. At the canopy scale and in mature forests, the works of Nichol et al. (2000; 2002), Nakaji (2006, 2007, 2008), Wu et al. (2010), Goerner et al. (2011), and the review of Garbulsky et al. (2011) support a negative relationship between PRI and LUE.

Although significant, the PRI vs. aPAR and PRI vs. LUE relationships at the seasonal scale are scattered and vary from one year to another (Figs. 2 and 3). Over shorter periods within the 20-day moving window, the signs of these relationships remain unchanged (+ for PRI vs. aPAR and – for PRI vs. LUE); however, the correlations are significantly improved (Figs. 4, 5, and 6). The highest correlations are most often observed over periods characterized by clear or slightly overcast skies. However, all the periods of clear skies do not involve improvements in the PRI vs. aPAR or PRI vs. LUE relationships. This finding is especially highlighted during the drought from day 175 to 240 in 2010 in Puéchabon forest (Fig. 5). During this period, the PRI vs. aPAR or PRI vs. LUE relationships are mostly nonsignificant, even though the weather is dominated by clear skies. Note also that during this period of drought, PRI increased, NDVI remained stable, and LUE has consequently been significantly reduced (Fig. 1).

These findings highlight the complexity of the nature of the relations that link PRI to bio-meteorological factors (GPP, LUE, aPAR, VPD, sky conditions, etc.). This complexity is illustrated from regression analyses using the Random forests approach in table 1 and figures 7, 8, and 9. In Fontainebleau (Fig. 7) over the six years of the study and in Puéchabon in 2011 (Fig. 9), PRI appears to be correlated to radiation and sky conditions, whereas in Puéchabon forest in 2010 (Fig. 8), which was characterized by a severe summer drought, PRI is essentially correlated to GPP. This result leads us to suggest that under non-water-stressed conditions, significant PRI vs. LUE relationships are mainly under the control of the incident radiation. This control is more pronounced under clear or slightly covered skies because of a greater range of variations of PRI, aPAR, and GPP and thus of LUE. Under stable overcast sky conditions, the range of variability of these variables appears to be less important, which may partially explain the loss of the PRI vs. aPAR and PRI vs. LUE relationships. Under water-limited conditions, the decline of the strength of the relationship between PRI and LUE in Puéchabon forest is difficult to explain; however, from a statistical point of view, the small

variations of LUE observed during the drought period may be a relevant reason (Fig. 1). In other words, in addition to physiological mechanisms that directly control PRI, small variations of LUE under severe stress conditions may explain the loss of the PRI vs. LUE relationship due to an insufficient signal-to-noise ratio.

The seasonal and interannual variability of PRI and thus the relationships between PRI, aPAR, and LUE are highly dependent on canopy foliage, which constitutes the main reflecting surface, and on the chlorophyll content because chlorophylls are the most important light-absorbing pigments in the visible spectrum. The dependency of PRI on canopy foliage dynamics can be clearly observed in Figure 1, which illustrates the similar seasonal patterns of PRI and NDVI. Strong relations between PRI and the leaf area index (LAI) and between PRI and the chlorophyll content have been established in previous studies (Sims et al. 2002; Stylinski et al. 2002; Nakaji et al. 2006; Garrity et al. 2011; Rahimzadeh-Bajgiran et al. 2012). Therefore, the relationships between PRI and LUE established over the entire season or for different years, such as those established using MODIS data (Drolet et al. 2005; Drolet et al. 2008; Hilker et al. 2010), are expected to be significantly affected by temporal changes in the structural and biochemical properties of the canopy.

Approaches such as those developed by Rahimzadeh-Bajgiran et al. (2012), who have developed a new spectral index that combines PRI and another spectral index as an indicator of chlorophyll content, may be used to explicitly consider the effects of temporal changes of chlorophyll content on PRI vs. LUE relationships. In our study, we suggest a different approach. Figure 10 illustrates the variation in the intercept (PRI_0) of the PRI vs. aPAR relationships, suggesting the possible presence of a temporal tendency that may reflect changes in structural and biochemical characteristics of the canopy. Because the amount of canopy foliage is likely constant, as suggested by the stability of NDVI during this period, this tendency can be explained by changes in the biochemical properties of the canopy, as observed in previous studies (Gond et al., 1999). Regardless of the cause of this tendency, it is important to note that once PRI_0 is subtracted from the measured PRI, the relationships between the corrected PRI and LUE for each year are significantly improved, and a stable multi-year model can be obtained. Nevertheless, further experimental studies are required to explain the temporal changes of PRI_0 during the season and to develop a more accurate disentangling approach to make PRI-based remote-sensing of leaf and ecosystem light-use efficiency less sensitive to spatial and temporal changes in the canopy structure and chlorophyll content.

5. Conclusions

Our study highlights the strong dependency between PRI and two categories of factors. At the seasonal scale, the temporal dynamics of PRI is primarily controlled by the phenology and the temporal dynamics of the structural and biochemical characteristics of the canopy. Thus, from this point of view, PRI is similar to other spectral indices sensitive to canopy structure such as NDVI and EVI and to some other spectral biochemical indices sensitive to leaf chlorophyll and carotenoid contents. At a shorter temporal scale – a few days – PRI has a wider dynamic range than NDVI and is mainly controlled by solar radiation and sky conditions. PRI increases when absorbed radiation increases and decreases rapidly in response to cloud cover. PRI is inversely correlated to light-use efficiency. At a short time scale, the relationships between PRI and LUE may be very significant. At seasonal and interannual scales, these relationships are more scattered, which may be partially due to the dependency of PRI on both the structural and biochemical properties of the canopy. Consequently, the relationships between LUE and PRI using satellite data such as MODIS should be interpreted with extreme caution. In our study, the intercepts of PRI vs. aPAR regressions established over short periods of a few days were interpreted as estimates of PRI at very low radiation and called PRI_0. The temporal changes of PRI_0 were used as indicators of temporal changes of the canopy state independent of the effects of radiation on the physiological mechanisms that control PRI. After subtraction of PRI_0 from the measured PRI, significant improvements in the corrected PRI vs. LUE relationships were observed. This approach of PRI correction must be studied in depth because it constitutes a very interesting method of considering the effects of temporal changes of canopy biochemical properties on PRI vs. LUE relationships at seasonal scales.

Chapitre 4. Analysis of PRI versus LUE relationship variability over a broad range of temporal scales in two contrasted sites. Scale effects and PRI representativity in multi-layer forest canopies

Hmimina G.[a]; Dufrêne E.[b]; Soudani K.[a]

[a] Univ. Paris-Sud, Laboratoire Ecologie Systématique et Evolution, UMR8079, F-91405 CNRS, Orsay, France

[b] CNRS, Laboratoire Ecologie Systématique et Evolution, UMR8079, F-91405, Orsay, France

Abstract

The Photochemical Reflectance Index (PRI) is increasingly used as a proxy of the LUE at several temporal and spatial scales; however, recent studies have highlighted the high spatial and temporal variability in PRI versus LUE relationships at canopy scale. While most of this variability could be explained at leaf scale or at low temporal scale by known confounding factors such as the PRI sensitivity to canopy pigment content, the extrapolation of such findings to broader scales is not trivial. The investigation of PRI potential at broad scales is considerably hampered by scale effects, by the interaction between those confounding factors, and by relationships between those factors and LUE. In this study, an accurate process-based deconvolution of PRI constitutive and facultative sources of variability is achieved over two contrasted sites totaling 6.5 years of half-hour resolution *in-situ* measurements of PRI and carbon fluxes. Both sources of variability are analyzed in the light of simulated ecophysiological variables. The predictive power and representativeness of PRI measurements are examined, and technical as well as fundamental limitations to the use of PRI as a proxy of ecosystem LUE are highlighted.

1. Introduction :

Forest ecosystems are an important carbon sink (Running et al. 2007), and play a key role in the mitigation of anthropogenic carbon dioxide emission (Houghton, 2003). Yet, they are expected to be particularly sensitive to climate changes, which may result in local changes in growing season length (Lebourgeois et al. 2010) or in water and nitrogen availability (Penuelas et al. 2012, Sheffield and Wood 2008). Canopy response to such abiotic constraints can be efficiently described by tracking changes in its light use efficiency (LUE), as defined in Monteith and Moss (1997). Many studies focused on the prediction of carbon fluxes at global scale by relying on process-based models (Running et al. 1993, White et al. 2000, Krinner et al. 2005, Turner et al. 2006). While the use of remote-sensing derived data (Demarty et al. 2007, Maselli et al. 2009) and the upscaling of flux-tower derived data (Jung et al. 2009) significantly improved the prediction of carbon fluxes, the evaluation of ecosystem responses to abiotic stress remains a major challenge (Gebermichael & Barros 2006, Jung et al. 2007, Anav et al. 2010).

One of the most promising answers to this issue is the use of the photochemical reflectance index (PRI) as proxy of the LUE. The PRI is an optical index based on an observed variation in leaf reflectance around 530 nm (Gamon et al. 1992, 1997) which was correlated to the de-epoxydation state of the Violaxanthin-Antheraxanthin-Zeaxanthin pigment pool, thus to changes in non-photochemical quenching (NPQ). When plants are submitted to a limitation due for instance to water or temperature stress, there is a drop in the amount of light which can be used in photochemical reactions and therefore a buildup of excess energy. In order to avoid photo inhibition, this excess of energy is mainly dissipated as heat, via the non-photochemical quenching (Yamamoto, 2006). This process was shown to be mostly regulated by a negative feed-back control mechanism involving the violaxanthin-based xanthophyll cycle (Yamamoto 1979, Pfundel and Bilger, 1993, Demmig-Adams & Adams, 1996). It was shown that the buildup of a proton gradient across the thylakoïd membrane trigger the conversion of violaxanthin into zeaxanthin. Violaxanthin inhibits the aggregation of light harvesting complexes, thus enabling the transfer of incoming energy to the photochemical mechanism. Zeaxanthin was shown to play the opposite role as it triggers the aggregation of light harvesting complexes, which diverts the incoming energy toward non-photochemical quenching (Ruban et al. 2012). The PRI may therefore enable us to track a key process of photosynthesis regulation.

Its use has been thoroughly evaluated at different spatial scales. While the PRI was shown to be correlated to the LUE at each scale, some issues were pinpointed. The PRI was shown to be highly sensitive to canopy structure and sun-view geometry (Barton et al. 2001, Hall et al. 2008, Hilker et al. 2009, Goerner et al. 2009). Moreover, the PRI sensitivity to leaf pigment content (Moran et al. 2000, Gamon and Sims 2002, Filella et al. 2004) was shown to impact PRI versus LUE relationships (Rahimzadeh-Bajgiran et al. 2012, Gamon and Berry 2012, Hmimina et al. 2013b, Soudani et al. submitted, Hmimina et al. submitted). Thus, the PRI is a composite signal, varying with canopy structural, biochemical, and physiological properties. A good understanding of these sources of PRI variability is therefore a prerequisite to its use as a LUE proxy, as reminded in Gamon and Berry. 2012, Hmimina et al. 2013b, Soudani et al. submitted.

Several methods allowing the deconvolution of PRI variability due to LUE changes from PRI variability due to angular effects (Hilker et al. 2011), or leaf pigment content (Gamon and Berry. 2012, Hmimina et al. 2013b, Hmimina et al. submitted) were developed, but another key issue has yet to be addressed. The LUE was indeed shown to exhibit a high spatial and temporal variability (Falge et al. 2002, Le Quere et al. 2009). Indeed, xanthophyll-based photo-protection mechanisms were shown to respond to PAR changes in a few minutes (Jahns & Holzwarth, 2012) and to effects of abiotic constraints such as water or nitrogen limitations which are highly variables over broader temporal scales. The timing and temporal resolution of PRI measurements are therefore expected to have a great impact on PRI vs LUE relationships (Hmimina et al. submitted). For instance, PRI variability due to confounding factors may mask the low variability due to LUE in measurements done around midday at a daily resolution under water stress, which would explain the reported loss of PRI versus LUE relationship under water stress (Soudani et al. submitted). Moreover, the correlation between in-situ PRI measurements and LUE was found to be greatly impacted by sky conditions (Hilker et al. 2009, Soudani et al. submitted), with a clear loss of correlation under diffuse light despite the fact that angular effects are supposed to be at a minimum. Also, since photosynthesis is known to be sensitive to the ratio between direct and diffuse radiation (Alton et al. 2007, Urban et al. 2007, Brodersen et al. 2008), it is expected that the vertical distribution of radiation within the canopy, and thus of photosynthesis, may induce a mismatch between PRI and LUE depending of canopy structure and sky conditions.

It is therefore necessary to investigate the relationship between PRI and ecophysiological processes in order to evaluate the potential of PRI measurement as a whole ecosystem LUE proxy. Because vertical distribution of biophysical and ecophysiological

processes cannot be directly accessed, multi-layer canopy process-based models such as CASTANEA (Dufrene et al. 2005) can be used in order to investigate dependencies between PRI and canopy functioning.

In this work, we investigate relationships between PRI, LUE and CASTANEA derived physiological variables to assess the impact of canopy structure and sky conditions under different climatic conditions.

2. Materials and methods

2.1. Study sites and in-situ measurements

This study focus on two contrasted FLUXNET sites (FR-Fon and FR-Pue; www.fluxnet.ornl.gov). The first flux tower site is located in Fontainebleau, near Paris, and is a temperate deciduous forest mainly occupied by two overstory species: pedunculate and sessile oaks (*Quercus robur* L. and *Quercus petraea* (Matt.) Liebl) and a dense understory of coppiced hornbeam (*Carpinus betulus* L.). Its maximum leaf area index is approximately 5.5 m^2/m^2. The second flux tower site is located in Puechabon, near Montpellier in the south of France and is an evergreen broadleaf forest dominated by a dense overstory of holm oak (*Quercus Ilex* L.). Its leaf area index is approximately 2.9 m^2/m^2. More details can be found in Soudani et al. 2012.

In both site, several meteorological variables are recorded along with water and carbon fluxes which are used to estimate the net carbon exchange (*NEE*) and the gross primary production (*GPP)* as described in Delpierre et al. 2012.

Moreover, NDVI and PRI measurements are done with a half-hour resolution since 2006 in Fontainebleau and 2009 in Puechabon, respectively. The NDVI is acquired using a laboratory-made sensor described in Pontailler et al. (2003) and in Soudani et al. (2012). The PRI is acquired using a SKR 1800 sensor manufactured by Skye Instruments, Ltd. (Llandrindod Wells, UK). They share a common observed area, facing downward at an angle of approximately 20° from vertical and oriented to the south. Both sensors are mounted at 7 m and 5 m from the top of the canopy, resulting in a field of view of 8 m^2 and 4m^2 in Fontainebleau and Puechabon, respectively.

The NDVI sensors measure the reflected radiances in two spectral bands centered on 650 nm and 800 nm respectively. The NDVI is then calculated as follows:

$$NDVI = \frac{(Rd_{800} - Rd_{650})}{(Rd_{800} + Rd_{650})} \qquad \text{(Eq. 1)}$$

The PRI sensors measure the incoming and reflected radiances in two 10 nm wide spectral bands centered on 531 nm and 570 nm. The PRI is then calculated based on the reflectances as follows:

$$PRI = \frac{(\rho_{530} - \rho_{570})}{(\rho_{530} + \rho_{570})} \qquad \text{(Eq. 2)}$$

These two spectral indices are measured every minute, and averaged over a half-hour span. The whole setup is described in details in Soudani et al. submitted.

2.2. CASTANEA model.

The CASTANEA model, described in details in Dufrene et al. (2005), was used in this work. Briefly, CASTANEA is a multi-layer canopy model. The canopy is vertically represented by a variable number of layers depending on the whole canopy LAI. The main biophysical and ecophysiological processes (extinction of radiation, photosynthesis, respiration and carbon allocation, etc.) are explicitly described. The model was previously calibrated over the two study sites in Delpierre et al. (2009) and Delpierre et al. (2012).

In this study, the model was first validated over both sites by comparing simulated GPP and GPP measured using the eddy-covariance method at stand level. Then, main ecophysiological variables are simulated at a half hour time resolution and over a 5 years period in Fontainebleau (2006 to 2010), and 1.5 year period in Puechabon (2009, 2010). Hereafter, aPAR, GPP, LUE and Rs (soil water content) correspond to variables simulated at the stand scale. $aPAR_s$ and LUE_s are simulated at layer level. In these simulations, each layer represents 0.1 point of LAI. Relationships between PRI and LUE are analyzed at stand and layer scales.

2.3. Deconvolution of constitutive and facultative sources of PRI variability and statistical analysis

In order to deconvolve the two main sources of PRI variability, the model described in Hmimina et al. submitted (Eq. 3) was fitted using data measured over a moving window period of 5 days.

$$PRI = PRI_{0j} + \Delta PRI_j * Erf\left(\frac{PAR}{PARsat_j}\right) \qquad \text{(Eq. 3)}$$

with $PRI_{0j,}$ ΔPRI_j and $PARsat_j$ the fitted PRI_0, PRI maximum range and saturating PAR values for day j respectively.

The constitutive PRI variability is then obtained as the seasonal variability in PRI_0. The facultative variability is obtained as $PRI_c = PRI - PRI_0$. The facultative PRI variability is defined as the LUE-related PRI variability, and the constitutive PRI variability is defined as the LUE unrelated PRI variability, as defined in Gamon & Berry 2012.

In order to assess the relevance of the deconvolution, we investigated the seasonal dynamic of the goodness of fit as well as the correlation between PRI_0 and saturating PAR and CASTANEA-derived ecophysiological variables. PRI_c is then related to measured and simulated LUE at stand and stratum scales. Strengths of relationships between PRI and ecophysiological variables were examined using linear regressions. Because the size of data was very high and for comparison purpose, the regressions were bootstrapped as 1000 samples of 100 randomly selected observations. The median of regressions coefficients and R^2 were considered over each group of 1000 samples.

3. Results

3.1. Validation of CASTANEA.

In order to validate the use of CASTANEA as a way to estimate canopy LUE in both sites, CASTANEA-based GPP and LUE were compared to flux-tower derived GPP and LUE as shown in Fig.1.

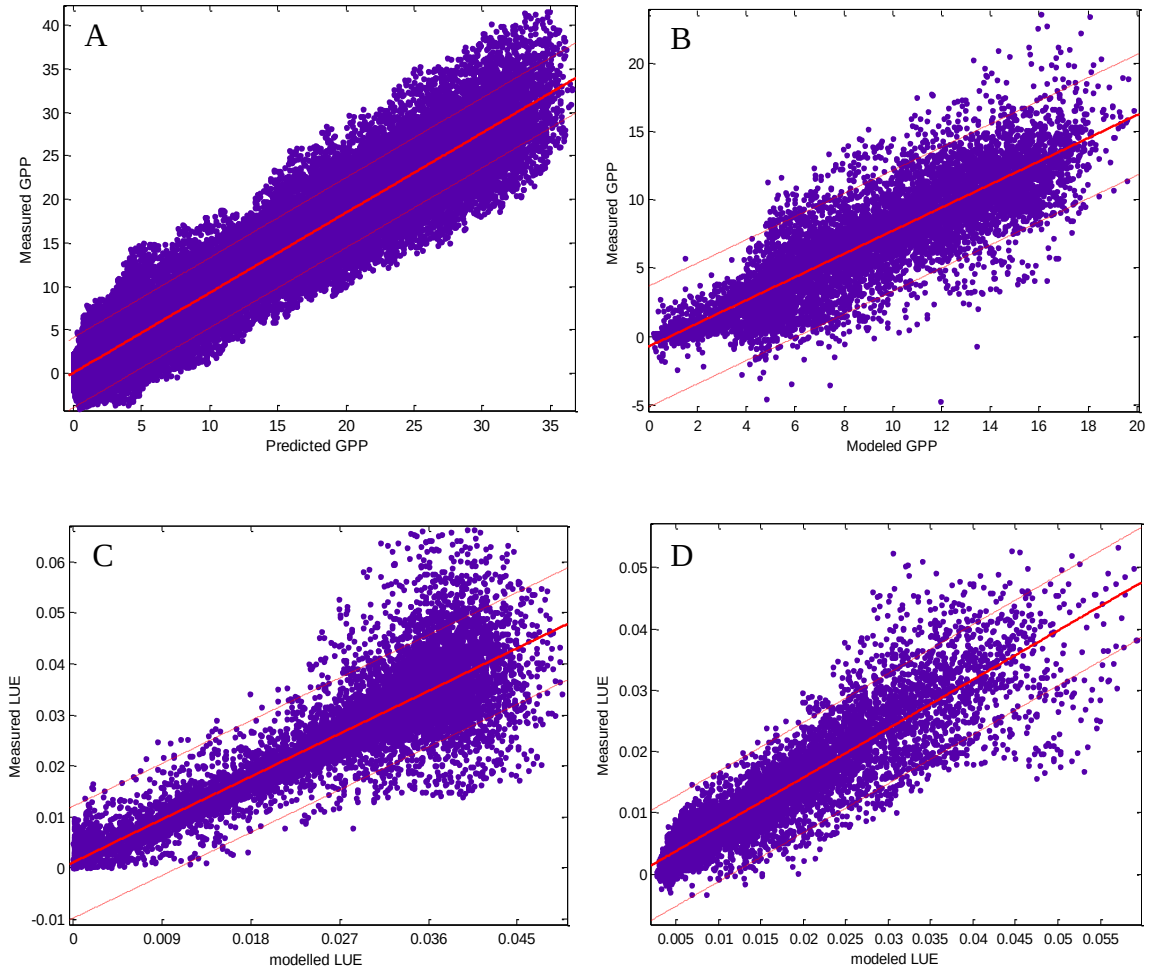

Figure 1: Regression between modeled and measured GPP (µmol CO_2/m²/s) (1.A and 1.B) and LUE (µmol CO_2 /µmol photon) (1.C and 1.D) in both study sites (Fontainebleau : 1.A and 1.C, Puechabon : 1.B and 1D).

The correlation between modeled and measured GPP and LUE are high in both sites. The residuals are normally distributed in both sites ($P < 0.01$ and $P < 0.03$ for the GPP and the LUE in Fontainebleau respectively, $P < 0.02$ and $P < 0.03$ in Puechabon). The relationship between predicted and measured LUE exhibits a high Heteroscedasticity, as shown by the increase in dispersion for high LUE values.

3.2. Temporal variability in PRI versus GPP and PRI vs LUE relationships.

The variability in PRI versus LUE relationship is then analyzed over the seasonal and infra-daily scale. R^2 are summarized in Figures 2.

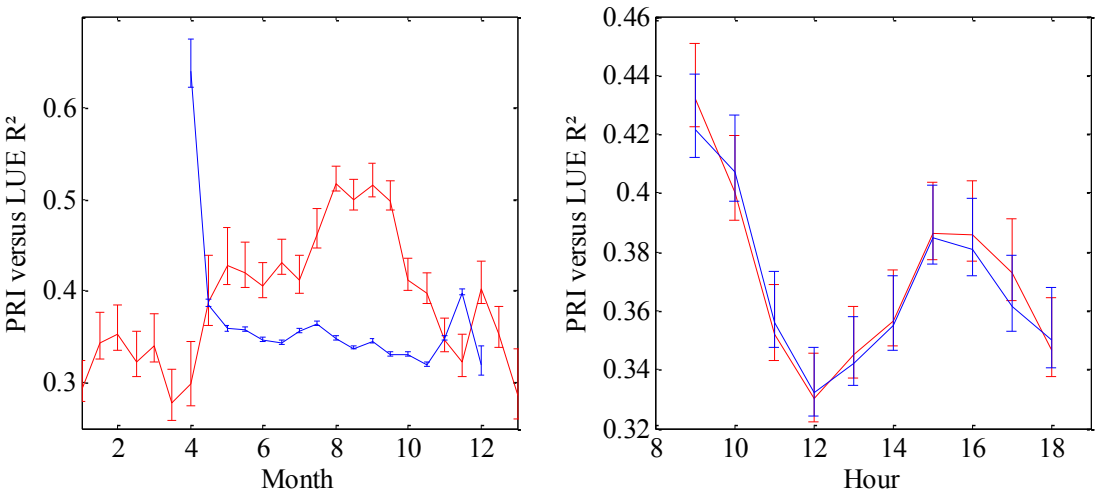

Figure 2: *Seasonal (left) and hourly (right) variability in PRI versus LUE relationship R² over both sites over a moving window of fifteen days (seasonal scale) and three hours (hourly scale). The blue line stands for the median over Fontainebleau site, and the red one for Puechabon. The bars indicate the 95% bootstrap confidence interval around the median.*

At the seasonal scale, the PRI versus LUE median R² exhibit contrasted patterns between both sites. In Fontainebleau, an increase in R² can be observed during the green-up and leaf senescence, while in Puechabon, the seasonal dynamic in PRI versus LUE R² is mostly characterized by an increase around October.

At hourly scale, the observed patterns are identical over both sites, and exhibit a decrease around midday and a high around 9 AM and 15 PM. The corresponding regression median slopes are shown in Figure 3.

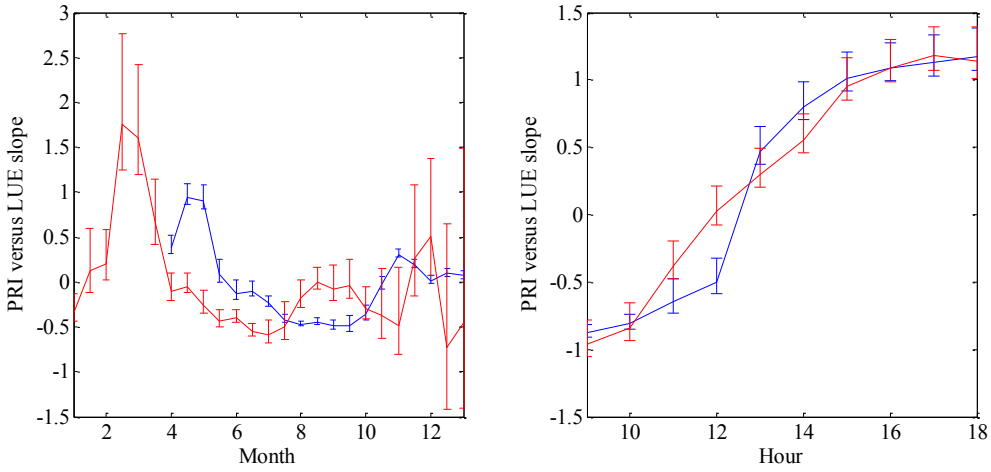

Figure 3: Seasonal (left) and hourly (right) variability in PRI versus LUE relationship slope over both sites. The blue line stands for the median over Fontainebleau site, and the red one for Puechabon. The bars indicate the 95% confidence interval around the median.

The median slope of the PRI versus LUE relationships exhibit a strong seasonal pattern, characterized by an inversion of the relationship during the green-up and leaf senescence in Fontainebleau, and around March in Puechabon (3.A).

The median slope also exhibits a high variability at hourly scale (3.B). Slopes of PRI versus LUE relationships are negative between 9 AM and midday and reverse in the afternoon.

Relationships between PRI and LUE are strongly improved when they are investigated at short time scales as shown in Figure 4 and Figure 5.

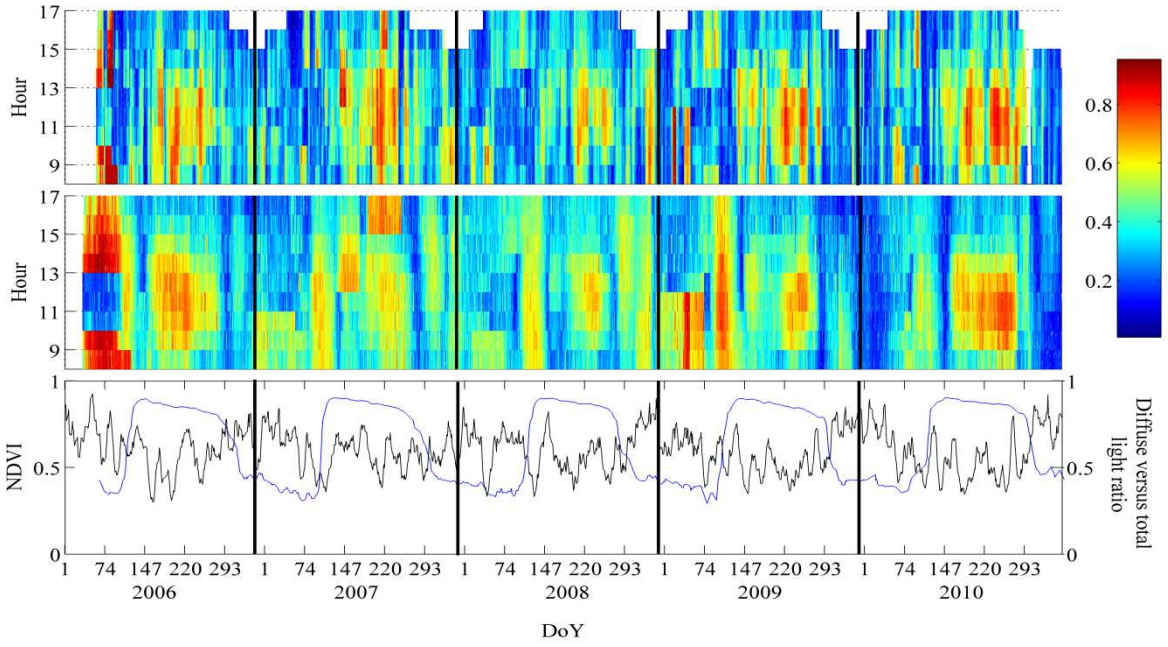

Figure 4: variation of the PRI versus LUE mean R^2 in Fontainebleau on the hour and daily scale, on 5 days moving window (higher panel) and 30 days moving window (middle panel). Seasonal variation of NDVI and ratio of diffuse light (lower panel).

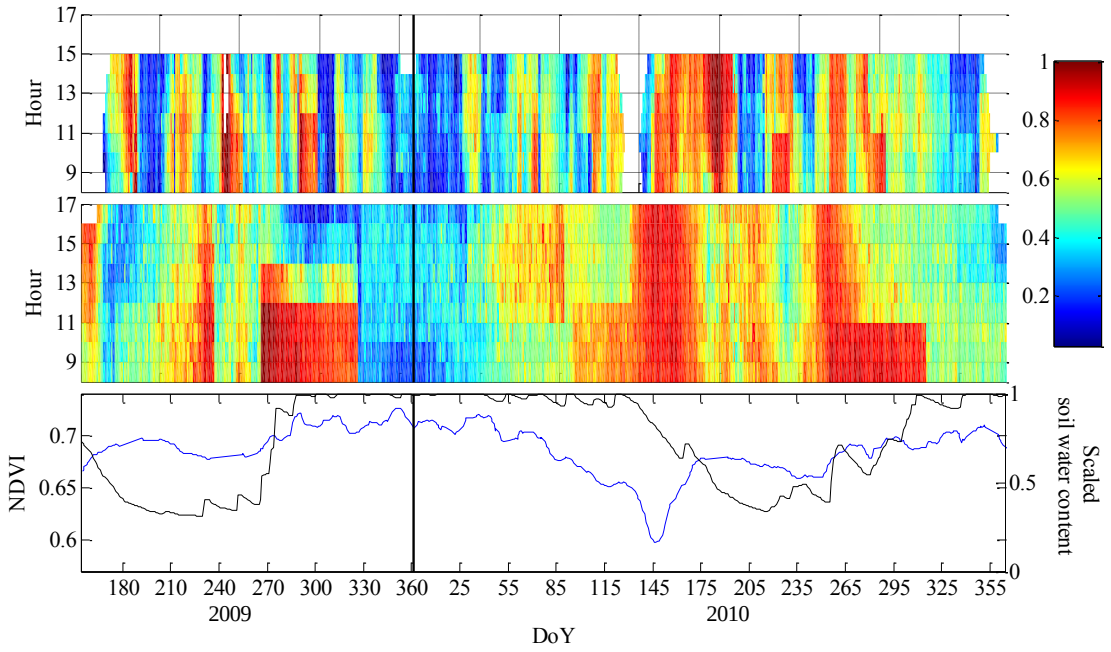

Figure 5: variation of the PRI versus LUE mean R² in Puechabon on the hour and daily scale, on 5 days moving window (upper panel) and 30 days moving window (middle panel). Seasonal variation of NDVI and scaled modeled soil water content (lower panel).

The patterns in PRI versus LUE relationship differ greatly between both temporal scales. A decrease in R^2 can be observed during green-up and senescence in Fontainebleau, as shown on the NDVI temporal profile. The overall patterns of the R^2 on a 5 days scale roughly match those of the diffuse light ratio as there is a visible loss of relationship between PRI and LUE under diffuse light. On a monthly scale, the R^2 seasonal patterns match those of the NDVI, with higher R^2 during the green-up and leaf senescence in Fontainebleau.

In the Puechabon site, the R^2 exhibits a slight decrease around midday and a high variability over a 5 days scale which didn't match the patterns of the measured variables. On a monthly scale, the R^2 are higher in the morning, and exhibit a pattern that does not match the pattern of the NDVI as opposed to the Fontainebleau site. Nevertheless, the LUE versus PRI R^2 increase with the variability in NDVI or soil water content.

While the relationship between PRI and LUE median R^2 do not differ significantly between morning and afternoon ($P > 0.57$), these relationships are mainly due to a strong relationship between the PRI and the aPAR.

3.3. Deconvolution of PRI variability

The PRI series were then fitted as PRI-aPAR light curves on a 5 days moving window using the model described in Eq.3. Those relationships, when significant at a 0.05 p-value threshold (76% of the obtained light curves, mean R^2=0.633 in Fontainebleau, 69% of the obtained light curves, mean R^2=0.57 in Puechabon) were used to derive the PRI_0, and saturating PAR.

The seasonal dynamics of these parameters are shown in Figure 6.

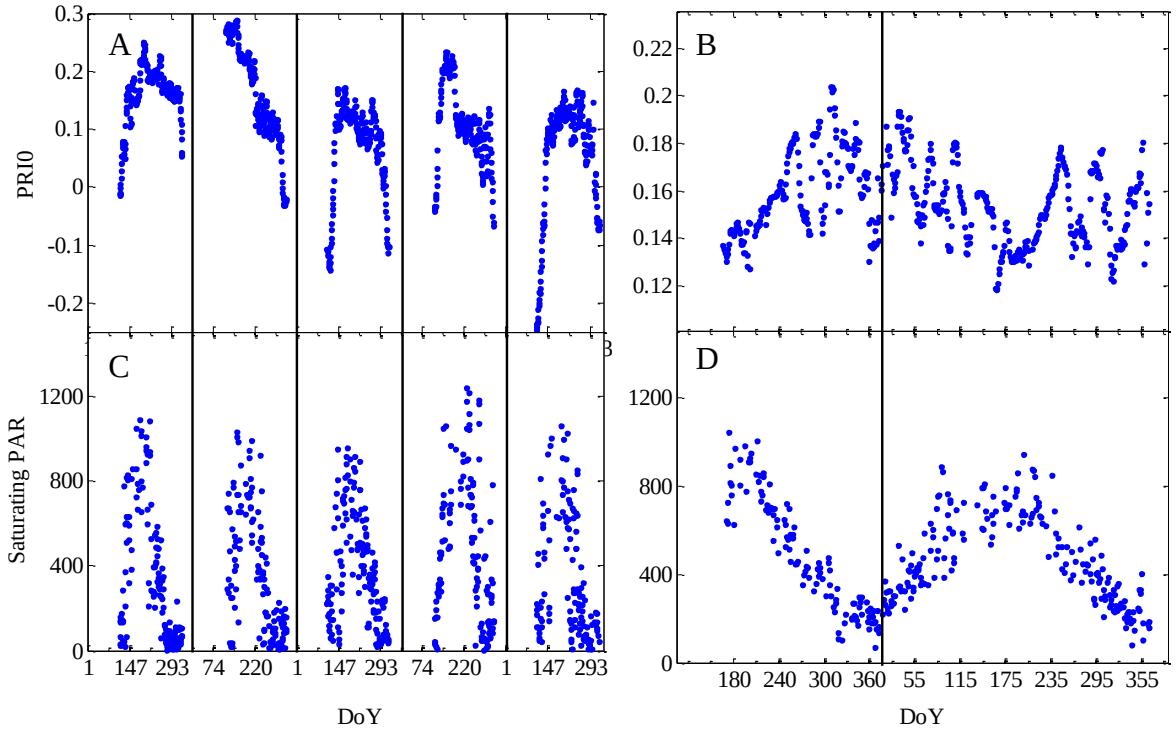

Figure 6: Seasonal dynamic of estimated PRI_0 (6.A and 6.B) and saturating PAR (µmol/m²/s) (6.C and 6.D) in Fontainebleau (6.A and 6.C) and Puechabon (6.B and 6.D) respectively.

The dynamic of the PRI0 are comparable to the dynamic of the NDVI (Soudani et al. 2012).

The relationships between PRI_0 and the NDVI are shown in Figure 7.

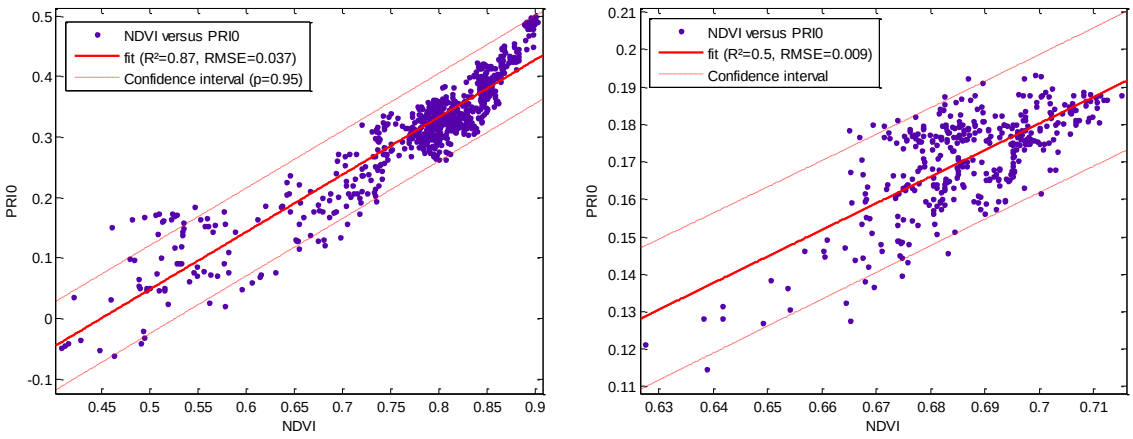

Figure 7: Relationship between PRI_0 and measured daily mean NDVI in Fontainebleau (left) and Puechabon (right).

The PRI_0 is highly correlated to the NDVI in Fontainebleau, but the PRI_0 versus NDVI relationship exhibits two distinct point clouds, one with low NDVI values, corresponding to the green-up and leaf senescence, and the other with high NDVI values, corresponding to the growing season. The correlation between PRI_0 and NDVI is high in each point cloud (R^2=0.79, RMSE=0.04 and R^2=0.8, RMSE=0.02 respectively), but their slope are significantly different (P <0.001). In Puechabon, the correlation between PRI_0 and NDVI is significantly lower, and the residuals are badly distributed. Nevertheless, we notice that a high correlation was found between soil water potential and PRI_0 during the drought events (R^2=0.83, RMSE=0.0061 for potentials under -0.15 MPa, R^2=0.015, RMSE=0.02 over the whole range).

As shown in Figure 6.C and 6.D, the saturating PAR could not be estimated precisely due to the strong non-linear shape of the PRI versus PAR relationship, and to the noise in PRI measurements which is particularly important in low PAR. The obtained seasonal dynamic is therefore noisy, particularly in Fontainebleau. Nevertheless, the estimated saturating PAR was highly correlated to soil water potential over the growing season in Fontainebleau (R^2=0.54, RMSE=166). The saturating PAR was correlated to the soil water potential for low values in Puechabon (R^2=0.68, RMSE=100). The slope of this relationship did not differ significantly from the one obtained in Fontainebleau (P > 0.12).

As done previously in chapter 3 (Fig 10, Soudani et al. submitted), the obtained PRI_0 (Fig.6) was then interpolated using a cubic spline in order to obtain continuous estimation and then subtracted to PRI in order to provide a corrected PRI_c. The relationship between PRI, PRI_c and LUE were compared over a broad range of time scales, and the resulting differences in R^2 are shown in Figure 8.

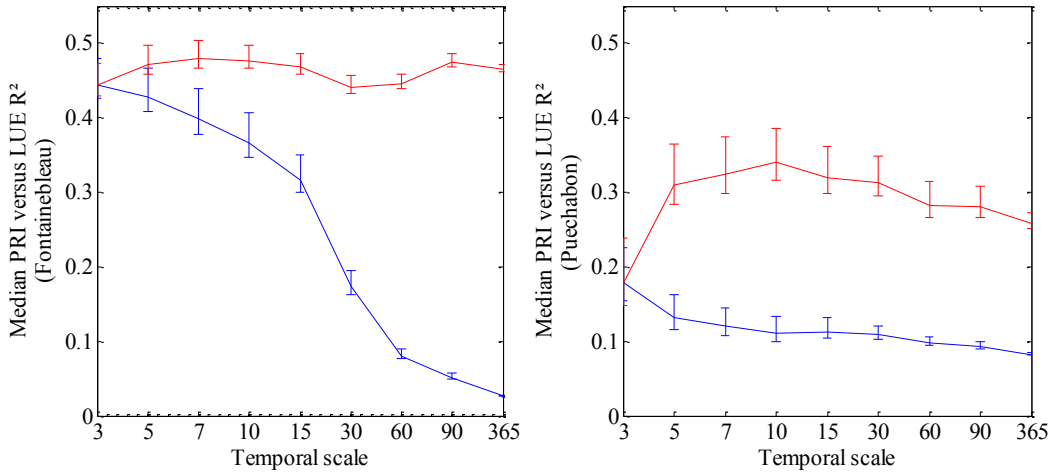

Figure 8: PRI and PRI_c versus LUE relationship R^2 in Fontainebleau (left) and Puechabon (right) over moving windows having different sizes (x-axis, days). The blue line stands for the PRI versus LUE median R^2, and the red line stands for the PRI_c versus LUE median R^2. The bars indicate the 95% confidence interval around the median.

The PRI versus LUE median R^2 decrease linearly with temporal scale (from 0.44 to 0.04 in Fontainebleau, and from 0.18 to 0.08 in Puechabon respectively). In comparison, the PRI_c versus LUE R^2 remain relatively stable over the range of temporal scales, except for an increase between 3 and 5 days and a slight decrease over periods longer than 10 days in Puechabon. Moreover, the obtained relationship parameters are stable over the whole range of temporal scales investigated as shown in Figure 8.

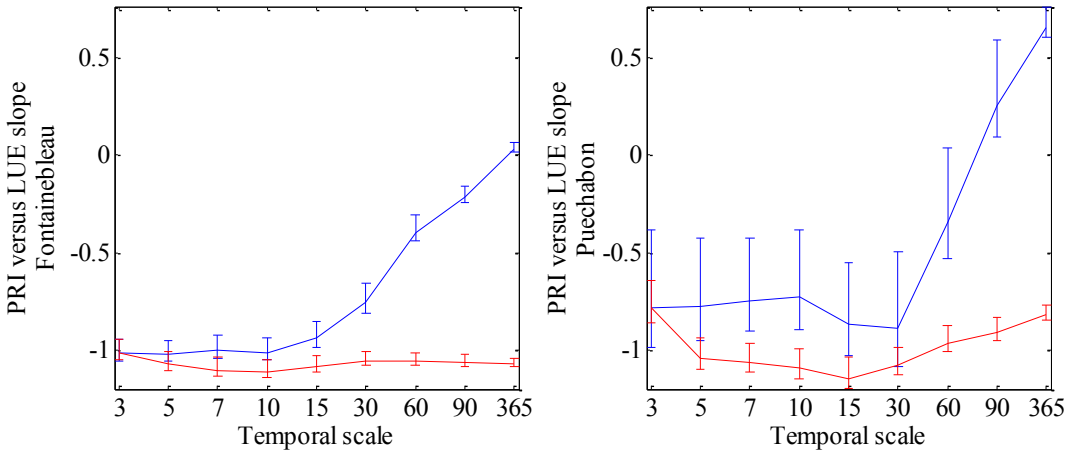

Figure 9: slope of the PRI versus LUE relationships in Fontainebleau (left) and Puechabon (right) over moving windows having different sizes (x-axis, days). The blue line stands for the PRI versus LUE median R^2, and the red line stands for the PRI_c versus LUE median R^2. The bars indicate the 95% confidence interval around the median

While the PRI versus LUE regression slope converge to zero with the increase of the temporal scale, the PRI_c versus LUE parameters remain stable. Moreover, the PRI versus LUE parameters variability is higher than the PRI_c versus LUE parameters variability which decreases with temporal scale. The parameters of most significant relationships over each bootstrap sample are similar for PRI_c, and similar to those of PRI_c for PRI, except for a higher variability.

3.4. Vertical variability in PRI versus LUE relationship.

After having corrected the PRI for the effect of seasonal changes in pigmentation and such, the stratification of the PRI_c versus CASTANEA-based LUE relationship is investigated and shown in Figure 10. The considered relationships are the one which exhibited the highest R^2 other each bootstrapped sample.

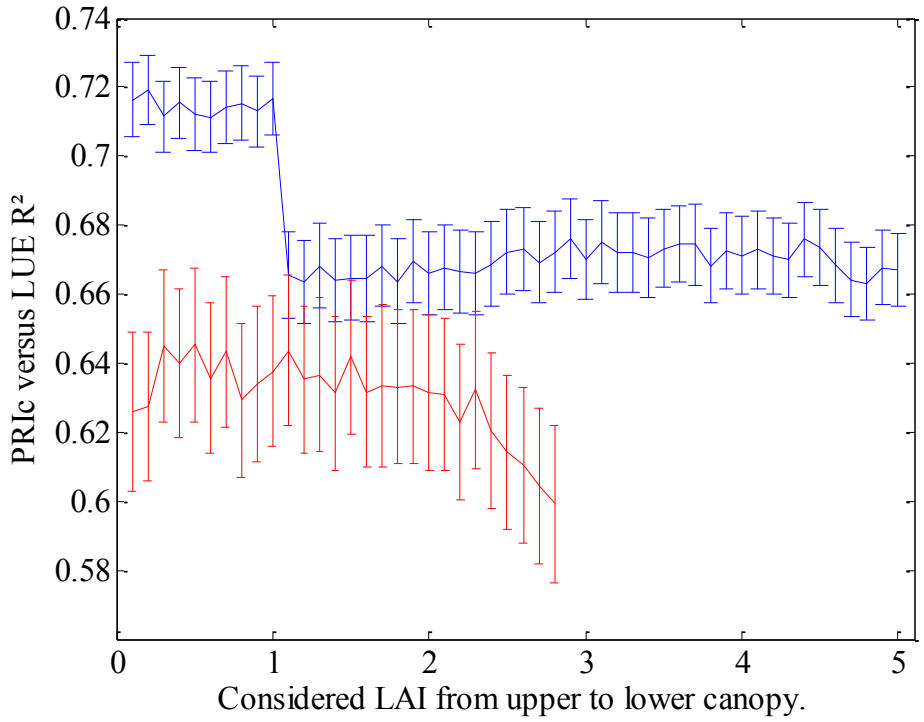

Figure 10: R-squares of the relationships between PRI_c and simulated LUE, as calculated on an increasing LAI from top to bottom in Fontainebleau (in blue) and Puechabon (in red). The bars indicate the 95% confidence interval around the median

The PRI_c versus LUE relationship drop sharply after the upper LAI point in Fontainebleau, whereas only a slight non-significant decrease for LAI above 2 can be seen in Puechabon. The temporal pattern in R^2 drop in Fontainebleau is detailed in Figure 11.

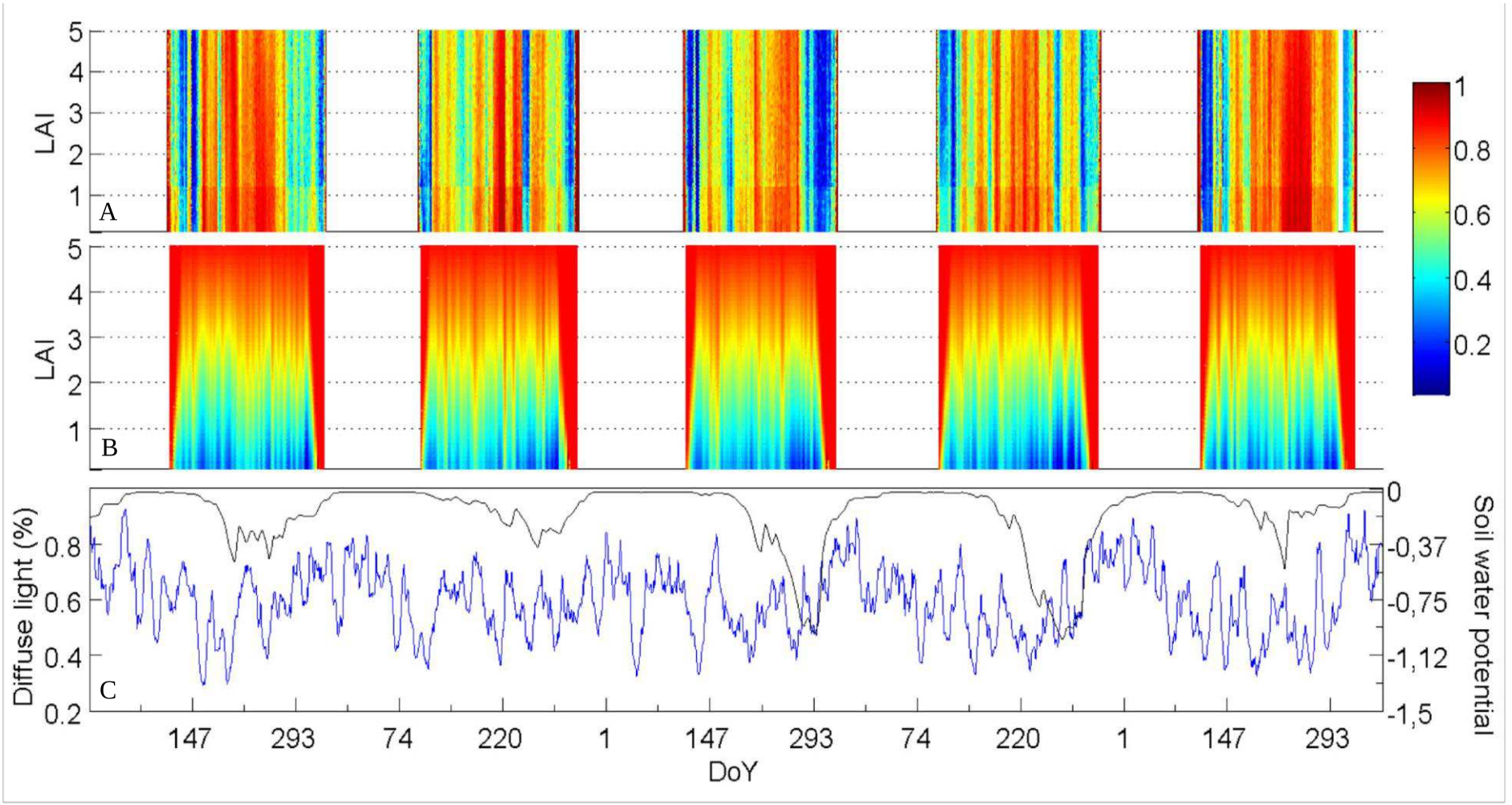

Figure 11: Relative loss in R^2 between PRIc and the LUE as calculated over an increasing LAI from the upper to bottom of the canopy (10.A). Relative contribution (%) of the aforementioned LAI units in the overall LUE (10.B). Seasonal dynamic of the diffuse versus total PAR ratio and of the soil water potential (10.C).

The drop in PRIc versus LUE R^2 around 1 point of LAI can be seen through the whole growing season, as long as the canopy total LAI is above a 2.5 m^2/m^2 value. On the other hand, the LAI responsible for 90% of the canopy LUE is highly variable, and is around 3.5 m^2/m^2 (+/-0.7). The broader patterns in PRIc versus LUE R^2 roughly match those of the soil water potential, while the finer patterns in PRIc versus LUE R^2 match those of the LUE relative contribution and diffuse versus total light ratio. The seasonal drop in PRIc response to high LAI derived LUE corresponds to stable low soil water potential, while the daily drop in PRIc response to high LAI derived LUE correspond to a higher contribution of low canopy strata to whole ecosystem LUE.

The median of simulated soil water potential and measured diffuse versus total light ratio is represented as a function of the relative loss of PRI_c versus LUE R^2 between the first layer of LAI and the whole ecosystem in Figure 12. The samples were drawn based on the relative loss of PRI_c versus LUE R^2 using a kmeans clustering algorithm.

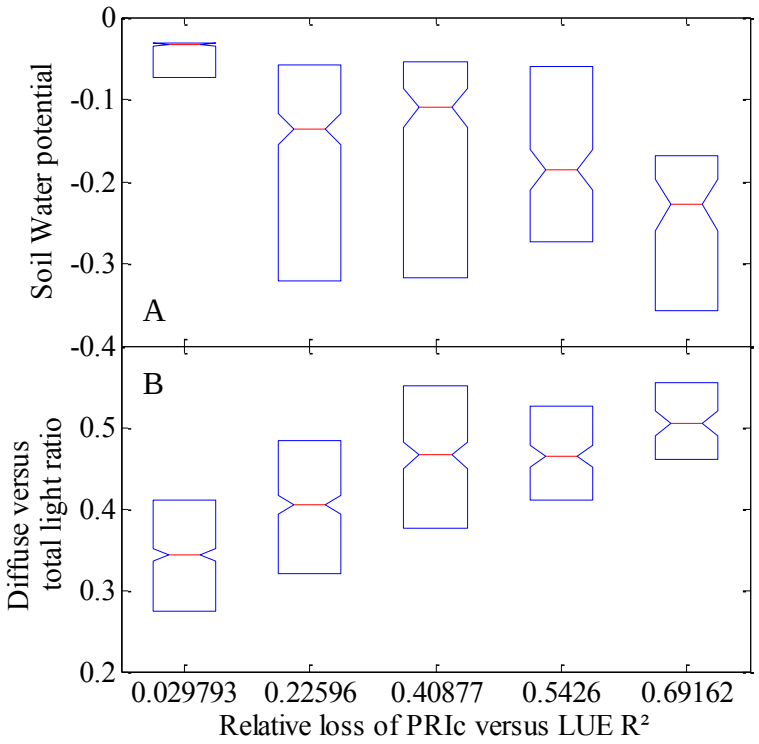

Figure 12: Median of soil water potential (12.A) and median of diffuse/total PAR ratio (12.B) versus daily relative loss of PRIc versus LUE R^2 between the first LAI layer and the whole ecosystem LAI. The red line stands for the median over each sample, the notches stand for the 95% confidence interval around the median, and the blue box stands for sample standard deviation.

While the linear correlation between soil water potential, diffuse versus total light ratio and the loss of PRI_c versus LUE R^2 is low (0.44 during the growing season), higher loss of correlation between PRI_c and LUE is shown to be associated with low soil water potential, and high diffuse light ratio.

4. Discussion

The two studied sites are greatly contrasted, and offer a wide range of situations which are particularly relevant to the estimation of PRI potential as a proxy of ecosystem LUE. The Fontainebleau site exhibit highly variable LAI and leaf chlorophyll content at the seasonal scale, and a relatively high maximum LAI which will allow us to investigate the vertical representativity of the measured PRI signal. The Puechabon site exhibit low LAI and leaf chlorophyll content variability, as well as a low maximum LAI, and is highly sensitive to drought.

The CASTANEA model, used in order to provide explanatory ecophysiological variables in this study, performs well over both sites. The validation of this model at the half-hour scale, as shown in Figure 1, shows that it was able to reproduce the infra-daily and seasonal patterns of GPP and LUE in both sites. In Fontainebleau, the residuals are randomly distributed, meaning that the patterns of GPP are accurately reproduced. The resulting LUE is modeled with a high accuracy, but the observed error increases with LUE. This phenomenon can also be explained by systematic errors in GPP measurement or estimation, which are amplified in low PAR. In Puechabon, a cloud of points can be observed for which the simulated GPP is overestimated, due to the difficulty to simulate the decrease in GPP due to the 2010 drought events. While the timing of the decrease in GPP is accurate, simulated values of GPP are slightly higher than those measured. This effect is partly alleviated when considering the LUE, due to its ratio structure.

In both sites, the seasonal PRI variability was higher than the daily variability. Peaks in correlation between PRI and LUE were found at seasonal scale in both sites (Figure 2.A), which were associated to a reversal of the PRI versus LUE slope (Figure 3.A). This indicates that the long-term relationship between PRI and LUE reflects fundamentally different phenomenon at the seasonal scale. At the hourly scale, two peaks in PRI versus LUE relationship were found in the morning and in the afternoon (Figure 2.B), showing an inversion in slope through the day (Figure 3.B). This phenomenon may be due to angular effects which may be predominant in the afternoon. The afternoon PRI versus LUE

relationship was indeed mostly due to a strong negative relationship between PRI and the incident PAR. In Fontainebleau, the periods exhibiting a high correlation between PRI and LUE occur mostly during green-up and senescence (Figure 4, middle panel and 4, lower panel). In Puechabon, those periods are associated to changes in NDVI, or in soil water content (Figure 5, higher panel and 5, lower panel). These facts confirm the high correlation between the PRI and canopy LAI and chlorophyll content which are also correlated to the LUE during these periods (Sims et al. 2002, Nakaji et al. 2006, Garbulsky et al. 2011, Hmimina et al. 2013b, Hmimina et al. submitted). While the patterns observed on a monthly scale in Puechabon reflect both changes in NDVI and soil water content (Figure 5, higher panel), the patterns shown in Fontainebleau reflect solely changes in NDVI, meaning that the LUE related PRI variability is masked by overwhelming phenology related variability (Figure 4, higher panel). Indeed, the patterns observed at 5-days scale are highly different than those observed at monthly scale, and mostly reflect changes in sky conditions in Fontainebleau (Figure 4, lower panel) or simulated soil water potential in Puechabon (Figure 5, lower panel). In several cases, periods of high correlation that shows at 5-days scale cannot be seen at monthly scale. The LAI and chlorophyll related relationship between PRI and LUE may therefore be a confounding factor rather than a mechanism of PRI versus LUE relationship at canopy scale. These effects are less visible in Puechabon due to a low temporal variability in pigment content.

Since the effect of phenology (ie : changes in LAI or canopy pigment content) interfere with the use of the PRI as a proxy of the LUE at the studied scale, the deconvolution approach introduced in Hmimina et al. submitted was applied to the measured signal in order to separate the PRI variability due to ecophysiological variables from the seasonal variability due to changes in canopy structure or biochemistry. The seasonal dynamic of the resulting PRI_0 defined as the estimated PRI of completely dark-adapted canopy exhibit patterns that are mostly similar to those of the NDVI (Figure 6.A and 6.B). The estimated PRI_0 are indeed highly correlated to the NDVI (Figure 7) in accordance to Rahimzadeh-Bajgiran et al. 2012, Gamon & Berry. 2013, Hmimina et al. 2013b, Hmimina et al. submitted. Although highly significant, this relationship arises from two distinct points clouds which exhibit different relationships. The overall relationship between PRI_0 and NDVI reflect the combination of the effect of changes in LAI and in leaves pigment content on PRI. It is therefore dependent of the site structural, biochemical and phenological characteristics. In Puechabon, the correlation between PRI_0 and NDVI is sensibly lower, which may be explained by the low NDVI variability. Nevertheless, this relationship is significantly different than those obtained in

Fontainebleau, indicating a complex combined effect of changes in LAI and canopy pigment content. The PRI_0 was also related to the soil water potential during drought events which may have a slight effect on canopy structural and biochemical properties in 2009. The estimated saturating PAR was correlated to the modeled soil water potential in Fontainebleau, in accordance with Hmimina et al. submitted. A comparable relationship with soil water potential was obtained in Puechabon during drought events, meaning that the saturating PAR, while it could not be estimated precisely, holds some physiological relevance. While the obtained relationship between PRI_0, saturating PAR and ecophysiological variables could not be used to provide a continuous estimation of the PRI_c, the PRI_0 was interpolated using a cubic spline and substracted to PRI measurement in order to derive an estimation of the PRI_c. As shown in Figure 8, the PRI_c allow a significant improvement in PRI versus LUE relationship, particularly over large temporal scales. While the PRI versus LUE R^2 quickly drop with temporal scale, the PRI_c yielded a stable relationship from a 3 days to a yearly temporal scale in both sites (Figure 8 and 9), meaning that most of the loss of PRI relationship which could be observed at the seasonal scale were due to the masking effect of changes in LAI or canopy biochemical properties. While the obtained increase in R^2 at broad temporal scales is sensibly lower than the one reported in Hmimina et al. submitted due to a lower temporal resolution (30 mn versus 5mn) and a higher noise in PRI measurement, it is of the same order of magnitude than the one reported in Soudani et al. Submitted, except for the Puechabon site where a significant improvement was obtained. Moreover, the bootstrapped maximum R^2, which were associated to models similar to the ones corresponding to the mean R^2 for PRI_c, are significantly higher than the one previously reported at comparable scales (Filella et al. 2004, Nakaji et al. 2008, Garbulsky et al. 2011, Soudani et al. submitted). The fact that similar and more stable relationships can be obtained on bootstrapped samples underlines the importance of random noise in PRI measurements. The resulting samples were used in the following analysis as ideally filtered series in order to minimize the effect of angular effects, measurement errors and residual confounding factors.

The R^2 of the relationship between PRI and the modeled LUE over an increasing LAI from the upper strata to the whole canopy, shown in Figure 10, exhibit a sharp drop in R^2 for LAI higher than 1 m^2/m^2 in Fontainebleau, while no clear stratification can be seen in Puechabon. This indicates the presence of a structural effect on the representativeness of the PRI measurement. The PRI only respond to changes of LUE in the first point of LAI, corresponding to sunlit leaves. The observed loss of R^2 is due to the contribution of lower leaves in whole canopy LUE. The temporal patterns of this contribution and of its effect on

the PRI_c versus LUE relationship shown in Figure 11 exhibit a high temporal variability. The R^2 between PRI and LUE quickly drop with LAI when the contribution of upper LAI strata in total LUE is low, which happens punctually due to high diffuse radiation ratio, and over prolonged period when high diffuse radiation ratio coincides with low soil water potential (Figure 12). The PRI versus LUE relationship may be lost at the ecosystem scale when lower leaves have access to an important amount of diffuse light while upper leaves photosynthesis is limited by water availability. In Fontainebleau, extrapolating the LUE calculated over the first LAI point to the whole canopy resulted in a 30% underestimation of predicted ecosystem LUE.

5. Conclusion

This work highlights the limitations of the use of the PRI as a proxy of the ecosystem LUE over several temporal scales over two contrasted ecosystems.

Firstly, PRI measurement acquired using standard broadband sensors and averaged over a 30 minutes time span proved to be sensible to angular effects and highly noisy, particularly in periods of low or diffuse radiation conditions. This issue could be resolved by using adaptive integration-time setting, such as the one described in Hmimina et al. submitted.

Moreover, it was shown that the confounding effect of changes or differences in LAI and leaf pigment explain most of the PRI patterns. While these factors mask physiologically related PRI variability during the growing season, they generate coincidental PRI versus LUE relationship during phenological events. These coincidental relationships are a major issue, since they may be misused in order to provide LUE estimations over broad spatial and temporal scales. While the effect of pigment content changes, or LAI changes may be accounted for by the use of several optical indices which could be used in order to correct the PRI, it was shown that there may be an interaction between the LAI and pigmentation effects, which would considerably hamper their deconvolution. No single relationship could be found over both sites between the estimated PRI_0 and NDVI or physiological variable available in this study. These effects may therefore depend on the canopy structural and biochemical properties, and may be site dependent. This constitutes a serious limitation of the use of PRI measurement over deciduous or contrasting sites, which could only be avoided thanks to the use of PRI light curve analysis in this study. While this method was shown to perform well over both sites, its use is limited by measurement temporal resolution, and accuracy, and

cannot be generalized over broader scales. A better comprehension of the obtained PRI_0 is clearly needed, and its temporal and spatial variability should be studied in depth.

Finally, the measured PRI vertical representativeness was shown to be limited to the sunlit foliage, which may hamper the use of the PRI as a LUE proxy over ecosystems exhibiting high LAI. In Fontainebleau, the surface of foliage representing most of the overall LUE was shown to be highly variable and to span beyond the scope of PRI measurements representativeness, notably during periods of diffuse light, and of abiotic stress. This result highlights a strong limitation of visible reflectance based remote-sensing as a way to study vegetal canopy functioning. The representativeness of such measurements should be studied in depth in link with both canopy structure and functioning. In this prospect, the coupling of proximal PRI measurement with multi-layered process based models was shown to hold a great potential.

Chapitre 5. Evaluation of the potential of MODIS satellite data to predict vegetation phenology in different biomes: an investigation using ground-based NDVI measurements

Hmimina G.[a], Dufrêne E.[a], Pontailler J-Y.[a], Delpierre N.[a], Aubinet M.[b], Caquet B.[d], de Grandcourt A.[d], Burban B.[e], Flechard C.[f], Granier A.[c], Gross P.[c], Heinesch B.[b], Longdoz B.[c], Moureaux C.[b], Ourcival J-M.[g], Rambal S.[g], Saint André L.[h], Soudani K.[a]

[a] University of Paris-Sud, CNRS, AgroParisTech, Laboratoire Ecologie Systematique et Evolution, Faculty of Sciences of Orsay, France.

[b] University of Liège - Gembloux Agro-Bio Tech (GxABT), Passage des Déportés 2, Gembloux, Belgium

[c] INRA, UMR EEF 1137 - INRA / University of Nancy, Champenoux, France

[d] CIRAD / CRDPI, France

[e] INRA, UMR Ecofog, Kourou, Guyane Française (French Guiana)

[f] INRA, Agrocampus Ouest, UMR 1069 SAS, Rennes, France

[g] CNRS, Centre d'Ecologie Fonctionnelle et Evolutive, Montpellier, France

[h] INRA - Unité Biogéochimie des Ecosystèmes Forestiers, Champenoux, France

Abstract

Vegetation phenology is the study of the timing of seasonal events that are considered to be the result of adaptive responses to climate variations on short and long time scales. In the field of remote sensing of vegetation phenology, phenological metrics are derived from time series of optical data. For that purpose, considerable effort has been specifically focused on developing noise reduction and cloud-contaminated data removal techniques to improve the quality of remotely-sensed time series. Comparative studies between time series composed of satellite data acquired under clear and cloudy conditions and from radiometric data obtained with high accuracy from ground-based measurements constitute a direct and effective way to assess the operational use and limitations of remote sensing for predicting the

main plant phenological events. In the present paper, we sought to explicitly evaluate the potential use of MODerate resolution Imaging Spectroradiometer (MODIS) remote sensing data for monitoring the seasonal dynamics of different types of vegetation cover that are representative of the major terrestrial biomes, including temperate deciduous forests, evergreen forests**,** African savannah, and crops. After cloud screening and filtering, we compared the temporal patterns and phenological metrics derived from *in situ* NDVI time series and from MODIS daily and 16-composite products. We also evaluated the effects of residual noise and the influence of data gaps in MODIS NDVI time series on the identification of the most relevant metrics for vegetation phenology monitoring. The results show that the inflexion points of a model fitted to a MODIS NDVI time series allow accurate estimates of the onset of greenness in the spring and the onset of yellowing in the autumn in deciduous forests (RMSE $\leq$ one week). Phenological metrics identical to those provided with the MODIS Global Vegetation Phenology product (MDC12Q2) are less robust to data gaps, and they can be subject to large biases of approximately two weeks or more during the autumn phenological transitions. In the evergreen forests, *in situ* NDVI time series describe the phenology with high fidelity despite small temporal changes in the canopy foliage. However, MODIS is unable to provide consistent phenological patterns. In crops and savannah, MODIS NDVI time series reproduce the general temporal patterns of phenology, but significant discrepancies appear between MODIS and ground-based NDVI time series during very localized periods of time depending on the weather conditions and spatial heterogeneity within the MODIS pixel. In the rainforest, the temporal pattern exhibited by a MODIS 16-day composite NDVI time series is more likely due to a pattern of noise in the NDVI data structure according to both rainy and dry seasons rather than to phenological changes. More investigations are needed, but in all cases, this result leads us to conclude that MODIS time series in tropical rainforests should be interpreted with great caution.

1. Introduction

Vegetation phenology is the study of the timing of seasonal events, such as leaf budburst and leaf senescence, that are considered to be the result of adaptive responses to climatic constraints. As such, an understanding of phenology brings important insights into both climate and vegetation interactions and their impacts on matter and energy exchange processes at local, regional and global scales. Because field phenological observations are work intensive and cannot be easily generalized, remote-sensing tools were developed to track Earth surface changes. The use of satellite-derived vegetation indices is now frequent in the literature and has been closely linked to canopy foliage biomass (Soudani et al., 2006), the onset of leaf greenness in the spring and the onset of leaf coloring in the autumn (Zhang et al., 2003; Soudani et al., 2008; Zhang and Goldberg, 2011). Remote sensing-based phenology began with the Advanced Very High Resolution Radiometer (AVHRR) (Reed et al. 1994) and has been significantly improved with the Moderate Resolution Imaging Spectroradiometer (MODIS) onboard Terra and Aqua satellites (Zhang et al. 2003). Data are acquired daily by AVHRR and MODIS sensors, but MODIS represents a significant improvement in terms of spatial resolution (250 m to 1 km vs. 1 km), spectral resolution (36 spectral bands vs. 6), geolocation accuracy [50 m at nadir (Wolfe et al., 2002) vs. 1 to 2 km (Box et al., 2006)], the atmospheric correction scheme and cloud screening (Heidinger et al., 2001) and sensor calibration (Justice et al., 1998). MODIS data are now used routinely for building the MODIS global vegetation phenology product that provides estimates of the timing of main vegetation seasonal cycles events at global scales. The first version of this product (MOD12Q2) was already evaluated, particularly in the studies of Zhang et al. (2003) and Soudani et al. (2008). Since 2009, a new version of the global vegetation phenology product (MCD12Q2) has been available that covers the period from 2001 through 2006. Compared to the first version, MCD12Q2 uses MODIS with both the Aqua and Terra platforms at higher spatial and temporal resolutions (500 m vs. 1 km and 8 days vs. 16 days). The first validation studies of this product are underway (Ganguly et al., 2010).

In the field of remote vegetation phenology sensing, considerable effort has been focused on developing noise reduction and cloud-contaminated data removal techniques [e.g., Best Index Slope Extraction (BISE) (Viovy et al., 1992), a CVA-MVC compositing algorithm used to produce MODIS-based global vegetation phenology products (Huete *et al.* 2002), an adaptive Savitzky-Golay filter (Chen et al., 2004) and a mean value iteration filter (Ma and Veroustraete, 2006)]. Different phenological markers were then derived from remotely-sensed

time series data after filtering and noise reduction pre-processing. These phenological markers may be categorized as follows (Soudani et al., 2008): (1) user-defined thresholds separating growing and dormancy seasons (White et al., 1997; Schwartz et al., 2002; White et al., 2002; Suzuki et al., 2003; Chen et al., 2004; White and Nemani, 2006; Delbart et al., 2006; Studer et al., 2007); (2) markers based on significant and rapid increases in remotely-sensed signals (Kaduk and Heimann, 1996; Moulin et al., 1997; Schwartz et al., 2002) and (3) parameters directly determined from functions fitted to remotely-sensed time series data (Jönsson and Eklundh, 2002; Zhang et al., 2003; Fisher et al., 2006; Beck et al., 2006; Soudani et al., 2008). These phenological markers are related to the vegetation cover types characterized by strong and rapid changes in leaf density that are sufficient to be detected by remote sensing sensors. These phenological markers focus on the beginning and end of the vegetation season, that is, the beginning and end of the period of canopy photosynthesis, respectively. These events are characteristic of the phenology of deciduous species. The timing of the beginning of the photosynthetically active period is associated with the emergence of buds and the first leaves. The timing of the end of this period is characterized by depigmentation, leaf yellowing and then leaf fall under the control of abscission processes. For evergreen species that show less seasonal change in foliage biomass, the noise inherent to satellite-based radiance measurements may completely mask the seasonal variations (Moulin et al., 1997). This interference may explain the fact that few studies have been devoted to the evergreen vegetation and that the potential use of remote sensing to monitor the seasonal dynamic of these biomes has not been sufficiently assessed.

Despite the technological maturity and significant progress achieved over the last 10 years, there remains a strong need for an effective and unbiased assessment of the potential and practical use of remotely-sensed data to monitor vegetation phenology. Indeed, the consequences of applying pre-processing techniques (atmospheric corrections, noise filtering, and compositing methods) on the performance of remotely-sensed time series for detecting phenological events have been evaluated under specific conditions through limited comparisons of one method against others without referring to field observations (Chen et al. 2004) or through comparisons with field observations that are themselves subject to multiple sources of uncertainty (operator bias, sampling density, temporal frequency, data compilation process, etc.). However, the multitude of remote sensing-based phenological metrics used can also make an accurate evaluation of the applicability of remote sensing for the detection of key vegetation phenological events much more difficult (White et al. 2009). Finally, from a practical point of view, phenological metrics provide many estimates that correspond to

different phenological situations, making their practical use in other studies problematic. Therefore, comparative studies between time series composed of satellite data in clear and cloudy conditions and of high-accuracy radiometric data obtained from ground-based measurements constitute a direct and effective way to assess the operational use and limitations of remote sensing in predicting the main plant phenological events. In this study, we sought to explicitly evaluate the potential use of MODIS remote sensing data for monitoring the seasonal dynamics of vegetation cover from *in situ* NDVI measurements in different vegetation cover types that are representative of the major terrestrial biomes, including temperate deciduous forests of oak and beech, an evergreen forest, a tropical rainforest, an African savannah, and a succession of crops. This assessment relies on tower-based measurements of NDVI at a half-hourly time step. After cloud screening and filtering, we will 1) compare temporal patterns and phenological metrics derived from *in situ* NDVI time series and from a MODIS daily and 16-day composite product. 2) evaluate the effects of residual noise and the influence of data gaps in the MODIS NDVI time series to identify the most relevant metrics for vegetation phenology monitoring.

2. Materials and methods

2.1. Study sites

This study was undertaken at seven experimental sites that are members of FLUXNET, the global network of eddy covariance flux towers measuring carbon, water and energy fluxes between the vegetation and atmosphere. These study sites cover three main bioclimatic regions (temperate, Mediterranean, and tropical) and the major plant functional types encountered: deciduous and evergreen forests, tropical moist evergreen forest, African savannah, and crops (Table 1). More details about these sites are provided in Soudani et al. (2012).

Site name	Type of Biome	Lat/Long	Altitude (m)	Average temperature (°C)	Average precipitation (mm)	Main vegetation species	Age (years)	Maximum Leaf Area Index (m^2/m^2)	Percent coverage of main species
Fontainebleau	Deciduous Broadleaf	48°28'35" N 2°46'48"E	120	10.2	720	Sessile and pedunculate Oaks (*Quercus petraea* (Matt.) Liebl and *Quercus robur* L.)	145	5	80%
Hesse	Deciduous Broadleaf	48°40'27" N 7°03'56"E	300	9.2	820	European beech (*Fagus sylvatica* L.,)	44	5.6	95%
Fougeres	Deciduous Broadleaf	48°22'59" N 1°11'05" W	140	11.2	900	European beech	40	-	95%
Puechabon	Evergreen Broadleaf forest	43°44'29" N 3°35'45" E	270	13.4	907	Holm Oak (*Quercus Ilex* L)	70	2.9	96%
French Guiana	Tropical rain forest	5°16'54" N 52°54'44" W	29	25.7	3136	150 species (DBH > 10 cm)/ha	-	7	-
Tchizalamou (Congo)	Herbaceous Savanna	4°17'210" S 11°39'23"E	82	25.7	1150	*Loudetia simplex*	-	1.6	75%
Lonzee (Belgium)	Succession of crops	50° 33' 8" N 04° 44' 42" E	165	10	800	Succession Wheat/Sugar beet/Wheat and mustard	-	-	100%

Table 1: Main characteristics of the study sites. Percent coverage quantifies the spatial representativity of the species "seen" by the in situ sensor over the MODIS pixel. This representativity is calculated on the basis of basal areas (or biomass in savanna) of the species present in the MODIS pixel from field inventories.

Briefly, the temperate deciduous forests are situated in the Fontainebleau, Hesse, and Fougeres regions in the Northern France. The two main overstory species are: sessile and pedunculate Oaks [*Quercus petraea* (Matt.) Liebl and *Quercus robur* L.] in the Fontainebleau forest, and beech (*Fagus Sylvatica* L.) in the Hesse and Fougeres forests. The Hesse site is described in more details in Granier et al. (2008)

The evergreen forests are situated in the Puechabon region in Southern France. The Puechabon site is a holm oak (*Quercus Ilex* L.) evergreen broadleaf forest. It is located on the northern Mediterranean coast, and is representative of the whole region. Holm oak is emblematic of Mediterranean sclerophyllous vegetation and is encountered in Southern Europe and the Arab Maghreb region in Northern Africa.

The tropical rainforest site is located in Paracou in French Guiana (Guyaflux experimental site). It is a mature forest with unknown human disturbance over the past centuries. This forest is characterized by a high diversity of plant species. The major species are in the

families of *Caesalpiniaceae*, *Lecythidaceae*, *Chrysobalanacae*, and *Sapotaceae*. More details about this experimental site are provided in Bonal et al. (2008).

The African savannah is located in the Tchizalamou study site (North-North-East of Pointe Noire – Congo). This site is part of the CARBOAFRICA network. It is composed of grassland dominated by the grass *Loudetia simplex* (Nees) Hubb., one of the most common species in this region of West Africa, with sparse shrubs of Annona arenaria (Schumach. & Thonn.). This area is burnt every year almost at the same date at the end of June. More details about this experimental site are provided in Castaldi et al. (2010).

The succession of crops is located in Lonzee in the Belgian province of Namur. It is composed of a succession of annual crops over three years at the same location as wheat (2007), sugar beet (2008), and wheat and mustard (2009). This site is part of CarboEurope-IP, and more details about this site and the farming operations are provided in Aubinet et al. (2009) and Dufranne et al. (2011).

For each site except the Guyaflux site, spatial representativity of the main species present in the MODIS pixel and "seen" by the *in situ* sensor is shown in Table 1. It is calculated as the ratio of basal areas (or biomass in Tchizalamou site) of species present in the field of view of *in situ* sensor to total basal area within MODIS pixel from field inventories. In forest stands field inventories were done on the whole MODIS pixel in Hesse and Fontainebleau sites (for Hesse forest, more details are given in Granier et al. (2008) and for Fontainebleau forest, data are unpublished but details about the forest stand are given in Delpierre et al. (2007)).In Fougere forest, field inventories were done in December 2010 on an area of approximately 10,000 m2 surrounding the flux tower. Both in and outside the sampled area, over the MODIS pixel, the stand is almost monospecific, composed of beech (unpublished data). In the Puechabon forest, inventory was made on 12 plots of 100m2 each around the tower. As shown in Table 1, the holm oak occupies about 96% of total basal area (31m ² / ha versus 32.3 m² / ha). This composition is considered as homogeneous on the 50 ha of the forest management unit and beyond, because the management over the past century was exactly the same across the whole forest region as shown in Goerner et al. (2009).In the tropical rainforest, as underlined above, there is a high specific diversity, including up to 180 different trees/ha, but no species is dominant. In the grassland savanna, Loudetia simplex, followed by Ctenium newtonii Hack. (Poaceae) accounted for more than 75% of the aerial total phytomass regardless of the season. The Lonzee herbaceous site, as shown in Dufranne et al. (2011), is a homogeneous agricultural area of about 12 ha.

2.2.*In situ* NDVI measurements and pre-processing

In situ measurements of NDVI were achieved using a laboratory-made sensor. More details about this NDVI sensor and the *in situ* measurement protocol are provided in Soudani et al. (2012). Briefly, NDVI sensors are made according to the design described in Pontailler et al. (2003) and Pontailler and Genty (1996). The body of the sensor is made of Teflon® installed into a stainless steel cylinder having a diameter of 3 cm and a height of 9 cm and is equipped with two photodiodes having spectral sensitivity in red and near-infrared bands. The two photodiodes are covered with two filters resulting in bandwidths of 640–660 nm and 780–820 nm for red and near infrared, respectively. The technical specifications of the components of the sensor are provided in Soudani et al. (2012). The sensor was calibrated against a spectroradiometer (LI-1800, LI-COR, Inc.). NDVI sensors are installed on towers above the vegetation, directed downward at a height of several meters above the top of the canopy. The sensor is inclined at approximately 30° from the vertical and oriented towards the south to avoid a hotspot effect. The field of view is 100°, but it is often collimated to account for viewing constraints encountered at each site. The area viewed is approximately tens to hundreds of square meters, depending on the site. The data were recorded at half-hour time steps in a data-storage central unit. The NDVI is computed for measured radiances reflected by the canopy.

The processing of *in situ* measurements of NDVI was achieved according to Soudani et al. (2012). Only daily radiance measurements acquired under clear sky conditions during the time of the MODIS overpass are considered in this study.

2.3.MODIS NDVI data and pre-processing

For this study, we used two MODIS products: MODIS NDVI MOD13Q1 V005 16-day composites and MOD09GQK daily surface reflectance at a 250 m resolution. The MOD13Q1 V005 16-day 250 m NDVI for years 2000 to 2009 were obtained through the MODIS Subset gateway for the pixels centered on the study sites. The MOD13Q1 NDVI values were built using the Constrained View Angle Maximum Value Composite (CV-AMVC) algorithm on a 16-day compositing period described in Huete *et al.*, (2002). The day of the year for each retained NDVI value is provided. The MODIS/TERRA surface reflectance daily L2G global 250 m V005 product (MOD09GQK) was obtained through the

Earth Observing System Data Gateway. We used the MODIS Reprojection Tool to extract the red and near-infrared bands and MODIS per-pixel quality assurance.

For each site, we used the pixel centered on the study site for each band and year, and we compiled them using MATLAB software (MATLAB 2008a, MathWorks, Natick, Massachusetts, USA). The NDVI was computed using MOD09GQK MODIS/Terra bands 1 (red: 630–690 nm) and 2 (near infrared: 780–900 nm) data produced at "ideal global quality".

$$NDVI = \frac{NIR-RED}{NIR+RED} \qquad (1)$$

Where *NIR* stands for the measured reflectance in the near infrared band and *RED* stands for the measured reflectance in the red band.

Unlike the MOD13Q1 products, which were already filtered using the 16-day CVA-MVC algorithm, daily MOD09GQK NDVI measurements are highly noisy despite the removal of pixels not flagged as "produced at ideal quality" in the pixel-level quality assurance (QA) image that provides QA descriptions about each pixel. Therefore, in this study, we developed the following scheme to improve the NDVI time series data. This scheme includes two steps:

- The removal of all values that can be considered unlikely considering what is known about the annual cycle of vegetation greenness using a Gaussian mixture model (GMM, McLachlan and Peel. 2000). For all studied biomes, we considered that the NDVI distribution is bimodal. The two modes correspond to low and high NDVI values. Low values coincide with the winter dormancy period in deciduous forests and periods of bare soils and low vegetation cover in crops and savannah. In evergreen forests, low NDVI values coincide with the short periods of leaf renewal that generally occur in the spring.
- The reduction of random noise using a moving-window mean filter based on the one described in Soudani et al. (2008).

First, to remove unlikely NDVI values contaminated by clouds and snow, a GMM was fitted on the distribution of NDVI values for each site and each year.

The two resulting Gaussian densities $N(\mu_1, \sigma_1)$ and $N(\mu_2, \sigma_2)$ with $\mu_1 < \mu_2$ provide three classes of NDVI values defined for each year, as follows:

- High NDVI values found in the $[\mu_2 - 2 * \sigma_2; \mu_2 + 2 * \sigma_2]$ interval.
- Intermediate values found in the $]\mu_1 + 2 * \sigma_1; \mu_2 - 2 * \sigma_2[$ interval.
- Low NDVI values found in the $[\mu_1 - 2 * \sigma_1; \mu_1 + 2 * \sigma_1]$ interval.

All NDVI values that were not within these bounds were discarded.

Second, we checked the distribution of NDVI acquisition dates in each of the three NDVI classes defined above. We assumed that the NDVI time series should exhibit coherent temporal patterns that predominate over noise and that most noisy observations correspond to low NDVI values. The few low NDVI observations occurring during periods that exhibit mostly high NDVI values are hereby considered as noise and vice versa. Formally, the NDVI filtering process was applied according the following rules:

- High NDVI values acquired on the dates that were closer to the modal date of the low NDVI values class than to the modal date of the high NDVI values class were discarded and vice versa.
- Intermediate values acquired during the dates that fell in the period of the high NDVI class were discarded.
- Low NDVI values acquired during the dates that fell in the period of the intermediate NDVI class were discarded.

After this first step of processing, the retained NDVI values were filtered and smoothed according to the algorithm presented in Soudani et al. (2008) using an 11-day moving window and excluding NDVI values lower than the average value minus the standard deviation of the NDVI values within the moving window.

2.4. Deriving phenological metrics from NDVI time series

For deciduous canopies, an asymmetric double-sigmoid function (ADS) was fitted to the NDVI time series independently for each year using the following equation:

$$NDVI(t) = p * t + (a + c) + \frac{1}{2} * (a - c) * \left(\tanh\left(b * (t - u)\right)\right) - \frac{1}{2} * (a - e) * \tanh\left(d * (t - v)\right) \quad (2)$$

tanh is the hyperbolic tangent, *t* is the time (day of year) and *a*, *b*, *c*, *d*, *e*, *u*, *v*, and *p* are the fitting parameters, where (*a* + *c*) is the winter NDVI value and (*a* - *e*) is the amplitude of the NDVI variation. *u* and *v* are the dates corresponding to the highest rates of change of *NDVI(t)* (maximum and minimum peaks of the first derivative of *NDVI(t)*) (Fig. 1). They are the dates of the two inflexion points when *NDVI(t)* increases during leaf expansion (*u*) and decreases during leaf senescence (*v*). *u* and *v* correspond to S_2 and A_2 shown in Figure 1, respectively.

Note that Eq. 2 is based on the equation of Zhang et al. (2003), rewritten as in Soudani et al. (2008) but modified by including two new parameters (*e* and *p*). The additional parameter *e* allows Eq. 2 to fit two different winter NDVI minima for the start and end of the year, and the parameter *p* accounts for the slight linear decrease observed in the NDVI time series during the winter and summer seasons (Fig. 1).

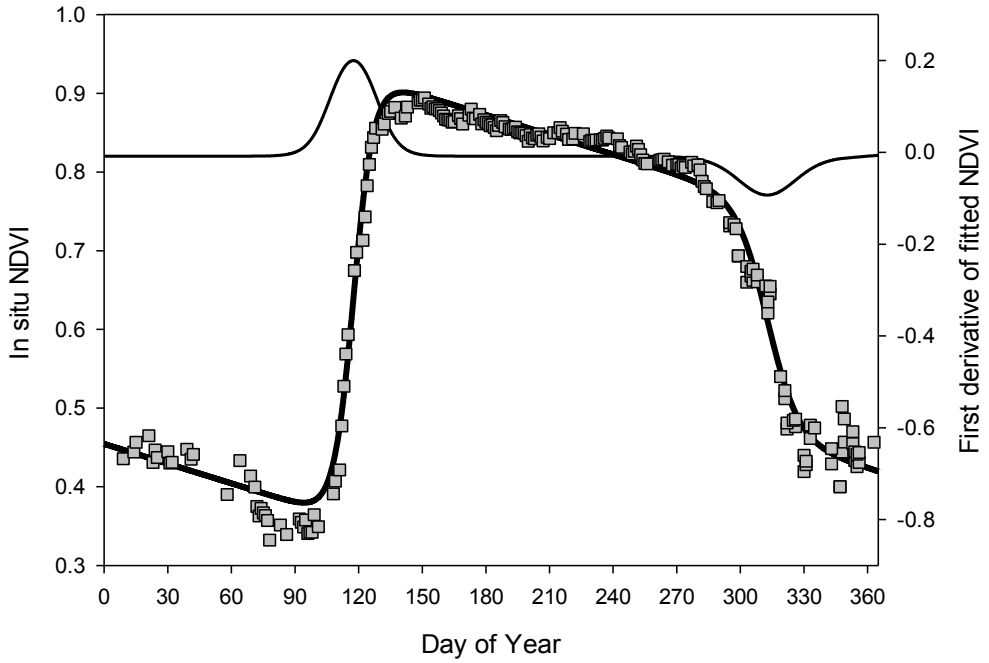

Figure. 1: In situ measured (gray square) and fitted NDVI time series (bold curve) over an oak forest stand in Fontainebleau during the year 2006. The rate of change given by the first derivative of the fitted NDVI time series (continuous curve – right axis). The vertical lines show six phenological markers derived from the fitted NDVI time-series (S and A refer to spring and autumn phenological events, respectively).

For the deciduous species and based on the fitted NDVI time series, we derived 6 metrics for both the spring (S_1 to S_3) and autumn (A_1 to A_3) seasons (Fig. 1). S_2 and A_2 are the dates of maximum increase and decrease of the NDVI (inflexion points) during the leaf expansion and leaf senescence phases, and they are directly given by *u* and *v* fitting parameters, respectively. The metrics S_1 and S_3 are the days of the year delimiting the leaf expansion phase in the spring. A_1 and A_3 are the days of year delimiting the leaf senescence phase in the autumn. S_1, S_3, A_1, and A_3 are determined from the local extrema of the third derivative of the fitted NDVI time series (Soudani et al. 2008). Note that S_1, S_3 and A_1, A_3 correspond to the onset of the greenness increase, the onset of the greenness maximum, the onset of the greenness decrease and the onset of the greenness minimum, respectively, given in the MODIS Vegetation phenology product (MCD12Q2). S_2 and A_2 are not given in the MCD12Q2 product.

For evergreen species whose phenological characteristics exhibit little change through time, and for crops and savannahs whose phenological characteristics exhibit irregular temporal patterns that cannot be modeled by the ADS function (Eq. 2), we used cubic splines to fit the NDVI time series because of their great flexibility for fitting data and because they are

differentiable, allowing for the implementation of the following phenological dates detection procedure:

- In a first step, the NDVI transition phases are localized by determining all local extrema. The duration of each phase is given by the duration between two successive extrema. Thus, each NDVI phase corresponds to a period of time where the NDVI varies in a monotonous manner.

- In a second step, all dates for which the ratio of the noise-to-signal metric described below (paragraph 2.5.1) is at a minimum and lower than the duration of the NDVI phase are considered as having a phenological significance. In other words, metrics that exhibit a noise-to-signal ratio higher than the duration of the NDVI transition phase were considered non-significant.

Figure 2 illustrates an *in situ* NDVI time series over an evergreen forest.

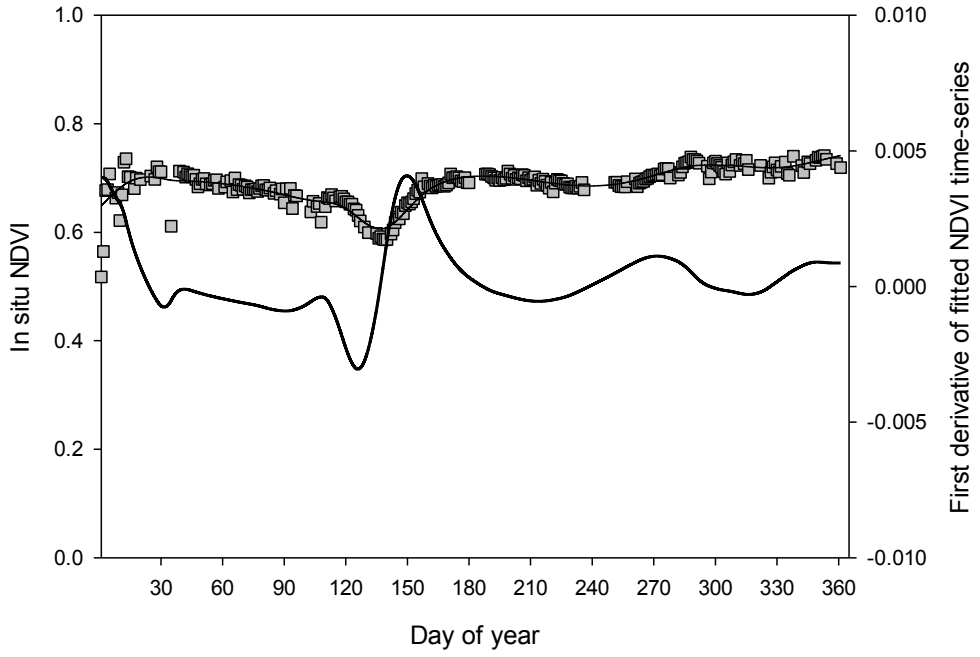

Figure 2: In situ measured (gray square) and fitted NDVI time series using cubic splines (continuous curve) over an evergreen broadleaf forest in Puechabon during the year 2009. First derivative of the fitted NDVI time series (continuous curve – right axis).

For every site, the dates of phenological events detected using MODIS daily and MODIS 16-days were compared to those detected using *in situ* NDVI time-series.

2.5. Theoretical assessment of the predictive power of vegetation phenology from *in situ* and satellite-based NDVI time series

2.5.1. Predictive power of vegetation phenological markers derived from *in situ* and satellite-based NDVI time series

Uncertainties on the dates of phenological events derived from NDVI time series are determined as follows. The NDVI time series may be written as:

$$NDVI\ (t) = fNDVI(t) + \varepsilon \quad (3)$$

$fNDVI(t)$ is the signal given by the fitted curve (ADS or cubic spline), and ε (fitting error) is a random noise with zero mean. This last assumption is discussed below.

The total variance of NDVI around time *t* describes the total information (signal and noise) contained in *NDVI(t)* and is given by the following equation (assuming independence between *NDVI* and ε):

$$Var\ (NDVI) = Var\big(fNDVI(t)\big) + Var(\varepsilon) \quad (4)$$

$Var\big(fNDVI(t)\big)$ may be locally approximated by:

$$Var\big(fNDVI(t)\big) \approx \left(\frac{dfNDVI(t)}{dt}\right)^2 * Var(t) \quad (5)$$

$\left(\frac{dfNDVI(t)}{dt}\right)^2$ gives the NDVI variance per unit of time and may be used as a measure of the information in the NDVI signal observed at time *t*. $Var(t)$ is the variance around time (t).

$Var(\varepsilon)$ corresponds to the variance of residuals between the predicted NDVI from the fit $fNDVI(t)$ and the observed NDVI values. $Var(\varepsilon)$ is equal to $RMSE(t)^2$ - i.e., the mean square error.

We define the predictive power of the NDVI time series locally at time (*t*) using the following expression:

$$pp(t) = \sqrt{\frac{RMSE^2}{\left(\frac{dfNDVI(t)}{dt}\right)^2}} \quad (6)$$

pp is expressed in days (time unit) and can be read as the number of days during which a monotonous variation in *NDVI(t)* should continue until it exceeds the noise. Therefore, *pp* is the theoretical uncertainty estimation of a given date (*t*) based on the NDVI change from the NDVI fit and taking into account the noise in the data around the fit. More generally, it corresponds to the noise-to-signal ratio and expresses the number of days necessary to obtain an NDVI temporal change higher than the NDVI noise.

The denominator is the first derivative of the NDVI fit because the estimation of the phenological metrics is based on the detection of an NDVI increase or decrease. The numerator term (*RMSE*) measures the NDVI noise. The noise is assumed to be constant over the year. For deciduous forests, this assumption is not strong after modifying the ADS function according to Eq. 2. Indeed, the examination of the NDVI time series shows a slight monotonic decrease in the NDVI throughout the seasons of winter and summer. The two parameters *p* and *e* were introduced to homogenize the distribution of residuals around the fit. However, over evergreen forests, the distribution of the residuals around the fit is not always homogeneous, as the flexibility of the spline that is used is not sufficient to account for all of the NDVI signal variations, which are particularly fast and short.

Eq. 6 was used to assess the potential error around an estimated phenological metric over both deciduous and evergreen forests.

2.5.2. Sensitivity analysis of MODIS-derived phenological metrics to data gaps in NDVI time series

To estimate the influence of data gaps due to clouds and snow in remotely-sensed NDVI time series on the ability to predict phenological events, we artificially introduced data gaps with several different lengths in *in situ* NDVI time series.

In a first step, the probability density function (pdf) of clear sky in the year at the time of the MODIS overpass was established using measurements of the sunshine duration acquired using a BF3 sunshine sensor (Delta-T devices) at a half-hour time step in the Fontainebleau tower-flux site during the year 2008. The year 2008 may be considered as a "normal year" representative of the regional cloud cover regime. We defined a clear sky as that in which the sunshine duration is at least 10 minutes per 30 minutes of measurements using the BF3 sensor. The pdf of clear sky days was determined using a non-parametric kernel smoothing density estimation fitted to the empirical histogram of clear days (Fig. 3). The pdf determines the conditional probability that the sky will be clear at the time of the

MODIS overpass on a given day of the year. For example, if it is assumed that half of the year is covered by clouds during the MODIS overpass and that all days are equally likely to be cloudy, then the probability of having a clear sky for a given day is: *(1/365) × 0.5*.

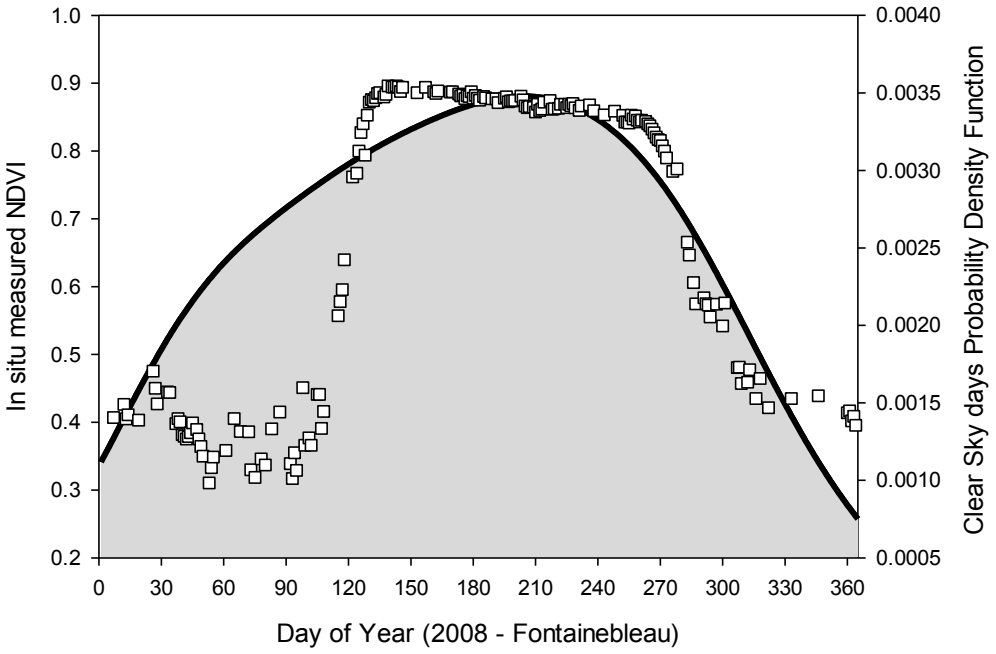

Figure 3: In situ measured NDVI in Fontainebleau forest for the year 2008 (empty square, left axis). The filled area under the continuous curve is the probability density of clear sky for each day of the year (the sky is considered clear when the sunshine duration is at least 10 min per period of 30 min at the time of the MODIS overpass (right axis)).

In a second step, an *in situ* NDVI time series is used to randomly generate an NDVI time series with gaps. We generate an NDVI time series with between 30 and 189 observations according to the probability density function for clear sky determined above. For each length of the NDVI time series, this operation is repeated 100 times. As a result, a total of 16,000 NDVI time series were created. Then, the ADS (Eq. 2) was fitted to each sample of the simulated NDVI time series, and the six phenological metrics defined above were estimated.

To quantify the strength of the NDVI signal of each simulated NDVI time series, we calculate the first derivative of the fitted NDVI at the date of each NDVI observation of the dataset. The absolute values of the first derivatives averaged over the series are used as a simple measure of the NDVI signal strength. For example, for a time series composed of very close NDVI values, it is expected that the curve fitted to the NDVI time series will be flat, the

first derivative calculated for each NDVI observation will be zero or close to zero and the average signal strength over all NDVI observations will also be zero or close to zero.

Finally, according to the strength of the NDVI signal, we grouped all samples into 100 classes using an unweighted pair group method with the arithmetic mean (Sokal and Michener, 1958). For each class, we determined the average length of the simulated NDVI time series within the class and the average RMSE between the estimates of the phenological marker determined from the simulated time series and full NDVI time series.

3. Results

3.1. Comparison between ground- and MODIS-based NDVI time series

Figure 4 shows the overall comparison between the *in situ*, daily and 16-day MODIS NDVI data.

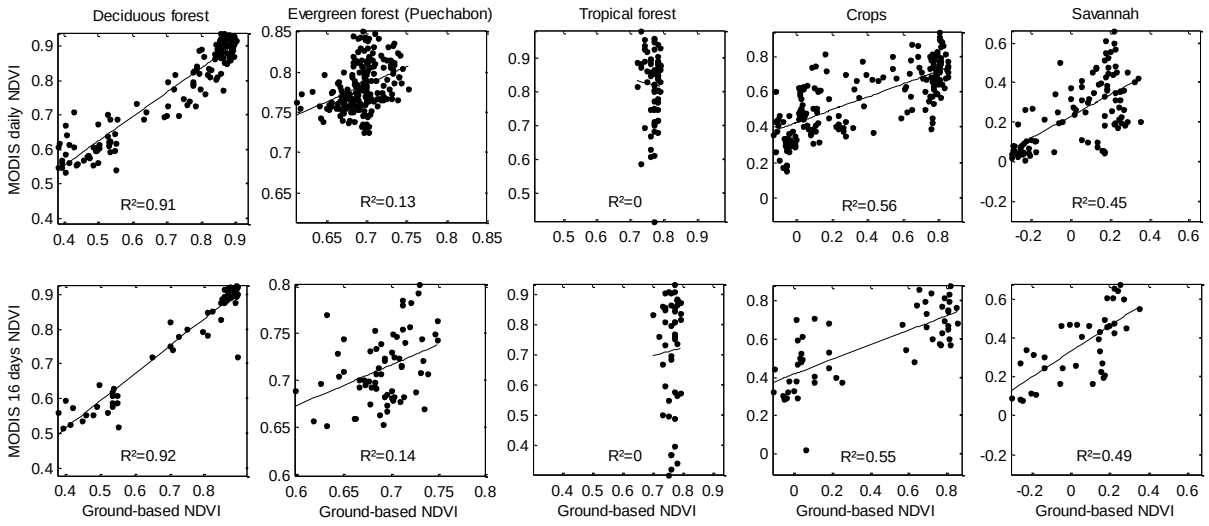

Figure 4: In situ NDVI (x-axis) versus daily (upper figures) and 16-day composite MODIS NDVI data for the different biomes. R²: Coefficient of determination.

For all vegetation types, the MODIS NDVI values are generally higher than those measured by *in situ* sensors. For the deciduous forests, the overall agreement between *in situ* and MODIS NDVI data is very good ($R^2 = 0.91$, $p < 0.00$). In the holm oak forest at Puechabon, the relationship is highly scattered due to small temporal changes in the canopy foliage area compared to the magnitude of the noise affecting the NDVI signal, even after filtering ($R^2 = 0.13$, $p < 0.00$). In the tropical forest, no significant relationship could be found ($R^2 = 0$, $p < 0.75$). In the succession of crops in Lonzee ($R^2 = 0.56$, $p < 0.00$) and in the

savannah site ($R^2 = 0.45$, $p < 0.00$), the relationships between *in situ* and MODIS NDVI measurements are significant but noisy despite the high *in situ* NDVI temporal changes.

In the deciduous forests, the linear relationships between the *in situ* and daily MODIS NDVI and between the *in situ* NDVI and MODIS 16-day composite data are similar for all sites (Fig. 4). While both filtering methods – CVA-MVC and GMM – appear to perform equally well, the filtering method based on a GMM applied to the daily MODIS NDVI time series provides a better temporal resolution and, as expected, preserves the intermediate values, which generally correspond to key phenological phases (leaf expansion and leaf senescence), as shown in Figure 4.

While the filtered MODIS NDVI observations are linearly correlated to the *in situ* NDVI measurements for deciduous forests, the evergreen forests exhibit a high level of noise in regard to the low *in situ* NDVI variability. The noise levels as estimated using RMSE between the observed and fitted NDVI time series in the evergreen forest in the Puechabon and deciduous forests are similar (0.03 versus 0.04), and the lack of correlation is mainly due to a low NDVI temporal variability (low seasonal variation of phenology). In the tropical forest of French Guyana, no significant relationship could be found between the MODIS and *in situ* NDVI observations ($p < 0.75$). The RMSE is larger than in the deciduous forests (0.12 versus 0.04), possibly due to the effects of sub-pixel cloud contamination not detected by a MODIS cloud mask algorithm and a failure in the filtering process.

Despite the noise in the data, the *in situ* and MODIS data reproduce similar temporal patterns in deciduous forests (Fig. 5). The NDVI time series show with high temporal resolution the phenological seasonality of these species, which is characterized by two phases: the growing season from mid-spring to summer and the dormancy season during late autumn and winter. These main phases are separated by two short transition phases delimited by two main phenological events: the onset of greenness when budburst starts in the spring and the onset of senescence in the autumn.

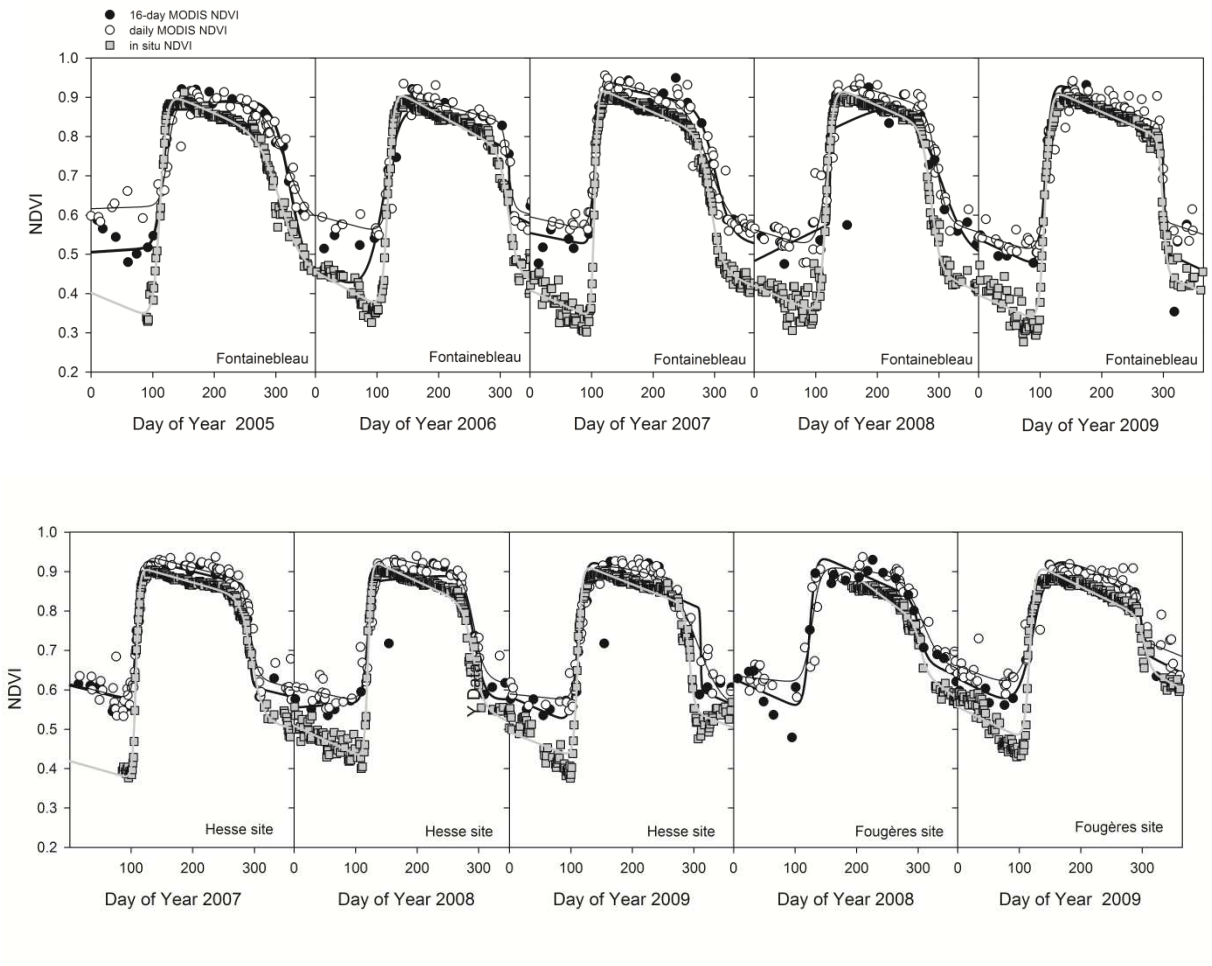

Figure 5: Time series of in situ NDVI (gray squares), daily MODIS NDVI (empty circles) and 16-day composite MODIS NDVI (filled circles) over deciduous forests.

For the evergreen broadleaf forest of Puechabon (Fig. 6), the *in situ* NDVI time series show clear phases of NDVI decrease during the spring despite small NDVI variations. This pattern is consistent with the phenology of the holm oak characterized by the partial foliage renewal each year from March to the middle of June. Note that in the Puechabon forest, an unexplained sensor dysfunction coinciding with strong rains explains the gap in NDVI measurements during the autumn of the year 2008. The MODIS daily and MODIS 16-day composite NDVI time series show small signal variations that do not coincide with the *in situ* NDVI measurements.

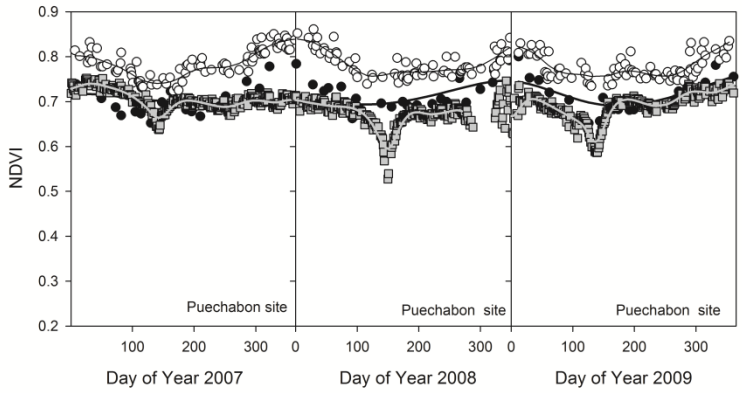

Figure 6: Time series of in situ NDVI (gray squares), daily MODIS NDVI (empty circles) and 16-day composite MODIS NDVI (filled circles) over an evergreen broadleaf forest in Puechabon. The continuous curves represent the series of cubic splines fitted to the NDVI data.

In the tropical forest (Fig. 7), *in situ* NDVI time series show two periods characterized by declines in the NDVI of variable magnitudes occurring around the middle of March for the first period and around days 300-320 (October) for the second period. For the first period, the decline in NDVI is clearly visible in 2007 and 2008. For the second period, the decline in NDVI appears only in 2008 and 2009. The first period of NDVI decline was much shorter than the second one. The second decline was more pronounced in 2009. Contrary to the *in situ* NDVI measurements, MODIS NDVI time series (Fig. 7) include so much noise that none of the tested filtering methods could provide a usable signal. The temporal pattern from the MODIS 16-day composite NDVI data is inconsistent with the *in situ* NDVI time series. This pattern is mainly characterized by two periods that coincide with the main rainy season from December to July (sometimes interrupted by a short dry season in March called the little summer of March) and the main dry season (July – November). The rainy season is characterized by abnormally low values of NDVI, and the second period is characterized by NDVI values at the same level as the daily MODIS NDVI data. This temporal pattern may arise from variations in noise intensity. As shown in figure 7, none of the tested filters could provide a good agreement between the *in situ* and MODIS observations.

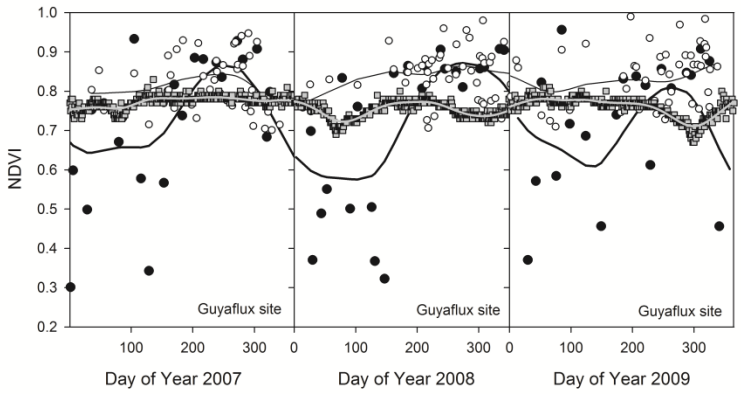

Figure 7: Time series of in situ NDVI (gray squares), daily MODIS NDVI (empty circles) and 16-day composite MODIS NDVI (filled circles) over the tropical forest in French Guyana. Continuous curves represent the series of cubic splines fitted to the NDVI data.

During the succession of crops at the Lonzee site (Fig. 8), the *in situ* NDVI measurements started in 2007 at the end of March, during the growth of winter wheat. For this crop, the *in situ* NDVI increases during the spring, reaches a peak at the end of April and then decreases during June and July to reach a minimum value a few weeks before the harvest at the beginning of August. After the harvest, the NDVI peaks again in the first week of September due to a re-growth of wheat and weeds. In 2008, during the growth of the sugar beet crop, the NDVI increases, reaches its maximum at the end of June and remains almost constant during the summer until the harvest at the beginning of November. In 2009, the *in situ* NDVI time series is bimodal, reproducing the phenology of a succession of two crops of winter wheat and mustard.

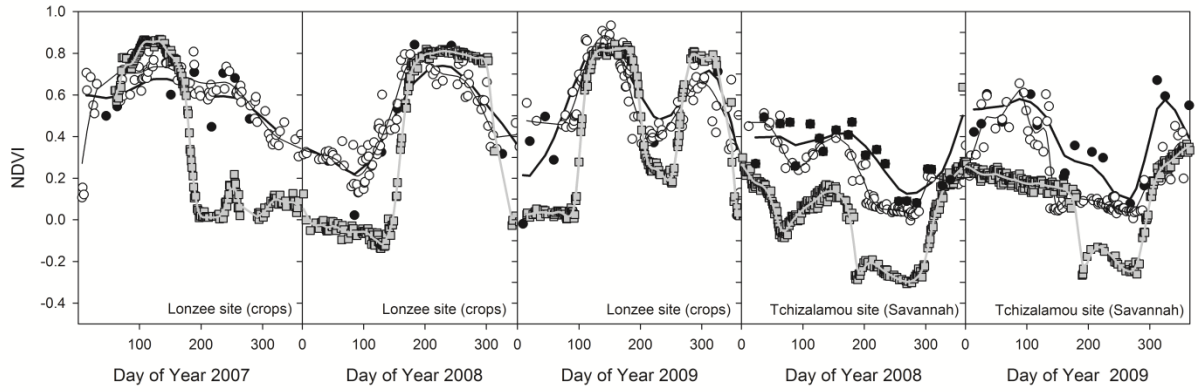

Figure 8: Time series of in situ NDVI (gray squares), daily MODIS NDVI (empty circles) and 16-day composite MODIS NDVI (filled circles) over herbaceous species in Lonzee (succession of crops) and at the Tchizalamou site (African savannah). Continuous curves represent the series of cubic splines fitted to the NDVI data.

In the succession of crops, the MODIS daily and 16-day composite signals (Fig. 8) exhibit strong noise, but the main temporal patterns associated with the phenology of this vegetation could be identified.

In the grass savannah at the Tchizalamou site (Fig. 8), the temporal patterns of the *in situ* NDVI measurements in 2008 and 2009 are similar, with the exception that the NDVI remains high during February and March 2009. The NDVI is at its maximum during the main wet season from October to May and at its minimum during the main dry season from May to October. The first decrease of the NDVI in 2008 is due to a short dry season, which may occur in February - March. For the two years, the sudden drop of NDVI at the end of the wet season is due to human-induced fire. Nevertheless, it is important to note that the mismatch between the *in situ* and MODIS observations in the savannah site occur during both the rainy and dry seasons, and it is most likely due to contamination of the data by clouds that are not detected by the filtering process.

3.2. Comparison of phenological metrics estimates derived from *in situ* and MODIS daily NDVI time series.

For the deciduous species, the comparative analysis for the 6 considered phenological metrics are shown in Figure 9 and Table 2.

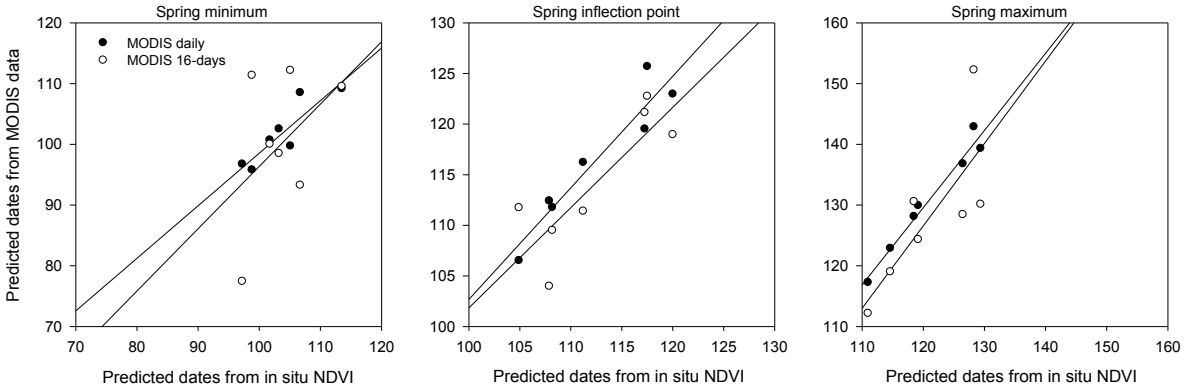

Figure 9: In situ NDVI-derived metrics (Day of Year) versus MODIS NDVI-derived metrics (Day of Year) for deciduous forests.

	S1		**S2**		**S3**		**A1**		**A2**		**A3**	
	MODIS daily	MODIS 16-day	MODIS daily	MODIS 16-day	MODIS daily	MODIS 16-day	MODIS daily	MODIS 16-day	MODIS daily	MODIS 16-day	MODIS daily	MODIS 16-day
MAE	2.5	9	4	3	10	7	11	11	4	5.5	15	12
Bias	-2	-3.5	4	1.5	10	7	-4	7.5	2.5	4	9	0.5
RMSE	3.	11	4.5	4	10	10.5	14.5	14	6	8	22	14
R^2	*0.8*	0.2	*0.9*	*0.7*	*0.97*	*0.59*	0.42	0.76	0.56	*0.47*	0.04	0.01
p	***0.007***	*0.312*	***0.001***	***0.019***	***0.000***	***0.043***	*0.115*	*0.102*	*0.052*	*0.09*	*0.668*	*0.825*

Table 2: Comparison between the phenological metrics derived from the in situ NDVI measurements (considered as reference) and MODIS data. (S_1, S_2, S_3) for the spring and (A_1, A_2, A_3) for the autumn. MAE (days): mean absolute error, bias (days): (+) MODIS overestimation, (-) underestimation, RMSE (days): root mean square error. R^2: coefficient of determination of the regression between the phenological markers based on the in situ and MODIS NDVI time series.

The best agreement between the predictions of the phenological dates based on the MODIS time series and *in situ* NDVI measurements is found for the two inflexion points S_2 and A_2 during the leaf expansion and the leaf senescence phases, respectively. The bias between the MODIS predictions and those based on *in situ* NDVI measurements is positive for S_2, S_3, A_2, and A_3 (MODIS-based phenological markers occur later). It is less important for S_2 and A_2 than for S_3 and A_3, which delimit the end of the two phases, i.e., the end of the leaf expansion phase in the spring (S_3) and the end of the leaf senescence phase in the autumn (A_3). In comparison with the daily MODIS series, the bias for S_2 is positive at approximately 4 days, and it is also positive for A_2 at 2.5 days. On both sides of the two inflexion points, the bias is negative for S_1 in early spring (MODIS-based phenology estimates are earlier) and positive for S_3 at the end of the leaf expansion phase. Furthermore, it is negative for A_1 in early autumn and positive for A_3 at the end of the leaf senescence phase. The relationships between the ground-based and MODIS daily spring metrics (S_1, S_2, S_3) are statistically significant ($p < 0.01$), while no statistically significant relationship could be found for the autumn metrics (A_1, A_2, A_3). The metrics derived from the MODIS 16-day series exhibit lower R^2, and only the S_2 and S_3 metrics could be significantly related to the ground-based metrics ($p < 0.02$ and $p < 0.04$, respectively).

3.3. Theoretical analysis of the predictive power of NDVI time series for phenology detection

Because the phenological metrics are based on the derivatives of the fitted NDVI time series, the RMSE of the first derivative ratio was used to quantify the expected theoretical uncertainty of any particular phenological metric regardless of the signal noise (Eq. 6). As described above, we recall that this ratio corresponds to the number of days needed to obtain a NDVI temporal change higher than the NDVI noise. Figures 10A and 10B illustrate the application of this method to track features and to estimate the uncertainties (in days) of main phenological metrics in a deciduous forest in Fontainebleau (10A) and in an evergreen forest in Puechabon (10B).

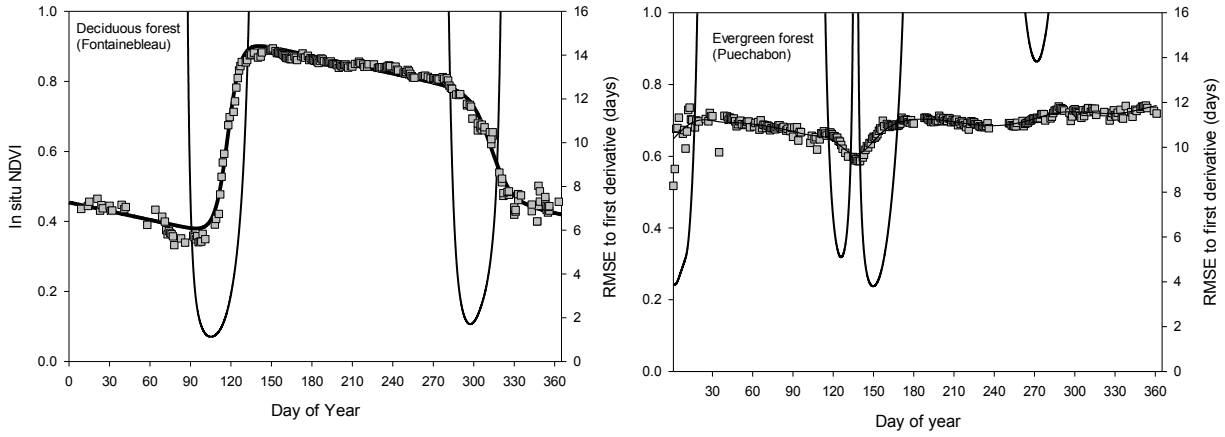

Figure 10 - A & B: In situ measured (gray squares) and fitted NDVI time series over a deciduous forest in Fontainebleau for year 2006 (A) and over an evergreen broadleaf forest of holm oak in Puechabon forest (B) during the year 2009. The continuous curve is the ratio between the RMSE and first derivative (right axis).

Summary statistics of uncertainty in the main phenological metrics over all deciduous forests and for all years are provided in Table 3.

	Theoretical uncertainty (days)	**S1**	**S2**	**S3**	**A1**	**A2**	**A3**
In situ NDVI	Average	2	0.7	2	6.5	2.5	6.0
	standard deviation	2.5	0.7	2.5	6.5	2.5	6.5
MODIS daily NDVI	Average	7.5	2	7.5	13	5	13
	standard deviation	8.5	2.5	8.5	16.5	6	16.5
MODIS 16-day NDVI	Average	8	2.5	8	14	5	14
	standard deviation	12	3.5	12	22	7	22

Table 3: Average and standard deviation of the theoretical uncertainties (from Eq. 6) calculated for six phenological metrics (Fig. 1) derived from the fitted NDVI time series over deciduous species and for all years (sample size=10). (S_1, S_2, S_3) for the spring and (A_1, A_2, A_3) for the autumn.

The uncertainties of phenological dates determined from the MODIS daily and 16-day NDVI products are similar. Nevertheless, the standard deviation is larger using the MODIS 16-day NDVI time series. In comparison with the *in situ* NDVI-derived phenological metrics, the theoretical uncertainty based on the daily and MODIS 16-day composite NDVI observations is higher, particularly for phenological markers associated with autumn. The phenological dates given by the inflexion points during the leaf expansion phase in the spring and the leaf senescence phase in the autumn are significantly more accurate than the other metrics. This result is of great importance because it demonstrates that the inflexion point metric is more robust for tracking the phenology from the NDVI time series in temperate broadleaf deciduous forests.

For the other biomes, summary statistics of uncertainty assessed over evergreen forests, savannah and crops are provided in Table 4.

	Theoretical uncertainty (days)	**Savannah**	**Crops**	**Evergreen forests**
In situ NDVI	Average	3.5	2.5	9.1
MODIS daily NDVI	Average	6.6	10.5	19.5
MODIS 16-days NDVI	Average	13.5	24.2	162.5

Table 4: Average theoretical uncertainty (from Eq. 6) for the significant phenological transitions derived from the fitted NDVI time series over crops, herbaceous savannah and evergreen forests.

For crops and the herbaceous savannah, the uncertainties obtained for the most significant transition dates derived from the *in situ* NDVI time series are comparable to those obtained for deciduous forests. For the evergreen forest of holm oak and the rainforest, the uncertainties are higher, differing from *in situ* NDVI measurements by approximately 10 days. In contrast, the daily and 16-day MODIS NDVI time series are not able to describe the phenology of these ecosystems with sufficient accuracy.

3.4. Influence of data gaps in the MODIS NDVI time series on the prediction accuracy of phenological metrics in deciduous forests

Based on the Fontainebleau 2008 *in situ* NDVI time series considered as a reference and by inserting artificial gaps into the actual data using the method described in 2.5.2, Figure

11 shows the differences between the phenological estimates from the full NDVI time series and the simulated (with data gaps) NDVI time series for the different phenological markers defined in Figure 1.

In Figure 11, the abscissa (x-axis) corresponds to the mean of the absolute values of the first derivatives of ADS fitted to the simulated NDVI time series. The first derivative is numerically calculated for every day of NDVI observation. Low values of the x-axis represent a loss of information (loss of NDVI signal) due to a bad compositing of the NDVI time series (decrease of the proportion of informative observations that are acquired during leaf expansion and leaf senescence phases), while the increase represents a relative gain of information due to the removal of uninformative observations (i.e., NDVI values during the winter and summer seasons). The two ordinate axes (left y-axis and right y-axis) correspond to the average RMSE between the estimates of the phenological marker determined from the simulated and full NDVI time series (left y-axis) and the average length of the simulated NDVI time series (right y-axis).

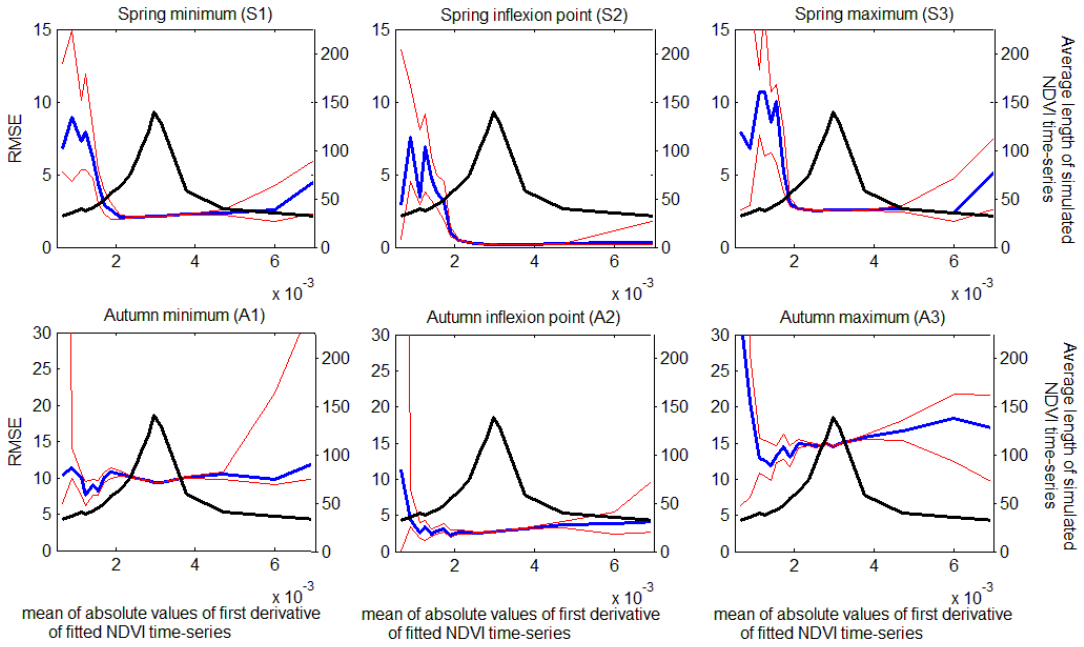

Figure 11: Relationships of phenology prediction error (days) (blue line, left y-axis) and the length of the simulated NDVI time-series (black line – right y-axis) versus the average of the absolute values of the first derivatives of fits of simulated NDVI time-series (x-axis). The red lines are the confidence limits (95%) of the phenology prediction error.

The general form of the relationships between the RMSE and the mean of the absolute values of the first derivatives of the fitted NDVI time series is concave up. The RMSE is minimal

around the middle of the x-axis and then increases rapidly on both sides for low and high values. In contrast, the general form of the relationships between the average length of simulated NDVI time series and the x-axis is concave down, indicating that the prediction errors of phenological metrics are lowest when the length of the simulated NDVI time series is high.

In Figure 11, both the level and extent of the central part of the RMSE curve, characterized by stable and low values, vary according to the phenological metric considered. The RMSE is lower and the region of error stability is wider for phenological metrics based on the inflexion points (S_2 and A_2) during the spring and autumn, respectively. For the spring phenological metrics, the point of inflexion S_2 is subject to the smallest error (< 1 day) for a length of NDVI time series varying between 35 and 140 observations. For the autumn phenological metrics, the prediction error at the point of inflexion (A_2) is higher and less stable at approximately 3 days for a range of sample sizes varying from 60 to 140 observations.

The extent of the portion of the curve where the RMSE is stable indicates the sensitivity of the phenological metrics to the length of the NDVI time series and to signal degradation due to cloud cover. Table 5 gives the range of the length of the simulated NDVI time series that bounds the region of RMSE stability (defined as the region having the lowest RMSE ± 1 day). This range gives the minimum number of NDVI observations retained without significantly degrading the predictive quality of the NDVI time series.

Phenological metrics:	**S1**	**S2**	**S3**	**A1**	**A2**	**A3**
Average length of simulated NDVI time series (n)						
[left-right*****]	83 - 73	75 - 51	94 -97	124-118	115-73	139-98
(in % of full NDVI dataset)	44%-39%	40%-27%	49%-51%	65%-62%	61%-40%	73%-51%
[left – right]						

Table 5: Sample sizes defining the stability region of the root mean square errors (lower RMSE ±1 day) of the phenological estimates in deciduous forests due to the introduction of artificial data gaps in the NDVI time series (first line). (Second line): Proportions of the remaining NDVI data (percentage of the total number of observations of the entire in situ NDVI time series, n=189). (S_1, S_2, S_3) for the spring and (A_1, A_2, A_3) for the autumn. ***** *[left-right] corresponds to both sides of the stability region for each phenological metric (see Figure 11).*

The results in Table 5 show that the average length of the simulated NDVI time series is considerably lower for S_2 and A_2 than for the other metrics, indicating that the phenological

metrics based on the inflexion points are less sensitive to data gaps and signal degradation due to cloud cover. The prediction error remains at its minimum by keeping only approximately 27% and 40% of the total number of NDVI observations in the best case (gaps or cloudy observations concentrated during the summer and winter) or approximately 40% and 61% of the total number of observations in the worst case (gaps or cloudy observations concentrated during the spring or autumn).

4. Discussion:

In situ NDVI measurements are made only a few meters above the canopy, and because NDVI is a normalized index, the effects of the sky conditions produce little noise. *In situ* NDVI measurements can thus be carried out under diffuse sky conditions, allowing for the monitoring of vegetation phenology at high temporal frequency in deciduous and evergreen forests for which the phenological variations are less pronounced. These data may be considered as a reference offering adequate empirical and theoretical frameworks for directly assessing the potential use of satellite data to predict vegetation phenology in different biomes and under different sky conditions. Nevertheless, when comparing coarse satellite data to ground measurements, spatial heterogeneity can become an important source of uncertainty in predicting phenology if certain precautions are not taken. In this study, the ground-based NDVI measurements benefited from an existing network of seven eddy covariance flux towers that were installed on flat terrain with relatively homogeneous vegetation cover, specifically chosen to satisfy the assumptions of the eddy covariance method and to avoid scaling issues and plant species heterogeneity (Chen et al. 2009, Metzger et al. 2012). In addition, for each study site, the homogeneity of the vegetation composition within the MODIS 250 m pixel was checked by visual photointerpretation complemented by the use of Landsat TM/ETM+ based NDVI subsets and ancillary ground-based observations. Nevertheless, it is important to note that these precautions do not completely remove the residual uncertainty due to the spatial heterogeneity in the MODIS pixel. We emphasize that ground-based NDVI measurements are acquired at a constant viewing angle, while MODIS data are acquired with different viewing geometries. BRDF effects lead to uncertainties of variable magnitude in the seasonal course of surface reflectance, and they may cause bias in the identification of vegetation phenological events (Tan et al. 2006; Hird and McDermid, 2009; Fensholt et al. 2010; Sims et al. 2011). In this study, we used the MODIS 16-day product derived from the CVA-MVC compositing methodology that preferentially select highest NDVI values with zenith view angle closest to nadir view (Huete et al., 2002). No

specific constraint on the viewing angle has been applied to daily MODIS data previously. Nevertheless, daily 250 m MODIS NDVI data were previously filtered using GMM and a moving-window mean filter to minimize the total noise due to variations in the atmospheric conditions, mismatch in the spatial scales between the MODIS data sets, and differences in radiometric data acquisition geometry.

In this study, a new filtering method based on mixture Gaussian models has been developed to remove spurious MODIS NDVI data in deciduous forests without altering their phenological patterns. This method showed good performance in terms of the similarity between the *in situ* and daily MODIS NDVI time series (Fig. 5). However, in evergreen forests, this method has a limited efficiency for filtering daily and 16-day MODIS NDVI time series because the magnitude of noise is of the same order as the phenological signal (Fig. 6 & 7).

After the removal of spurious NDVI observations, both MODIS and *in situ* NDVI time series allow us to predict with good accuracy the two main phenological events in temperate deciduous forests: the date of the onset of greenness in the spring and the date of the onset of leaf senescence in the autumn (Fig. 9, Table 2). The MODIS daily NDVI derived onset of greenness metrics was shown to be well correlated to the *in situ* NDVI metrics, while the related senescence metrics may still be challenging. The use of the MODIS 16-day NDVI series yielded more variable results, which is probably due to the loss of intermediate NDVI values.

The inflexion points during NDVI increase and NDVI decrease phases in the spring and autumn constitute the best predictors in terms of robustness to data gaps and prediction accuracy. These results are in agreement with Fischer et al. (2006), Soudani et al. (2008), and Busetto et al. (2009). For inflexion-point-based phenological metrics, the biases between *in situ* and MODIS-based NDVI time series estimates are positive and vary between 2 and 4 days for the daily and 16-day composite MODIS NDVI time-series, respectively. For the spring minimum (S_1) and autumn maximum (A_1) metrics derived from the daily MODIS time series (Table 2), the biases are negative, meaning that MODIS tends to detect the onset of greenness earlier. Negative bias in S_1 was also reported by Fisher et al. (2006) and Soudani et al. (2008). This result can be explained by the greater sensitivity of (S_1, S_3) and (A_1, A_3) to a lack of NDVI observations during short periods at the beginning and end of the leaf expansion and leaf yellowing phases, respectively. A lack of NDVI measurements has the effect of

shifting the start of the sigmoid to the left at S_1 and A_1 and to the right at S_3 and A_3. This point will be discussed in detail below.

The use of the method based on the noise-to-signal ratio developed in this study (Eq. 6) provided a quantitative insight about the uncertainty of each phenological metric and its reliability, accounting for the initial NDVI signal, filtering, and fitting techniques in both deciduous and evergreen forests. In deciduous forests (Table 3), whether the data were obtained from the *in situ* or MODIS NDVI time series, the theoretical uncertainty yielded significantly lower values for the phenological transition dates based on the inflexion points for both the spring and autumn phases. This result may be explained by two reasons. First, the rate of change of the NDVI during these two periods is higher, and thus, the noise-to-signal ratio is lower, allowing a better fit of the data. Second, the inflexion point of the NDVI curve is more stable due to the constraint of symmetry around this position. During the leaf expansion phase, this date is constrained by two NDVI plateaus in the winter and summer. During leaf senescence, it is constrained by two other plateaus in the summer and autumn/winter. For these two reasons, a relatively small number of NDVI measurements that are of good quality and are well distributed over the seasons (winter, leaf expansion and senescence phases, summer and autumn) may be sufficient to obtain good estimates. The dates of the NDVI minimum increase and the NDVI maximum are not constrained, and it is necessary to have high-quality NDVI data during these periods to obtain accurate estimates.

The conclusions underlined above are confirmed by the results of the sensitivity analysis of the phenological markers to the lack of NDVI data conducted on the 2008 year in Fontainebleau site, which exhibit strong phenological pattern and low noise, as summarized in Figure 11 and Table 5. The dates of spring and autumnal phenological transitions derived from inflexion points are the most accurate and most robust. The use of the inflexion point may even be necessary to estimate the date of leaf senescence with sufficient accuracy because of the strong instability of the other two indices (A_1 and A_2), as shown in Figure 11 and Table 5. However, during the autumnal phase, the NDVI decline is generally slower and less pronounced than during leaf expansion in the spring because it depends on biological and physical mechanisms (leaf yellowing, browning, leaf fall, marcescence, and the mechanical influence of wind and precipitation) that may vary from year to year. Marcescence, which means that leaves die but do not fall off of trees in the autumn, is frequent in temperate deciduous forests and may influence the NDVI decline. In addition, it is highly likely that the contribution of the soil covered with newly fallen leaves may also significantly affect the NDVI signal and may explain (at least partially) the slow decline of the NDVI during the

autumn and throughout the winter, as shown in previous studies (Van Leeuwen and Huete, 1996; Nagler et al. 2000). These factors may shift the position of the inflexion point to the right and cause an overestimation of the date of leaf yellowing and senescence in the autumn.

The results of the sensitivity analysis (Fig. 11) also show that the inflexion point is the most robust remote sensing-based phenological metric to gaps in the NDVI time series. The spring phenological transition prediction error remains less than one week when the number of NDVI observations is less than 30, corresponding to one observation every two weeks, which is equivalent to the multi-temporal MODIS NDVI 16-day composite product. This leads us to the conclusion that the MODIS 16-day composite NDVI data may allow accurate predictions of spring phenology using the inflexion point of the NDVI curve provided that the NDVI observations are not contaminated by clouds and that they are well distributed over the main transition phases. When those two conditions are not met, the use of MODIS 16-day composite NDVI may lead to hazardous prediction, as shown in the left part of the graphs (Fig. 11). However, it is difficult to predict the timing of autumnal phenological transition with one week of accuracy using the MODIS 16-day NDVI data, and it is still highly unlikely that such accuracy can be achieved by using the criteria A_1 and A_3, even when the MODIS daily NDVI data are used (Table 3).

In the evergreen forest in Puechabon and the tropical rainforest (Fig. 6, 7 & Table 4), the *in situ* NDVI time series show low NDVI variations. In the evergreen Mediterranean forest of holm oak, the NDVI variations are consistent with the phenology of this species, which is mainly characterized by two major events: the sprouting of leaves and shoots in the spring and the shedding of leaves, which is particularly important during the phase of leaf sprouting in the spring and occasionally autumn (Soudani et al. 2012; La Mantia et al. 2003). In the tropical rainforest in French Guiana, the interpretation of the NDVI temporal patterns is more complex because of the high species diversity in such forests. Nevertheless, the two periods of NDVI decline, which are observed occasionally during the first short dry season in February - March and during the second (main) dry season from the end of August to the end of October, are concomitant with two periods of lower rainfall and higher solar radiation. The NDVI decline during the second dry season coincided with a peak of litterfall, as shown by measurements of the litterfall regime based on the use of litter traps placed beneath the canopy in this forest (Soudani et al. 2012).

The seasonal phenological features derived from the daily MODIS NDVI time series measured over the evergreen forests are quite poor because only a slight decrease of the NDVI in the spring in the Puechabon forest was detected. However, 16-day composite

MODIS NDVI time series could not provide a sufficient certainty to precisely detect any of the phenological features of the evergreen forests.

In the tropical forest (Fig. 7), the MODIS NDVI time series exhibited strong noise, so none of the temporal features detected in ground-based NDVI time series could be found in the MODIS NDVI data. In contrast, the wave shapes observed in the 16-day composite and daily (with a lower magnitude for the latter) NDVI time series are mainly driven by seasonal variations in noise intensity. We note that during the main dry season, this pattern is opposite to that observed in the *in situ* NDVI time series. It is also important to note that the seasonal patterns of the MODIS 16-day composite NDVI shown in Figure 7 are similar to those obtained in previous works (Huete et al. 2006; Saleska et al. 2007). These studies concluded that there is an increase in the canopy greenness during dry periods. Our results suggest that this pattern may not reflect a phenological signal but a variation of the noise intensity in the NDVI observations. The use of the MODIS daily or 16-day composite data without any ground-based reference may therefore be misleading.

The results from the savannah and crop sites (Fig. 8, Table 4) pinpoint an important limitation of the MODIS NDVI time series in the detection phenological features: while the actual features were detected, strong errors occurred due to mixed pixels or bad sky conditions coinciding with phenological events. These errors could not be addressed by the tested filters or by the noise-to-signal ratio. At the savannah site, which may be heterogeneous at the MODIS pixel scale, some comparable features could be found between the *in situ* and MODIS series such as the NDVI drop due to a short dry period in March 2008, and the green-up at the end of 2009, while there were localized mismatches, notably around June, when the area is burnt. This observation may indicate a possible scale mismatch between the *in situ* and MODIS observations.

5. Conclusion

In this study, *in situ* NDVI time series allowed us to directly assess the accuracy of MODIS-derived phenological estimates. In deciduous forests, inflexion points of a double sigmoid model fitted to NDVI data allow for the most accurate estimates of the onset of greenness in the spring and the onset of yellowing in the autumn (RMSE $\leq$ one week). Phenological metrics delimiting the leaf expansion phase in the spring and the leaf senescence phase in the autumn, which are identical to those provided in MODIS Global Vegetation Phenology product (MDC12Q2), are less robust to data gaps, and they can be subject to large

biases of approximately two weeks or more during the autumn phenological transitions. The inflexion point detection was shown to be more precise and less sensitive to data gaps than these metrics. However, the use of the date at the beginning of the NDVI decline in the autumn (identical to the onset of the greenness decrease in MDC12Q2) instead of the date at the inflexion point can be justified because of the slow, monotonic decline of the NDVI during the autumn and winter, which could be due to the contribution of freshly fallen leaf litter and because the phenomenon of marcescence can cause a shift to the right of the inflexion point that could lead to overestimation of the onset of leaf yellowing. In the evergreen forests, *in situ* NDVI time series describe the phenology with high fidelity despite small temporal changes in the canopy foliage. However, MODIS is unable to provide consistent phenological patterns. In savannah and crops, the detection of phenological patterns could be achieved but was hampered by a seasonal variation of noise amplitudes. Similarly, in the tropical rainforest, the temporal pattern exhibited in the MODIS 16-day composite NDVI time series is more likely due to a pattern of noise in the NDVI data, structured according to both rainy and dry seasons rather than to phenological changes. More investigations are needed, but in all cases, this result leads us to conclude that the MODIS time series in tropical rainforests should be interpreted with great caution.

Synthèse et Discussion générale

Le PRI – Photochemical Reflectance Index- est un indice optique initialement conçu sur la base de mécanismes observés à des échelles fines, cellulaire et foliaire. Suite aux premiers travaux de Gamon et al. (1992, 1997) et Penuelas et al. (1997, 1998), de nombreuses évaluations de l'usage du PRI à des échelles plus larges ont été réalisées (Nichol et al. 2000, 2002 ; Drolet et al. 2005 ; Nakaji et al. 2006). Lorsque l'équipe d'écophysiologie végétale du laboratoire ESE a entamé la mise en place d'un réseau de mesures proximales de NDVI et de PRI, en 2005/2006, de nombreuses études reliant le PRI à divers indicateurs du rendement de la photosynthèse étaient disponibles à des échelles temporelles et spatiales diverses, illustrant généralement la capacité du PRI à répondre aux variations du rendement de la photosynthèse. La généralisation de l'usage du PRI aux échelles larges a cependant mis en évidence une variabilité de la relation entre PRI et LUE entre écosystèmes (Grace et al. 2007). Lorsque ce travail a été initié en 2010, la difficulté de généraliser à l'échelle de l'écosystème l'usage du PRI conçu et validé à l'échelle de la feuille était donc connue, ainsi que des causes potentielles de la variabilité observée des relations entre PRI et LUE entre sites. Néanmoins, aucune démarche cohérente permettant le transfert d'échelle de la feuille à l'écosystème intégrant la complexité et l'hétérogénéité structurale et fonctionnelle de ce dernier n'avait été entreprise.

C'est dans ce contexte que s'inscrit ce travail, conçu et structuré de manière à évaluer l'apport du PRI en tant que proxy du LUE depuis les échelles fines jusqu'aux échelles larges, à la fois spatiales (feuille, mini-couvert, peuplement, parcelle) et temporelles (de la minute à l'année). Dans ce développement, les résultats décrits et discutés précédemment au fil d'une démarche de transfert de l'échelle de la feuille à l'échelle de l'écosystème seront synthétisés et replacés dans un contexte général.

1. De la réponse des signaux de télédétection à la structure et au fonctionnement des couverts végétaux de l'échelle de la feuille à celle de l'écosystème

Trois indices optiques ont été étudiés dans le cadre de ce travail :

- Le NDVI - Normalised Difference Vegetation Index -, à l'échelle de jeunes couverts végétaux, de peuplements adultes et à l'échelle du pixel satellitaire, en tant qu'indicateur de la structure des couverts végétaux et de sa variabilité temporelle intra et interannuelle.
- Le $mNDI_{705}$, - modified Normalised Difference Index - à l'échelle de la feuille et de jeunes couverts végétaux, en tant qu'indicateur de l'état biochimique à l'échelle saisonnière.
- Le PRI, à l'échelle de la feuille, de jeunes couverts végétaux, et de peuplements adultes, en tant qu'indicateur du rendement de la photosynthèse de l'échelle de la minute à l'échelle de l'année.

Ces trois indices optiques ont été utilisés conjointement pour décrire à différentes échelles la structure, l'état biochimique et le fonctionnement des couverts végétaux. Le NDVI et le $mNDI_{705}$ (dont la variabilité est essentiellement saisonnière et est peu corrélée au LUE) sont ici considérés en tant que « grille de lecture » du PRI.

1.1. Du potentiel du NDVI en tant qu'indicateur de la phénologie et de la structure des couverts végétaux

Le NDVI est principalement utilisé pour détecter des variations de biomasse foliaire due à la variabilité structurale du couvert, principalement sous le contrôle du cycle phénologique qui lui-même est sous le contrôle de la variabilité climatique ou sous les effets de stress intenses lorsqu'ils sont accompagnés par des chutes ou des décolorations foliaires significatives (Soudani et al. 2008 ; Soudani et al. 2012 ; Hmimina et al. 2013a). Soudani et al. 2012 illustrent le potentiel de mesures proximales de NDVI pour suivre la structure de couverts végétaux, et détecter des phénomènes variés tels que le débourrement et la sénescence dans les forêts décidues tempérées, la succession de cohortes de feuilles dans les forêts sempervirentes de chêne vert, de pin maritime et tropicale humide, la dynamique temporelle de la savane herbacée du site de Tchizalamou (Congo) sous le contrôle principal de la succession saison sèche et saison humide ou l'impact des pratiques culturales sur la dynamique du couvert végétal dans une succession de cultures en Belgique et les et les feux de brousse sur le site de Tchizalamou.

Le chapitre 5, qui se situe dans le prolongement de Soudani et al. 2012, exploite les séries NDVI in situ et a permis de définir un cadre conceptuel permettant l'exploitation systématique de séries temporelles de NDVI satellitaire en tant qu'indicateur de la

dynamique de la structure du couvert. Le développement théorique entrepris et détaillé dans ce chapitre s'inscrit dans le prolongement des conclusions de Zhang et al. 2003, Fischer et al. 2006 et Soudani et al. 2008 qui ont souligné l'importance de la résolution temporelle dans l'estimation des dates phénologiques clés en forêts décidues. Dans ce travail, la résolution temporelle effective des séries de mesures NDVI est estimée à l'aide d'un rapport bruit/signal, et est dépendante de la précision de la mesure, des propriétés du couvert concerné et de sa phénologie.

Cette analyse démontre la capacité de mesures proximales de NDVI à un pas de temps semi-horaire à :

- suivre des variations de structure des couverts végétaux, telles que celles importantes générées par la sénescence et le débourrement des peuplements décidus (Chapitre 5, Figure 5), les variations fines liées à la mise en place de nouvelles cohortes de feuilles au sein du peuplement de chêne vert de Puechabon (Chapitre 5, Figure 6) ou les variations subtiles de la structure du couvert dans la forêt tropicale humide (Guyane) expliquées partiellement par la chute foliaire (Chapitre 5, Figure 7).
- Déterminer des dates des évènements phénologiques rapides tels que le débourrement ou progressifs tels que la sénescence avec une précision de l'ordre du jour (Chapitre 5, Figure 10.A), et des évènements ponctuels et fins tels que la mise en place de nouvelles cohortes de feuilles avec une précision de l'ordre de la semaine (Chapitre 5, Figure 10.B)

La comparaison des séries temporelles du NDVI in situ à celles issues de l'instrument satellitaire MODIS a permis d'étudier l'effet des conditions atmosphériques et la dégradation de la résolution temporelle sur l'estimation des dates phénologiques clés et de la dynamique du couvert dans les différents biomes cités ci-dessus. De cette analyse découlent trois principales conclusions :

- Les mesures satellitaires MODIS à une résolution temporelle journalière ne permettent pas de détecter les faibles variations de structure telles que celles liées à la phénologie dans les forêts sempervirentes.
- Les séries temporelles obtenues en climat tropical sont contaminées par un bruit important qui génère des tendances qui ne reflètent pas une dynamique saisonnière réelle de la forêt. Ce résultat a des implications d'autant plus importantes qu'une polémique porte actuellement sur l'interprétation du pattern temporel de la structure de ces forêts (Huete et al. 2006, Saleska et al. 2007).

- La précision avec laquelle un phénomène rapide tel que le débourrement peut être détecté dans des conditions optimales d'acquisition (absence de nuages aux dates importantes) est de l'ordre du jour, tandis que la précision avec laquelle un phénomène progressif tel que la sénescence peut être détecté est supérieure à 3 jours dans les mêmes conditions. Cette précision tombe à 10 et 15 jours pour des phénomènes impliquant une variabilité plus faible du signal mesuré tels que le début et la fin de la sénescence de peuplements décidus, respectivement. Enfin, quel que soit la résolution temporelle de la série NDVI, le point d'inflexion pendant les phases d'expansion et de sénescence foliaire demeure le meilleur estimateur des dates phénologiques clés. Les autres indicateurs actuellement utilisés dans le produit phénologique MODIS MDC12Q2 fourni en routine à l'échelle globale sont moins performants (Chapitre 5, Figure 11).

Ces conclusions concernant le potentiel des mesures de NDVI MODIS en tant qu'indicateur de la dynamique de la structure des couverts végétaux sont à situer dans le cadre de l'étude du potentiel du PRI MODIS en tant que proxy du LUE. Cette démarche d'évaluation de l'effet de la résolution temporelle sur le potentiel de détection pourrait être appliquée à d'autres indices spectraux satellitaires mais nécessite l'accès à des séries longues de mesure in-situ.

1.2. Du potentiel du $mNDI_{705}$ en tant qu'indicateur de l'état biochimique des couverts végétaux

Le $mNDI_{705}$ résulte de l'introduction par Sims et Gamon (2002) d'une bande de référence centrée sur 445 nm à un indice optique basé sur la translation du « red-edge » (point d'inflexion du spectre de couverts végétaux à la limite du spectre d'absorption de la chlorophylle, vers 725 nm). Cette bande de référence varie peu avec les concentrations foliaires en chlorophylles et caroténoïdes et permet de corriger les effets additifs systématiques. Cet indice optique est fortement corrélé au contenu en chlorophylle des feuilles (Sims et Gamon 2002, Le Maire et al. 2004), et au contenu en chlorophylle et au LAI de couverts végétaux (Zhao et al. 2007). Cette corrélation est confirmée dans ces travaux à l'échelle de la feuille grâce à une comparaison entre cet indice et des dosages de chlorophylles sur des feuilles de hêtre et de chêne (Chapitre 1, Figure 3). En outre, les variations saisonnières du $mNDI_{705}$ s'avèrent différentes de celles du NDVI (Chapitre 2, Figure 1), et concordent avec des observations antérieures concernant la dynamique saisonnière du contenu en chlorophylle, notamment sur le hêtre (Damesin et al. 2003).

Le $mNDI_{705}$ mesuré à l'échelle de la feuille et de jeunes peuplements est fortement corrélé aux variations entre feuilles et saisonnières du PRI (Chapitre 1, Figure 10 et Chapitre 2, Figure 6 respectivement). Ce résultat concorde avec les résultats de Sims et Gamon 2002 et ceux de Rahimzadeh-Bajgiran et al. 2012. A l'échelle de la feuille, cette corrélation est attribuable à la capacité du $mNDI_{705}$ à décrire la composition biochimique des feuilles. A l'échelle de la canopée, la corrélation entre $mNDI_{705}$ et les variations saisonnière du PRI est forte alors même que le NDVI, indicateur de la structure des couverts, est stable et n'est pas significativement corrélé à ces variations. Cette relation est donc également attribuable à la capacité du $mNDI_{705}$ à décrire la composition biochimique du couvert, et non uniquement à l'effet de variations du LAI. Au reste, une corrélation forte a été mise en évidence entre LAI et $mNDI_{705}$ (Zhao et al. 2007), et ce travail ne permet pas de distinguer la variabilité du $mNDI_{705}$ due aux changements de composition biochimique du couvert de celle due aux changements de structure du couvert.

1.3. Du potentiel du PRI en tant qu'indicateur du rendement de la photosynthèse

De nombreux travaux mettent en évidence la réponse du PRI aux changements de LUE à différentes échelles (Garbulsky et al. 2011). L'existence d'une réponse cohérente de la bande spectrale centrée sur 530 nm au PAR, et du PRI aux variations de LUE a dans un premier temps été vérifiée. A l'échelle de la feuille, une réponse des réflectances autour de 525 nm et 540 nm aux variations du PAR a été mise en évidence, conformément aux travaux et Gamon et al. 1997 (Chapitre 1, Figures 6 et 7). Une réponse similaire a été mise en évidence à l'échelle de couverts végétaux (Chapitre 2). Le PRI varie en conséquence avec le PAR de façon exponentielle, et avec le LUE de manière linéaire tant à l'échelle de la feuille (Chapitre 1, Figures 8 et 11) qu'à l'échelle de jeunes canopées (Chapitre 2, Figures 5 et 9) et de peuplements matures (Chapitre 3, Figures 2, 3 et 6). Ces corrélations entre PRI et PAR ou LUE sont mises en évidence sur une période d'une demi-heure à l'échelle de la feuille et d'un jour à quelques jours à l'échelle de la canopée. Elles se caractérisent par une forte variabilité inter-feuilles, ou par l'impact important de la variabilité saisonnière du PRI à l'échelle de la canopée (Chapitre 4, Figures 4, 5 et 9).

La variabilité inter-feuille et saisonnière du PRI indépendamment du PAR et du LUE a été isolée à l'aide d'analyses de courbes de réponses du PRI au PAR. Le PRI_0, introduit et défini dans ce travail comme étant le PRI d'une feuille ou d'un couvert idéalement adapté à l'obscurité est utilisé pour décrire cette variabilité. Cette démarche originale va dans le sens

de celle proposée récemment par Gamon et Berry (2012) qui décrivent et séparent deux sources de variabilités du PRI, une variabilité constitutive due à des variations de la composition biochimique des feuilles, et une variabilité facultative due à l'activité du cycle xanthophylle en lien avec la régulation du LUE.

Dans nos travaux, nous avons montré qu'il est possible de mesurer directement le PRI_0 dans des conditions de faible lumière en supposant que le cycle de xanthophylle n'a pas été activé. Il est également possible de l'estimer à partir des courbes de réponse du PRI au PAR en utilisant l'ordonnée à l'origine de la relation PRI en fonction du PAR (PRI d'un couvert idéalement adapté à l'obscurité). La première approche a été validée à l'échelle de la feuille. La seconde approche a été validée de l'échelle de la feuille à l'échelle du couvert végétal et à différentes échelles temporelles (de 30 mn à plusieurs jours). Cependant, des études complémentaires sont nécessaires afin d'affiner l'estimation du PRI_0 en particulier dans des conditions de stress.

Le PRI_0, fortement corrélé à la composition biochimique des feuilles (Chapitre 1, Figure 10 ; Chapitre 2, Figure 6) et à la structure du couvert (Chapitre 4, Figure 7), a permis de corriger les mesures de PRI réalisées de manière à obtenir un PRI_c mieux corrélé au LUE et indépendant ou du moins peu sensible à la variabilité des propriétés du couvert (Chapitre 1, Figure 11, Chapitre 2, Figure 9, Chapitre 3, Figure 11, Chapitre 4, Figure 8).

Ce travail a donc mis en évidence la nature composite du signal PRI, qui répond effectivement aux variations du LUE, mais également à la variabilité spatiale et temporelles de la structure et de la composition biochimique à l'échelle de la feuille et du couvert, conformément aux travaux de Gamon et Berry 2012 et de Filella et al. 2004. L'importance relative de cette variabilité facultative et constitutive du PRI est en outre susceptible de varier d'un peuplement à l'autre et avec les conditions d'acquisition en particulier les résolutions spatiale, temporelle et spectrale.

2. Des effets d'échelle, et de la pertinence des signaux de télédétection aux différentes échelles considérées

Le constat de la sensibilité de la relation entre PRI et LUE au contenu en pigment et au LAI des couverts végétaux soulève un important problème lié à l'interprétation du signal PRI à l'échelle du couvert et de la parcelle. Si ce phénomène laisse présager une perte de la

relation entre PRI et LUE aux échelles larges on observe a contrario dans la littérature une grande diversité de relations dont la plupart sont hautement significatives. Ainsi, Nichol et al. 2000 et 2002 (repris par Grace et al. 2007) obtiennent des relations entre PRI et LUE significatives, mais différentes sur des peuplements décidus et de conifères. Garbulsky et al. 2011 qui synthétisent les résultats des études précédentes obtiennent pour des peuplements décidus, herbacés et conifères des relations de formes et de paramètres différents, qui une fois combinées dessinent une relation exponentielle statistiquement significative.

S'il en découle qu'une relation unique entre PRI et LUE peut émerger de l'agrégation de relations différentes obtenues sur des peuplements différents, la pertinence de telles relations doit être évaluée aux différentes échelles temporelles impliquées.

2.1. Effet du contenu en chlorophylle foliaire

Alors qu'à l'échelle de la feuille, la variabilité inter-feuille n'a pas permis de dégager une unique relation PRI-LUE sur une saison de croissance et sur deux espèces feuillues (Chapitre 1, Figure 11), une relation comparable à celle mise en évidence par Garbulsky et al. 2011 est obtenue à l'échelle de jeunes couverts végétaux en combinant les observations réalisées sur les 3 espèces suivies (deux décidus de LAI différents, et un conifère). Cette relation est hautement significative, et est également de forme exponentielle (Chapitre 2, Figure 9). De même à l'échelle de peuplements adultes, alors que les relations entre PRI et LUE obtenues sur des échelles temporelles fines sont linéaires (Chapitre 3, Figure 6), les relations obtenues à l'échelle de la saison sont de forme exponentielle (Chapitre 3, Figure 11). A l'échelle de jeunes couverts, la soustraction du PRI_0 aux mesures de PRI fait entièrement disparaitre cette forme exponentielle de la relation entre PRI et LUE, et la corrélation entre le PRI_c obtenu et le LUE est linéaire, et significativement supérieure (Chapitre 2, Figure 11). Cette relation exponentielle, similaire à celle observée par Garbulsky et al. 2011 semble donc due à la variabilité constitutive du PRI, et ne rend pas compte de sa variabilité facultative. Ce phénomène n'est pas directement observable à l'échelle de peuplements adultes (Chapitre 3, Figure 11), probablement du fait de la résolution temporelle inférieure et du bruit important sur le signal PRI mesuré sur les sites de Fontainebleau et de Puéchabon, qui rendent difficile l'estimation du PRI_0 à l'aide de régressions linéaires (Chapitre 3, Figure 10).

La variabilité spatiale (ici, inter sites ou inter-espèces) et la variabilité temporelle (saisonnière, due à la phénologie) du contenu en pigment des couverts végétaux entrainent donc une variabilité constitutive du PRI, qui non seulement masque sa variabilité facultative, mais est

également susceptible de générer une relation entre PRI et LUE indépendamment du cycle de xanthophylle (Chapitre 3, Figures 10 et 11).

2.2.Effet de l'indice foliaire du couvert

A l'échelle de peuplements adultes et de l'année, cette variabilité du contenu en pigment des couverts végétaux n'est pas clairement dissociable de la variabilité de sa structure. Ainsi, sur les sites de Fontainebleau et de Puechabon, une forte corrélation PRI vs LUE est observée pendant les phases de forte dynamique du NDVI (Chapitre 4, Figures 2 et 4) qui coïncident avec le débourrement et la sénescence à Fontainebleau et pendant la succession de cohortes de feuilles à Puechabon. Aux échelles fines, cette relation expliquée par la variabilité du NDVI disparait.

Alors que les variations saisonnières du PRI_0 coïncident avec celle du NDVI (Chapitre 4, Figure 5), une relation composite entre NDVI et PRI_0 est mise en évidence (Chapitre 4, Figure 6) suggérant la mise en jeux de mécanismes distincts :

- une variation rapide du LAI lors du débourrement et de la sénescence et la chute foliaire sur le site de Fontainebleau, et lors de l'apparition de nouvelles cohortes de feuilles sur le site de Puéchabon. Cette variation du LAI est à l'origine d'une relation entre NDVI et PRI pendant ces phases phénologiques bien prononcées.
- Une variation continue du contenu en pigments de la canopée tout au long de la saison de végétation.

Dans les deux cas, cette corrélation entre PRI_0 et NDVI est positive sur les deux sites étudiés. Cette relation est donc inverse de celle décrite précédemment à l'échelle de jeunes couverts. Cette inversion est probablement due à la différence entre la réponse spectrale des capteurs PRI utilisés sur les sites de Fontainebleau et de Puéchabon et la méthode de calcul du PRI sur la base de spectres de réflectance à l'échelle de jeunes couverts. La réponse du PRI à la structure et au contenu en pigment des couverts végétaux est donc probablement fortement dépendante du capteur utilisé.

En conséquence, la sensibilité aux variations du NDVI est à l'origine d'une relation PRI et LUE inverse selon les périodes considérées. L'inclusion de périodes de variations du NDVI influe donc sur les réponses PRI vs LUE (Chapitre 4, Figures 2 et 3).

A la lumière de ces résultats, il n'apparait pas réaliste de corriger le PRI à l'aide d'indices spectraux sensibles à la fois à la structure et à la composition biochimique des couverts végétaux sans la déconvolution de ces deux catégories de facteurs comme évoqué dans les chapitres 1 et 2. En plus d'être potentiellement site-dépendante, une telle correction devrait nécessairement être capteur-dépendante.

2.3. Effet de la stratification de la photosynthèse

S'il n'est pas actuellement envisageable de proposer une correction unique du PRI pour les effets de structure et de composition biochimique des couverts végétaux, il a néanmoins été possible de corriger ces mesures grâce à l'estimation du PRI_0 sur les sites de Fontainebleau et de Puéchabon. En outre, les pentes des relations entre PRI et LUE obtenues sur des échelles temporelles fines sont comparables à celles obtenues entre PRI_c et LUE (Chapitre 4, Figure 9), ce qui indique que la variabilité du PRI à court-terme reste principalement due au LUE.

La qualité de ces relations reste cependant extrêmement variable à l'échelle saisonnière (Chapitre 3, Figure 4 et 5, Chapitre 4, Figures 11). Les périodes montrant de forts R^2 se caractérisent par un ratio de lumière diffuse faible sur le site de Fontainebleau, et par une forte variabilité du potentiel hydrique du sol sur le site de Puéchabon. L'influence de ces deux variables est confirmée par l'analyse par « random forest » du PRI sur ces deux sites ; les trois principales variables explicatives du PRI sur le site de Fontainebleau sont des variables liées au rayonnement, dont le ratio de lumière directe (Chapitre 3, Figure 7), tandis que les principales variables explicatives du PRI sur le site de Puéchabon sont la GPP et le LUE, en rapport avec la sécheresse qui s'est manifestée durant l'été 2010.

L'influence du potentiel hydrique du sol sur le site de Puéchabon peut s'expliquer par l'impact du stress hydrique sur la réponse du PRI et du LUE au PAR. Il a été montré (Chapitre 2, Figures 6 et 8, Chapitre 4, Figure 6) que le LUE comme le PRI saturent à une valeur de PAR qui décroit avec le contenu en eau du sol. La variabilité du PRI et du LUE mesurée à intervalle fixe de 30 mn décroit donc avec le contenu en eau du sol, ce qui entraine mathématiquement une baisse de la corrélation entre PRI et LUE. Un effet similaire est attendu par ciel couvert en raison d'une faible variabilité du PAR et donc une faible variabilité du PRI. Par ciel clair, la saturation du PRI à partir d'environ 1000 µmol/m²/s (Chapitre 4, Figure 6) suggère que les pics de R^2 observés entre LUE et PRI ne semblent pas être seulement expliqués par une augmentation de la variabilité du PRI.

La lumière diffuse ayant un effet connu sur la stratification de la photosynthèse et sur le LUE à l'échelle de l'écosystème (Alton et al. 2007), la corrélation entre le PRI_c et le LUE d'un pourcentage croissant de la surface foliaire de la canopée de Fontainebleau a été examinée. Il en découle une chute de la corrélation entre PRI_c et LUE au-delà du premier mètre carré de feuille par mètre carré au sol (Chapitre 4, Figures 10). Le PRI répond donc principalement aux variations de LUE de la première unité de LAI. Ce résultat est d'autant plus important que la contribution relative de ce premier point de LAI est extrêmement variable à l'échelle de la saison (Chapitre 4, Figure 11) ; la présence de lumière directe stimule la photosynthèse des couches inférieures de la canopée, tandis qu'un faible potentiel hydrique du sol inhibe la photosynthèse de la couche supérieure de la canopée en abaissant sa valeur de PAR saturant. Il en résulte une forte variabilité saisonnière de la représentativité verticale du PRI mesuré (Chapitre 4, Figure 11), celle-ci diminuant avec le ratio de lumière diffuse et avec la disponibilité en eau pour un LAI important (Chapitre 4, Figure 12). L'extrapolation du LUE estimé sur cette unité de LAI dans la couche supérieure du couvert à l'ensemble de l'écosystème résulterait en l'occurrence en une sous-estimation de l'ordre de 30% de la GPP.

3. Limites du PRI en tant que proxy du LUE à l'échelle de l'écosystème

Si le PRI est effectivement un indicateur du LUE particulièrement prometteur, l'impact de sa sensibilité à la structure et à la composition biochimique des couverts végétaux sur les relations PRI -LUE est largement sous-estimé. L'examen de ces relations le long d'un gradient d'échelles spatiales et temporelles met en évidence la complexité de l'interprétation du signal PRI. Ce travail démontre de l'échelle de la feuille à l'échelle du peuplement le caractère composite du signal PRI. Cet indice répond principalement aux variations de LUE aux échelles temporelles fines, et aux variations de structure et de composition biochimique des couverts végétaux aux échelles larges. Son usage en tant que proxy du LUE à des résolutions temporelles faibles (mesures aéroportées ou satellitaires) est donc particulièrement compromis, et risque de donner lieu à des erreurs importantes d'interprétations du PRI, donc d'estimation du LUE.

Il a été montré que la correction du PRI est localement possible à l'aide d'un approche basée sur l'analyse des courbes de réponses du PRI au PAR ou par mesure directe à faible lumière. Si l'application de cette approche nécessite la mise en place de mesures sensibles à de faibles rayonnements et réalisées à une haute résolution temporelle et n'est donc pas généralisable à

grande échelle, elle représente cependant un outil majeur en vue de décrire et de comprendre la variabilité du PRI au sein de différents écosystèmes.

Malgré l'existence d'indices optiques permettant de suivre la structure et la composition biochimique des couverts végétaux, une correction précise à l'échelle globale du PRI satellitaire pour ces effets n'a pas encore été testée. Si des relations entre PRI_0 et indices optiques indépendants ont pu être trouvées dans le cadre de ce travail, il a également été montré qu'elles sont potentiellement site-dépendantes du fait de la dépendance entre la structure et la composition des couverts végétaux, et qu'elles sont également capteur-dépendante. En raison de l'étroitesse de la bande spectrale sensible au cycle des xanthophylles et la faiblesse du signal, il nécessaire d'accorder une importance particulière aux propriétés spectrales du capteur utilisé, aussi bien pour la bande sensible que pour la bande de référence.

En outre, une limitation inévitable à l'usage du PRI en tant que proxy du LUE a été mise en évidence. De par sa nature, le PRI a une représentativité limitée au feuillage visible des couverts végétaux. Même dans des conditions idéales, l'usage du PRI risque donc de générer une sous-estimation dans les écosystèmes à fort LAI en raison de la sensibilité du LUE au rayonnement diffus. L'impact de cette limitation en terme de potentiel de prédiction du LUE devrait être étudié sur une large gamme d'écosystèmes différents, soumis à des climats différents.

Une approche couplant des modèles de fonctionnement multi-couches à base de processus biophysiques et écophysiologiques à un modèle de reflectance intégrant l'effet du cycle des xanthophylles permettrait de mieux comprendre la variabilité de la reflectance, en particulier dans les bandes PRI en réponses à la variabilité du fonctionnement, de la structure et des propriétés biochimiques du couvert.

Bibliographie

Alton PB, North PR, Los SO. 2007. The impact of diffuse sunlight on canopy light-use efficiency, gross photosynthetic product and net ecosystem exchange in three forest biomes. Global Change Biology **13**, 776–787.

Anav A, D'Andrea F, Viovy N, Vuichard N. 2010. A validation of heat and carbon fluxes from high-resolution land surface and regional models. Journal of Geophysical Research **115**, G04016.

Arkebauer TJ, Weiss A, Sinclair TR, Blum A. 1994. In defense of radiation use efficiency: a response to Demetriades-Shah et al.(1992). Agricultural and forest meteorology **68**, 221–227.

Asner G. 1998. Biophysical and biochemical sources of variability in canopy reflectance. Remote Sensing of Environment **253**, 234–253.

Asner GP, Nepstad D, Cardinot G, Ray D. 2004. Drought stress and carbon uptake in an Amazon forest measured with spaceborne imaging spectroscopy. Proceedings of the National Academy of Sciences of the United States of America **101**, 6039–44.

Aubinet M, Moureaux C, Bodson B, Dufranne D, Heinesch B, Suleau M, Vancutsem F, Vilret A. 2009. Carbon sequestration by a crop over a 4-year sugar beet/winter wheat/seed potato/winter wheat rotation cycle. Agricultural and Forest Meteorology **149**, 407–418.

Baker NR. 2008. Chlorophyll Fluorescence: A Probe of Photosynthesis In Vivo. Annual Review of Plant Biology **59**, 89–113.

Baldocchi D, Falge E, Gu L, Olson R, Hollinger D, Running S, Anthoni P, Bernhofer C, Davis K, Evans R, *et al.* 2001. FLUXNET: A New Tool to Study the Temporal and Spatial Variability of Ecosystem–Scale Carbon Dioxide, Water Vapor, and Energy Flux Densities. Bulletin of the American Meteorological Society **82**, 2415–2434.

Barton CVM, North PRJ. 2001. Remote sensing of canopy light use efficiency using the photochemical reflectance index: Model and sensitivity analysis. Remote Sensing of Environment **78**, 264–273.

Beck PSA, Atzberger C, Høgda KA, Johansen B, Skidmore AK. 2006. Improved monitoring of vegetation dynamics at very high latitudes: A new method using MODIS NDVI. Remote Sensing of Environment **100**, 321–334.

Berk RA. 2008. *Statistical learning from a regression perspective*. Springer.

Bonente G, Howes BD, Caffarri S, Smulevich G, Bassi R. 2008. Interactions between the photosystem II subunit PsbS and xanthophylls studied in vivo and in vitro. The Journal of biological chemistry **283**, 8434–45.

Bréda N, Huc R, Granier A, Dreyer E. 2006. Temperate forest trees and stands under severe drought: a review of ecophysiological responses, adaptation processes and long-term consequences. Annals of Forest Science **63**, 625–644.

Breiman L. 2001. Random forests. Machine learning **45**, 5–32.

Brodersen CR, Vogelmann TC, Williams WE, Gorton HL. 2008. A new paradigm in leaf-level photosynthesis: direct and diffuse lights are not equal. Plant, cell & environment **31**, 159–64.

Busch F, Hüner NPA, Ensminger I. 2009. Biochemical constrains limit the potential of the photochemical reflectance index as a predictor of effective quantum efficiency of photosynthesis during the winter spring transition in Jack pine seedlings. Functional Plant Biology **36** , 1016–1026.

Busetto L, Colombo R, Migliavacca M, Cremonese E, Meroni M, Galvagno M, Rossini M, Siniscalco C, Morra Di Cella U, Pari E. 2010. Remote sensing of larch phenological cycle and analysis of relationships with climate in the Alpine region. Global Change Biology **16**, 2504–2517.

Carnicer J, Coll M, Ninyerola M, Pons X, Sánchez G, Peñuelas J. 2011. Widespread crown condition decline, food web disruption, and amplified tree mortality with increased climate change-type drought. Proceedings of the National Academy of Sciences **108**, 1474–1478.

Castaldi, S de Grandcourt, A Rasile, A Skiba, U Valentini R. 2010. Fluxes of CO2, CH4 and N2O from soil of burned grassland savannah of central Africa. Biogeosciences Discuss **7**, 4089.

Chen J, Jönsson P, Tamura M, Gu Z, Matsushita B, Eklundh L. 2004. A simple method for reconstructing a high-quality NDVI time-series data set based on the Savitzky–Golay filter. Remote Sensing of Environment **91**, 332–344.

Chiesi M, Fibbi L, Genesio L, Gioli B, Magno R, Maselli F, Moriondo M, Vaccari FP. 2011. Integration of ground and satellite data to model Mediterranean forest processes. International Journal of Applied Earth Observation and Geoinformation **13**, 504–515.

Chiesi M, Maselli F, Moriondo M, Fibbi L, Bindi M, Running SW. 2007. Application of BIOME-BGC to simulate Mediterranean forest processes. Ecological Modelling **206**, 179–190.

Coops NC, Black TA, Jassal R (Paul) S, Trofymow JA (Tony), Morgenstern K. 2007. Comparison of MODIS, eddy covariance determined and physiologically modelled gross primary production (GPP) in a Douglas-fir forest stand. Remote Sensing of Environment **107**, 385–401.

Coumou D, Rahmstorf S. 2012. A decade of weather extremes. Nature Climate Change.

Damesin C. 2003. Respiration and photosynthesis characteristics of current-year stems of Fagus sylvatica: from the seasonal pattern to an annual balance. New Phytologist **158**, 465–475.

Delbart N, Le Toan T, Kergoat L, Fedotova V. 2006. Remote sensing of spring phenology in boreal regions: A free of snow-effect method using NOAA-AVHRR and SPOT-VGT data (1982–2004). Remote Sensing of Environment **101**, 52–62.

Delpierre N. 2009. du déterminisme des variations interannuelles des échanges carbonés entre les écosystèmes forestiers européens et l'atmosphère: une approche basée. Thèse de doctorat pour obtenir le grade de Docteur en Sciences de l'Université Paris XI Orsay,208.

Delpierre N, Soudani K, François C, Le Maire G, Bernhofer C, Kutsch W, Misson L, Rambal S, Vesala T, Dufrêne E. 2012. Quantifying the influence of climate and biological drivers on the interannual variability of carbon exchanges in European forests through process-based modelling. Agricultural and Forest Meteorology **154–155**, 99–112.

Demarez V. 1999. Seasonal variation of leaf chlorophyll content of a temperate forest. Inversion of the PROSPECT model. International Journal of Remote Sensing **20**, 879–894.

Demarty J, Chevallier F, Friend AD, Viovy N, Piao S, Ciais P. 2007. Assimilation of global MODIS leaf area index retrievals within a terrestrial biosphere model. Geophysical Research Letters **34**, L15402.

Demetriades-Shah TH, Fuchs M, Kanemasu ET, Flitcroft I. 1992. A note of caution concerning the relationship between cumulated intercepted solar radiation and crop growth. Agricultural and Forest Meteorology **58**, 193–207.

Demmig-Adams B, Adams WW. 1996. The role of xanthophyll cycle carotenoids in the protection of photosynthesis. Trends in Plant science **1**, 21–26.

Demmig-Adams B, Adams WW. 2006. Photoprotection in an ecological context: the remarkable complexity of thermal energy dissipation. New Phytologist **172**, 11–21.

Drolet GG, Huemmrich KF, Hall FG, Middleton EM, Black TA, Barr AG, Margolis HA. 2005. A MODIS-derived photochemical reflectance index to detect inter-annual variations in the photosynthetic light-use efficiency of a boreal deciduous forest. Remote Sensing of Environment **98**, 212–224.

Drolet GG, Middleton EM, Huemmrich KF, Hall FG, Amiro BD, Barr AG, Black TA, McCaughey JH, Margolis HA. 2008. Regional mapping of gross light-use efficiency using MODIS spectral indices. Remote Sensing of Environment **112**, 3064–3078.

Dufranne D, Moureaux C, Vancutsem F, Bodson B, Aubinet M. 2011. Comparison of carbon fluxes, growth and productivity of a winter wheat crop in three contrasting growing seasons. Agriculture, Ecosystems & Environment **141**, 133–142.

Dufrêne E, Davi H, François C, Maire G Le, Dantec V Le, Granier a. 2005. Modelling carbon and water cycles in a beech forest. Ecological Modelling **185**, 407–436.

Ensminger I, Sveshnikov D, Campbell DA, Funk C, Jansson S, Lloyd J, Shibistova O, Öquist G. 2004. Intermittent low temperatures constrain spring recovery of photosynthesis in boreal Scots pine forests. Global Change Biology **10**, 995–1008.

Evain S, Flexas J, Moya I. 2004. A new instrument for passive remote sensing: 2. Measurement of leaf and canopy reflectance changes at 531 nm and their relationship with photosynthesis and chlorophyll fluorescence. Remote Sensing of Environment **91**, 175–185.

Falge E, Baldocchi D, Tenhunen J, Aubinet M, Bakwin P, Berbigier P, Bernhofer C, Burba G, Clement R, Davis KJ, *et al.* 2002. Seasonality of ecosystem respiration and gross primary production as derived from FLUXNET measurements. Agricultural and Forest Meteorology **113**, 53–74.

Filella I, Amaro T, Araus JL, Peñuelas J. 1996. Relationship between photosynthetic radiation-use efficiency of barley canopies and the photochemical reflectance index (PRI). Physiologia Plantarum **96**, 211–216.

Filella I, Peñuelas J, Llorens L, Estiarte M. 2004. Reflectance assessment of seasonal and annual changes in biomass and CO2 uptake of a Mediterranean shrubland submitted to experimental warming and drought. Remote Sensing of Environment **90**, 308–318.

Filella I, Porcar-Castell A, Munné-Bosch S, Bäck J, Garbulsky MF, Peñuelas J. 2009. PRI assessment of long-term changes in carotenoids/chlorophyll ratio and short-term changes in de-epoxidation state of the xanthophyll cycle. International Journal of Remote Sensing **30**, 4443–4455.

Fisher JI, Mustard JF, Vadeboncoeur MA. 2006. Green leaf phenology at Landsat resolution: Scaling from the field to the satellite. Remote Sensing of Environment **100**, 265–279.

Gamon J a., Berry J a. 2012. Facultative and constitutive pigment effects on the Photochemical Reflectance Index (PRI) in sun and shade conifer needles. Israel Journal of Plant Sciences **60**, 85–95.

Gamon JA, Field CB, Bilger W, Björkman O, Fredeen AL, Peñuelas J. 1990. Remote sensing of the xanthophyll cycle and chlorophyll fluorescence in sunflower leaves and canopies. Oecologia **85**, 1–7.

Gamon JJ, Field CC, Fredeen A AL, Thayer S. 2001. Assessing photosynthetic downregulation in sunflower stands with an optically-based model. Photosynthesis Research **67**, 113–125 LA – English.

Gamon JA, Peñuelas J, Field CB. 1992. A narrow-waveband spectral index that tracks diurnal changes in photosynthetic efficiency. Remote Sensing of Environment **41**, 35–44.

Gamon JA, Serrano L, Surfus JS. 1997. The photochemical reflectance index: an optical indicator of photosynthetic radiation use efficiency across species, functional types, and nutrient levels. Oecologia **112**, 492–501 LA – English.

Gamon JA, Surfus JS. 1999. Assessing leaf pigment content and activity with a reflectometer. New Phytologist **143**, 105–117.

Ganguly S, Friedl MA, Tan B, Zhang X, Verma M. 2010. Land surface phenology from MODIS: Characterization of the Collection 5 global land cover dynamics product. Remote Sensing of Environment **114**, 1805–1816.

Garbulsky MF, Peñuelas J, Gamon J, Inoue Y, Filella I. 2011. The photochemical reflectance index (PRI) and the remote sensing of leaf, canopy and ecosystem radiation use efficiencies: A review and meta-analysis. Remote Sensing of Environment **115**, 281–297.

Garrity SR, Eitel JUH, Vierling LA. 2011. Disentangling the relationships between plant pigments and the photochemical reflectance index reveals a new approach for remote estimation of carotenoid content. Remote Sensing of Environment **115**, 628–635.

Gebremichael M, Barros AP. 2006. Evaluation of MODIS Gross Primary Productivity (GPP) in tropical monsoon regions. Remote Sensing of Environment **100**, 150–166.

Genty B, Briantais J-M, Baker NR. 1989. The relationship between the quantum yield of photosynthetic electron transport and quenching of chlorophyll fluorescence. Biochimica et Biophysica Acta (BBA) - General Subjects **990**, 87–92.

Goerner A, Reichstein M, Rambal S. 2009. Tracking seasonal drought effects on ecosystem light use efficiency with satellite-based PRI in a Mediterranean forest. Remote Sensing of Environment **113**, 1101–1111.

Goerner A, Reichstein M, Tomelleri E, Hanan N, Rambal S, Papale D, Dragoni D, Schmullius C. 2011. Remote sensing of ecosystem light use efficiency with MODIS-based PRI. Biogeosciences **8**, 189–202.

Gond V, de Pury DGG, Veroustraete F, Ceulemans R. 1999. Seasonal variations in leaf area index, leaf chlorophyll, and water content; scaling-up to estimate fAPAR and carbon balance in a multilayer, multispecies temperate forest. Tree physiology **19**, 673–679.

Grace J, Nichol C, Disney M, Lewis P, Quaife T, Bowyer P. 2007. Can we measure terrestrial photosynthesis from space directly, using spectral reflectance and fluorescence? Global Change Biology **13**, 1484–1497.

Guanter L, Frankenberg C, Dudhia A, Lewis PE, Gómez-Dans J, Kuze A, Suto H, Grainger RG. 2012. Retrieval and global assessment of terrestrial chlorophyll fluorescence from GOSAT space measurements. Remote Sensing of Environment **121**, 236–251.

Guo J, Trotter CM. 2004. Estimating photosynthetic light-use efficiency using the photochemical reflectance index: variations among species. Functional Plant Biology **31**, 255–265.

Hall FG, Hilker T, Coops NC, Lyapustin A, Huemmrich KF, Middleton E, Margolis H, Drolet G, Black TA. 2008. Multi-angle remote sensing of forest light use efficiency by observing PRI variation with canopy shadow fraction. Remote Sensing of Environment **112**, 3201–3211.

Hanson P, Amthor J. 2004. Oak forest carbon and water simulations: model intercomparisons and evaluations against independent data. Ecological … **74**, 443–489.

Hartel H, Lokstein H, Grimm B, Rank B. 1996. Kinetic Studies on the Xanthophyll Cycle in Barley Leaves (Influence of Antenna Size and Relations to Nonphotochemical Chlorophyll Fluorescence Quenching). Plant Physiology **110** , 471–482.

Heidinger AK, Anne VR, Dean C. 2001. Using MODIS to Estimate Cloud Contamination of the AVHRR Data Record. Journal of Atmospheric and Oceanic Technology **19**, 586–601.

Heinsch FA, Zhao M, Running SW, Kimball JS, Nemani RR, Davis KJ, Bolstad P V, Cook BD, Desai AR, Ricciuto DM, *et al.* 2006. Evaluation of remote sensing based terrestrial productivity from MODIS using regional tower eddy flux network observations. Geoscience and Remote Sensing, IEEE Transactions on **44**, 1908–1925.

Hieber AD, Kawabata O, Yamamoto HY. 2004. Significance of the Lipid Phase in the Dynamics and Functions of the Xanthophyll Cycle as Revealed by PsbS Overexpression in Tobacco and In-vitro De-epoxidation in Monogalactosyldiacylglycerol Micelles. Plant and Cell Physiology **45** , 92–102.

Hilker T, Coops NC, Hall FG, Black TA, Wulder MA, Nesic Z, Krishnan P. 2008*a*. Separating physiologically and directionally induced changes in PRI using BRDF models. Remote Sensing of Environment **112**, 2777–2788.

Hilker T, Coops NC, Wulder MA, Black TA, Guy RD. 2008*b*. The use of remote sensing in light use efficiency based models of gross primary production: A review of current status and future requirements. Science of the Total Environment **404**, 411–423.

Hilker T, Hall FG, Coops NC, Lyapustin A, Wang Y, Nesic Z, Grant N, Black TA, Wulder MA, Kljun N, *et al.* 2010. Remote sensing of photosynthetic light-use efficiency across two forested biomes: Spatial scaling. Remote Sensing of Environment **114**, 2863–2874.

Hilker T, Lyapustin A, Hall FG, Wang Y, Coops NC, Drolet G, Black TA. 2009. An assessment of photosynthetic light use efficiency from space: Modeling the atmospheric and directional impacts on PRI reflectance. Remote Sensing of Environment **113**, 2463–2475.

Hirose T, Bazzaz FA. 1998. Trade-off Between Light- and Nitrogen-use Efficiency in Canopy Photosynthesis . Annals of Botany **82** , 195–202.

Hmimina G, Dufrêne E, Pontailler J-Y, Delpierre N, Aubinet M, Caquet B, de Grandcourt A, Burban B, Flechard C, Granier A, *et al.* 2013. Evaluation of the potential of MODIS satellite data to predict vegetation phenology in different biomes: An investigation using ground-based NDVI measurements. Remote Sensing of Environment **132**, 145–158.

Hmimina G, Dufrêne E, Soudani K. 2014. Relationship between PRI and leaf ecophysiological and biochemical parameters under two different water statuses: toward a rapid and efficient correction method using real-time measurements. Plant, Cell & Environment, n/a–n/a.

Holt NE, Zigmantas D, Valkunas L, Li X-P, Niyogi KK, Fleming GR. 2005. Carotenoid cation formation and the regulation of photosynthetic light harvesting. Science **307**, 433–436.

Houghton R. 2003. Revised estimates of the annual net flux of carbon to the atmosphere from changes in land use and land management 1850–2000. Tellus B, 378–390.

Huete A, Didan K, Miura T, Rodriguez EP, Gao X, Ferreira LG. 2002. Overview of the radiometric and biophysical performance of the MODIS vegetation indices. Remote Sensing of Environment **83**, 195–213.

Huete a, Justice C, Liu H. 1994. Development of vegetation and soil indices for MODIS-EOS. Remote Sensing of Environment **49**, 224–234.

Hwang T, Kang S, Kim J, Kim Y, Lee D, Band L. 2008. Evaluating drought effect on MODIS Gross Primary Production (GPP) with an eco-hydrological model in the mountainous forest, East Asia. Global Change Biology **14**, 1037–1056.

Inoue Y, Peñuelas J. 2006. Relationship between light use efficiency and photochemical reflectance index in soybean leaves as affected by soil water content. International Journal of Remote Sensing **27**, 5109–5114.

Jahns P. 1995. The Xanthophyll Cycle in Intermittent Light-Grown Pea Plants (Possible Functions of Chlorophyll a/b-Binding Proteins). Plant Physiology **108** , 149–156.

Jahns P, Holzwarth AR. 2012. The role of the xanthophyll cycle and of lutein in photoprotection of photosystem II. Biochimica et Biophysica Acta (BBA)-Bioenergetics **1817**, 182–193.

Johnson MP, Davison P a, Ruban A V, Horton P. 2008. The xanthophyll cycle pool size controls the kinetics of non-photochemical quenching in Arabidopsis thaliana. FEBS letters **582**, 262–6.

Jönsson P, Eklundh L. 2002. Seasonality extraction by function fitting to time-series of satellite sensor data. IEEE Transactions on Geoscience and Remote Sensing **40:8, s. 1**.

Jung M, Reichstein M, Bondeau a. 2009. Towards global empirical upscaling of FLUXNET eddy covariance observations: validation of a model tree ensemble approach using a biosphere model. Biogeosciences **6**, 2001–2013.

Jung M, Vetter M, Herold M, Churkina G, Reichstein M, Zaehle S, Ciais P, Viovy N, Bondeau A, Chen Y, *et al.* 2007. Uncertainties of modeling gross primary productivity over Europe: A systematic study on the effects of using different drivers and terrestrial biosphere models. Global Biogeochemical Cycles **21**, n/a–n/a.

Justice CO, Vermote E, Townshend JRG, Defries R, Roy DP, Hall DK, Salomonson V V, Privette JL, Riggs G, Strahler A, *et al.* 1998. The Moderate Resolution Imaging Spectroradiometer (MODIS): land remote sensing for global change research. Geoscience and Remote Sensing, IEEE Transactions on **36**, 1228–1249.

Kaduk J, Heimann M. 1996. A prognostic phenology scheme for global terrestrial carbon cycle models. Climate Research **6**, 1–19.

Keenan T, García R. 2009. understanding of drought controls on seasonal variation in Mediterranean forest canopy CO 2 and water fluxes through combined in situ measurements and. Biogeosciences …, 2285–2329.

Kemanian AR, Stöckle CO, Huggins DR. 2004. Variability of barley radiation-use efficiency. Crop science **44**, 1662–1672.

Krinner G, Viovy N, de Noblet-Ducoudré N, Ogée J, Polcher J, Friedlingstein P, Ciais P, Sitch S, Prentice IC. 2005. A dynamic global vegetation model for studies of the coupled atmosphere-biosphere system. Global Biogeochemical Cycles **19**, n/a–n/a.

Kumar M, Monteith JL. 1981. Remote sensing of crop growth. Plants and the daylight spectrum, 133–144.

Lafont S, Zhao Y, Calvet J-C, Peylin P, Ciais P, Maignan F, Weiss M. 2012. Modelling LAI, surface water and carbon fluxes at high-resolution over France: comparison of ISBA-A-gs and ORCHIDEE. Biogeosciences **9**, 439–456.

Lebourgeois F, Pierrat J-C, Perez V, Piedallu C, Cecchini S, Ulrich E. 2010. Simulating phenological shifts in French temperate forests under two climatic change scenarios and four driving global circulation models. International journal of biometeorology **54**, 563–81.

Li Z, Wakao S, Fischer BB, Niyogi KK. 2009. Sensing and responding to excess light. Annual review of plant biology **60**, 239–260.

Limousin J-M, Rambal S, Ourcival J-M, Rodríguez-Calcerrada J, Pérez-Ramos IM, Rodríguez-Cortina R, Misson L, Joffre R. 2012. Morphological and phenological shoot plasticity in a Mediterranean evergreen oak facing long-term increased drought. Oecologia **169**, 565–577.

Ma M, Veroustraete F. 2006. Reconstructing pathfinder AVHRR land NDVI time-series data for the Northwest of China. Advances in Space Research **37**, 835–840.

Maselli F, Chiesi M, Moriondo M, Fibbi L, Bindi M, Running SW. 2009. Modelling the forest carbon budget of a Mediterranean region through the integration of ground and satellite data. Ecological Modelling **220**, 330–342.

Maxwell K, Johnson GN. 2000. Chlorophyll fluorescence—a practical guide. Journal of Experimental Botany **51** , 659–668.

Menzel A, Fabian P. 1999. Growing season extended in Europe. Nature, 1996.

Meroni M, Rossini M, Picchi V, Panigada C, Cogliati S, Nali C, Colombo R. 2008. Assessing Steady-state Fluorescence and PRI from Hyperspectral Proximal Sensing as Early Indicators of Plant Stress: The Case of Ozone Exposure. , 1740–1754.

Monteith JL, Moss CJ. 1977. Climate and the Efficiency of Crop Production in Britain [and Discussion]. Philosophical Transactions of the Royal Society of London. B, Biological Sciences **281** , 277–294.

Morales F, Abadía A, Abadía J. 1990. Characterization of the xanthophyll cycle and other photosynthetic pigment changes induced by iron deficiency in sugar beet (Beta vulgaris L.). Plant Physiology **94**, 607–613.

Morales P, Sykes MT, Prentice IC, Smith P, Smith B, Bugmann H, Zierl B, Friedlingstein P, Viovy N, Sabate S, *et al.* 2005. Comparing and evaluating process-based ecosystem model predictions of carbon and water fluxes in major European forest biomes. Global Change Biology **11**, 2211–2233.

Moran JA, Mitchell AK, Goodmanson G, Stockburger KA. 2000. Differentiation among effects of nitrogen fertilization treatments on conifer seedlings by foliar reflectance: a comparison of methods. Tree Physiology **20** , 1113–1120.

Moreno A, Maselli F, Gilabert MA, Chiesi M, Martínez B, Seufert G. 2012. Assessment of MODIS imagery to track light-use efficiency in a water-limited Mediterranean pine forest. Remote Sensing of Environment **123**, 359–367.

Moulin S, Kergoat L, Viovy N, Dedieu G. 1997. Global-Scale Assessment of Vegetation Phenology Using NOAA/AVHRR Satellite Measurements. Journal of Climate **10**, 1154–1170.

Mu Q, Zhao M, Heinsch FA, Liu M, Tian H, Running SW. 2007. Evaluating water stress controls on primary production in biogeochemical and remote sensing based models. Journal of Geophysical Research: Biogeosciences (2005–2012) **112**.

Muchow RC, Sinclair TR, Bennett JM. 1990. Temperature and solar radiation effects on potential maize yield across locations. Agronomy journal **82**, 338–343.

Myneni RB, Los SO, Asrar G. 1995. Potential gross primary productivity of terrestrial vegetation from 1982–1990. Geophysical Research Letters **22**, 2617–2620.

Myneni RB, Los SO, Tucker CJ. 1996. Satellite-based identification of linked vegetation index and sea surface temperature Anomaly areas from 1982-1990 for Africa, Australia and South America. Geophys. Res. Lett. **23**, 729–732.

Nakaji T, Ide R, Oguma H, Saigusa N, Fujinuma Y. 2007. Utility of spectral vegetation index for estimation of gross CO< sub> 2</sub> flux under varied sky conditions. Remote Sensing of Environment **109**, 274–284.

Nakaji T, Ide R, Takagi K, Kosugi Y, Ohkubo S, Nishida K, Saigusa N, Oguma H, Nasahara KN. 2008. Utility of spectral vegetation indices for estimation of light conversion efficiency in coniferous forests in Japan. Agricultural and Forest Meteorology **148**, 776–787.

Nakaji T, Oguma H, Fujinuma Y. 2006. Seasonal changes in the relationship between photochemical reflectance index and photosynthetic light use efficiency of Japanese larch needles. International Journal of Remote Sensing **27**, 493–509.

Nichol CJ, Huemmrich KF, Black TA, Jarvis PG, Walthall CL, Grace J, Hall FG. 2000. Remote sensing of photosynthetic-light-use efficiency of boreal forest. Agricultural and Forest Meteorology **101**, 131–142.

Nichol CJ, Lloyd J, Shibistova O, Arneth A, Röser C, Knohl A, Matsubara S, Grace J. 2002. Remote sensing of photosynthetic-light-use efficiency of a Siberian boreal forest. Tellus B **54**, 677–687.

Nilkens M, Kress E, Lambrev P, Miloslavina Y, Müller M, Holzwarth AR, Jahns P. 2010. Identification of a slowly inducible zeaxanthin-dependent component of non-photochemical quenching of chlorophyll fluorescence generated under steady-state conditions in Arabidopsis. Biochimica et Biophysica Acta (BBA) - Bioenergetics **1797**, 466–475.

Ogaya R, Peñuelas J. 2003. Comparative field study of Quercus ilex and Phillyrea latifolia: photosynthetic response to experimental drought conditions. Environmental and Experimental Botany **50**, 137–148.

Ort DR. 2001. When there is too much light. Plant Physiology **125**, 29–32.

Pan Y, Birdsey R, Hom J, McCullough K, Clark K. 2006. Improved estimates of net primary productivity from MODIS satellite data at regional and local scales. Ecological Applications **16**, 125–132.

Peguero-Pina J, Morales F, Flexas J, Gil-Pelegrín E, Moya I. 2008. Photochemistry, remotely sensed physiological reflectance index and de-epoxidation state of the xanthophyll cycle in Quercus coccifera under intense drought. Oecologia **156**, 1–11 LA – English.

Penuelas J, Filella I, Comas P. 2002. Changed plant and animal life cycles from 1952 to 2000 in the Mediterranean region. Global Change Biology, 531–544.

Penuelas J, Filella I, Gamon JA. 1995. Assessment of photosynthetic radiation-use efficiency with spectral reflectance. New Phytologist **131**, 291–296.

Peñuelas J, Filella I, Llusia J, Siscart D, Piñol J. 1998. Comparative field study of spring and summer leaf gas exchange and photobiology of the Mediterranean trees Quercus ilex and Phillyrea latifolia. Journal of Experimental Botany **49**, 229–238.

Peñuelas J, Garbulsky MF, Filella I. 2011. Photochemical reflectance index (PRI) and remote sensing of plant CO2 uptake. New Phytologist **191**, 596–599.

Peñuelas J, Llusia J, Pinol J, Filella I, Penuelas J. 1997. Photochemical reflectance index and leaf photosynthetic radiation-use-efficiency assessment in Mediterranean trees. International Journal of Remote Sensing **18**, 2863–2868.

Peñuelas J, Sardans J, Rivas-ubach A, Janssens I a. 2012. The human-induced imbalance between C, N and P in Earth's life system. Global Change Biology **18**, 3–6.

Pfündel E, Bilger W. 1994. Regulation and possible function of the violaxanthin cycle. Photosynthesis Research **42**, 89–109.

Pontailler J-Y, Genty B. 1996. A simple red:far-red sensor using gallium arsenide phosphide detectors. Functional ecology **10**, 535–540.

Pontailler J-Y, Hymus GJ, Drake BG. 2003. Estimation of leaf area index using ground-based remote sensed NDVI measurements: validation and comparison with two indirect techniques. Canadian Journal of Remote Sensing **29**, 381–387.

La Porta N, Capretti P, Thomsen IM, Kasanen R, Hietala AM, Von Weissenberg K. 2008. Forest pathogens with higher damage potential due to climate change in Europe. Canadian Journal of Plant Pathology **30**, 177–195.

Potter CS, Randerson JT, Field CB, Matson PA, Vitousek PM, Mooney HA, Klooster SA. 1993. Terrestrial ecosystem production: a process model based on global satellite and surface data. Global Biogeochemical Cycles **7**, 811–841.

Prince SD, Goward SN. 1995. Global primary production: a remote sensing approach. Journal of biogeography, 815–835.

Le Quere C, Raupach MR, Canadell JG, Marland et al. G. 2009. Trends in the sources and sinks of carbon dioxide. Nature Geosci **2**, 831–836.

Rahimzadeh-Bajgiran P, Munehiro M, Omasa K. 2012. Relationships between the photochemical reflectance index (PRI) and chlorophyll fluorescence parameters and plant pigment indices at different leaf growth stages. Photosynthesis Research **113**, 261–271.

Rascher U, Agati G, Alonso L, Cecchi G, Champagne S, Colombo R, Damm a., Daumard F, de Miguel E, Fernandez G, *et al.* 2009. CEFLES2: the remote sensing component to quantify photosynthetic efficiency from the leaf to the region by measuring sun-induced fluorescence in the oxygen absorption bands. Biogeosciences **6**, 1181–1198.

Rascher U, Nedbal L. 2006. Dynamics of photosynthesis in fluctuating light. Current Opinion in Plant Biology **9**, 671–678.

Raven, P.H., Evert, R.F., Eichhorn, S.E., & Bouharmont, J. (2003). Biologie végétale, Traduction de la 7e édition américaine par J. Bouharmont avec la collaboration de C.M. Evrard, 1 ère édition, De Boeck Université, Paris-Bruxelles, ISBN : 2-7445-0102-6, xxii

Reed BC, Brown JF, Vander Zee D, Loveland TR, Merchant JW, Ohlen DO. 1994. Measuring phenological variability from satellite imagery. Journal of Vegetation Science **5**, 703–714.

Rosati A, Dejong TM. 2003. Estimating Photosynthetic Radiation Use Efficiency Using Incident Light and Photosynthesis of Individual Leaves . Annals of Botany **91** , 869–877.

Rosema a, Verhoef W, Schroote J, Snel J. 1991. Simulating fluorescence light-canopy interaction in support of laser-induced fluorescence measurements. Remote Sensing of Environment **37**, 117–130.

Ruban A V, Johnson MP, Duffy CDP. 2012. The photoprotective molecular switch in the photosystem II antenna. Biochimica et biophysica acta **1817**, 167–81.

Running SW, Thornton PE, Nemani R, Glassy JM. 2000. Global terrestrial gross and net primary productivity from the Earth Observing System. Methods in ecosystem science, 44–57.

Sarlikioti V, Driever SM, Marcelis LFM. 2010. Photochemical reflectance index as a mean of monitoring early water stress. Annals of Applied Biology **157**, 81–89.

Schoenholtz S., Miegroet HV, Burger J. 2000. A review of chemical and physical properties as indicators of forest soil quality: challenges and opportunities. Forest Ecology and Management **138**, 335–356.

Schreiber U, Bilger W. 1993. Progress in Chlorophyll Fluorescence Research: Major Developments During the Past Years in Retrospect. In: Behnke H-D, Lüttge U, Esser K, Kadereit J, Runge M, eds. Progress in Botany / Fortschritte der Botanik SE - 8. Springer Berlin Heidelberg, 151–173.

Schwartz MD, Reed BC, White MA. 2002. Assessing satellite-derived start-of-season measures in the conterminous USA. International Journal of Climatology **22**, 1793–1805.

Sheffield J, Wood E. 2008. Projected changes in drought occurrence under future global warming from multi-model, multi-scenario, IPCC AR4 simulations. Climate Dynamics **31**, 79–105.

Sims DA, Gamon JA. 2002. Relationships between leaf pigment content and spectral reflectance across a wide range of species, leaf structures and developmental stages. Remote Sensing of Environment **81**, 337–354.

Soudani K, François C, le Maire G, Le Dantec V, Dufrêne E. 2006. Comparative analysis of IKONOS, SPOT, and ETM+ data for leaf area index estimation in temperate coniferous and deciduous forest stands. Remote Sensing of Environment **102**, 161–175.

Soudani K, Hmimina G, Delpierre N, Pontailler JY, Aubinet M, Bonal D, Caquet B, De Grandcourt A, Burban B, Flechard C, *et al.* 2012. Ground-based Network of NDVI measurements for tracking temporal dynamics of canopy structure and vegetation phenology in different biomes. Remote Sensing of Environment **123**, 234–245.

Soudani K, le Maire G, Dufrêne E, François C, Delpierre N, Ulrich E, Cecchini S. 2008. Evaluation of the onset of green-up in temperate deciduous broadleaf forests derived from Moderate Resolution Imaging Spectroradiometer (MODIS) data. Remote Sensing of Environment **112**, 2643–2655.

Spitters CJT. 1989. Crop growth models: their usefulness and limitations. VI Symposium on the Timing of Field Production of Vegetables 267.349–368.

Studer S, Stöckli R, Appenzeller C, Vidale P. 2007. A comparative study of satellite and ground-based phenology. International Journal of Biometeorology **51**, 405–414.

Stylinski C, Gamon J, Oechel W. 2002. Seasonal patterns of reflectance indices, carotenoid pigments and photosynthesis of evergreen chaparral species. Oecologia **131**, 366–374 LA – English.

Suárez L, Zarco-Tejada PJ, González-Dugo V, Berni JAJ, Sagardoy R, Morales F, Fereres E. 2010. Detecting water stress effects on fruit quality in orchards with time-series PRI airborne imagery. Remote Sensing of Environment **114**, 286–298.

Suárez L, Zarco-Tejada PJ, Sepulcre-Cantó G, Pérez-Priego O, Miller JR, Jiménez-Muñoz JC, Sobrino J. 2008. Assessing canopy PRI for water stress detection with diurnal airborne imagery. Remote Sensing of Environment **112**, 560–575.

Suzuki R, Nomaki T, Yasunari T. 2003. West-east contrast of phenology and climate in northern Asia revealed using a remotely sensed vegetation index. International Journal of Biometeorology **47**, 126–138.

Szabó I, Bergantino E, Giacometti GM. 2005. Light and oxygenic photosynthesis: energy dissipation as a protection mechanism against photo-oxidation. EMBO reports **6**, 629–634.

Takizawa K, Cruz JA, Kanazawa A, Kramer DM. 2007. The thylakoid proton motive force in vivo. Quantitative, non-invasive probes, energetics, and regulatory consequences of light-induced pmf. Biochimica et Biophysica Acta (BBA) - Bioenergetics **1767**, 1233–1244.

Thenot F, Méthy M, Winkel T. 2002. The Photochemical Reflectance Index (PRI) as a water-stress index. International Journal of Remote Sensing **23**, 5135–5139.

Thornley J. 1998. Dynamic model of leaf photosynthesis with acclimation to light and nitrogen. Annals of Botany, 421–430.

Trotter GM, Whitehead D, Pinkney EJ. 2002. The photochemical reflectance index as a measure of photosynthetic light use efficiency for plants with varying foliar nitrogen contents. International Journal of Remote Sensing **23**, 1207–1212.

Turner DP, Ritts WD, Cohen WB, Gower ST, Running SW, Zhao M, Costa MH, Kirschbaum AA, Ham JM, Saleska SR, *et al.* 2006. Evaluation of MODIS NPP and GPP products across multiple biomes. Remote Sensing of Environment **102**, 282–292.

Turner DP, Ritts WD, Cohen WB, Gower ST, Zhao M, Running SW, Wofsy SC, Urbanski S, Dunn AL, Munger JW. 2003. Scaling Gross Primary Production (GPP) over boreal and deciduous forest landscapes in support of MODIS GPP product validation. Remote Sensing of Environment **88**, 256–270.

Turner DP, Ritts WD, Cohen WB, Maeirsperger TK, Gower ST, Kirschbaum AA, Running SW, Zhao M, Wofsy SC, Dunn AL. 2005. Site-level evaluation of satellite-based global terrestrial gross primary production and net primary production monitoring. Global Change Biology **11**, 666–684.

Turner DP, Urbanski S, Bremer D, Wofsy SC, MEYERS T, GOWER ST, GREGORY M. 2003. A cross-biome comparison of daily light use efficiency for gross primary production. Global Change Biology **9**, 383–395.

Urban O, Janouš D, Acosta M, Czerný R, Marková I, Navrátil M, Pavelka M, Pokorný R, Šprtová M, Zhang R, *et al.* 2007. Ecophysiological controls over the net ecosystem exchange of mountain spruce stand. Comparison of the response in direct vs. diffuse solar radiation. Global Change Biology **13**, 157–168.

Verstraete M, Pinty B, Myneni R. 1996. Potential and limitations of information extraction on the terrestrial biosphere from satellite remote sensing. Remote Sensing of Environment **4257**.

Viovy N, Arino O, Belward AS. 1992. The Best Index Slope Extraction (BISE): A method for reducing noise in NDVI time-series. International Journal of Remote Sensing **13**, 1585–1590.

White MA, Nemani RR. 2006. Real-time monitoring and short-term forecasting of land surface phenology. Remote Sensing of Environment **104**, 43–49.

White MA, Nemani RR, Thornton PE, Running SW. 2002. Satellite Evidence of Phenological Differences Between Urbanized and Rural Areas of the Eastern United States Deciduous Broadleaf Forest. Ecosystems **5**, 260–273.

White MA, Thornton PE, Running SW. 1997. A continental phenology model for monitoring vegetation responses to interannual climatic variability. Global biogeochemical cycles **11**, 217–234.

White M a., Thornton PE, Running SW, Nemani RR. 2000. Parameterization and Sensitivity Analysis of the BIOME–BGC Terrestrial Ecosystem Model: Net Primary Production Controls. Earth Interactions **4**, 1–85.

Wolfe RE, Nishihama M, Fleig AJ, Kuyper JA, Roy DP, Storey JC, Patt FS. 2002. Achieving sub-pixel geolocation accuracy in support of MODIS land science. Remote Sensing of Environment **83**, 31–49.

Wu C, Niu Z, Tang Q, Huang W. 2010. Revised photochemical reflectance index (PRI) for predicting light use efficiency of wheat in a growth cycle: validation and comparison. International Journal of Remote Sensing **31**, 2911–2924.

Xu L, Baldocchi DD. 2003. Seasonal trends in photosynthetic parameters and stomatal conductance of blue oak (Quercus douglasii) under prolonged summer drought and high temperature. Tree Physiology **23** , 865–877.

Yamamoto HY. 1979. Biochemistry of the violaxanthin cycle in higher plants. Pure & Applied Chemistry **51**, 639–648.

Yamamoto HY. 2006. Functional roles of the major chloroplast lipids in the violaxanthin cycle. Planta **224**, 719–724.

Zarco-Tejada PJ, Berjón A, López-Lozano R, Miller JR, Martín P, Cachorro V, González MR, de Frutos A. 2005. Assessing vineyard condition with hyperspectral indices: Leaf and canopy reflectance simulation in a row-structured discontinuous canopy. Remote Sensing of Environment **99**, 271–287.

Zarco-Tejada PJ, González-Dugo V, Berni JAJ. 2012. Fluorescence, temperature and narrow-band indices acquired from a UAV platform for water stress detection using a micro-hyperspectral imager and a thermal camera. Remote Sensing of Environment **117**, 322–337.

Zarco-Tejada P., Rueda C., Ustin S. 2003. Water content estimation in vegetation with MODIS reflectance data and model inversion methods. Remote Sensing of Environment **85**, 109–124.

Zhang X, Friedl MA, Schaaf CB, Strahler AH, Hodges JCF, Gao F, Reed BC, Huete A. 2003. Monitoring vegetation phenology using MODIS. Remote Sensing of Environment **84**, 471–475.

Zhang X, Goldberg MD. 2011. Monitoring fall foliage coloration dynamics using time-series satellite data. Remote Sensing of Environment **115**, 382–391.

Annexes

L’article Soudani et al. 2012, publié dans le journal Remote Sensing of environment, ainsi que les articles Hmimina et al. 2013a et Hmimina et al. 2013b, publiés dans les journaux Remote Sensing of Environment et Plant, Cell & Environment respectivement sont présentés dans les Annexes suivantes.